

*WA Davis*

**NATIONAL ACADEMIES OF SCIENCES AND ENGINEERING  
NATIONAL RESEARCH COUNCIL  
of the  
UNITED STATES OF AMERICA**

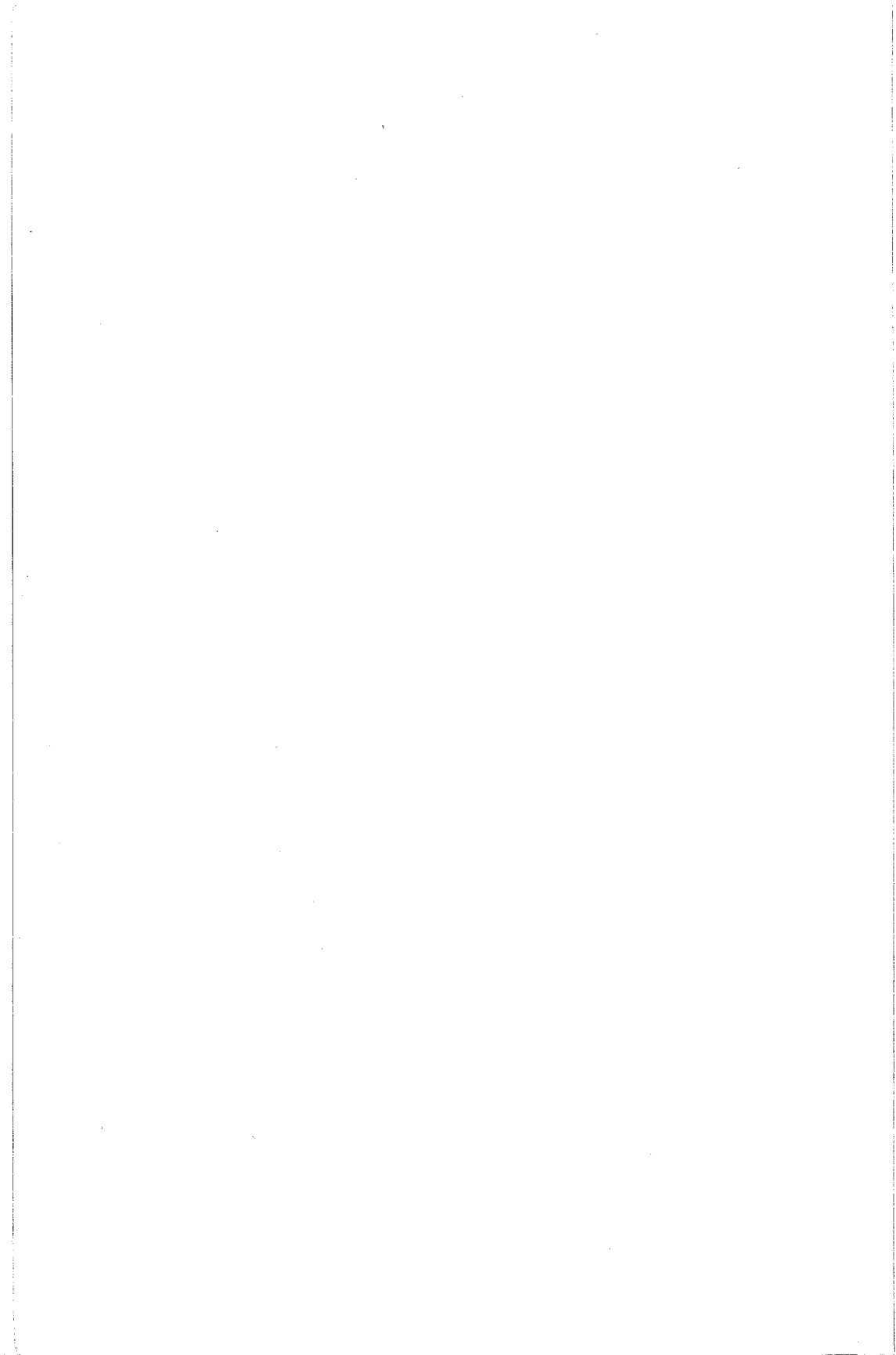
**UNITED STATES NATIONAL COMMITTEE  
International Union of Radio Science**



National Radio Science Meeting  
4 - 7 January 2006

Sponsored by USNC/URSI

University of Colorado at Boulder  
Boulder, Colorado  
USA



United States National Committee  
International Union of Radio Science

# ABSTRACTS

National Radio Science Meeting  
4–7 January 2006

University of Colorado, Boulder

Sponsored by USNC/URSI

## Table of Contents

| Session                          | Page No. | Session         | Page No. |
|----------------------------------|----------|-----------------|----------|
| Membership Information . . . . . | iii      | F2 . . . . .    | 157      |
| Description of URSI . . . . .    | iv       | F3 . . . . .    | 163      |
| Plenary Session . . . . .        | vii      | G1 . . . . .    | 171      |
| A1 . . . . .                     | 1        | G2 . . . . .    | 185      |
| A2 . . . . .                     | 7        | G3 . . . . .    | 199      |
| A/D1 . . . . .                   | 15       | G4 . . . . .    | 211      |
| B1 . . . . .                     | 23       | G/H1 . . . . .  | 221      |
| B2 . . . . .                     | 31       | G/H2 . . . . .  | 235      |
| B3 . . . . .                     | 39       | G/H3 . . . . .  | 247      |
| B4 . . . . .                     | 47       | H1 . . . . .    | 257      |
| B5 . . . . .                     | 61       | H/G1 . . . . .  | 269      |
| B6 . . . . .                     | 73       | H/G2 . . . . .  | 279      |
| B7 . . . . .                     | 81       | H/G3 . . . . .  | 291      |
| B/E1 . . . . .                   | 89       | J1 . . . . .    | 299      |
| B/F1 . . . . .                   | 97       | J2 . . . . .    | 309      |
| B/F2 . . . . .                   | 105      | J3 . . . . .    | 321      |
| B/F3 . . . . .                   | 117      | J/B1 . . . . .  | 335      |
| C1 . . . . .                     | 125      | J/B2 . . . . .  | 349      |
| D1 . . . . .                     | 133      | K1 . . . . .    | 361      |
| E1 . . . . .                     | 139      | K2 . . . . .    | 367      |
| F1 . . . . .                     | 145      | Index . . . . . | 379      |

# Membership

United States National Committee  
INTERNATIONAL UNION OF RADIO SCIENCE

|                          |                            |
|--------------------------|----------------------------|
| Chair:                   | Piergiorgio L.E. Uslenghi* |
| Secretary & Chair-Elect: | Yahya Rahmat-Samii*        |
| Immediate Past Chair:    | Umran S. Inan*             |
| Treasurer:               | Gary S. Brown              |

## Members Representing Societies, Groups, and Institutes:

|   |                        |
|---|------------------------|
| American Astronomical Society:                | Donald Backer          |
| American Geophysical Union:                   | David Hysell           |
| American Meteorological Society:              | Richard J. Doviak      |
| IEEE Antennas and Propagation Society:        | Susan C. Hagness       |
| IEEE Geosciences and Remote Sensing Society:  | Edgeworth R. Westwater |
| IEEE Microwave Theory and Techniques Society: | Tatsuo Itoh            |

## Members-at-Large

Susan C. Hagness  
Steven C. Reising  
Jennifer T. Bernhard  
Paul A. Bernhardt  
Jacqueline Hewitt  
Nader Engheta  
Yahya Rahmat-Samii  
Robert Gardner

## Chairs of the USNC-URSI Commissions:

|              |                   |
|--------------|-------------------|
| Commission A | Vijay Nair        |
| Commission B | David R. Jackson  |
| Commission C | Dev Palmer        |
| Commission D | L. Wilson Pearson |
| Commission E | Cynthia Ropiak    |
| Commission F | Roger Lang        |
| Commission G | John Matthews     |
| Commission H | Meers Oppenheim   |
| Commission J | David Woody       |
| Commission K | Gianluca Lazzi    |

## Officers, Chairs and Vice Chairs of Commissions of URSI residing in the United States

|                          |                    |
|--------------------------|--------------------|
| URSI Honorary President  | William E. Gordon  |
| URSI Vice President      | Chalmers M. Butler |
| Chair, Commission C      | A. F. Molisch      |
| Vice Chair, Commission D | Franz Kärtner      |

\*Member of USNC/URSI Executive Committee

## Description of the International Union of Radio Science

The International Union of Radio Science is one of the world scientific unions organized under the International Council of Scientific Unions (ICSU). It is commonly designated as URSI from its French name, Union Radio Scientifique Internationale. Its aims are (1) to promote the scientific study of radio communications, (2) to aid and organize radio research requiring cooperation on an international scale and to encourage the discussion and publication of the results, (3) to facilitate agreement upon common methods of measurement and the standardization of measuring instruments, and (4) to stimulate and to coordinate studies of the scientific aspects of telecommunications using electromagnetic waves, guided and unguided. The International Union itself is an organizational framework to aid in promoting these objectives. The actual technical work is largely done by the National Committee in the various countries.

The officers of the International Union are:

|  |  |
|--|--|
| President:                                     | François Lefevre (France)  |
| Past President:                                | Kristian Schlegel (Germany)  |
| Vice Presidents:                               | Chalmers M. Butler (USA)<br>Gert Brussaard (Netherlands)<br>Martti Hallikainen (Finland)<br>Phil Wilkinson (Australia) |
| Secretary-General:                             | Paul Lagasse (Belgium)   |
| Assistant Secretary General:                   | Femke Olyslager (Belgium)  |
| Assistant Secretary General<br>(Publications): | W. Ross Stone (USA)  |
| Executive Secretary:                           | Inge Heleu (Belgium)   |
| Administrative Secretary                       | Inge Lievens (Belgium)   |

The Secretary General's office and the headquarters of the organization are located c/o INTEC, Ghent University, Sint-Pietersnieuwstraat 41, B-9000 Ghent, Belgium. The Union is supported by contributions (dues) from 44 member committees. The International Union, as of the XXVIIIth General Assembly held in New Delhi, India, 23–29 October, 2005, has ten bodies, called Commissions, for centralizing studies in principal fields.

Every three years the International Union of Radio Science holds a meeting called the General Assembly. The next is the XXIXth, to be held in Chicago, Illinois, USA, on 7–16 August, 2008. The Secretariat prepares and distributes the Proceedings of the General Assemblies. The International Union arranges international symposia on specific subjects pertaining to the work of one or several Commissions and also cooperates with other Unions in international symposia on subjects of joint interest.

Radio is unique among the fields of scientific work in having a specific adaptability to large-scale international research programs, since many of the phenomena that must be studied are worldwide in extent and yet are in a measure subject to control by experimenters. Exploration of space and the extension of scientific observations to the space environment are dependent on radio for their research. One branch, radio astronomy, involves cosmic phenomena, URSI thus has a distinct field of usefulness in furnishing a meeting ground for the numerous workers in the manifold aspects of radio research; its meetings and committee activities furnish valuable means of promoting research through exchange of ideas.

Steering Committee:

P.L.E. Uslenghi, University of Illinois at Chicago

K. Grosland, CU Conference Services, University of Colorado

Technical Program Committee:

P. Uslenghi, Chair

Y. Rahmat-Samii, Secretary

S. Reising, Student Paper Competition

(A) V. Nair

(F) R. Lang

(B) D. Jackson

(G) J. Matthews

(C) D. Palmer

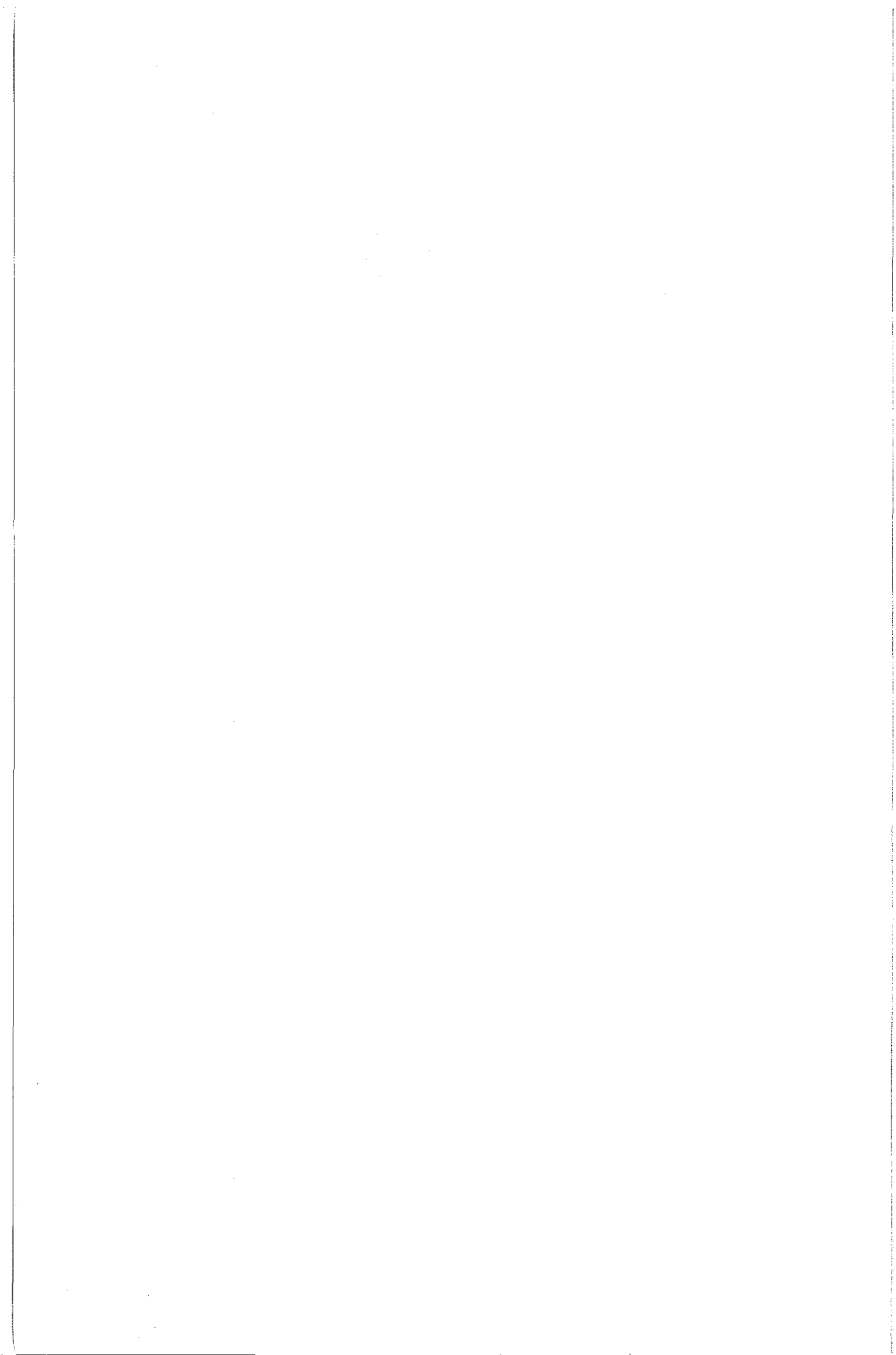
(H) M. Oppenheim

(D) L.W. Pearson

(J) D. Woody

(E) C. Ropiak

(K) G. Lazzi





Plenary Session, 10:15 – Thurs.

Gasiewski, A.J., Clegg, A.W.

## Plenary

SPECTRUM MANAGEMENT AND INTERFERENCE MITIGATION IN PASSIVE EARTH REMOTE SENSING

Gasiewski, A.J.<sup>2</sup>

<sup>1</sup>NOAA Environmental Technology Laboratory, Boulder, CO, USA

<sup>2</sup>Department of Electrical and Computer Engineering, University of Colorado, Boulder, CO, USA

Increasing use of previously quiet radio bands for communications and radar applications imposes a growing problem for passive remote sensing of many key environmental variables, including soil moisture, sea surface temperature, water vapor, ocean surface winds, cloud water content, and rain rate. We review in this talk the status of major passive microwave environmental observing systems, sensitivity and spectral requirements for Earth remote sensing, useful RFI mitigation techniques, and major regulatory issues affecting passive Earth remote sensing.

The problem of anthropogenic radio frequency interference (RFI) in passive Earth remote sensing is similar to that of RFI in radio astronomy, thus engendering a mutual interest among users of the Earth Exploration Satellite Service (EESS) and Radio Astronomy Service (RAS) to regulate emissions in several key bands of common interest. Being that the two services are based upon distinct viewing geometries and locations, integration times, spectral features, and applications of the data, however, there are a number of vexing issues specific to Earth remote sensing. Foremost among these distinctions is the need in passive Earth remote sensing to maintain interference-free operation while regularly viewing downward over the entire globe, including (and especially) major urban and coastal areas. In addition, certain key bands necessary for passive microwave surface observation have never been provided primary EESS allocation.

Progress over the past several years in developing RFI mitigation techniques for passive Earth remote sensing has been substantial, and the use of such techniques promises to at least temporarily sustain environmental observation capabilities. Countering this trend, we anticipate that new applications of passive microwave sensors relying upon direct assimilation of data into modern numerical models will further magnify the impact of RFI as these models improve their representational accuracy.

DC TO DAYLIGHT: SPECTRUM MANAGEMENT AND THE NEW  
RADIO ASTRONOMY

Clegg, A. W.

National Science Foundation, 4201 Wilson Blvd, Arlington VA 22230

Radio astronomers are increasingly outfitting existing radio telescopes with the capability to acquire data well outside of bands allocated to the radio astronomy service. Envisioned next-generation radio telescopes, such as the Square Kilometer Array, will go one step further by *requiring* this capability to carry out some of their fundamental scientific goals. At the same time, the general population (including radio astronomers) is driving unprecedented demand for access to the radio spectrum by licensed services and unlicensed devices for the provision of cellular phone communications, wireless networks, satellite radio and television, and a wide range of other ubiquitous modern conveniences. As a result, radio astronomers face a number of significant issues that impact the future of radio astronomy:

1) The increased reliance on interference mitigation and excision techniques that, although promising, remain nascent and unproven on a large scale. Out-of-band observing will increasingly require robust hardware and software that can simultaneously contend with strong signals originating from a multitude of directions at multiple frequencies and with differing modulation waveforms.

2) The development of cognitive radios, software-defined radios, and other opportunistic transmission technologies that will make it harder to predict the specific nature of interfering signals. In addition, many concepts for listen-before-transmit schemes to be used in cognitive and software radios either cannot or do not take into account the existence of sensitive and purely passive services such as radio astronomy. At the same time, radio astronomers hoping to increase the efficiency of out-of-band observing may draw upon some of the opportunistic techniques developed for cognitive radios.

3) The increased non-regulation of new and potentially interfering technologies as "unlicensed devices," a designation that tends to increase the penetration rate of the devices while simultaneously complicating the ability to identify the specific source(s) of interfering transmissions. Ultrawideband (UWB) transmitters, vehicular radars, and Broadband over Power Line (BPL) systems are examples.

4) The deployment of next-generation millimeter and sub-millimeter radio telescopes that portend the need to extend radio astronomy frequency allocations, and the allocation tables themselves, beyond the present 275 GHz limit.

5) Consideration of "out-of-the-box" concepts such as possible trade-offs in the blanket designation of protected radio astronomy bands in exchange for enhanced regulatory protection in the vicinity of radio astronomy observatories.

Session A1, 08:35 – Fri.

**MEASUREMENT AND MODELING  
ISSUES**

Co-Chairs: W.A. Davis, C.E. Baum



DESIRABLE ANTENNA CHARACTERISTICS FOR LATE-TIME  
TARGET IDENTIFICATION

Baum, Carl E.  
University of New Mexico

An antenna is required to send an interrogating electromagnetic wave at a target. An antenna (a different antenna or the same antenna) is required to receive the scattered wave from the target. In both cases the antenna characteristics mix with the target-response function to complicate the target identification. What, then, can we do to simplify this problem? The antennas can be designed to give the best possible transient response (or, equivalently, transfer function).

As we know, antennas cannot radiate DC (to the far field). As such, within physical limits an antenna cannot radiate a pure delta function (impulse). Exciting the radiating antenna with a step function, the antenna will radiate a wave with at least one zero crossing. The area (complete time integral) of the radiated waveform must be zero. In reception, the antenna response is the time integral of its response in transmission.

An important class of antennas for use with transients is that of impulse-radiating antennas (IRA's), which come in a least three types: reflector, lens (including small-angle TEM horns), and array. An important characteristic is that they radiate an approximate delta function when driven by a step-function voltage. Even then, however, the foregoing limitations concerning zero area still apply. The same applies to their receiving response to a delta function.

This leads to the question discussed in this paper. Which of these types of IRAs is most suited for use in late-time target identification?

All antennas, being limited in their low-frequency response, cannot radiate only an approximate delta function. The remaining part(s) of the pulse (to give net zero area, or complete time integral) can appear before and/or after the delta function. For late-time target identification we find here that these other parts are better placed before rather than after the approximate delta function.

STATISTICAL AND 'FUZZY POLE' CHARACTERIZATION OF  
THE COMPLEX POLES OF A CONDUCTING SPHERE AND A  
WIRE

Joshi, G. G., Davis, W. A., Stutzman, W. L.

Virginia Tech Antenna Group, Bradley Dept. of Electrical and Com-  
puter Engineering, Virginia Tech

Developments in ultra-wideband radar, communications and surveillance systems require reliable scatter characterization and modeling. Time-domain, scatter-response characterization based on the Singularity Expansion Method (SEM) has been a popular approach (C. E. Baum, IEEE Antennas and Prop. Society Symp. 11, 459462, 1973). Early SEM research emphasized the accuracy of various extraction methods and algorithms for noisy time-domain data. Some research has also focused on the accuracy of the poles extracted from the noisy data in terms of the percentage error. However, no effort has been undertaken to demonstrate the distribution of complex poles in the presence of noise. Here, analytical as well as measured scatter responses of a conducting sphere and a straight wire will be analyzed for various noise levels. The complex poles will be extracted from the time domain response using the Matrix Pencil Method (T. K. Sarkar, and O. Pereira, IEEE Antennas and Prop. Mag., 37, 4855, 1995).

Empirically observed distributions of the extracted complex poles for various noise levels will be matched to known distributions using iterative search of the distribution parameters. The real and imaginary components of the complex poles or resonances will be treated separately. These advances in the statistical characterization of complex poles will contribute to the development of a comprehensive wideband channel model that incorporates scatterer response.

Complex poles extracted from empirical data form clusters due to the measurement noise. Fuzzy cluster representations of the time-frequency domain signatures are widely used to model buried targets. A similar approach will be applied to characterize a cluster of complex poles by a single fuzzy pole using the Fuzzy Cluster Mean (FCM) algorithm (J. Bezdek, J. Cybernetics, 3, 5871, 1974). The FCM algorithm iteratively searches for a fuzzy pole by minimizing a cost function as in a constrained optimization problem. Advances in fuzzy pole representation will provide characterization of target signatures using fewer complex poles.



## GAP ERROR MITIGATION VIA MODAL ANALYSIS FOR MATERIAL CHARACTERIZATION IN COAXIAL LINE TEST FIXTURES

Fehlen, R. G.<sup>1</sup>, Havrilla, M. J.<sup>1</sup>, Frasc, L. L.<sup>2</sup>, Choi, C.<sup>2</sup>

<sup>1</sup>Department of Electrical and Computer Engineering, Air Force Institute of Technology, Wright Patterson AFB, OH 45433

<sup>2</sup>The Boeing Company, St. Louis, MO 63166

Electromagnetic material characterization is the process of determining the complex permittivity and permeability of a test sample. The well-defined *TEM* field propagation characteristics of a coaxial transmission line are ideal for material measurements provided the test sample uniformly fills the cross-sectional dimensions of the guiding structure. If gaps are introduced between the material sample and the conducting boundaries, higher-order modes are excited which introduce error into material characterization measurements. Gaps are typically the result of imperfect machining of the test sample or different thermal expansion rates of the test sample and conducting boundaries in high temperature experiments. Additionally, softer material may be machined with an intentional air gap to reduce sample-compression error. Mitigating gap error ensures the accuracy of the measurement and simplifies the mounting process. Existing techniques quantify gap error through lumped circuit element models of the coaxial transmission line and material. This paper will use a full wave analysis to accommodate higher-order mode excitation in quantifying the gap error.

Consider a sample of length  $d$  occupying the region  $0 < z < d$  along the guiding axis of an empty coaxial line. If an air gap along the radial direction is subsequently introduced between the inner or outer conducting boundary of the coaxial fixture and the test sample, then higher-order modes will be scattered. If it is assumed that the air gap is axially symmetric, then it can be shown that  $TM_{0n}$  modes will be excited in the surrounding region of the sample discontinuity (note, a *TEM* mode can only be supported in the regions  $z < 0$  and  $z > d$ ). A mode-matching technique can be implemented to enforce continuity of tangential electric and magnetic field components at the front and back interfaces of the sample. This modal analysis leads to a matrix equation that can subsequently be solved to determine the theoretical *TEM* mode scattering parameters ( $S_{11}^{thy}$ ,  $S_{21}^{thy}$ ) of the test sample. A two-dimensional root search algorithm can be utilized to iterate and determine the sample permittivity and permeability values until the theoretical and experimental S-parameters are equal, namely

$$\begin{aligned} S_{11}^{thy}(\omega, \epsilon, \mu) - S_{11}^{exp}(\omega) &= 0 \\ S_{21}^{thy}(\omega, \epsilon, \mu) - S_{21}^{exp}(\omega) &= 0 \end{aligned}$$

Experimental results for several sample materials and gap scenarios will be provided and compared with the ideal uniformly-filled case. The effects of different gap scenarios will be explored.<sup>a b</sup>

<sup>a</sup>STUDENT PAPER submission and presentation

<sup>b</sup>The views of the authors expressed in this article do not reflect the official policy of the U.S. Air Force, Department of Defense, or the U.S. Government.

## NEW EXPRESSION OF APPROXIMATE TRANSITION BOUNDARY CONDITIONS FOR UNIAXIAL BIANISOTROPIC THIN LAYERS

Jiang Bin-hao , Liu Yong-tan

<sup>1</sup>Harbin Institute of Technology , Research Institute of Electronic Engineering<sup>2</sup>Harbin Institute of Technology , Research Institute of Electronic Engineering

Approximations boundary conditions can be usefully employed to simplify a large variety of electromagnetic field problems involving complex geometries and materials. In any given case there may be several different approximate conditions that could be employed, each derived by considering a simplified (canonical) problem whose solution can be found. For uniaxial bianisotropic thin layers, a pair of differential vector equations relating the tangential components of the fields and their second-order tangential derivatives has been obtained for higher-order transition boundary conditions by using averaging method [1,2]. Although the boundary conditions are well approximated over a reasonably wide range of parameters and have been used to serve as the foundation for related electromagnetics problems, we believe that the potentialities of the conditions have not been fully exploited. By using the basic field equations and some manipulations of vectors, this paper presents a new expression of the approximate transition boundary conditions for the uniaxial bianisotropic thin layers.

The obtained boundary conditions contain only the first order polynomials in the normal derivatives, and the present results shall be referred to as the first-order conditions. The normal differential operators on the tangential field vectors can be used to better simulate the spatial variation of the fields since the influence of the uniaxial layers on the electromagnetic fields in the normal direction is more strong than ones in the tangential directions. For guided propagation in normal direction the obtained conditions can also be degraded into the forms of expression in which no derivatives of the fields are included. In addition, the new representation is now geometry independent (the coordinate-free vector formulation), therefore we can generalize its expression to a curved boundary.

[1] D. Y. Khaliullin and S. A. Tretyakov. IEE Proc. Microwaves, Antennas and Propagations, 145, 163-168, 1998.

[2] S. A. Tretyakov and A. S. Cherepanov. Radio Science, 26, 523-528, 1991.

Session A2, 10:15-Fri.

**DIELECTRIC SPECTROSCOPY  
AND DIELECTRIC DETECTION  
METHODS**

Co-Chairs: J. Baker-Jarvis, M. Janezic



## BROADBAND COMPLEX PERMITTIVITY MEASUREMENTS OF LIQUIDS

Janeizc, M.D., Baker-Jarvis, J.  
NIST, 325 Broadway, Boulder, CO 80305, USA

In this paper we report on broadband complex permittivity measurements of various liquids using a shielded open-circuited sample fixture. We discuss the various metrological aspects of this method, including the calibration of the fixture and the full-mode model used to determine the complex permittivity of a liquid from measurements of the shielded open-circuited fixture's reflection coefficient.

The need for accurate, broadband dielectric measurements of liquids is important for applications in the biotechnology, petroleum, chemical, and food industries. The dielectric properties of many liquids can vary dramatically as a function of frequency and temperature, making accurate measurements difficult. Traditional resonator methods offer the highest accuracy, but only at single frequencies, while transmission-line techniques offer broad frequency coverage, often at the expense of measurement accuracy.

The shielded open-circuited method can be used for broadband dielectric measurements while maintaining a high level of accuracy. Other advantages of this technique include the ability to perform rapid measurements, simplicity of fixture design, and ease of inserting and removing liquid from the fixture. However, the difficulties of this method, which we address in this paper, include a complex model for determining the permittivity of the liquid from measurements of the fixture's reflection coefficient and the difficulty of fixture calibration.

We developed a full-mode model for the shielded open-circuited fixture that includes not only the fundamental TEM mode, but also the evanescent  $TM_{0n}$  modes that are excited at the boundaries of impedance mismatches within the shielded open-circuited fixture. The inclusion of the higher-order evanescent modes is an improvement over previous models that include only the fundamental TEM mode, and we present permittivity results comparing the full-mode model with previous models.

Calibration of the shielded open-circuited fixture is complicated by the fact that the calibration is performed at a reference plane that is separated from the liquid by a polymer bead. We examined two possible calibration methods. The first method requires a calibration at the connector of the shielded open-circuited holder and then performs a reference-plane rotation through the polymer bead. The second method eliminates the need to rotate the calibration reference plane through the polymer bead by taking a ratio of reflection coefficient measurements at the connector of the fixture.

## DIELECTRIC RELAXATION, SPECTRAL ENTROPY, AND EXTRACTION OF RELAXATION TIMES

Baker-Jarvis, J., Janezic, M. D.  
NIST, Boulder, CO, NIST, Boulder, CO

In this paper we study the relationship of time-dependent entropy and entropy production to dielectric measurements. The paper includes a discussion of the frequency-domain form of the entropy and its relationship to the permittivity, permeability, impedance, and dielectric measurements. An understanding of entropy and its evolution in electromagnetic interactions bridges the boundaries between electromagnetism and thermodynamics and is another diagnostic tool for characterizing high-frequency properties of materials. The approach used here is a Liouville-based statistical-mechanical theory. We show that the microscopic entropy is reversible and the macroscopic entropy satisfies a H-theorem. We derive new equations for the entropy and entropy production and apply them to functions of the polarization, magnetization, and macroscopic fields. We begin by proving a new, exact H-theorem for the entropy, progress to application of time-dependent entropy in electromagnetics, and then apply the theory to relevant applications in electromagnetics. The use of time-dependent entropy in the analysis of electromagnetic dielectric and magnetic interactions with materials has been isolated to a few applications. Much of the work performed to date has been limited to static and quasi-static analyses that describe adiabatic demagnetization and depolarization. As electromagnetic measurements on the microscale become common place, it is important for theoretical understanding to keep pace. Knowledge of entropy and its evolution bridges the boundaries between electromagnetism and nonequilibrium thermodynamics. For static fields the electromagnetic interaction is modeled as action at a distance and the change in entropy occurs only through flow of heat into or out of the system. For nonequilibrium states the entropy changes due to relaxation.

## MEASURING THE DIELECTRIC PROPERTIES OF A CONCRETE WALL USING AN ULTRA-WIDEBAND, TIME-DOMAIN MEASUREMENT SYSTEM

Chriss Grosvenor, Ben Davis, Robert Johnk  
, David Novotny, Nino Canales  
National Institute of Standards and Technology

The National Institute of Standards and Technology designed a new measurement system for determining the permittivity and loss tangent of a large concrete wall. This report will discuss the measurement system, the digital signal processing technique, the genetic algorithm, and the results of our measurements. These results will then be used in a database of other building materials in order to accurately simulate business or residential environments. The concrete walls were designed according to current building code specifications and include 1) a concrete wall without rebar, 2) a concrete wall with rebar, and 3) a rebar mesh as would be found in the previous concrete wall. This technique was developed to provide a portable system capable of measurements in an in-situ environment, such as the inner wall of a residential or office building. Currently, a modified form of the system is used to measure the shielding effectiveness of aircraft and is also used to measure targets in a cluttered environment. The system is an ultra-wideband, time domain measurement system using transmitting and receiving TEM half-horn antennas, a vector network analyzer, and a portable ground plane. The portability of this system allows us to move from our laboratory to other locations. Digital signal processing and the unique design of our TEM half-horn antennas allow us to isolate the sample from the rest of the measurement environment, thus simulating a measurement in free-space. The free-space transmission and reflection coefficients are used to extract the permittivity and loss tangent of the concrete wall using digital signal processing and a genetic algorithm optimization.

## BROADBAND MICROWAVE MEASUREMENTS OF LIQUIDS IN MICROFLUIDIC STRUCTURES

James C. Booth

National Institute of Standards and Technology, 325 Broadway, Boulder, CO 80305

We report on efforts at NIST to develop wideband dielectric spectroscopy techniques for bio- and/or chemical- analysis of small volumes of liquid samples. Rapid and accurate detection and/or identification of minute biological or chemical samples is essential for the development of effective homeland security technologies. Electromagnetic characterization can be a viable alternative to chemical or optical detection schemes to analyze biological or chemical liquids. One option in dielectric characterization is dielectric spectroscopy: the measurement of a samples dielectric permittivity across a very broad range of frequencies. This technique has the potential to rapidly characterize a wide variety of biological or chemical materials, from macromolecules like hemoglobin to live bacterial samples to proteins and DNA. By combining lithographically-defined broadband microwave structures with microfluidic chambers produced by state-of-the-art microfabrication techniques, it is possible to determine the dielectric response of small sample volumes (sub-microliters) over several decades in frequency. Integration with other microelectromechanical systems (MEMS), as well as microfluidic pumps and circuits, could enable rapid analysis of large numbers of different samples in high-throughput screening systems. Here we report on the design, fabrication, and evaluation of integrated microfluidic/microelectronic test structures for the determination of the dielectric properties of fluids over a broad frequency range. Our integrated devices allow for accurate S-parameter measurements utilizing on-wafer calibration techniques on sample volumes as small as 0.1 microliter, over the frequency range from 1 MHz to 40 GHz. We analyze our calibrated S-parameter measurements using 2-dimensional quasi-static electromagnetic simulations in order to obtain accurate values for the complex relative permittivity over this entire frequency range. Comparisons to bulk measurements on reference fluids such as methanol and de-ionized water show reasonable agreement over this frequency range.



## MILLIMETER WAVE SPECTROSCOPY OF ROCKS AND FLUIDS

Scales, J. A., Batzle, M.

Colorado School of Mines, Golden, Colorado 80401

One region of the electromagnetic spectrum that is relatively unexploited for materials characterization is the millimeter wave band (frequencies roughly between 40 and 300 GHz). Millimeter wave techniques involve free-space (non-contacting) measurements which have a length scale that makes them ideal for characterizing bulk properties of multicomponent composites where the scale of homogeneity is on the order of millimeters. These composites include granular materials such as rocks, fluid mixtures, suspensions and emulsions.

In this talk we will show data on partially saturated rocks and an oil/water mixture which demonstrate that millimeter wave spectroscopy is a sensitive, yet rapid measure of changing composition. The sensitivity of the dielectric permittivity to the moisture content make millimeter wave techniques idea for characterizing water content. In addition, we will show how dielectric anisotropy can be related to the mesoscopic structure of the sample.

The measurements are performed in a quasi-optical setup with state-of-the-art vector network analyzer. The millimeter waves are generated by a sweepable centimeter wave source (i.e., microwaves; in this case from 8-18 GHz). These centimeter waves are harmonically multiplied by Schottky diodes, coupled into waveguide and eventually radiated into free space by a scalar horn antenna. A polyethylene lens focuses the beam and a sample is placed in the focal plane. The transmitted field is then collected by an identical lens/horn combination, detected by another Schottky harmonic detector and fed to a vector receiver which mixes the centimeter waves down to more easily manageable frequencies where the signal is digitized. Reflected waves are also collected by the transmitting horn and routed via a circulator and isolator to the vector receiver. The source and receiver oscillators are phase-locked. The experiments described here were performed in the W band (nominally 75-110 GHz); other bands are readily accessible by changing waveguides and sources/detectors.



Session A/D1, 13:15 – Thurs.

**MULTI-STANDARD, MULTI-  
SERVICE WIRELESS UNIVERSAL  
RECEIVERS: DESIGN AND  
DEVELOPMENT**

Co-Chairs: A.E. Fathy, V.K. Nair

A/D1

## MXN RADIO PLATFORM INTEGRATION CHALLENGES

Nair, V., Pan, K., Kolinski, J., Kini, V.

Corporate Technology Group, Intel Corporation, Hillsboro, OR 97124

Future communication devices should support key usage models such as simultaneous voice and data transmissions, multi-media applications that scale across networks, seamless handoff, location-based services etc. [V. Nair et al., Universal Communicator: Next Generation Wireless Handset, in Annual Review of Communications, Volume 57, International Electronic Consortium; Nov. 2004]. Such a mixed network (MxN) communication device necessitates high-level integration of high speed digital, analog and RF circuitries in small form factor platforms. System-level modeling and accurate RF characterization of multiple radios are needed to fully understand the complex RF interactions and to develop a consistent platform design methodology. RF interferences due to the placement of multiple radiating elements in a small form factor device will have to be thoroughly investigated.

RF component technologies for wireless systems have been steadily advancing over the years. Low power consumption RFICs, highly linear power amplifiers, embedded passives and advanced filter technologies are being developed to meet the system requirements. During the last few years, film bulk acoustic resonator (FBAR) filters have also been incorporated in cell phones. RF micro electro mechanical systems (MEMS) technology advanced significantly over the last few years to realize practical circuit functions for wireless applications. Another key challenge is to combine front-end antenna with filters, switches and rest of the RF module in a unique packaging platform. Antenna concepts like reconfigurable antenna and multi-band antenna have to be developed for small form factor devices. Some of the innovative antenna concepts and receiver technologies required for MxN radios are discussed in the paper by Fathy et al. [A. Fathy, S. El-Ghazaly, H. Chunna, S. Yang and V. Nair., Reconfigurable Antennas and RF Front ends for Wireless Receivers, 2005 URSI General Assembly, New Delhi, Oct. 2005]

In a multi-radio platform, noise mitigation and interference minimizations are very critical. Noise interference in MxN radios can be categorized into three areas: a) platform-to-radio noise, b) radio-to-radio noise, and c) radio-to-platform noise. Each of these noise interferences requires separate mitigation techniques. In order to study the platform integration challenges of MxN radios, we designed several proof-of-concept (POC) devices. The POC device included WirelessLAN, Bluetooth, WCDMA and GPS radios integrated into a very small form factor handheld platform. Individual radio performance and the radio co-existence were characterized to determine multi-radio operation efficiency. For example, GPS radio characterization showed that the receiver sensitivity decreased about 3 dB when the application processor was turned on. An additional 2 dB of desensitization occurred when the base band processor was powered up. Impact of other radios in the platform was also determined in order to develop a mixed network radio platform design methodology.

This paper will discuss the advances and challenges in the MxN radio platform integration.

## LOW COST 60 GHZ GB/S RADIO

Laskar, J., Pintel, S., Lee, C-H

, Sarkar, S., Perumana, B., Mukhopadhyay, R.

Georgia Electronic Design Center, School of Electrical and Computer Engineering, Georgia Institute of Technology

## Abstract

The demand for ultra-high data rate wireless communication systems is increasing daily with the emergence of a multitude of multimedia applications. In particular, the needs become urgent for ultrahigh speed personal area networking and point-to-point or point-to-multipoint data link. This demand has since pushed the development of technologies and systems operating at the millimeter-wave frequencies, and overcome the current limitations of alternative solution such as 802.11n and UWB. This trend has also been reinforced by the exponentially growth of the emerging automotive collision avoidance radar applications. Indeed, the availability of several GHz band-width unlicensed ISM bands in the 60GHz spectrum represents a great opportunity for ultra-high speed short-range wireless communications. Since the mid-90s, many examples of MMIC chip-set have been reported for 60 GHz radio applications using GaAs FET and InP pHEMT technologies. Despite their commercial availability and their outstanding performances, these technologies struggle to enter the market because of their prohibitive cost and their limited capability to integrated advanced base-band processing. In addition, the combination, of a low cost highly producible module technology, featuring low loss and embedded function such as antenna, is required to enable a high volume commercial use of the 60 GHz systems. The recent advances of CMOS and SiGe process technologies have now made the design of low-cost highly integrated millimeter-wave radios possible in Silicon. In combination with an optimum organic Liquid Crystal Polymer packaging approach, this represents a unique opportunity to develop Gb/s radio that could address the increasing demand in term of data rate throughput of the emerging broadband wireless communication systems. In this paper we discuss the circuit and module challenges that will enable a successful deployment of 60GHz gigabits wireless systems.

## TOWARDS MULTI-SERVICE WIRELESS UNIVERSAL RECEIVER+

Yongping Han<sup>1</sup>, Chunna Zhang<sup>1</sup>, Songnan Yang<sup>1</sup>,  
 , Helen K Pan<sup>2</sup>, Aly E. Fathy<sup>1</sup>, Samir El-Ghazaly<sup>1</sup> , Vijay K. Nair<sup>2</sup>

<sup>1</sup>Department of Electrical and Computer Engineering, University of Tennessee, Knoxville, TN 37996, U.S.A.

<sup>2</sup>Intel Corporataion, JF2-86, 2111 N.E.25th Ave., Hillsboro, OR 97124, U.S.A.

In anticipation of an impending realization of integrated computing and functional communication silicon chips, we believe researchers should presently begin addressing potential interfacing problems. This includes the utilization of multi-standards, multi-bands, and multi-functions receivers as developed by many wireless service providers. In particular, there is a need for adaptable, reconfigurable antennas and RF front ends, as opposed to wide band or multi-band antennas with many individual receivers to address the demands of these various services.

Fortunately, a current trend in industry is to develop compact multifunctional integrated systems or subsystems, and universal wireless receivers are excellent examples of this new trend. We need to utilize one receiver set that supports many standards (GSM, CDMA, GPRS, EDGE and UMTS/3GSM) for cell-phones as well as many other services like Bluetooth, WLAN, WiMax, UWB, Zigbee, GPS and potentially more to come. We believe reconfigurable structures and circuits using MEMs technology will significantly aid in addressing this problem.

Hence, we have developed various reconfigurable antennas that can surpass the performance of both conventional multi-band and wide band antennas. In this paper, we will specifically present some examples of such developments including the Maze-loop[1], the CPW-fed reconfigurable monopole[2], and the Nested patch antennas, and we will report on the performance of these newly developed antennas as well as other antenna configurations.

Additionally, we have considered the development of one universal RF front end rather than use one for each service. The universal receiver includes a reconfigurable low noise amplifier, a tunable oscillator, and an adjustable RF power amplifier for both gain and linearity (i.e. IIP2 and IIP3). Concepts, implementations, and measured results will be presented.

+This work was sponsored by Intel Corp., Hillsboro, Or, USA.

1 A Novel Reconfigurable Maze Antenna for Multi-service Wireless Universal Receivers, by Songnan Yang, Helen K Pan, Aly E. Fathy, Samir El-Ghazaly and Vijay K Nair, to be presented at IEEE Radio and Wireless Symposium, Jan., 2006, San Diego, CA.

2 Reconfigurable Antennas and RF Front Ends for the Development of a Universal Wireless Receiver, by Chunna Zhang, Yongping Han, Songnan Yang, Aly E Fathy, Samir El-Ghazaly, Vijay K. Nair, to be presented at IEEE Radio and Wireless Symposium, Jan., 2006, San Diego, CA.

## RADIATION AND BEAM-STEERING OF A W-BAND TROUGH WAVEGUIDE ANTENNA USING MEMS PERTURBATIONS

Huff, G. H., Bernhard, J. T.

Electromagnetics Laboratory, University of Illinois at Urbana-Champaign

The trough waveguide has been investigated for many applications, ranging from a source for microwave heating to sustained plasma generation, which make use of both its open structure and the wide bandwidth provided by the dominant guided TE mode [W. Rotman and A. Maestri, IRE Int. Convention Record, 8, Mar. 1960, pp. 67-83]. In the initial stages of development, the trough waveguide made use of mechanically controlled perturbations within the waveguide as a means to facilitate radiation and beam-steering from the open structure. Although these techniques proved very effective, the cam and gear methods available at the time of development were mechanically limited and somewhat cumbersome. Making use of micromachining techniques, this structure is revisited here with the goal of developing a radiating structure for highly integrated radar and communication systems.

In this work, radiation from the trough waveguide is facilitated through electro-mechanical cantilever-type perturbations which are hinged across the bottom of the center fin on both sides of the guiding structure. This design separates itself from previous work on this type of antenna, as the actuated cantilevers are used primarily to provide the desired phase and amplitude distribution across the effective aperture instead of significantly altering the guided wavelength. This effect has been observed in field plots of the waveguide for different actuation schemes. Using the cantilevers, the traveling wave encounters the antipodal asymmetry periodically every distance  $a$ , which is where the electric field of the TEM mode on the aperture experiences a peak value. Since the design does not significantly alter the guided wavelength, the characteristic impedance of the guide is not adversely affected and the use of symmetrical tuning elements is not needed as they were in many previous designs that placed solid perturbations the guide. In addition to facilitating radiation, the cantilevers can be actuated in such a manner that they provide amplitude tapering along the effective aperture (open end of the guide). To achieve this tapering - with minimal effect on the guided wavelength - the degree of actuation (angle) of the cantilever can be properly set to convert a given amount of energy into the radiating TEM mode. Discussion of this traveling wave antenna will include a W-band design intended for micromachined actuators and an S-band design for laboratory investigation, along with the feed structures used to excite the trough waveguide and the possible electromechanical perturbations that can operate in the guide.



ALTERNATIVE IMPLEMENTATION OF RECONFIGURABLE  
METAMATERIAL-BASED LEAKY-WAVE APERTURESSungjoon Lim, Tatsuo Itoh

University of California, Los Angeles, Electrical Engineering

The backward wave propagating capability in left-handed metamaterials (LHMs) is commonly used in leaky-wave antennas. By combining forward and backward wave propagation, a metamaterial-based leaky-wave antenna has an advantage for full space scanning, while a conventional leaky-wave antenna can scan only a half space. In addition, when varactor diodes are loaded on this periodic antenna, it provides additional functions while maintaining a full space scanning capability.

The radiation direction can be controlled by the varactor diodes voltage at a fixed frequency. Furthermore, the beamwidth can also be controlled in two different electronic manners. In this paper, the two methods will be discussed and compared to each other.

In both methods, the beamwidth controllability is possible because the propagation constant of each unit cell can be independently controlled. The first way to control beamwidth is achieved by distributing a non-uniform beamdirection from each unit cell. Each beam is combined into a total beam pattern based on an array factor. In the second method, beamwidth control can be achieved by changing the radiation aperture size. A leaky-wave aperture can be made non-radiating if the operating point of structure is in the slow wave region but can be made radiative if the operating point is in the fast wave region. Therefore, the radiation aperture size is determined by the size of the structure that is in the fast wave region. Due to the independent electronic controllability of each unit cell, any portion of the structure can be made either radiative or non-radiative region.

In terms of radiation efficiency, the first method is more efficient because all unit cells radiate so that a higher gain is achieved with the same beamwidth. In the second method, the gain is lower since only a portion of the structure radiates. Directivity is lower also. However, in the second method, the non-radiating aperture can be used as either a phase delay or phase advance line. In the proposed structure, it is shown to be used as a phase advance line operating in the slow wave region. A wide phase tuning range is observed in the left-handed region. The integration of a phase shifter and a leaky-wave antenna simplifies a scanning array system. The bias ranges of the varactor diodes are different in both cases. In the first case, variable bias is given depending on the location of the unit cell. In the second case, a uniform bias is given over the nonradiating section, while a differently uniform bias is applied over the radiating section for a given radiation direction.



Session B1, 10:15 – Wed.

**THEORETICAL CONSIDERATIONS  
IN ELECTROMAGNETICS**

Co-Chairs: C.E. Baum, P.L.E. Uslenghi



## UNIFORM ASYMPTOTIC DESCRIPTION OF THE MAIN SIGNAL

Cartwright, N.A., Oughstun, K.E.

College of Engineering and Mathematical Sciences, University of Vermont, Burlington, VT 05401

The determination of the dynamical evolution of a signal in a dispersive medium or system is a problem of central importance in the area of electromagnetic pulse propagation. Consider the following canonical problem in the theory of ultrawideband pulse propagation through a temporally dispersive, absorptive material: Let the half-space  $z < 0$  be vacuum, while the half-space  $z \geq 0$  is occupied by a dielectric material whose temporal frequency dispersion is described by the causal, single-resonance Lorentz model (H. A. Lorentz, *The Theory of Electrons*, 1906). Let the wave field traveling in the positive  $z$ -direction on the plane  $z = 0^+$  be a unit step function modulated sinusoidal plane wave of fixed carrier frequency  $\omega_c > 0$  with turn-on time at  $t = 0$ . With this initial field, determine the temporal evolution of the propagated signal on any given plane  $z > 0$ .

The exact, formal solution to this problem is given by the Fourier-Laplace integral representation

$$E(z, t) = \frac{1}{2\pi} \int_{ia-\infty}^{ia+\infty} \tilde{E}(0, \omega) \exp[i\tilde{k}(\omega)z - \omega t] d\omega, \quad (1)$$

for  $z \geq 0$  and  $a > 0$ . Here  $\tilde{E}(0, \omega) = i/(\omega - \omega_c)$  is the Fourier transform of the initial electric field component  $E(0, t) = u(t) \sin(\omega_c t)$ ,  $u(t)$  is the unit step function, and  $\tilde{k}(\omega) = (\omega/c)n(\omega)$  is the complex wave number in the dispersive dielectric, where  $c$  denotes the speed of light in vacuum. For a single-resonance Lorentz model dielectric, the complex index of refraction is given by

$$n(\omega) = \left( 1 - \frac{\omega_p^2}{\omega^2 - \omega_0^2 + 2i\delta\omega} \right)^{1/2}, \quad (2)$$

with plasma frequency  $\omega_p$ , undamped resonance frequency  $\omega_0$ , and phenomenological damping constant  $\delta$ . For an ultrawideband wave form whose spectrum spans a wide range of frequencies over which  $\tilde{k}$  may vary in a complicated manner, the group velocity approximation is not a valid approximation for propagation distances greater than one absorption depth into the dispersive material.

Because of the exponential appearing in the integrand of (1), the Fourier-Laplace representation is ideally suited for analysis by asymptotic expansion techniques that are valid as  $z \rightarrow \infty$ , as originally done by Brillouin (*Wave Propagation and Group Velocity*, 1960) using the method of steepest descents. An improved asymptotic approximation was later provided by Oughstun and Sherman (*Electromagnetic Pulse Propagation in Causal Dielectrics*, 1994) with the use of modern, uniform asymptotic techniques. However, the approximation of Oughstun and Sherman showed discontinuities in the propagated field and gave incorrect approximations for the pole contribution when the value of the carrier frequency of the input pulse lies within or above the absorption band of the material. Here, we provide a completely uniform asymptotic approximation to this problem. This refined asymptotic description results in a continuous evolution of the propagated field for all space-time points.

## PROPAGATION CONSTANTS OF COHERENT WAVES IN RADIATIVE TRANSFER THEORY AND IN WAVE THEORY

Saba Mudaliar

AFRL/SNHE, 80 Scott Drive, Hanscom AFB, MA 01731

It is popular to formulate and study scattering and propagation in random media using the phenomenological radiative transfer (RT) approach. One important quantity in the RT theory is the differential scattering cross section. The optical theorem then relates this quantity to the propagation constant of the coherent waves. On the other hand, in the wave approach we formulate the problem as a system of partial differential equations and boundary conditions for the Green's functions of the problem. On averaging this system we arrive at the Dyson equation, which may be solved using, for example, the bilocal approximation to the mass operator. The ability to solve this problem depends very much on the geometry under consideration. For the unbounded random medium with statistical homogeneity we can solve this equation and obtain closed form solution for the mean propagation constants. However, for bounded structures such as layered random media the problem is more complicated and it appears that we have to impose further approximations. It turns out that for the case of unbounded random medium the coherent propagation constants obtained by the RT approach and the wave approach are identical. However, in the case of layered media, we find that the expressions obtained are different. In the RT approach, the coherent propagation constants depend only on the statistical characteristics of the random medium. On the other hand, in the wave approach, the propagation constants depend not only on the statistical characteristics of the medium but also on the boundary reflection coefficients and the thickness of the layer. As a consequence we find that in the RT approach, the propagation constants depend on polarization only if the spectral density of the random medium and/or the medium itself is anisotropic. But in the wave approach we find that the propagation constants depend on polarization even if the medium and the spectral density are isotropic. The anisotropy in this case is due to the layer geometry. This leads to considerable complication in subsequent analysis and in the calculation of field covariances. Thus it is important to know about the significance of the influence of the layer geometry on the coherent propagation constants. If it turns out that in the problem under study the influence of layer geometry on the propagation constants is not significant the subsequent analysis and indeed the equation for field covariance are considerably simplified. We consider some numerical examples to assess the propagation characteristics in a random medium layer and their dependence on the layer geometry. We find that, in general, the effects of boundaries on propagation constants are not significant in most situations encountered in applications.

## THE FORWARD-SCATTERING THEOREM APPLIED TO THE SCATTERING DYADIC

Baum, Carl E.

University of New Mexico

From the forward-scattering theorem we have relations between the absorption and scattering cross sections, and the forward scattering. The scattered fields are represented by a scattering dyadic times the incident plane wave. This allows one to reformulate the results in terms of the scattering dyadic, exhibiting some general characteristics of this dyadic.

In [C.E. Baum, "Scattering of the Transient Plane Waves", Interaction Note 473, 1980] the forward-scattering theorem was considered in both time and complex-frequency domains. This relates the power absorbed and scattered by an object to that scattered in the forward direction. This is a classical problem; the references in the above can be consulted in this regard. Note that various authors also call this the cross-section theorem or optical theorem.

Here we have used the radar convention in which the scattering dyadic is related to an incident plane wave. This is also sometimes considered as scattering amplitude (as in amplitude or magnitude, and phase, not very appropriate to a dyadic-or matrix-valued function). Some authors instead use this term (scattering matrix) to refer the scattering to some kind of incoming wave scattering into an outgoing wave. For present purposes, let us call this form a reversal matrix (or dyadic or operator) in which form we can also state the results of this paper.

The forward-scattering theorem and its extensions give various interesting results. This is particularly useful for the case of lossless scatterers, since we do not need to solve the scattering problem for the absorption by the scatterer.

One of the interesting extensions concerns the analytic continuation into the  $s$  plane away from the  $j$  axis. This gives some analytic properties of the scattering dyadic. Besides relating LHP and RHP behavior (including natural modes and high-frequency asymptotics), there may be some additional properties to be discovered.

## THE ADVANTAGE OF USING COMBINED FIELDS IN INVERSE SCATTERING

Uslenghi, P. L. E.

Department of Electrical and Computer Engineering, University of Illinois at Chicago

Combined fields were introduced and used many years ago by several authors, including Bateman, Rumsay, Itoh, and Baum and Singaraju. They consist of linear combinations of electric and magnetic fields, have the dimension of an electric field, and render the introduction and use of magnetic fields unnecessary, at least when dealing with fields in linear, homogeneous and isotropic media. The boundary conditions may be reformulated in terms of combined fields. Each combined field is proportional to its own curl. The use of combined fields has also been advocated by several authors, e.g. Harrington and Mautz, to simplify calculations based on the numerical solution of integral equations.

Recently, this author has introduced combined fields to simplify the formulation of the Stratton-Chu equations (P. L. E. Uslenghi, Proc. of ICEAA'05, Turin, Italy, September 2005). In the usual Stratton-Chu equations, both electric and magnetic fields appear, whereas in the combined field formulation only one type of combined field appears in each equation. This simplification leads, in particular, to a simple relationship between near field and far field, that is especially useful in inverse scattering and remote sensing problems.

In this work, the relation between far combined field and the corresponding near field is examined in detail. Starting from a preassigned far field, the corresponding near field is determined in two steps. Since only the transversal component of the far field is given, the inverse problem is not uniquely solvable, i.e. the same far field yields a set of near fields. The properties of this set are discussed. For each near field, an inverse Fourier transform allows for the determination of both the shape of the near field surface and the combined current distribution on that surface.



## SCATTERING FROM SINUSOIDAL SURFACES OF SMALL PERIOD

Black, T., Brown, G.S. <sup>2</sup>

, ElectroMagnetic Interactions Laboratory, Virginia Tech

Scattering from conducting surfaces having a sinusoidal height profile is a topic that has seen a significant degree of activity. While such surfaces are not abundant in nature, they do provide the opportunity to understand some basic scattering properties of a special class of periodic surfaces. Most of the research that has appeared in the literature relative to this problem has been analytical in nature. The purpose of this paper is to investigate the usefulness of numerical techniques for a specific topic that has no known solution. It is well known that if a sinusoidal surface has a very large period relative to the electromagnetic wavelength of the incident radiation, the Kirchhoff approximation does a reasonable job of predicting the current induced on the surface except when a Bragg order of the scattered field exits the surface at grazing. Conversely, when the height of the surface is small compared to a wavelength, perturbation does a reasonable job of predicting the scattering assuming the surface has a period that is not too different from that of the incident radiation. However, when the height of the surface is the order of the electromagnetic wavelength and the wavelength of the surface is smaller than the wavelength of the incident radiation, there is little data available to determine just how the current is behaving in this instance. It is very important to understand just exactly how the surface current behaves as the wavelength of the surface becomes much smaller than that of the incident radiation. It is clear that eventually the current will eventually only "see" the crests or tops of the sinusoidal surface and this surface will behave as a flat surface in its scattering properties. In this paper, we apply the Method of Ordered Multiple Interaction (MOMI) to compute the current induced on the surface. We use the results to compute the far zone radiation pattern and the field very near to the surface for the purpose of estimating when the sinusoidal surface behaves as a planar surface in its scattering properties. We also show how the current on the small wavelength surface starts to act like the planar surface current. All of the studies are carried out at normal incidence.



Session B2 13:15 – Wed.

**GUIDED WAVES**

Co-Chairs: S. Rengarajan, A. Yaghjian



BIDIRECTIONALITY OF UNIFORM AND PERIODIC WAVEGUIDES MADE OF RECIPROCAL MATERIAL

Yaghjian, A.D.

AFRL/SNHA, Hanscom, AFB, MA 01731, USA

If the geometry and electromagnetic material parameters of an open or closed waveguide are symmetric about a plane perpendicular to the propagation axis ( $z$  axis), then it is obvious from a simple symmetry argument that every time-harmonic ( $e^{-i\omega t}$ ) traveling wave propagating with  $e^{i\beta z}$  dependence can also propagate in the opposite direction with  $e^{-i\beta z}$  dependence, where  $\beta$  is the complex propagation constant. Thus, a waveguide possessing this "reflection symmetry" can be said to be "bidirectional."

If the waveguide does not possess this reflection symmetry, it may not be bidirectional, and thus it becomes of interest to obtain general conditions that are sufficient for a waveguide to be bidirectional (P.A. Chorney, MIT Technical Report 396, 1961). Toward this end, McIsaac (*IEEE MTT Trans.*, **39**, 1808–1816, 1991) has proven that a uniform waveguide that contains only lossless reciprocal material is bidirectional for traveling waves with real propagation constants  $\beta$ . In this paper, a general theorem is proven that states that both uniform and periodic waveguides containing lossy or lossless reciprocal material are bidirectional in that every traveling wave with complex propagation constant  $\beta$  has an associated traveling wave with propagation constant  $-\beta$ . This theorem is proven indirectly using two reciprocal antennas separated by asymptotically large distances along the waveguide. Direct application of the Maxwell differential equations also proves that every complex wave with  $e^{i\beta z}$  dependence on a lossless reciprocal waveguide has an associated complex wave with  $e^{-i\beta^* z}$  dependence, where the  $*$  indicates the complex conjugate.

These theorems imply that complex waves on lossless reciprocal waveguides come in quadruplets, one bidirectional pair with propagation constants  $\pm\beta$ , and another bidirectional pair with propagation constants  $\mp\beta^*$ . An important consequence of the theorems is that for traveling waves with real propagation constants on lossless reciprocal periodic waveguides, the  $kd$ - $\beta d$  diagram need cover only the range of  $\beta d$  from 0 to  $\pi$ , where  $k = \omega/c$  with  $c$  denoting the free-space speed of light, and  $d$  is the spatial period of the periodic waveguide. It is noted that, although waveguides containing nonreciprocal material are not in general bidirectional, some nonreciprocal waveguides retain the property of bidirectionality.

## TUNABLE BRAGG GAP IN A PERIODICALLY CORRUGATED WAVEGUIDE

Pogrebnyak, V.A.<sup>1</sup>, Whalen, J.J.<sup>2</sup>, Kucukaltun, A.N.<sup>1</sup>, Bargach, K.<sup>2</sup>

<sup>1</sup>Department of Electrical and Electronics Engineering, Faculty of Engineering and Architecture, Cukurova University, Adana, 01330 TURKEY

<sup>2</sup>Department of Electrical Engineering, Faculty of Engineering, State University of New York at Buffalo, 322 Bonner Hall, NY 14260-1920

The principal physical phenomenon in wave propagation caused by periodicity is Bragg reflection. It results in the opening of the forbidden gap in the spectrum of the periodic structure. The Bragg reflection occurs both in the case of unbounded periodic medium as well as in a case of a bounded periodic structure like a periodic waveguide.

We investigated experimentally the microwave transmission properties of a hollow rectangular metallic waveguide, having lower and upper walls with the identical sinusoidal profile  $y(x) = \xi \cos(qx)$  and smooth side walls. Where  $\xi$  and  $a$  are an amplitude and a period of the corrugations equal correspondingly to 0.415 cm and 3.15 cm. Thickness and width of the waveguide were 5.4 cm and 6 cm. The upper periodic plate could slide with respect to the lower forming the phase shift  $\Delta x$  between the plates.

It was predicted theoretically that the Bragg gap (and accordingly transmission coefficient) varied from zero to a maximum value upon a shift of one periodic plate with respect to another in accordance with formula (V.A.Pogrebnyak, *Opt. communications* **232**, 201-207, 2004)

$$\delta\omega = \left[ \frac{2\sqrt{2}\xi}{3d} (1 - \cos(q\Delta x))^{1/2} \right] \omega_{cutoff}. \quad (1)$$

In this paper, we are reporting on experimental observation of this phenomenon in the rectangular periodically corrugated waveguide.

A standard microwave setup with the HP8510 network analyzer was used for measuring of the transmission characteristics of the periodic waveguide at a frequency range 6-18 GHz. We investigated propagation of the TE wave along the x-axis and having the polarization vector parallel to grooves of the corrugation (the z-axis). The 1.36 GHz band gap in vicinity of the cutoff frequency of the 3rd mode has been observed when a shift between plates equals  $a/2$ . The gap closed when the shift between the plates vanished.

Thus transmission through the waveguide could be tuned from the maximum value down to 30 dB upon a shift of one periodic plate with respect to another on the half period of the corrugation.

The tuning mechanism can be used in different microwave, optoelectronic, and photonic applications.

## ANALYSIS OF PARALLEL PLATE WAVEGUIDE T AND STEP JUNCTIONS

Sembiam R. Rengarajan

Department of Electrical and Computer Engineering, California State University, Northridge, CA 91330

Parallel plate waveguide T and step junctions are used in applications such as continuous transverse stub (CTS) and other antennas. An analysis of the T junction in such a structure has been presented in the prior literature (K.H. Park, H.J. Eom, Y. Yamaguchi, IEEE Trans. Microwave Theory Tech., vol. 42, no. 2, pp. 356-358, Feb. 1994). In that paper, the continuity of the tangential component of the magnetic field and the continuity of the Fourier transform of the electric field are enforced. We present a method of moments solution to the integral equation for the aperture electric field at the junction. Boundary conditions for the tangential components of the electric and magnetic fields are applied, with the use of the parallel plate Green functions. The numerical analysis in our method is simpler. Step discontinuities in parallel plate waveguides are employed in CTS-type antennas for impedance transformations. A precise knowledge of the junction susceptance is required in the analysis and design of such structures. A moment method solution to the tangential component of the electric field at the junction and the scattering parameters of the step discontinuity are also presented in this paper.

Numerical results obtained for the T junction compare well with previously published results. Computed results are also validated by the power balance conditions which are satisfied to great precision. The scattering parameters and coupled power for a range of values of waveguide heights, and dielectric constants will be presented at the meeting. These results are applicable in the analysis and design of antennas and microwave circuits such as power dividers, couplers and impedance transformers.

## COMPUTATIONAL S-PARAMETER EXTRACTION OF AN INHOMOGENEOUS DIELECTRIC SLAB LOADED WAVEGUIDE

Barba, P., Bogle, A., Crossmann, S. , Kempel, L.C., Rothwell, E.

Michigan State University

The measurement of the transmission and reflection coefficients from a dielectric sample (inside a waveguide) is a crucial step in extracting its unknown constitutive parameters. The traditional method for measuring an unknown sample is to fill the cross-section of the waveguide with a sample having parallel front and back faces. Unfortunately, during the material research phase of a development, an insufficient quantity of the sample may be available for such an experiment. Hence, it is advantageous to develop a constitutive extraction method that does not require so much material. In previous work, the authors have developed a method that requires a small sample placed on the centerline of the waveguide. Increasingly, determining the sensitivity of an experimental technique is important to quantify the quality of the measurement. In the method mentioned above, there are a variety of potential error sources. Placing the dielectric sample inside the waveguide can result in a source of error by introducing unwanted shifting (right or left) relative to the cross-section centerline. By simulating the shifting of the slab and comparing these results with the experimental data, the impact of these errors can be better determined. To assess the error due to a lateral shift, a forward model is required that provides that S-parameters with the reference planes at the front and back surface of the sample. This can be accomplished using LSE- and LSM-modes. The formulation, however, is rather involved. In addition, more flexible computational electromagnetics models allow assessment of other types of sample shapes such as the case where the front and back faces are no longer parallel to each other. An example of such an analysis method is the finite element method (FEM). The authors have found that the finite element method, when used with the thru-reflect-line (TRL) calibration procedure, has proven to be an efficient and reliable technique to simulate the electromagnetics of dielectric discontinuities within a rectangular waveguide. The formulation and examples of this technique will be presented at the meeting.



## LOSS REDUCTION TECHNIQUE OF VERTICAL STRIP TRANSMISSION LINE AT MILLIMETER-WAVE FREQUENCY

Furoshi Kuroki, Hiroshi Ohta  
Kure National College of Technology

Printed transmission lines such as a microstrip line and a coplanar waveguide are preferable for applications at centimeter wave frequencies, but they suffer from a lot of transmission loss at millimeter frequencies due to their conduction loss. Another candidate as a transmission medium for millimeter wave integrated circuits is the vertical strip line, which consists of metal strip vertically inserted in a below cut-off parallel metal plate waveguide. It is expected that the transmission loss is smaller than that of other printed transmission lines because the field distribution expands around the vertical metal strip. To investigate its capability to apply the vertical strip line into low-loss printed circuits, we measured the transmission loss at 60 GHz. The spacing of the parallel metal plate waveguide was selected at 2.25 mm so as to be less than half a free-space wavelength at 60 GHz. The metal strip was etched on a glass-Teflon substrate with a thickness of 0.264 mm. A relative dielectric constant and a loss tangent of the glass-Teflon substrate are 2.6 and 0.001, respectively. The transmission loss was estimated by measuring un-loaded Q factors, and was measured to be 20 dB/m. It was obvious that the transmission loss of the vertical strip line was smaller than that of the microstrip line, whose transmission loss was measured to be 60 dB/m at 50 GHz. Transmission loss of the vertical strip line was calculated to be 10 dB/m by HFSS. It is considered that the discrepancy between the calculated and measured transmission losses is caused by roughness of the metal strip surface attached to the glass-Teflon substrate. With this in mind, we devised a new structure of the vertical strip line, where the metal strips are etched on the both sides of the glass-Teflon substrate and have equi-voltage. In this structure, there is no current distribution on the metal strip surface attached to the glass-Teflon substrate, and hence, loss reduction. The measured transmission loss of the new vertical strip line was 9 dB/m at 60 GHz.



Session B3, 15:15 – Wed.

**COMPUTATIONAL  
ELECTROMAGNETICS**

Co-Chairs: R.J. Adams, R.J. Pogorzelski



## EFFICIENT INVERSION OF THE IMPEDANCE MATRIX IN AN OVERLAPPING, LOCALIZING BASIS

Robert J. Adams<sup>1</sup>, Gang Wang<sup>1</sup>, Francis X. Canning<sup>2</sup><sup>1</sup>University of Kentucky, Lexington, KY 40503<sup>2</sup>Simply Sparse Technologies, Inc., Morgantown, WV

Numerical solutions of integral equation formulations of time-harmonic electromagnetic phenomena involve solving linear systems of the form

$$ZJ = E^i \quad (1)$$

where  $Z$  is the impedance matrix. The use of integral equations to determine (1) usually leads to a full impedance matrix. This has led to the development of a large number of fast iterative solution strategies. Iterative methods, however, have certain well known limitations restricting the class of problems to which they can be usefully applied.

It has recently been shown for scalar problems in two dimensions that a reduced-complexity, error-controllable direct solution of (1) is obtained by expanding and inverting the impedance matrix in a complete set of nonradiating local-global solution (LOGOS) modes. A nonradiating LOGOS mode consists of an excitation/solution pairing,  $(E_m^i, J_m)$ , for which the current and the incident field are both localized to a (usually) small region of a larger simulation domain. Unfortunately, the relative computational efficiencies of previously reported LOGOS representations is approximately  $O(N^{1.5})$  in 2-D and  $O(N^2)$  in 3-D. Such limitations are directly related to the non-overlapping nature of the nonradiating LOGOS modes.

This paper summarizes an improved LOGOS direct solution algorithm for PEC scattering problems in 2-D. It is shown that the solution algorithm requires  $O(N \log N)$  floating point operations to determine an  $O(N)$  factored representation of the inverse of the impedance matrix. These reduced complexities are obtained using an overlapping basis of LOGOS modes defined on a dual-grid multilevel quad tree.

The direct solution algorithm proceeds by projecting the sparse,  $O(N)$ , MLSSM representation of the impedance matrix (Zhu *et. al.*, 2005) onto overlapped LOGOS modes defined at successively coarser levels of the dual-grid quad tree. Interactions between the main and offset grids of the dual-grid tree are minimized by imposing an appropriate orthogonality condition on the LOGOS modes defined on the main and offset grids. The latter condition is efficiently enforced using a so-called  $R\Theta$  factorization of the MLSSM representation of the impedance matrix.

ON THE REDUCTION OF INTER-MATCHPOINT ERROR IN  
POINT-MATCHED NUMERICAL SOLUTION OF INTEGRAL  
EQUATIONS

Pogorzelski, R. J.

Jet Propulsion Laboratory, California Institute of Technology

In solving computationally, electromagnetics problems formulated in terms of integral equations, the induced current is expanded in a set of basis functions and the equation itself is commonly imposed via matching the right and left sides at a selected set of matchpoints on the boundary over which the integral is carried out. The result is a set of simultaneous linear equations for the unknown coefficients in the current expansion. This set can be solved by matrix inversion for modest size problems but for large problems an iterative approach is commonly used in which the iterations, designed to reduce the residuals at the matchpoints, are continued until a suitable error level is attained. The error referred to here is the error at the matchpoints. The error between the matchpoints is typically much larger but is commonly ignored because its impact on the far-zone radiation field is small due to its rapidly oscillatory character. Nevertheless, this error can adversely impact near-field calculation and the calculation of parameters such as the input impedance at ports defined in the problem. While this error can always be reduced by increasing the number of matchpoints and perhaps also the number of basis functions, such increase can be prohibitively costly in terms of computation time and storage. Thus, an efficient and simple means of reducing this error is desirable.

This paper introduces a new iterative approach to inter-matchpoint error reduction. It is as follows. By Fourier transformation, the boundary residual can be partitioned into high and low spatial frequency portions. Once this has been done, the low frequency portion can be treated via re-application of the previously calculated inverse of the system matrix or by repeat of the iterative solution. Subsequently, the new residual is again partitioned and again the low frequency portion used to drive the system. After several such iterations, all of the remaining error resides in the high spatial frequency portion of the spectrum and can be accurately treated using a local planar approximation to the boundary. This approach has been implemented in both the Method of Moments and the Method of Auxiliary Sources and shown to be both efficient and rapidly convergent.

COUPLING OF THE FIELD OF AN EXTERIOR MONOPOLE  
THROUGH AN APERTURE IN A PEC SCREEN TO A LOADED  
THIN WIRE IN A CYLINDRICAL/COAXIAL CAVITY

Bopp III, C. L., Butler, C. M.  
Clemson University

The electromagnetic field coupling to a loaded thin wire in a cylindrical/coaxial cavity is investigated. The wire and cavity are excited by a monopole antenna resting on a PEC screen and the coupling from the antenna to the wire inside the cavity takes place through a circular aperture in the screen that is backed by a cylindrical/coaxial cavity containing a thin wire. There is an interest in understanding how electromagnetic fields couple to wires and tubes that may be present in an enclosed structure and in how to efficiently analyze this coupling as part of an overall system. The cavity may consist of multiple cascaded coaxial and circular cylindrical sections with sections coupled through apertures and conducting elements common to more than one section. The sections may have different axial and radial dimensions and may be filled with material having different magnetic and electric properties. Previously, a Greens function method for analyzing the coupling to a thin wire inside a circular cavity was presented. Here, we build upon this internal coupling to include excitation by a source external to the cavity structure. Aperture theory is used to separate the problem into one internal to the cavity and one external to the cavity above the PEC screen. A set of coupled integral equations is developed to determine the unknown aperture field and wire current. For the purpose of demonstrating the accuracy of the procedure and numerical solutions obtained from this analysis, a cavity model is constructed and measurements made on the laboratory model are compared with computed results. The measured input impedance of the monopole and the impedance at the point where the cavity is truncated are compared with values obtained computationally.

NUMERICAL SIMULATION OF ELECTRIC DIPOLE ANTENNAS  
IN THE INNER MAGNETOSPHERE

Timothy W. Chevalier, Umran S. Inan, Timothy F. Bell  
, Michael W. Chevalier

Stanford University, STAR Laboratory, Electrical Engineering Department

The study of the radiation properties of electric dipole antennas in the magnetosphere has been an area of active research in recent years because of interest in pitch angle scattering of highly energetic electrons from the Earth's radiation belts. Previous analytical work has provided much insight into the properties of such antennas, but is limited to certain geometries and operating conditions to solve the closed form solutions. As a way to circumvent these limitations, the current distribution and input impedance of electric dipole antennas operating in a low density cold magnetoplasma at VLF (Very Low Frequency) are determined through simulation. A full wave solution of Maxwell's equations utilize the FDTD (Finite Difference Time Domain) method to simulate electromagnetic wave propagation in this highly anisotropic medium.

The PML (Perfectly Matched Layer) ABC (Absorbing Boundary Condition) is an effective and well established method for the absorption of electromagnetic waves in numerical simulations; however, the PML has been found to exhibit instabilities in the form of non-physical wave amplification in this environment. The instabilities are a result of waves that possess anti-parallel group and phase velocities within the PML medium. Various methods have been developed to circumvent these difficulties and include FIR (Finite Impulse Response) filtering of the time domain Maxwell's equations and a new PML, which utilizes information about the wave normal vector  $\vec{k}$  to damp these unstable modes. The new PML is applicable to whistler mode propagation and exhibits reflection coefficients as low as -40dB. It has been found that the current distribution for electrically short antennas is roughly triangular. Calculated variations of input impedance for several case studies are given and compared with existing analytical work.



## MODELING PERIODIC STRUCTURES BY SPECTRAL-FDTD METHOD

Nader Farahat, Abraham Diaz, Daniel Santiago  
Polytechnic University of Puerto Rico

In this paper we use the Spectral-FDTD [1] method to analyze periodic structures used as frequency selective surfaces (FSS). This method shows a significant advantage over the split-field method [2] for simulation of the incident illuminations close to the grazing angles. In split-field method, for which the angle of incident is fixed in each simulation the stability condition becomes a function of incident angle and thus the large time steps must be chosen in order to maintain the stability. Therefore the technique becomes inefficient for wide angles of incident. In the spectral-FDTD method, on the other hand, the wavenumber is fixed instead of the incident angle. Consequently in a single simulation different frequencies are impinging on the FSS with different angles. This allows one to simulate the wide angles of incident efficiently. However in the end an interpolation is required to map the data for certain wavenumber solutions to the angles of incident over the entire band of frequency. We use each node of 32-node Beowulf PC cluster for one wavenumber simulation and in the end we map the data from wavenumber-frequency plane into the angle-frequency plane using the interpolation. It seems that this technique can be used without instability problem for any wavenumber and easily obtain the results for the desired angular domain. However it should be noted that if one needs the response to one or two angles (especially close to normal incident) it is more efficient to use the split-field technique. The impedance and reflection coefficient of several periodic structures for different polarizations and angle of incident will be presented and compared with other techniques.

References: 1-Amir Aminian, Fan Yang, and Yahya Rahmat-Samii, Surface Impedance Characterizations Using Spectral FDTD Method: A Unified Approach to Analyze Arbitrary Artificial Complex Surfaces, 2004 URSI International Symposium on Electromagnetic Theory, Pisa, Italy, May 23-27, 2004. 2- P. H. Harms, A. Roden, J. Maloney, M. Kesler, E. Kuster, and S. D. Gedney, "Numerical Analysis of Periodic Structures Using the Split Field Update Algorithm", The Thirteenth Annual Review of Progress in Applied Computational Electromagnetics, Monterey, CA, March 17-21, 1997



Session B4, 12:55 – Thurs.

**ELECTROMAGNETIC  
APPLICATIONS OF  
METAMATERIALS**

Co-Chairs: N. Engheta, J.L. Volakis



## A VOLUMETRIC NEGATIVE-REFRACTIVE-INDEX METAMATERIAL BASED ON UNIPLANAR TRANSMISSION-LINE LAYERS

Ashwin K. Iyer, George V. Eleftheriades

The Edward S. Rogers Sr., Department of Electrical and Computer Engineering, University of Toronto, Toronto, Ontario, Canada

This talk will describe a new class of volumetric negative-refractive-index (NRI) metamaterials based on two-dimensional uniplanar transmission-line NRI layers. The layers consist of the series interconnection of transmission lines loaded in a dual configuration and can alternatively be perceived as an array of loaded metallic rings. The effective medium response of the constituent layers is revealed through a periodic analysis, and an equivalent circuit is developed to produce the dispersion characteristics of the volumetric medium formed by stacking the layers. This equivalent circuit also yields the effective permittivity and permeability of the volumetric medium. Various volumetric designs employing both discrete and printed lumped loading elements, as well as different ring topologies, are proposed and studied for their dispersion and transmission properties using full-wave simulations. They are shown to exhibit a relatively broad NRI bandwidth that can be predicted well by the proposed equivalent circuit model. It is also shown that the volumetric layered medium can be designed for a closed stopband, or to be impedance-matched to free-space with a refractive index of  $-1$ , thus meeting the requirements of Veselago's slab lens. We shall also discuss the possibility of scaling the proposed volumetric layered medium to terahertz frequencies and beyond.

### References

1. G. V. Eleftheriades, A. K. Iyer, and P. C. Kremer, "Planar negative refractive index media using periodically  $L$ - $C$  loaded transmission lines," *IEEE Trans. on Microwave Theory and Tech.*, vol. 50, no. 12, pp. 2702-2712, Dec. 2002.
2. F. Elek and G. V. Eleftheriades, "A two-dimensional uniplanar transmission-line metamaterial with a negative index of refraction," *New J. Phys.*, vol. 7, no. 163, August 2005.
3. A. K. Iyer and G. V. Eleftheriades, "A volumetric layered transmission-line metamaterial exhibiting a negative refractive index," *J. Opt. Soc. Am. B Focus Issue on Metamaterials*, accepted.
4. V. G. Veselago, "The electrodynamics of substances with simultaneously negative values of  $\epsilon$  and  $\mu$ ," *Sov. Phys. Usp.*, vol. 10, no. 4, pp. 509-514, Jan.-Feb. 1968.

DIRECT MEASUREMENTS OF EVANESCENT WAVE GROWTH  
INSIDE PASSIVE SPLIT-RING-RESONATOR BASED METAMATERIALS

Popa, B.-I., Cummer, S. A.

Duke University, Electrical and Computer Engineering Department,  
Durham, NC 27708, USA

It has been shown theoretically (J. B. Pendry, *Phys. Rev. Lett.*, **85**, 3966, 2000) that evanescent waves in air are exponentially enhanced inside a finite negative index of refraction slab having the relative permittivity and permeability equal to -1. Recent experiments (A. Grbic and G. V. Eleftheriades, *Phys. Rev. Lett.*, **90**, 137401, 2003) demonstrated subwavelength focusing in a 2D transmission line analog of a NIM, it has yet to be shown directly that this phenomenon occurs through the evanescent wave growth that was theoretically predicted. Fabricating an electromagnetic metamaterial NIM with the material parameters required, however, is challenging because the normally material must be tuned to have the relative permittivity and permeability extremely close to -1.

To circumvent the extreme sensitivity of the evanescent wave enhancement property to the material parameters, we show that the basic phenomenon occurs under relaxed conditions for a single transverse wavenumber and use this approach in our measurements. More specifically, we analyze theoretically and experimentally a three slab configuration (air-material-air) inside a rectangular metallic waveguide excited below its cutoff frequency. This type of excitation produces evanescent waves of known transverse wavenumber inside the waveguide. We use this property to show that there is always a frequency for which an evanescent wave of a selected transverse wavenumber (for example the  $TE_{10}$  mode) is enhanced inside an isotropic negative-permeability-positive-permittivity metamaterial composed of split-ring-resonators (SRRs). We further show how this frequency can be found experimentally, and present measurements of the electric field distribution inside the three slabs considered above that closely match the theoretically predicted fields, thus confirming the behavior of evanescent waves in a finite NIM predicted by Pendry.

We also analyze the effect of the loss on the performance of the particular metamaterial considered and show that despite losses the magnitude of the enhancement of the chosen mode is comparable to what would be obtained inside an ideal, lossless metamaterial.

DISPERSION CHARACTERISTICS OF GUIDED-WAVE STRUCTURES WITH ENZ MEDIA

Silveirinha, M.G.<sup>2</sup>, Engheta, N.<sup>1</sup>

<sup>1</sup>University of Pennsylvania, Department of Electrical and Systems Engineering, Philadelphia, Pennsylvania 19104, U.S.A.

<sup>2</sup>University of Coimbra, Department of Electrical Engineering, Coimbra, Portugal

Materials with relative effective permittivity (or relative permeability) near zero (ENZ or MNZ) are a class of metamaterials with unusual characteristics in their interaction with electromagnetic waves. These materials have become the subjects of study in recent years (e.g., R. W. Ziolkowski, Propagation in and scattering from a matched metamaterial having a zero index of refraction, *Phys. Rev. E*, 70, 046608 (2004); N. Engheta, M. G. Silveirinha, A. Alu and A. Salandrino, Scattering and reflection properties of low-epsilon metamaterial shells and bends. ICEAA05, Torino, Italy, Sept. 12-16, 2005, pp. 101-104.; A. Alu, F. Bilotti, N. Engheta, and L. Vegni, How Metamaterials May Significantly Affect the Wave Transmission through a Sub-Wavelength Hole in a Flat Perfectly Conducting Screen, Workshop on Metamaterials for Microwave and (Sub) millimetre Wave Applications: Photonic Bandgap and Double Negative Designs, Components and Experiments, London, UK, November 24, 2003.) In such ENZ or MNZ materials, the refractive index can be near zero, and thus the phase variation inside such media can be slow; however, the intrinsic impedance of plane waves in such media can be significantly different from that in conventional media. In our previous work, we have shown how ENZ or MNZ properties can provide interesting features in reducing the total scattering cross section of objects, and how this type of materials can affect the guided wave propagation around a bend in a waveguide.

In the present work, we focus our attention on the more general problem of guided wave propagation in waveguides partially filled with ENZ media. Following our work on wave tunneling through ENZ sections of waveguides with ENZ-filled bends, here we study more general features of such waveguides, e.g., group velocities, phase velocities, and field singularities of modes in these structures. We will also discuss characteristics of tunneling and reflection properties due to the ENZ section of the guides. For the case of partially filled ENZ waveguides, modal distributions and dispersion properties will also be studied. In this talk, we will present some of our theoretical results in this area and we will discuss physical intuitions behind these findings.

THREE-DIMENSIONAL NEGATIVE-REFRACTIVE-INDEX  
META-MATERIALS COMPOSED OF SPHERICAL DIELECTRIC  
RESONATORS

Tetsuya Ueda, Tatsuo Itoh  
Dept. of Electrical Engineering, UCLA

Propagation characteristics have been numerically investigated in the three-dimensional lattice structures which are composed of dielectric spheres in a host dielectric medium in an attempt to obtain the negative-refractive index near the resonant frequency of the spheres. For simplicity, we have assumed that they have the periodicity in the calculation but it is not essential for the operation. The mechanisms to be considered here are classified into two schemes; the first is the one-sphere scheme that is based on the spatial coupling between neighboring homogeneous dielectric resonators, and the second is the two-sphere scheme that is made of a combination of heterogeneous spheres with spherical TE and TM resonant modes. The former is the extension to the three-dimensional structure of the concept that is well-known for designing the microwave bandpass filters using dielectric resonators [1]. Here, the magnetic coupling between the spheres with TE resonant mode can give rise to the left handed wave transmission along a series of the dielectric resonators. On the other hand, for the two-sphere scheme, the sphere with a TE dielectric resonant mode and the one with a TM mode behave like a split ring resonator and thin wire, respectively, so that the negative effective permeability and permittivity are realized simultaneously [2].

For the one-sphere scheme, we have investigated various types of lattice structures such as simple cubic, body-centered cubic, and face-centered cubic lattices, and so forth. The left handed characteristics are confirmed in the dispersion diagrams for the face-centered cubic lattice in any propagation directions near the spherical TE resonant frequencies. The behavior of the EM wave propagation is mainly governed by the resonant conditions of spheres, but not by Bragg scattering in the periodic structure that is used for designing band gaps in photonic crystals [3]. It is found that there are still some problems of anisotropy, polarization dependence of the EM wave, and undesired secondary scattering modes that show forward wave characteristics. In addition, we have also investigated the cases where additional spheres are doped in the unit cell of the lattice to attempt to improve the dependence of propagation direction and polarization.

For the two-sphere scheme, the dispersion diagrams for the periodic structure and the scattering parameters for finite unit cells are obtained that verify the left handed transmission characteristics when a plane wave is assumed to be normally incident to a specific direction.

[1] Y. Konishi, *Microwave Integrated Circuits*, Dekker, 1991.

[2] C. L. Holloway et al., *IEEE Trans. Antennas Propagat.*, 51, 2596, 2003.

[3] M. Notomi, *Phys. Rev. B*, 62, 10696, 2000.



ULTRACOMPACT SUB-WAVELENGTH PLASMONIC CAVITY  
RESONATOR ON A NANOWIRE

Li, Jingjing, Engheta, N

University of Pennsylvania, Department of Electrical and System Engineering

An electromagnetic cavity resonator with deep sub-wavelength size is considered theoretically on plasmonic nanowires with the permittivity modulated periodically. In this work, plasmonic nanowires are treated as cylindrical waveguides made of materials with negative permittivity in a certain band of frequency (such as silver or gold nanowires), and their dispersion characteristics are briefly reviewed first. In such waveguides, due to the negative value of the real part of permittivity, a slow-wave TM mode with no cut-off radius is present, i.e., even for a very small radius, this TM mode with the guided wavelength much smaller than the free-space wavelength is tightly bound to the nanowire. These epsilon-negative cylindrical waveguides (ENG CW) with periodically varied permittivity is then studied analytically using the space harmonic method. Dispersion relations for this slow guided mode inside and outside the band gap are calculated numerically, and evanescent modes near the center of band gap are studied in details. By properly creating a defect on such a sub-wavelength periodically modulated ENG CW (PM-ENG CW), a cavity on this nanowire can be synthesized whose dimension along the nanowire is determined by the guided wavelength and the decay rate of the evanescent mode, resulting in an ultracompact cavity resonator with a size much smaller than the free space wavelength. This size can be made even smaller by reducing the nanowire radius, since the thinner the wire radius, the shorter the guided wavelength and the higher the decaying constant. The effective size of this cavity is calculated numerically, and Finite Element Method (FEM) is used to demonstrate the cavity mode. The quality factor ( $Q$ ) of such an ultracompact resonating mode is discussed. It was found that the material loss, more than the radiation leakage, is a determining parameter in  $Q$  evaluation. Candidate materials, e.g., some of the noble metals, suitable for making this structure are suggested and method of realizing such a resonating structure using only one material is also mentioned. Finally, the quantum limit of this theory is also discussed.

EFFICIENT ELECTRICALLY SMALL ANTENNA DESIGN USING  
A DIPOLE ANTENNA LOCATED NEAR AN EPSILON NEGATIVE  
(ENG) SPHERE

Aycan Erentok, Richard W. Ziolkowski  
University of Arizona

A metamaterial-based electrically small antenna design using a shell of homogenous, isotropic double negative medium (DNG) was first introduced analytically in (R. W. Ziolkowski and A. Kipple, Application of double negative metamaterials to increase the power radiated by electrically small antennas, *IEEE Trans. Antennas Propagat.*, vol. 51, no. 10, pp. 2626-2640, October 2003). Different from the classical ideas; such as using passive or active lumped elements to obtain a matching network, a DNG shell medium was used as a distributed matching element to the electrically small dipole antenna to obtain large radiated power efficiency and large fractional bandwidth. A different design methodology that replaced the DNG shell with an epsilon negative (ENG) shell was introduced in (R. W. Ziolkowski and A. Erentok, Metamaterial-based efficient electrically small antennas, submitted to *IEEE Trans. Antennas Propagat.*, June 2005). Here, we extend this concept by introducing an electrically small cylindrical dipole antenna antenna outside of an ENG sphere.

It will be shown that the antenna-ENG sphere system may have advantages over the previously presented dipole-ENG shell work for practical implementations. A finite element model, ANSOFT's High Frequency Structure Simulator (HFSS), was used as the computational electromagnetic (CEM) modeling tool for this investigation. The antenna-ENG sphere system was designed at 300MHz using an electrically small cylindrical dipole antenna with a length located next to an ENG sphere with a radius  $r$ . The ENG sphere located at the origin and the front face of the antenna was placed a distance  $h$  from it along the  $y$ -axis. The resonant interactions of dipole-ENG sphere system were studied for different  $h$  values. A resonant dipole-ENG sphere system showed a 64dB radiated power gain at 300MHz agreeing with the previous dipole-centered-ENG shell results.

It will also be demonstrated that for a given electrically small antenna, the distance  $h$  can be optimized to produce an electrically small system with a zero input reactance and an input resistance that is matched to a specified source resistance and that these antenna resonances occur where the corresponding radiated power gains and radiation efficiencies are maxima. The radiation patterns of the dipole antenna do not show any degradation at the far-field region. The quality factor and the fractional bandwidth of this dipole-ENG sphere system and its comparison to the Chu limit with and without dispersion characteristics will be discussed.

MINIATURE ANTENNAS EMBEDDED WITHIN FINITE EXTENT  
DEGENERATE BAND EDGE CRYSTALS

G. Mumcu, S. Yarga, K. Sertel, J. L. Volakis

The Ohio State University, Electro Science Lab, Department of Electrical and Computer Engineering, 1320 Kinnear Rd, Columbus, OH 43212 USA

Magnetic photonic crystals (MPCs) and degenerate band edge (DBE) crystals alleviate the issues of transmittance/matching and amplitude growth associated with slow modes in regular band edge (RBE) crystals. A direct consequence of these slow modes is large amplitude growth of the incoming wave at certain directions, making them promising for high gain miniature antennas and arrays. Earlier characterizations of the frozen mode (amplitude growth, transmittance, minimum thickness) showed that the amplitude growth phenomenon can indeed be realized in finite thickness MPCs (G. Mumcu, K. Sertel, J. L. Volakis, A. Figotin, and I. Vitebsky, to appear in IEEE Transactions on Antennas and Propagation). Further, modeling of printed dipoles embedded within such finite thickness MPCs (infinitely planar) demonstrated that such large amplitude growth within the crystal translates into higher gain antennas (G. Mumcu, K. Sertel and J. L. Volakis, 2005 IEEE International Symposium on Antennas and Propagation Symposium, Washington, DC, USA). DBE crystals are obtained by removing the magnetic layer of the MPCs and are matched better due to the relatively flat band edge. As a result, field amplitude increase can be achieved using less unit cells as compared to RBE crystals. In a recent presentation (J. L. Volakis, G. Mumcu, and K. Sertel, International Conference on Electromagnetics in Advanced Applications (ICEAA), 12–16 September 2005, Torino, Italy) we considered the DBE crystals and demonstrated that printed dipoles in finite thickness DBE crystals also exhibit higher gain. Specifically, more than 10dB increase in the received power and significant narrowing of the half beamwidth ( $76^\circ$  down to  $10^\circ$ ) is observed once the same dipole is placed inside the DBE crystal as compared to a simple dielectric layer of the same thickness.

In contrast to the above studies, this paper considers for the first time the performance of small dipoles embedded within DBE crystals in full three-dimensional setting (i.e. finite thickness and finite slab size). We will specifically discuss the effects of truncation on the receiving properties of the DBE loaded antenna. Induced currents on the dipole will be found via the surface integral equation formulation employing the dyadic Green's function of the uniaxial crystals. Of course, since the DBE crystal consists of many layers with large dielectrics, the resulting matrix system will be large, implying some challenges in its implementation. Our analysis focusses on the slow modes and effects of DBE loading on the receiving and transmitting properties of the small dipoles. We will present the analysis method along with the representative results for radiating and receiving elements placed within different size DBE crystals.

## INVESTIGATION OF LEAKY-WAVE ANTENNAS MADE FROM METAMATERIALS

Giampiero Lovat<sup>1</sup>, Paolo Burghignoli<sup>1</sup>  
, David R. Jackson<sup>3</sup>, Donald R. Wilton<sup>3</sup>

<sup>1</sup>Department of Electrical Engineering, 00184 Rome, Italy

<sup>2</sup>Department of Information Engineering, University of Siena , 53100 Siena, Italy

<sup>3</sup>Department of ECE, University of Houston, Houston, TX 77204-4005

One of the interesting uses of metamaterials is in the development of high-gain leaky-wave antennas (LWAs). LWAs have the inherent advantage of a high directivity that is typically achievable with a rather simple structure, since the guiding structure itself provides the radiation mechanism while a simple source is often used to launch the leaky wave. LWAs may be constructed in various ways, with the focus here being on planar structures composed of planar dielectric and/or metallic layers. A simple source such as an electric or magnetic dipole may be used to launch a cylindrical leaky wave that propagates outward on such a structure, producing a radiation pattern that is either conical at some scan angle, or a pencil beam at broadside. A line source excitation may be used if a fan beam is desired.

In the past, planar LWAs have been constructed using dielectric layers, in which a high-permittivity superstrate layer is placed over a substrate layer. More recently, planar LWAs have also been constructed from periodic metallic patch or slot arrays that form a partially reflecting surface (PRS) that is placed over a substrate layer. Although the PRS was constructed from a periodic structure, these previous LWAs did not use a metamaterial substrate.

With the advent of recent interest in metamaterials, it has been observed that high-directivity antennas using a metamaterial layer, e.g., a layer with a relative permittivity near zero, may be realized. Although not initially appreciated, it will be shown that such novel antennas are in fact LWAs by nature, and hence a comparison with other planar LWAs is warranted. The properties of such metamaterial LWAs will be explored, and comparisons will be made with LWAs realized with conventional substrates. The use of a wire medium to obtain a quasi-homogeneous artificial low-permittivity layer will be explored, and results will be presented to show that LWAs based on such a medium behave as expected from the homogeneous-layer analysis. The possible use of other artificial metamaterial layers will also be examined, including metamaterial layers with both low and high values of permittivities and permeabilities.

NUMERICAL SIMULATION AND EXPERIMENTAL RESULTS OF  
A GRADED NEGATIVE INDEX OF REFRACTION LENS WITH A  
GENERAL ANISOTROPIC MATERIAL

Parazzoli, G. C., Koltenbah, B. E., Greigor, R. B.  
, Lam, T. A., Tanielian, H. M.  
Boeing Phantom Works

Numerical Simulation and Experimental Results of a Graded Negative Index  
of Refraction Lens with a General Anisotropic Material

Claudio G. Parazzoli, Benjamin E.C. Koltenbah, Robert B. Greigor, Tai A.  
Lam, Minas H. Tanielian

Boeing Phantom Works, Seattle Washington 98124

Abstract

In this paper we discuss the numerical simulation of a Graded Refractive Index (GRIN) lens with a general anisotropic medium and compare it with an equivalent non-graded Positive Index of refraction Material (PIM) one with isotropic medium. The lens performance is first evaluated with the help of a generalized eikonal equation for an arbitrary anisotropic medium. The methodology for the rigorous solution of the eikonal equation in a general medium will be fully discussed. We start with the general form of Maxwell Equations, apply the eikonal approximation and derive the corresponding dispersion relation for a general medium. The dispersion relation is the eikonal equation. This equation is a first order, non-linear partial differential equation. It is solved with the standard method of the characteristics and thus reduced to a set of seven ordinary differential equations. The software developed for the numerical integration of the ordinary differential equations in a Matlab environment will be described in detail. Subsequently, a full Finite Difference Time Dependent (FDTD) simulation was performed to verify the validity of the eikonal calculations. The performance of the GRIN lens improved significantly over the equivalent PIM one. The GRIN lens is also five to ten times lighter than the equivalent PIM. A GRIN lens operating at 15 [GHz] was fabricated at Boeing. The comparison between the simulation, by the eikonal equation and the FDTD, and the experimental results of this lens will be reported. The agreement between the experiment and the simulation is excellent. We will discuss several applications of Negative Index Material lenses and present experimental and simulation results for these applications.

## EFFICIENT AND ACCURATE TECHNIQUES TO SIMULATE ELECTROMAGNETIC CRYSTALS

Femke Olyslager<sup>1</sup>, Davy Pissort<sup>1</sup>, Jan Fostier<sup>1</sup>, Ignace Bogaert<sup>1</sup>, Jurgen De Zaeytijd<sup>1</sup>, Eric Michielssen<sup>2</sup><sup>1</sup>Department of Information Technology, Ghent University, Belgium<sup>2</sup>Electrical Engineering and Computer Science, University of Michigan

In the optics community electromagnetic crystals (ECs) are usually simulated with FDTD. This technique is prone to phase errors and it was our purpose to develop accurate full-wave frequency domain techniques that are sufficiently fast.

In first instance we focused on two-dimensional problems consisting of a number of circular dielectric cylinders embedded in a host medium which were simulated by an angular Fourier decomposition of the field around each cylinder combined with a multiple scattering technique. In order to reduce the simulation time and memory consumption this was augmented by the MLFMA. To reduce the number of iterations different preconditioners were investigated. To simulate semi-infinite length EC waveguides, that excite the structure, a technique was developed to simulate this by a truncated finite length waveguide by continuing a few periods in the complex plane. To simulate an EC consisting of a number of cylinders omitted in an otherwise infinite periodic crystal a technique was developed to limit the unknowns to those corresponding to the omitted cylinders and to obtain immediately a very sparse interaction matrix that allows extremely fast simulations in the band gap. The technique was also extended to simulate a finite thickness dielectric slab pierced by a number of cylindrical holes. To take into account the radiation out of the plane of the slab a PML based technique was established.

In a second approach the two-dimensional scattering problem was treated using a Huygens source based boundary integral equation, where each cylinder boundary was divided into a number of segments, hence allowing for the inclusion of non-circular cylinders as well. Again this was augmented with the MLFMA and a special preconditioner was used. To gain more speed on the lowest levels of the MLFMA an SVD was used to compactly represent the translation matrices. Simulations with tens of thousands of cylinders were easily performed.

The developed techniques clearly demonstrate the possibility to simulate very large EC devices accurately using limited computation resources.

ON SIGN AND BRANCH OF CERTAIN PARAMETERS FOR SIMPLE, LOSSY DOUBLE-NEGATIVE MATERIALS

Arslanagic, S.<sup>1</sup>, Breinbjerg, O.<sup>2</sup>

<sup>1</sup>The University of Arizona, Electrical and Computer Engineering Department, P.O. Box 210104, 1230 E. Speedway Boulevard, 85721 Tucson, Arizona, USA

<sup>2</sup>Technical University of Denmark, Oersted-DTU, Electromagnetic Systems, Build. 348, Oersteds Plads, DK-2800 Kgs. Lyngby, Denmark

Double-negative (DNG) materials, first considered by V.G. Veselago in the late 1960s, have a negative real part of their permittivity as well as permeability, and these materials thus possess several unfamiliar electromagnetic properties (V. G. Veselago, *Sov. Phys. Usp.*, **10**, 509-514, 1968). In recent years, a great interest in exploring and exploiting the electromagnetic characteristics and properties of DNG materials has emerged, and a considerable amount of work, of theoretical as well as practical importance, has already been performed; e.g., see (N. Engheta *et al.*, *IEEE Trans. Microw. Theory Tech.*, **53**, 1535-1556, 2005) and the works referenced therein. Specifically, the sign and branch of certain parameters - such as wave number, intrinsic impedance, and refractive index - in DNG materials have been subjects of some discussion and disagreement (D.R. Smith *et al.*, *Phys. Rev. Lett.*, **85**, 2933-2936, 2000), (R. W. Ziolkowski *et al.*, *Phys. Rev. E.*, **64**, Paper 056625, 2001), (C. Caloz *et al.*, *J. Appl. Phys.*, **90**, 5483-5486, 2001), (R. A. Shelby *et al.*, *Science*, **292**, 77-79, 2001), (I. V. Lindell *et al.*, *Microwave Opt. Tech. Lett.*, **31**, 129-133, 2001), (A. L. Pokrovsky *et al.*, *Solid State Commun.*, **124**, 283-287, 2002). There is thus a need to re-examine these parameters.

In this work we investigate the sign and branch of wave number, intrinsic impedance, and refractive index for simple, lossy DNG materials. The investigation takes into account at the outset the obvious yet important fact that Maxwell's equations include only permittivity and permeability, but not wave number, intrinsic impedance, and refractive index. These parameters are introduced for convenience, and their introduction requires, of course, a consistent and proper choice of definitions. Each involves a square root quantity and, hence, requires a choice of the sign and branch of these parameters. One definition may be more convenient, or perhaps even more advantageous, than another but the correct solution to a given problem can be obtained with either definition as long as it is used stringently and the resulting physical quantities are consistent with expectations. Starting with lossless DPS materials (double-positive materials with positive real parts of the permittivity and permeability) the investigation extends to include lossy DNG materials. As an example illustrating the present findings, the problem of scattering by a circular DPS or DNG cylinder illuminated by an exterior, nearby electric line source is considered, and the exact eigenfunction solution is obtained with different choices of the sign of the wave number.





Session B5, 08:15 – Fri.

**APERTURE ANTENNAS AND  
ARRAYS**

Co-Chairs: M.E. Kowalski, G. Lazzi



MODELING CASSEGRAIN REFLECTOR SYSTEM USING FINITE  
DIFFERENCE TIME DOMAIN METHOD OF BODIES OF REVOLU-  
TION

Carrion, J., Sanchez, J., Farahat, N.

Polytechnic University of Puerto Rico, P.O. box 192017 , San Juan, PR  
00919

In this paper we model an entire Cassegrain reflector antenna including the feed, the subreflector and the reflector using the Body of Revolution (BOR) version of the Finite Difference Time Domain (FDTD) Method. The reflector system consists of a corrugated horn as the feed and axially-symmetric shaped subreflector and reflector. The corrugations in the feed (more than 100 corrugations for long horns) must be accurately modeled in order to predict its far-field pattern as well as the return loss. In addition it has been shown that the return loss can also be affected by the presence of the subreflector which rules out the individual modeling of the components.

Typically, due to the large electrical dimensions of reflector antennas, the design and analysis are carried out using approximated techniques such as physical optics and ray tracing. However accurate calculation of the important parameters such as return loss and side lobe level are required for todays modern communication systems which cannot be achieved with these methods. Rigorous volumetric techniques such as FDTD are desired. However the direct simulation of the entire reflector system requires high memory and cpu-time. Therefore to achieve the necessary accuracy and efficiency of simulation the axially-symmetric nature of the system can be used to extract the azimuthal variation and therefore model the antenna in two-dimensional plane using the BOR-FDTD method. This enables one to accurately design the entire system in a timely manner.

We model the entire Cassegrain reflector antenna on SGI Altix 350 PC cluster. The cluster is integrated by two modules each with two nodes of 2 Gbytes. The cluster as a whole unit can carry out the simulations requiring up to 8 Gbytes of shared memory. The numerical results including the far-field pattern and return loss will be presented.

A SHAPING METHOD FOR CIRCULARLY SYMMETRIC DUAL REFLECTOR ANTENNAS SOLVING NONLINEAR ALGEBRAIC EQUATIONS

KIM, Y., LEE, T.H.

THE OHIO STATE UNIVERSITY, ELECTROSCIENCE LABORATORY, US SATELLITE INDUSTRY COMPUTER CODE CONSORTIUM

This work presents a shaping method for a circularly symmetric dual reflector antenna. Conventional dual reflectors have amplitude taper at the main reflector aperture that results in reduced focused power in the desired direction. Therefore, reflector surfaces need to be shaped to obtain desired aperture distribution. The shaped reflector surfaces in many literatures (V. Galindo, *Design of Dual-Reflector Antenna with Arbitrary Phase and Amplitude Distribution*, *IEEE Trans. On Antenna and Propagation*, **AP-12**, 403-408, July 1964) are often determined by solving partial differential equations based on the principles of geometrical optics (GO), including power conservation and Snells law. However, in this research several nonlinear algebraic equations are formulated based on these principles and geometrical properties of conventional dual reflector antennas, and solved numerically with a certain approximation for a shaped dual reflector surface and caustic line.

The shaping method in this work creates and combines electrically small conventional local dual reflector systems with its own caustic location determined to produce a desired amplitude distribution at the corresponding aperture. Nevertheless, the shaped dual reflectors preserve properties of conventional dual reflectors. Consequently, the caustic location is no longer fixed in shaped dual reflector system and the amplitude of reflected field is controlled by the distance between caustic point and the reflection point on subreflector. The power is accordingly redistributed over the shaped dual reflector system, so that the desired aperture distribution is obtained. Caustic behavior explains how this shaping method works.

To formulate the shaped surface equations, the initial conditions should be provided. Those are unshaped initial geometry, feed power pattern, desired aperture distribution and initial points. The initial points for the subreflector, main reflector and caustics are pre-determined by ray conditions as in (Y. Kim, *Shaping of a Circularly Symmetric Three Dimensional Dual Reflector Antenna*, *MS Thesis, The Ohio State University, Department of Electrical Engineering, Columbus, Ohio, 2004*). They are the starting points for the shaping process. Then, a new set of caustics, subreflector and main reflector points are determined such that an incremental power from the feed is captured and redistributed through the reflectors to produce the desired incremental plane wave at the aperture. The new set of points becomes initial points for the next set of incremental dual reflector surface. The process is then carried to cover the overall desired aperture field distribution.

Non-uniform as well as uniform aperture amplitude distribution with constant phase can be prescribed. Ring-focus dual reflector antennas can be shaped to avoid subreflector blockage. Considerably reasonable result is obtained using this shaping method.

EQUIVALENT STRIP WIDTH FOR CYLINDRICAL WIRE:  
EXPERIMENTAL AND NUMERICAL VERIFICATION

Rajagopalan, H., Rahmat-Samii, Y.

Department of Electrical Engineering, University of California, Los Angeles, Los Angeles, CA-90095.

Reflector antennas with mesh surfaces are used in many satellite and ground antenna systems. These mesh structures have either strip-aperture or wire-grid characteristics. Butler determined that the equivalent diameter for a single narrow conducting strip is one-half its width (C. Butler, *IEEE Transactions on Antennas and Propagation*, **30**, 755-758, 1982). This equivalence has not been verified in practice for mesh reflector structures. The motivation of this work is to verify the equivalent strip width for a cylindrical wire with measurement and numerical analysis.

The study was divided into two tasks. The first task was to verify experimentally the correlation between the strip width and the wire diameter using measured data, and the second task was to numerically verify the correlation using the strip model and the wire model. For measurement purposes, X band waveguide (8 - 12.4 GHz) was used. Copper strips of similar width were cut and taped to the face of the waveguide using electrically conductive tape. These strips were positioned such that the periodicity of the structure was maintained. The transmission and reflection characteristics of the waveguide were measured using a network analyzer by connecting the waveguide with the strips between waveguide adapters. A similar experiment was performed using copper wires. For numerical analysis, a model of the experimental setup was designed and simulated in High-Frequency Structure Simulator (HFSS). By exciting the dominant waveguide mode, the transmission and reflection characteristics were obtained. A periodic strip model was simulated both in HFSS and periodic Method of Moments (MoM).

Comparing the measurement and HFSS simulated results confirmed that the numerical model was accurate. Using HFSS, it was verified that the equivalent strip width for a cylindrical wire is almost twice ( $\approx 1.9$ ) the wire diameter (for an infinitely thin strip) for mesh reflector structures. A convergence study was performed on the model in HFSS to obtain an optimum meshing surface. The effect of the thickness of the strip was studied and it was observed that as the strip thickness increases, the transmission goes down proportionally. The periodic strip model in HFSS was simulated using the plane wave incidence at different angles, as was the model in periodic MoM. Transmission and reflection characteristics obtained from the two simulations were found to be similar.

## DUAL-BAND, HIGHLY-STEERABLE MICROSTRIP PATCH PHASED-ARRAYS

Marc E. Kowalski, Brian DeWitt

L-3 Communications Randtron Antenna Systems, 130 Constitution Drive, Menlo Park, CA 94025

Reported are the results of an investigation to design, build and test low-profile antennas suitable for airborne datalinks. Airborne datalink antennas ideally have high-gain pencil beams steerable to optimize the SNR of the channel. In the past, these requirements have been met by dual-axis, mechanically steered antennas. Although this renders the high-gain requirement more practicable, these designs generally result in large protrusions from the conducting surface of an airborne platform. In addition to possible RCS concerns, such obtrusions generally result in a significant increase in the aerodynamic drag of the platform. Minimizing this effect while maintaining coverage throughout a specified cone has traditionally lead to the use of mechanically steered antennas with almost hemispherical coverage, in an effort to minimize the number of antennas used. Nonetheless, the impact on fuel efficiency and range on airborne platforms from the addition of datalink antennas is far from satisfactory.

In this work, the use of phased-array microstrip antennas to meet the aforementioned performance requirements is explored. In particular, a challenging dual-band datalink is pursued, with center frequencies of the two bands having a ratio of approximately 1.5:1. This bandwidth requirement is not easily met by microstrip elements, so a variety of broadbanding and dual-banding element design techniques have been investigated, including various combinations of multilayer stacking, aperture coupling, slotting patches and shorting patches. Even with an element that provides satisfactory bandwidth, it is far from trivial to implement an array that maintains this bandwidth while permitting steering from on-boresight to near-horizon. Some of the array design considerations investigated include architectures for time-delay beamforming networks, sub-arraying beamforming techniques, element active (mutual) impedance, impact of scan blindness, and surface-wave phenomena.

## INCREASING CHANNEL CAPACITY FOR LINEAR ARRAYS USING POLARIZED ANTENNAS

Gupta, G., Konanur, A. S., Hughes, B. L., Lazzi, G.

Department of Electrical and Computer Engineering, North Carolina State University, Raleigh, NC 27695-7914, USA

MIMO antennas have been used in wireless communications to increase channel capacity. Conventional MIMO systems employ antenna elements with  $\approx \lambda/2$  spacing in rich scattering environment to achieve decorrelation of fading path gains. For applications with area constraints like mobile communications this limits the number of antennas that can be used. In these scenarios compact yet reliable antennas are needed. Recently it was proposed that the use of polarized antennas can lead to a potentially three fold increase in capacity (M. R. Andrews, *Nature*, **409**, 316-318, Jan, 2001).

Linear array antennas are very versatile and find a variety of applications. In this paper we study the benefits of polarized antennas for linear arrays. A mathematical framework to analyze the radiated fields is developed. We show that for linear arrays there is a three fold increase in the degrees of freedom with the use of polarized antennas. This implies the existence of three orthogonal channels under suitable scattering conditions. To quantify the performance improvement, a co-located tripole antenna has been designed. This is important because if the antennas are not co-located then space diversity can also improve the performance. The individual elements of the tripole are printed dipoles. The antennas have been first optimized using simulations and then fabricated. The return loss for each element is below  $-10$  dB and mutual coupling between individual elements below  $-20$  dB.

To evaluate the performance benefits in a realistic scenario, channel measurements were performed in an indoor NLOS environment using linear arrays of tripoles. The scatterers were placed in the azimuthal plane at randomly generated angles with uniform probability density function. This is a popular model for azimuthal distribution of scatterers. The average capacity for the system using tripole antennas shows a  $\approx 3$  fold increase in capacity for a wide range of received SNRs as compared to the system using same number of dipole antennas. Simulations were performed using more detailed channel models and the results are in good agreement. This demonstrates that compact polarized antennas can be used to achieve significant improvement in capacity performance for linear arrays.

## MODELING OF PHASE-CONJUGATING ARRAYS FOR MULTIPATH COMPENSATION IN A MARITIME ENVIRONMENT

B. O. Takase, K. S. Y. Wong, C. R. Kawakami  
, G. S. Shiroma, W. A. Shiroma  
Dept. of Electrical Engineering, University of Hawaii

Unmanned Surface Vehicles (USVs) are increasingly used in high-risk intelligence, surveillance, and reconnaissance missions. Mission success is dependent largely upon maintaining a reliable communications link between the USV and the controller. However, in maritime communications, multipath fading due to reflections off the ocean surface can disrupt the link, potentially causing a loss of contact with the USV.

In this work, we use ray-tracing methods to model the potential use of phase-conjugating arrays to compensate for multipath fading and signal level variation in maritime communications. The work is based on a previously reported method in which up to 30 dB of improvement in signal-level variation was experimentally observed in a simulated severe-multipath environment (J. Tuovinen, G. S. Shiroma, W. E. Forsyth, and W. A. Shiroma, *2003 IEEE MTT-S Int. Microwave Symp. Dig.*, pp. 1681-1684, June 2003). The method does not eliminate multipath, but uses it advantageously in conjunction with a phase-conjugating array to eliminate deep fades.

Modifications to the canonical two-ray ground-reflection model were made using both a planar and sinusoidal seawater boundary. Results were first obtained for communications between omnidirectional antennas as a baseline, and then with an omnidirectional-to-phase-conjugating antenna link. The resulting model can be used to determine the minimum requirements, such as the number of array elements, for reliable communication for a given range. Since phase conjugation cannot compensate for the time delay of the data traveling on the direct path and multipath, the model is also used to analyze how the difference in path lengths affects the maximum data rate.



## A NOVEL DESIGN METHODOLOGY FOR APERIODIC ANTENNA ARRAYS USING PARTICLE SWARM OPTIMIZATION

Nanbo Jin, Yahya Rahmat-Samii

Department of Electrical Engineering, University of California, Los Angeles

Aperiodic antenna arrays have received great attention since 1960's with the advances in both radio astronomy and radar techniques. Using uniform-amplitude excitations, a narrow beamwidth and a low peak SLL can be achieved by an aperiodic array with much fewer elements than using a conventional periodic antenna array, due to the flexibility in its element spacings. Aperiodic arrays can be categorized into *sparse arrays* and *thinned arrays*. In the last forty years, many efforts have been expanded on the design of aperiodic arrays (either sparse arrays or thinned arrays) with the lowest peak SLL, yet all fail in approaching the optimum design obtained by brute-force investigations. A strategy that trades off multiple factors (the peak SLL, the beamwidth and the number of elements) of an aperiodic antenna array also remains unavailable, which results in a very challenging engineering problem.

This paper presents a novel design methodology for aperiodic antenna arrays using particle swarm optimization (PSO) technique. A randomized Newtonian mechanics model is proposed to describe the swarm behavior, which is formulated as an iterative process and applied to different types of optimizations. In aperiodic array applications, an attractive feature of PSO algorithm is that the variables to be optimized can be either real numbers (RPSO) or binary strings (BPSO). This enables the algorithm to be applied in the design of sparse arrays and thinned arrays, respectively. Specifically, RPSO determines the position of each element in a sparse array, and BPSO determines the on/off state of each element in a thinned array. The objective of both optimizations is to achieve the lowest peak SLL. The effectiveness of the algorithm is validated by comparing the optimized aperiodic arrays to some representative designs of existing methodologies.

The applicability of the PSO algorithm in aperiodic antenna array designs is further expanded by its multi-objective implementations (MORPSO and MOBPSO). With multiple design criteria defined by appropriate fitness functions, a sparse array is optimized to achieve a lower peak SLL with a narrow beam, and a thinned array is designed for a lower SLL using the least number of elements. For instance, A 10-element,  $10\lambda$  linear sparse array is observed to have a -19dB peak SLL while keeping the same beamwidth as a periodic array. The non-dominated designs obtained on the pareto front is shown to be substantially advantageous to some existing aperiodic array designs, and dramatically improve the limit between multiple design criteria given by the probabilistic-based method. It is believed by the authors that this paper is the first systematical study of aperiodic antenna arrays using an evolutionary algorithm, and the methodology can be applied to design arbitrary, multi-dimensional aperiodic antenna arrays with steered beams and directional elements for practical applications.

## OPTIMIZATION OF WIRELESS ARRAYS WITH ARBITRARILY LOCATED ELEMENTS

Young, W.F.<sup>1</sup>, Kuester, E.F.<sup>2</sup>, Holloway, C.L.<sup>3</sup>

<sup>1</sup>Sandia National Laboratories, Networked Systems Survivability and Assurance Department, Albuquerque, NM 87185-0785, USA

<sup>2</sup>Department of Electrical and Computer Engineering, University of Colorado, 425 UCB, Boulder, CO 80309, USA

<sup>3</sup>National Institute of Standards and Technology, 325 Broadway, Boulder, CO 80305, USA

We are investigating the potential of using arbitrarily placed wireless transceivers to increase the probability of maintaining a communication link in an electrically harsh environment. Specifically, we examine the performance of a well-known matrix-based array optimization technique applied to the case when the antenna elements exist in a complex environment and the observation point is not in the far-field of the array. Study of array performance in a non-ideal setting represents an important step in determining the feasibility of using this optimization technique for *ad hoc* wireless arrays within a building.

Array directivity or gain optimization techniques based on the general eigenvalue equation and Hermitian matrices are well covered in past literature, (e.g., É. I. Krupitskii, *Sov. Phys. Dokl.*, **7**, 257-259, 1962; R. F. Harrington, *IEEE Trans. Ant. Prop.*, **13**, 896-903, 1965; and D. K. Cheng, et al., *IEEE Trans. Ant. Prop.*, **13**, 973-974, 1965), as well as in a more recent publication (T. S. Angell et al., *Optimization Methods in Electromagnetic Radiation*, Springer, 2004). However, we apply the optimization technique differently from the typical approach in three key ways. First, the observation point, or the desired point of optimum radiation is now located within the volume of the array (which requires the use of a slightly modified expression for “gain” or “directivity” as a performance index). Second, we examine the statistical behavior of the optimized performance, e.g., average gain, by optimizing 200 sets of random element and observation point locations. Third, the effects of some simple boundary surfaces are included through the use of Green’s functions and first order impedance boundary conditions. This last item relates to work on arrays in arbitrary environments (S. P. Morgan, *Bell Syst. Tech. J.*, **44**, 23-47, 1965).

Simulation results for the directivity or gain of the array in the presence of several boundary configurations will be presented. These boundary scenarios include both perfect electric conductor (PEC) and approximated building surfaces for horizontal and vertical ground planes to model array performance in the presence of a building floor or wall. Array performance with a corner reflector boundary created from the intersection of horizontal and vertical surfaces is also simulated to examine corner impacts. Finally, we present results for an array between two parallel PECs to study the impacts of resonance on the optimized directivity. Our directivity results for arrays in free space are comparable to previously published results on arrays optimized for far-field radiation. In addition, our results indicate on average that the optimized directivity or gain with simple boundaries is within 3dB of that for the optimized configuration in free space.

## STEERABLE ARRAY ANTENNAS WITH DIELECTRIC PHASE SHIFTERS FOR 77 GHZ AUTOMOTIVE RADAR APPLICATIONS

Junho Cha, Yasuo Kuga

Department of Electrical Engineering, University of Washington

The 77 GHz collision avoidance radar in an automobile requires a beam scanning mechanism. In this paper, a new design is proposed for a mechanically controllable millimeterwave phase shifter and array antennas. Numerical simulations using Ansoft HFSS and Designer have been conducted. We have demonstrated that a movable dielectric slab placed on a coplanar waveguide (CPW) could be used as a phase shifter for automotive radar applications at 77 GHz. The effective dielectric constant and the characteristic impedance are calculated as a function of the movable dielectric slab position on the CPW transmission line. One of the advantages of this newly proposed phase shifter design is that the whole antenna can be designed without using solid state phase shifters or MEMS devices. The length of the dielectric material placed on a CPW is 1.82 mm, 3.64 mm, and 5.46 mm which corresponds to  $180^\circ$ ,  $360^\circ$ , and  $540^\circ$ , respectively. The required dielectric constant of  $\epsilon_r=5.60$  can be designed using a common ceramic material. The microstrip transmission line to WR-12 waveguide transition for an initial feeding point has been studied. Seven element patch array antennas were investigated for this application. The array antenna was designed to scan with a phase difference of  $-90^\circ$  to  $+90^\circ$  with an expected beam scan angle of  $-20^\circ$  to  $+20^\circ$ . The element separation was set to 2.922 mm which corresponds to  $0.75\lambda$ . The left and right dielectric slabs were alternatively and repeatedly inserted into the CPW. In addition, preset delays lines are added to minimize the number of dielectric slabs. We have designed the proposed antenna on a Duroid 5880 substrate ( $\epsilon_r=2.2$ ) with a thickness of 10 mil (0.254 mm).

## A PLANAR ANTENNA WITH NO-GRATING LOBES AT 60 GHZ

Futoshi Kuroki<sup>1</sup>, Ken-ichi Masaki<sup>1</sup>, Tsukasa Yoneyama<sup>2</sup><sup>1</sup>Kure National College of Technology<sup>2</sup>Tohoku Institute of Technology

Millimeter waves have attracted much attention for construction of novel wireless applications such as car radar systems and high bit-rate wireless communications. Indeed, several kinds of millimeter wave front-ends have been developed in many institutes and companies. It is important that the development of antennas compatible with millimeter wave integrated circuits is an indispensable technology for high performance millimeter wave systems. Actually, printed transmission lines such as a microstrip line and a coplanar waveguide were used as antenna feeders. These printed transmission lines have good performance at centimeter frequencies, but they suffer from a considerable conductor loss at millimeter wave frequencies. To solve this problem, a planar antenna fed by a high permittivity LSE-NRD guide radiator was designed at 60 GHz. Grating lobes in a previously-developed planar antenna were suppressed because the planar antenna consists of radiating slots, which were spaced by a period of less than a free space wavelength on a dielectric substrate and were fed by an oversized waveguide with filling of the Teflon material. A pencil beam was observed at the broadside direction, but the direction of the main beam was tilted by 15 degrees compared with that of a theoretical result. It is considered that this issue was caused by change of an effective relative dielectric constant of the oversized waveguide because a Teflon surface and a surface of the dielectric substrate with the radiating slots may be not attached each other due to deflection of the dielectric substrate. With this in mind, we developed a planar antenna fed by an oversized hollow metal waveguide to obtain a pencil beam in the broadside direction. To suppress the grating lobes, the spacing of the slotted arrays was set at 0.95 wavelengths. In this structure, the antenna gain and the antenna efficiency were measured to be 33 dBi and 40 percent, respectively.

Session B6, 12:55 – Fri.

**APPLICATION-FOCUSED  
ANTENNA CONSIDERATIONS**

Co-Chairs: J. Bernhard, W. Shiroma



COMPACT NOVEL RECONFIGURABLE ANTENNAS FOR  
MULTI-BAND OPERATION

Chunna Zhang<sup>1</sup>, Songnan Yang<sup>1</sup>, Helen K Pan<sup>2</sup>  
, Aly E. Fathy<sup>1</sup>, Samir El-Ghazaly<sup>1</sup>, Vijay Nair<sup>2</sup>

<sup>1</sup>Department of Electrical and Computer Engineering, University of  
Tennessee, Knoxville, Tennessee 37996

<sup>2</sup>Intel Corporation, JF2-86, 2111 N.E. 25th Ave., Hillsboro, Oregon  
97124

There are numerous wireless services that operate over wide frequency ranges and demand different operating electrical characteristics. For example, E-GSM systems operate within 0.89 to 0.96GHz, GPS within 1.57 to 1.58GHz, and UMTS within 1.92 to 2.17 GHz. Meanwhile, WLAN systems utilize different frequency bands (2.4 and 5.2GHz) with additional ranges for other services including Bluetooth, Zigbee, Wimax, among others. Radiation patterns of most of these antennas are omni-directional; however, some of these services require circularly polarized antennas. Antennas at these low frequencies are generally large in size and therefore unwieldy, especially at the 0.80 to 0.90GHz range. Hence, due to their inconvenient size, it is not practical to dedicate one antenna for each service, as they would occupy large real estate area. In addition, their proximity will cause significant performance degradation. Many of these services, such as wireless, are used only when needed, while there may be the need for the continuous use of others, such as Bluetooth and GPS. Therefore, in most cases, we would require automatic switching between the different modes, bands, and standards of operations. Reconfigurable structures are excellent candidates for this purpose, because they can be dynamically reconfigured to address most of these cases and their performance could surpass other configurations[1]. We have developed various reconfigurable antennas where their design is aimed at minimizing the number of switching devices and their overall size. MEMS are used and are preferred for switching, because of their low power dissipation. Eventually, the fabrication of these MEMs would be compatible with CMOS technology. In this paper, we will present the modeling and design of two original concepts: the maze and nested loop antennas. The maze-loop antenna[2] is based on reconfigurable fractal structure, where we would require slight tuning to adjust its fractal resonances to a selected set of frequencies[2]. But recently, we significantly reduced the size of these loop antenna structures at these low-operating frequencies by using symmetry planes and virtual short circuits. In addition, we have developed a novel concept for nesting various patches to obtain a multi-band or reconfigurable multi-band antenna, whenever MEMs devices are used for switching. Efforts to reduce their sizes and minimize the number of utilized switches for reconfiguration will be discussed here in detail.

[1] Reconfigurable Antennas and RF Front Ends for the Development of a Universal Wireless Receiver by C. Zhang, et al., to be presented at the IEEE Radio and Wireless Symposium, Jan., 2006, San Diego, CA.

[2] A Novel Reconfigurable Maze Antenna for Multi-service Wireless Universal Receivers, by S. Yang, et al. to be presented at the IEEE Radio and Wireless Symposium, Jan., 2006, San Diego, CA.

## RF MEMS INTEGRATION IN RECONFIGURABLE BENT MONOPOLE ANTENNA DESIGN

Pan, Helen K.<sup>1</sup>, Atkins, Phill<sup>2</sup>, Nair, Vijay K.<sup>1</sup>, Bernhard, Jennifer T.<sup>2</sup><sup>1</sup>Intel Corporation, JF2-86, 2111 NE. 25th Ave, Hillsboro, OR 97124<sup>2</sup>ECE Department, University of Illinois at Urbana-Champaign, Urbana, IL 61801

The next-generation wireless communication devices are developing toward the multifunction systems—ones that provide users with options of connecting to different wireless services for different purposes at different times [M. Brandolini, P. Rossi, D. Manstretta and F. Svelto, *IEEE Trans. Microwave Theory and Techniques*, **53**, 1026-1038, 2005]. One of these emerging technologies is *software defined radio* (SDR). With SDR, multiple signaling and modulation schemes can be implemented in software as long as the radio hardware can operate within the desired bands. Another wireless technology of the future is *multiple-input multiple-output* (MIMO) systems. MIMO technology provides dramatic increases in throughput by using multiple antennas at both the transmitter and receiver. One of the most significant challenges to the maturation of SDR and MIMO technologies is the design of antennas that can be adjusted or tuned to deliver the desired functionality over a wide range of frequencies in a variety of packages or form factors. Reconfigurable antennas are good candidates to deliver the flexibility in frequency tunability, pattern formation [G. H. Huff, J. Feng, S. Zhang and J. T. Bernhard, *IEEE Microwave and Wireless Components Lett.*, **13**, 57-59, 2003] and polarization selection [F. Yang and Y. Rahmat-Samii, *IEEE Microwave and Wireless Components Lett.*, **12**, 96-98, 2002]. In many cases, reconfigurability is achieved with RF switches placed at various locations to change the dimension of the antenna structure [W.H. Weedon, W. J. Payne and G. M. Rebeiz, *IEEE AP-S International Symposium*, **3**, 654-657, 2001] or the current distribution on the structure [F. Yang, and Y. Rahmat-Samii, *IEEE AP-S International Symposium*, **1**, 462-465, 2002].

Various RF switch technologies can be integrated in reconfigurable antenna designs such as pin diodes MESFETs and RF MEMs switches. RF MEMs switches have the best characteristics for reconfigurable antenna designs in terms of insertion loss, high frequency range and low power consumption. While most of reconfigurable antenna system designs implement hard-wired or lumped equivalent circuit model for proof of concept, the actual RF MEMs switch integration with antenna designs are not usually addressed. In this paper, we will address the RF MEMs integration factor in terms of switch location, parasitic, size and 50 ohms characteristic impedance matching. This study is based on reconfigurable bent monopole antenna that incorporates three RF MEMs switches (Teravicta Technologies, Austin TX, USA) operated in 4 bands from 1.8 to 5 GHz. Simulated and measured results of frequency switching behavior will be shown during the presentation.



## EFFECT OF MATCHING NETWORKS FOR VECTOR ANTENNAS ON MIMO CHANNEL CAPACITY

Konanur, A.S, Krishnamurthy, S.H, Hughes, B.L , Lazzi, G  
Department of Electrical and Computer Engineering, North Carolina  
State University, Raleigh, NC

The channel capacity that can be achieved in a MIMO system is dependent on the properties of the multi-element antennas employed. The elements of these antennas must all be well matched at a common frequency and the coupling between elements must be minimal. Good antenna design allows for these goals to be realized to a substantial extent. However, very compact MIMO antennas required for portable devices are not ideal, perfectly matched, uncoupled antennas. Thus, it is necessary to investigate methods that optimize the performance of realistic antennas in a MIMO configuration. Vector Antennas are a class of compact MIMO antennas that consist of co-located elements (eg. loops and dipoles) that can sense more than one component of the incident Electromagnetic field at a point (Konanur et al, *IEEE Trans. Microwave Theory and Techniques*, **53**, 1837-1844, June 2005). In this paper the use of lossless filters to enhance the MIMO channel capacity that can be achieved by Vector Antennas is explored.

The use of a lossless matching network between the load and the receiving antenna has been proposed (J.W. Wallace, A.Jensen, *IEEE Trans. Wireless Commun*, **3**, 1317-1325, July 2004) as a means of efficiently transferring power from the antenna to the load network. We design and use such filters in conjunction with various practical vector MIMO antennas. These antennas are placed in a realistic indoor scattering environment and the channel matrices are measured for different channel realizations. Subsequently, the Expected Mutual Information (EMI), with and without the filters, is calculated and the increase in EMI is evaluated. The expected mutual information serves as a lower bound on the achievable ergodic capacity. The increase in capacity is primarily a result of better power transfer to the loads, achieved as a result of a conjugate match between the antenna and input impedance of the filter on the one hand and the output impedance of the filter and impedance of the load on the other hand.

Preliminary results indicate that for a four-element MIMO antenna consisting of a loop and three dipoles, a 4-dB gain in SNR can be achieved by using the filter network. The feasibility of implementing a practical filter network with passive elements will also be explored.

## ANTENNAS FOR PICOSATELLITE APPLICATIONS

J. M. Akagi, J. D. Roque, W. A. Shiroma  
Dept. of Electrical Engineering, University of Hawaii

Picosatellites have recently shown promise as a practical, low-cost alternative to larger conventional satellites. The advantages of these small satellites include lower development and launch costs, shorter development cycles, and the ability to support newer technologies and experimental payloads. Another advantage is that a collaborative network of small satellites gives rise to capabilities that rival those of a single large satellite, since the network can reconfigure itself for different missions. The inherent redundancy of a small-satellite network also implies that it is more tolerant to single-point failures.

For the satellite-earth station link, early prototype picosatellites employed quarter-wavelength monopole antennas operating in the amateur radio UHF band, due to the prevalence of amateur radio earth stations in this band. However, this limited data rates to only the simplest types of telemetry, with 1200 baud being the standard protocol. Realizing the need for higher data rates to accommodate applications such as imaging, more recent picosatellites have been designed with transceivers at *S* band or higher. However, monopole antennas in this higher frequency range do not provide the same, nearly omnidirectional coverage as it provides in the UHF range, due to the smaller relative size of the antenna in comparison to the picosatellite structure. To establish a reasonable communication link, the monopole must be mounted on the side of the satellite, which reduces the signal strength on the opposite side of the satellite. As an alternative, we report the use of microstrip patch and inverted F antennas specifically designed to be mechanically and electrically conducive to a  $10 \times 10 \times 15 \text{ cm}^3$  picosatellite structure that is used in a mission to capture geo-referenced images from low-earth orbit.

In addition to the satellite-earth station link, crosslink communications between satellites is necessary to establish collaborative picosatellite networks. Omnidirectional antennas are the natural choice for picosatellites too small to accommodate attitude control systems, due to the unknown relative positions and orientations of the satellites within the network. However, omnidirectional antennas are susceptible to third-party eavesdropping, and waste a considerable amount of power for picosatellites which have limited power resources in the first place. We report progress in using circularly polarized retrodirective antenna arrays for two-dimensional self-steering crosslinks at *X* band.

## ANALYSIS OF MUTUAL COUPLING OF ANTENNAS ON A 47-FOOT COAST GUARD VESSEL

DeMinco, N.

U.S. Department of Commerce, NTIA/ITS.E

Isolation between the VHF transmitter and receiver antennas is an important issue for achieving satisfactory operation of the communication system on a Coast Guard vessel. For this study, the current antenna configuration, and several different antenna configurations on the 47-foot Coast Guard boat were modeled numerically to determine the isolation between the transmitter and receiver antennas. Some measured data were available of antenna isolation performance that was measured for the current antenna configuration on the vessel. An antenna on a metallic Coast Guard vessel located on the sea does not behave as if it were in free space or over a perfectly conducting ground plane. The gain, impedance, and antenna patterns are a function of the antenna geometry, antenna materials used, antenna height above the ground or sea, ground or sea conductivity, ground or sea dielectric constant, frequency, elevation angle, and azimuth angle. The performance of an antenna near or on the surface of the Earth or sea is also very dependent on the interaction with the Earth or sea, and the metallic vessel structure.

Computational electromagnetics using analytical mathematical expressions are difficult to apply to these types of practical problems, but the use of numerical techniques such as the method-of-moments makes the solution of this problem more tractable. The method-of-moments technique in the Numerical Electromagnetics Code (NEC) was used to model these antennas in this complex environment. The computational mode employed determines electromagnetic fields for antenna structures that are above an imperfect interface such as the ground or the sea, and the algorithms are also valid for antennas close to the interface.

Conventional methods could not be used here due to the close proximity of the antennas with respect to a sea environment and the metallic boat. The results of this analysis will show how the presence of the boat and the sea affect the antenna performance. The NEC model can also determine near fields that are very close to the antenna structure, in addition to antenna far fields, so that it can be used for antenna coupling calculations to determine antenna-to-antenna isolation.

The 47-foot vessel was modeled using wire segments, since there was more flexibility and freedom in using wire only segments, rather than a combination of patches and wire segments. Engineering drawings of the 47-foot Coast Guard vessel were used to generate the model. The model contains just under 10,000 wire segments, which includes the hull, cabin, and vessel superstructure. The 47-foot vessel model also includes details of the antennas mounted on the buoyancy chamber and antennas on the mast above the buoyancy chamber in addition to the HF whip antenna mounted on the port side of the vessel. The model was used successfully to determine antenna isolation and antenna performance characteristics. The mutual coupling prediction resulted in good agreement with the measured isolation.

USING THE TRANSMISSION-LINE METHOD TO DERIVE A CLOSED-FORM EXPRESSION TO LOCATE THE MICROSTRIP ANTENNA 50-OHM FEEDING POINT.

Hao Lin<sup>1</sup>, Xing Ping Lin<sup>2</sup>

<sup>1</sup>Graduate school, Tsinghua University, Peking, China, Address: Room 104, Building 28, Tsinghua University, Peking, China

<sup>2</sup>TRW Automotive

Patch antennas have been widely used in the wireless communication industry due to their low profile and small size. Available space allowed in applications for the antenna is getting smaller all the time. Different dimensions of rectangular patch antennas will yield different impedances at different feeding points. It is desired to have a 50-ohm feeding point in most applications. A transmission-line method has been widely used to characterize the rectangular patch antenna. In this paper, by using the transmission-line method, we obtain a closed-form expression for the relationship between the rectangular microstrip patch antenna feeding position and the input impedance. It is simple, unique, and easy to use.

Given the input impedance, the feeding position in terms of the microstrip patch antenna width, substrate height, relative permittivity and frequency is determined. The 50-ohm feeding point can be found in a simple way by using the equation derived here.

A transmission-line method was used to express the input impedance of the patch antenna at any location (distance  $d$  from the source to the edge along the center line) in terms of the end slot radiation impedance, patch dimensions, and dielectric constant. The resulting equation was a complicated one, and it was difficult to solve for  $d$ . We simplified the analysis by limiting the patch antenna open-end effect. Then the source distance  $D$  from an ideal  $1/2$ -wavelength patch antenna edge was obtained as

$$D = \frac{\lambda}{2\pi} \tan^{-1} \left( \sqrt{\frac{2y - y_{in}}{y_{in}y^2 - 2y}} \right),$$

where  $y_{in}$  is the normalized input admittance of the patch (normalized to the microstrip patch characteristic admittance) and  $y$  is the normalized patch slot radiation admittance.

The actual distance  $d$  of the source from the edge was obtained by subtracting the equivalent microstrip open-end length from the value of  $D$ . This equation has been applied to three cases with different patch dimensions operating at 1.8 GHz and 2.4 GHz to find the 50-ohm input impedance location. The 3D CST microwave studio software simulation tool had been used to locate the 50-Ohm input feeding location for these three cases. The tool was also used to verify the equation with input impedances different than 50 ohms. The simulation results are in good agreement with the results from the equation.

Session B7, 07:55 – Sat.

**MILLIMETER WAVES,  
COMPONENTS, AND CIRCUITS**

Co-Chairs: R.J. Pogorzelski, J. Venkatesan



## NEW TYPE OF NRD GUIDE BEAM-LEAD DIODE MOUNT AT 60 GHz

Futishi Kuroki<sup>1</sup>, Yu-suke Murata<sup>1</sup>, Ryo-ta Masumoto<sup>1</sup>,  
Tsukasa Yoneyama<sup>2</sup>

<sup>1</sup>Kure National College of Technology

<sup>2</sup>Tohoku Institute of Technology

An NRD guide, which consists of rectangular-shaped dielectric strips sandwiched by parallel metal plates with a separation of half a wavelength, is a transmission medium for construction of high performance millimeter-wave integrated circuits. This guide has good advantages such as low loss nature and no radiation at curved sections and discontinuities. Teflon was usually selected as the dielectric strip because of its low loss nature in millimeter-wave region, and the height and width were set at 2.25mm and 2.5mm, respectively. To date, NRD guide active devices such as a frequency converter and an ASK modulator have been successfully fabricated by using a beam-lead type Schottky barrier diode, where the diode was bonded across a gap between two rectangular shaped electrodes attached on the cross sectional surface of the dielectric strip. In this structure, a high permittivity sheet was inserted between the dielectric strip and the diode-mount so as to make a good impedance matching, although the high permittivity sheet was almost costly. To reduce the cost of the diode mount, we developed a new type of diode-mount without the high permittivity sheet. In the present diode-mount, the beam-lead type Schottky barrier diode was bonded between a gap, provided in a vertical strip transmission line, and the vertical strip transmission line, etched on a dielectric substrate together with chock circuits to apply a bias voltage, was connected to the NRD guide. The new type of NRD guide beam-lead diode mount was successfully designed at 60 GHz, and hence, decreasing the cost of the diode-mount.

## POLARIZATION-SENSITIVE ANTENNA-COUPLED BOLOMETER ARRAYS

Arnold, K.S.<sup>1</sup>, Holzapfel, W.L.<sup>1</sup>, Lee, A.T.<sup>1</sup>

, Mehl, J.<sup>1</sup>, Myers, M.J.<sup>1</sup>, Richards, P.L.<sup>1</sup>

, Tran, H.T.<sup>1</sup>, Engargiola, G.<sup>3</sup>, Spieler, H.<sup>4</sup>, Ade, P.<sup>2</sup>

<sup>1</sup>Department of Physics, University of California, Berkeley, Berkeley, California 94720

<sup>2</sup>School of Physics and Astronomy, Cardiff University, Cardiff, Wales, United Kingdom

<sup>3</sup>Department of Astronomy, University of California, Berkeley, Berkeley, California 94720

<sup>4</sup>Lawrence Berkeley National Laboratory, Berkeley, California 94720

Bolometers are the most sensitive broadband detectors of millimeter wavelength radiation. For bolometer experiments probing the Cosmic Microwave Background (CMB), the detector noise is often limited by the photon noise of the signal. To increase overall sensitivity, experiments of the future must employ an increased number of bolometers. A polarization experiment, designed to probe signals one to two orders of magnitude below the temperature anisotropy in the CMB, certainly requires this type of increased sensitivity. There has recently been much progress in the multiplexed SQUID (Superconducting Quantum Interference Device) readout of bolometers, facilitating this type of focal plane bolometer array.

We are developing a lithographed array of antenna-coupled bolometers for polarization studies of the CMB. The planar antennas are crossed double slot dipoles, with the beam pattern of each pixel optimized by direct contact with a dielectric lens. Superconducting niobium microstrip filters are used to define the frequency bands, and microstrip transmission lines couple the power to suspended bolometers. The antenna array is multichroic, with single-color pixels distributed among three frequency bands. The bands have been designed to optimize retrieval of astrophysical information while minimizing atmospheric contamination. These arrays are being developed for use in the ground-based PolarBear experiment, and they would also be a good match for other future experiments.

Verification of the eight layer process used to fabricate the arrays will be discussed. Results will be shown from the testing of the electrical and thermal properties of the suspended transition-edge sensors, as well as the electromagnetic properties of the antenna and microstrip.



NEW NARROW TO AVERAGE BAND-WIDTH DUAL-BAND  
PASSBAND FILTER DESIGN USING STEP-IMPEDANCE RES-  
ONATORS AND ZERO PHASE FEED STRUCTURE

Mokhtaari, M.<sup>2</sup>, Bornemann, J.<sup>2</sup>, Amari, S.<sup>2</sup>

<sup>1</sup>University of Victoria, ECE Department, , EOW A107, Computational  
Electromagnetics Lab, , P.O. Box 3055, Victoria, BC, CANADA

<sup>2</sup>Royal Military College of Canada, ECE Department, , PO Box 17000,  
Station Forces, Kingston, Ontario, CANADA K7K 7B4

In this paper, some new configurations of the concurrent dual-band filter design are presented. Stepped impedance resonators (SIRs) are used to implement the dual-band characteristics of bandpass filters due to their tunable spurious response properties. The new filters have actually a new dual-band feature of two controllable passbands at desired frequencies, high out of band suppression as well as wide stop band region. It should be noted that the ratio of resonance frequencies depends on that of characteristic impedances of transmission lines ( $K$ ) and they are briefly described as follows:  $f_2/f_1 \geq 2$  if  $K \leq 1$   $f_2/f_1 = 2$  if  $K = 1$   $f_2/f_1 \leq 2$  if  $K \geq 1$

where  $f_2$  and  $f_1$  are the center frequencies of the second and first passbands respectively. The above essential conditions are utilized to design dual-band filters with different frequency ratios. Transmission zeros can be created by appropriate inter-coupled between resonators, zero phase feed structure and somehow input and output cross-coupling. The new dual-band filter topologies save more than half the circuit size in comparison with those of the switch-type. They also have smaller size in comparison with former similar configurations with no input and output matching networks. Several dual-band passband filters with new topologies including Comb-line, Rectangular, Triangular and Circular Schemes adapted with different microwave circuits have been designed on RT-Duroid 6006 substrate and simulated by Ansoft Designer using the MOM. The result shows good agreement between theory and simulation and confirms the theory and new dual-band topologies to make dual-band filters with narrow to average bandwidths, one strong transmission zero between the passbands and more transmission zeroes on the upper and lower stopband regions.

## NOVEL VERSION OF THE DOUBLE-Y BALUN: MICROSTRIP TO COPLANAR STRIP TRANSITION

Jaikrishna Venkatesan

JPL, California Institute of Technology

The double-Y balun has been investigated in the past for use with balanced mixers and pulsed antennas. Various versions of the balun have been reported in technical literature, among them: (1) microstrip to slotline, (2) coplanar waveguide (CPW) to slotline, (3) CPW to coplanar strip (CPS), and CPW to parallel microstrip. The double-Y balun transitioning from a CPW to a CPS line has been shown to offer maximum bandwidth when compared to the other versions of the double-Y balun described above. However, parasitic resonances caused by the CPW section of the balun degrade the passband performance of the balun. In addition, the inductance of CPW bridges (required for proper operation of the balun) cause a shift in the  $\pi/8$  resonance of the balun, further limiting the performance of the balun. The requirement for CPW bridges also increases manufacturing complexity of the balun. In this work, a novel version of the double-Y balun is designed for feeding a complementary spiral. The balun transitions from an unbalanced microstrip line to a balanced CPS line. The use of a microstrip line with finite ground plane improves the passband performance of the balun by avoiding parasitic resonances caused by CPW lines. In addition, the new version of the double-Y balun described in this work does not require the use of bridges at the junction, hence avoiding the shift in the  $\pi/8$  resonance of the balun and reducing manufacturing complexity as well. The new version of the double-Y balun, transitioning from a microstrip line to a CPS line is analyzed numerically using Momentum (Agilents 2.5-D Method of Moments Code), and numerical results are compared with preliminary experimental results consisting of VSWR and insertion loss measurements.

## DEVELOPMENT OF MM AND SUB-MM-WAVE FERRITE CIRCULATORS BASED ON DIELECTRIC IMAGE GUIDES

Joshua L. Wilson<sup>1</sup>, Suren Gigoyan<sup>1</sup>, Yoon W. Kang<sup>2</sup>, Aly E. Fathy<sup>1</sup>

<sup>1</sup>Department of Electrical and Computer Engineering, University of Tennessee, Knoxville, Tennessee, 37996, U.S.A.

<sup>2</sup>Spallation Neutron Source Project, Oak Ridge National Laboratory, MS-6474, Oak Ridge, TN 37831, U.S.A.

Recently, interest has increased in ferrite devices, especially in the mm-wave frequency range for various communications system and antenna applications. To develop ferrite devices, a great deal of knowledge and understanding of magnetic material properties are needed. In this paper, we will discuss our development efforts of mm-wave circulator structures. At mm-wave frequencies, it is difficult to manufacture ferrite-based devices on rectangular metallic waveguide or microstrip lines, since a serious matching problem would exist between the ferrite material and the waveguide structure. Hence, we based our mm-wave circulator design on dielectric image guide structure to circumvent these matching problems.

The developed circulator structure was designed for the 26-40 GHz frequency range and its performance was both theoretically and experimentally investigated. Insertion loss was less than 0.4 dB, and isolation exceeded 35 dB. However, the design can be easily extended to much higher frequencies [1]. In addition, the developed circulator is lightweight, small in size, and would be relatively simple to manufacture. The cross section of the DIG rectangular rod was chosen to allow only a single E<sub>11y</sub> mode propagation, and was fabricated using nearly-pure semiconductor silicon material. The rod material has a relative permittivity of 11.8, which is close to that of the ferrite material, significantly simplifying the silicon-ferrite matching.

In this paper we will discuss the circulator design as well as the waveguide to DIG design and performance. In addition, we will demonstrate the effect of the bias magnetic field on the ferrite circulator. By employing a variable magnetic field, it is possible to achieve a compact-sized wideband mm or sub-mm wave circulator with extremely low insertion loss and high isolation.

++ Prof. S. Gigoyan is a visiting Fulbright scholar at the University of Tennessee from the Institute of Radio Physics Electronics, IRPHE Ashtarak -2, Armenia 378410.

[1] Low-Inertial Optically Controlled Circuits in 110-130 GHz Range Based on Dielectric Image Guides, by S. Gigoyan et al, to be presented at the IEEE Radio Wireless conference, Jan. 2006, San Diego, CA.

## NEW TYPE OF FERRITE RESONATOR FOR NRD GUIDE CIRCULATOR AT 60 GHZ

Futoshi Kuroki<sup>1</sup>, Sho-hei Ishikawa<sup>1</sup>, Yu-suke Takigawa<sup>1</sup>,  
Tsukasa Yoneyama<sup>2</sup>

<sup>1</sup>Kure National College of Technology

<sup>2</sup>Tohoku Institute of Technology

A promising candidate for millimeter-wave transmission media is the NRD guide, which consists of dielectric strips inserted in a below cutoff parallel metal plate waveguide and features no radiation at curved sections and discontinuities. Actually, several types of passive and active devices, such as a mode suppressor, band pass filters, transformers, a Gunn oscillator, and mixers, have been successfully developed by using the NRD guide. From among these NRD guide circuit components, an NRD guide circulator with a ferrite resonator is one of indispensable devices in the NRD guide circuit components, because it was usually employed as a duplexer and an iso-circulator. The ferrite resonator, used for the NRD guide circulator to date, consists of two Ni-Zn circular ferrite disks attached on the upper and lower metal plates, which were supported by a Teflon tube between these ferrite disks. In this structure, the Teflon tube has to be made by accuracy of less than several micron orders, and thus, the cost of the ferrite resonator may increase. With this in mind, a new type of ferrite resonator, using a Teflon cylinder instead of the Teflon tube, was devised. The Teflon cylinder can be easily fabricated, and hence, the cost reduction. The new ferrite resonator was analyzed based on the 3-dimensional finite-element method. The circulator having the present ferrite resonator was fabricated and its performances were measured. From this result, it was obvious that agreement between the measured and calculated resonance frequencies was quite satisfactory, and thus, the simple structure and low cost NRD guide circulator was successfully developed.

Session B/E1, 10:15 – Sat.

**PENETRATION OF EM  
RADIATION AND COUPLING  
INTO CAVITIES, INCLUDING  
EFFECTS ON DIGITAL  
ELECTRONICS**

Co-Chairs: D. Erricolo, F.M. Tesche

B/E1

## EFFICIENT TECHNIQUES FOR THE CALCULATION OF EM PEN- ETRATION INTO CAVITIES

Chatrpol Lertsirimit , David R. Jackson, Donald R. Wilton  
University of Houston

The calculation of electromagnetic fields inside of a cavity enclosure due to exterior signals that impinge on the cavity is an important topic in EMI/EMC. However, an accurate and efficient calculation of the fields inside complex cavities is challenging for various reasons. A discussion of techniques that aid in overcoming some of these challenges is the topic of this presentation.

One of the difficulties encountered in such cavity EMI/EMC calculations arises from the sharp resonances that may be encountered due to the high-Q nature of the cavities. This is especially true when the cavities have relatively small apertures, so that radiation leakage is fairly small. In the frequency-domain, moment-method solutions may become ill-conditioned near such resonance peaks. Furthermore, many calculations may be required to accurately characterize the resonance peaks since the frequency variation of the cavity response is very large near a resonance. Since moment-method solutions of complex cavity problems are usually numerically expensive, this results in a large computational expense. An efficient method for obtaining a CAD formula that characterizes the response of a cavity near a particular resonance will be presented. In this method the cavity response (e.g, for the voltage drop  $V(f)$  between two points inside the cavity) is represented as a first-order system near a resonance, as

$$V(f) = \frac{A_0}{1 + j2Q \left( \frac{f}{f_0} - 1 \right)} + C,$$

where  $Q$  is the quality-factor of the cavity and  $f_0$  is the resonance frequency. The number of unknown real parameters is six (two complex coefficients  $A_0$  and  $C$ , and two real parameters  $Q$  and  $f_0$ ). Algebraic manipulations allow for the response function to be re-written in terms of three unknown complex parameters. Further manipulation allows for the three complex parameters to be obtained by solving a  $3 \times 3$  linear system of equations, using three sample points in the frequency domain.. Numerical results will be presented to show the utility of the method for an actual complex cavity EMI problem.

Another numerical challenge for cavity problems when using the method of moments is the efficient calculation of the cavity Greens function. For rectangular cavities, the cavity Greens functions may be dramatically accelerated using the Ewald method. Formulas have been derived for how to optimally choose the splitting parameters  $E$  in this method, how to choose the summation limits, and when to switch from the Ewald method to a pure-spectral cavity Greens function when the vertical separation between the source and observation points becomes sufficiently large.

## EXPERIMENTAL STUDY OF ELECTROMAGNETIC INTERFERENCE (EMI) ON PCBs AND CABLES ENCLOSED IN COMPLEX STRUCTURES

Zulfiqar A. Khan, Yakup Bayram, John L. Volakis  
ElectroScience Lab., The Ohio State University

EM coupling on cables and circuits is an important problem in EMI/EMC. However, complex surrounding structures and countless geometrical configurations of cables and PCBs makes it challenging for conventional EM solvers to evaluate induced voltages on circuits and cables in the system. Recently, new hybrid numerical and semi-analytical methods were proposed for the EMC/EMI analysis of complex shielding enclosures. These include, EM coupling onto cable bundles [Bayram and Volakis, *IEEE Trans. EMC*, Vol. 47, Issue 2, May 2005 pp 234-246], EMI effects on PCB traces [Bayram and Volakis, 2005 *IEEE AP-S Int. Symp.*], and coupling of penetrating wires to shielding enclosures [Lertsirimit et al, 2004 *IEEE Symp. Ant Prop.*, Vol. 1, pp 375-378]. All these methods concentrated on solving the individual pieces/components, whereas it is desirable to investigate EMI/EMC coupling at system level. As we aspire to coming at system level analysis, it is important to generate reference data based on measurements for future validation.

This work presents an experimental study of EMI/EMC effects on cables and printed circuit boards enclosed within a complex structure comprising several cavities. To this end, a multi-cavity structure was constructed, with several measurement ports to evaluate EMI coupling for various enclosure configurations. The measurement setup employs multiple rectangular and cylindrical cavities, penetrating wires and analog/digital circuits. This complex structure will be illuminated by a plane wave and the induced fields and load voltages will be measured within 1-3 GHz band. Shielding degradation due to penetrating wires and apertures connecting adjacent structures will also be considered. The measurement data will be validated using conventional solvers and will be used as a reference for validation of the aforementioned semi-analytical and numerical methods.



## EXPERIMENTAL AND THEORETICAL ANALYSIS OF DIGITAL MODULATION SCHEMES AND RF POWER AMPLIFIERS SUBJECT TO ELECTROMAGNETIC INTERFERENCE

Yakup Bayram<sup>1</sup>, Suk K Myoung<sup>2</sup>, Seok J Doo<sup>2</sup>  
, Patrick Roblin<sup>2</sup>, John L. Volakis<sup>1</sup>

<sup>1</sup>Electro Science Laboratory, The Ohio State University

<sup>2</sup>Nonlinear RF Laboratory, The Ohio State University

We will present experimental and theoretical evaluation of digital modulation schemes (incorporating a RF Power Amplifier) subject to intentional Electromagnetic Interference (EMI). We particularly consider constant and non-constant envelope modulation schemes to evaluate performance (Error Vector Magnitude, Upset or Failure) subject to in-band and out-of-band EMI. To observe device level EMI effects, we perform a detailed analysis of EMI effects on a RF-Power Amplifier with emphasis on non-linear effects on the device due to high power EMI illuminations. Measurements and simulations are carried out to observe EMI effects on both system and device level.

The performance of digital modulation schemes such as Quadrature Phase Shift Keying (QPSK), Quadrature Amplitude Modulation (QAM) and binary modulation schemes such as Binary Phase Shift Keying (BPSK) is evaluated by computing the Error Vector Magnitude (EVM). Both in-band and out-of-band frequencies are injected into the system to study the vulnerability of the modulation schemes on intentional EMI. We are able to associate the overall effects with either direct deterioration of the modulated signals or an overall upset on the electronic modules that process the modulated signals. To do so, an RF-power amplifier was employed prior to the transmission stage and examined device effects on the modulated signal by measuring the EMV.

We observed that device level upset is predominantly seen when the power amplifier is forced into the nonlinear regime when high power EMI is injected to gate terminal. Based on the measurements and corresponding simulations, we demonstrate that intermodulation products lead to significant degradation of the power amplifier gain. The amplifier performance is further exacerbated due to thermal effects stemming from large DC power consumption.

In addition to direct EMI injection, we also exposed the power amplifier inside a metallic enclosure to high power plane wave illumination to examine external EMI effects in a more practical setting. For such a complex system, our analysis incorporates a hybrid S-parameter matrix for system modeling of the entire structure. Specifically, we integrate full wave EM models of the structure with a Harmonic Balance Circuit analysis. for modeling the PCBs and RF (as well as digital) devices. Such analysis very general and allows for complete realistic evaluation of performance deterioration associated with active RF devices in realistic settings.

ESTIMATES OF THE NEAR FIELD EM ENVIRONMENT OF  
A PYRAMIDAL HORN ANTENNA, WITH APPLICATIONS TO  
VULNERABILITY TESTING OF COMMON ELECTRICAL APPLI-  
ANCES

Fredrick M. Tesche<sup>1</sup>, Chalmers M. Butler<sup>1</sup>, Adam Schreiber<sup>1</sup>  
, David V. Giri<sup>2</sup>

<sup>1</sup>Holcombe Department of Electrical and Computer Engineering, 336  
Fluor Daniel EIB, Clemson University, Clemson, SC, 29634-0915 USA

<sup>2</sup>Pro-Tech, 11-C Orchard Court, Alamo, CA 94507-1541

To better understand the effects of high power EM (HPEM) effects on electrical systems, there is a need for determining the EM field thresholds at which upsets or failures in electrical systems can occur. Conventional EMC compliance testing does not provide information on such thresholds, since this type of test only proves that the equipment under test (EUT) will not fail when exposed to a specified or mandated EM field level.

A common frequency that is found in both industrial and household locations is 2.4 GHz. Many types of consumer goods are exposed to this intermittent CW environment, and such signals arise from cell phones, Bluetooth appliances, microwave ovens and other unlicensed radiators. To obtain the upset and damage thresholds for common commercial electronics at this frequency, Clemson University has undertaken an experimental effort to test to failure a variety of commercial equipment. The testing was conducted in an anechoic chamber with a magnetron source from a commercial microwave oven feeding an S-band pyramidal horn through a section of WR340 waveguide. This test was similar to one conducted earlier by Kaelin and Giri (see D. V. Giri, **High-Power Electromagnetic Radiators: Nonlethal Weapons and Other Applications**, Harvard Press, Nov. 2004), which showed damaging effects of EM field at this frequency, but did not examine upset or failure thresholds.

For the Clemson testing, a commercial H-field probe was used to measure the three H-field components at various locations within the chamber, and this provided information as to the EM field environment experienced by the EUT. Unfortunately, the probe had a maximum H-field measurement capability of about 2.1 A/m ( 800 V/m) and consequently, field points close to the horn could not be measured directly. To estimate the EM field environment near the antennas, a near-field pyramidal horn model was developed and the field strengths at these test locations were inferred from a measurement of the field farther away, where the probe could function safely.

This presentation concentrates not on the measurement program and results, but on the computational model used to characterize the excitation EM field in the near-field region of the horn. The model uses the equivalence theorem with an assumed TE<sub>10</sub> field distribution over the horn aperture. Close to the antenna, the usual Fresnel and Fraunhofer approximations cannot be invoked, and the 2-dimensional aperture field integration must be performed numerically. This procedure yields both the on-axis and off-axis fields. In this presentation, we describe the computational model and compare the results with other near-field calculations reported elsewhere in the literature.

## CURRENT ON A CONDUCTING CYLINDER IN AN ELLIPTIC CHANNEL EXCITED THROUGH A SLOT IN A CONDUCTING SCREEN BY AN INCIDENT FIELD TE TO THE SLOT AXIS

Schreiber, A. W.<sup>1</sup>, Butler, C. M.<sup>1</sup>, Erricolo, D.<sup>2</sup>

<sup>1</sup>Holcombe Department of Electrical and Computer Engineering, Clemson University, Clemson, SC 29634-0915 USA

<sup>2</sup>Department of Electrical and Computer Engineering, University of Illinois at Chicago, Chicago, IL 60607-7053 USA

The authors determine the current induced by a TE source on a perfectly conducting cylinder in a semielliptic channel behind a slotted ground plane. The edges of the slot in the conducting plane coincide with the foci of the semiellipse (channel wall), and the medium inside the channel and that outside are the same or they may be isorefractive to one another. The excitation may be due to a source either inside or outside the channel, provided the resulting field is TE to the slot axis and axially invariant. If desirable, the conducting cylinder may reside outside the channel.

The electric field due to an axially-directed magnetic line current can be determined in closed form at all points inside and outside the channel (P. L. E. Uslenghi, IEEE Trans. Ant. and Propagat, 52, pp. 1473-1480, June 2004). This electric field, expressed as a series of products of radial and angular Mathieu functions, is adopted as a Green's function of an electric field integral equation for the unknown magnetic surface current on the cylinder in a model of the field outside the cylinder. The forcing function of this integral equation is the tangential-to-the cylinder electric field due to the independent TE source radiating in the present of the channel-backed slotted plane but in the absence of the cylinder. From the solution of this integral equation, i.e., from the surface magnetic current, one can determine the surface electric current induced on the surface of the conducting cylinder. The Green's function and incident field are discussed, and the formulation and numerical solution of the integral equation are described. Also described is the ancillary computation of the electric surface current induced on the perfectly conducting surface of the cylinder from knowledge of the equivalent magnetic current (solution of the integral equation) and the incident field.

Solutions of the integral equation and the electric current induced on the cylinder are obtained for various cylinder locations and cross-sections, for selected excitations, and for specified channel and slot dimensions.

## ANALYTICAL AND NUMERICAL STUDY OF MULTILAYERED PARABOLOIDAL RADOMES.

Liang, J., Uslenghi, P. L. E.

Department of Electrical and Computer Engineering, University of Illinois at Chicago

A paraboloidal radome made of several layers of materials isorefractive to free space is considered. The primary field is a plane electromagnetic wave axially incident on the convex side of the structure. The analysis is conducted in the frequency domain. This scattering problem is amenable to an exact solution by geometrical optics. Such a solution was recently presented by Liang and Uslenghi (IEEE-APS Intl. Symposium and URSI Meeting, Washington, D.C., July 2005), and is based on an extension of the exact geometrical optics solution for axial scattering by an isorefractive paraboloid previously obtained by Roy and Uslenghi (IEEE Trans. Antennas Propag., vol. 45, p. 1563, October 1997). For a radome consisting of one or two layers, the solution is obtained explicitly, whereas for multiple layers a chain-matrix algorithm is employed.

The purpose of the present work is to conduct a comparison between the exact solution outlined above and purely numerical approaches to the same problem, based on either the Method of Moments or an FDTD formulation. In numerical approaches, as well as in practice, the extent of the paraboloidal surface of the radome is finite. Therefore, an important result of our comparisons is to establish how far from the nose of the paraboloid (in terms of wavelengths) one has to extend the surface considered in the numerical analysis in order to obtain sufficiently accurate results, both for surface fields (in amplitude and phase) and for far fields, the latter especially for backscattering and for small bistatic angles.

A similar analytical-numerical comparison is performed for a metallic paraboloid coated by layers of different isorefractive materials. This second study is important for the validation of general-purpose codes developed for radar-absorbing materials on curved surfaces.

Session B/F1, 08:15 – Wed.

**COMPLEX MEDIA AND  
ENVIRONMENTS**

Co-Chairs: E. Bahar, N. Engheta

**B/F1**

## A NOVEL PROTOTYPE FOR UWB MIMO VECTOR ANTENNA

Rajagopalan, A., Lazzi, G.

Department of Electrical and Computer Engineering, North Carolina State University, Raleigh, NC 27695-7914, USA

Since the 3.1-10.6 GHz frequency spectrum has been allotted for UWB applications considerable efforts have been expended in developing Ultra-Wideband antennas. Most of these antennas have been broadband dipoles such as bowties, disc monopoles and Vivaldi antennas. This talk presents a new prototype for a co-located UWB MIMO vector antenna system. A vector antenna is a system where each individual component of the electromagnetic signal is sensed. As such, all available degrees of freedom are utilized. These antennas are to be employed as ultra wide-band counterparts to narrow band vector antennas and find applications in wireless communications and biomedical imaging.

Co-located loops and dipoles with low coupling between them have been shown to provide an increase in capacity as compared to single antennas. The current research was motivated by the extension of this principle to ultra-wideband systems. The antenna system consists of a wideband loop antenna operating from 2-7 GHz and two coplanar bowtie patches that operate in the same frequency range. All the antennas are fabricated on a single substrate with relative permittivity 2.6. The loop antenna is similar to a clover leaf structure fed at the center. This ensures constant phase of the current in each individual sector which preserves the radiation pattern of the loop as a magnetic dipole. The two bowties are two sided patch antennas that are placed orthogonal to each other and coplanar with the loop. The performance of each individual antenna with respect to return loss, radiation pattern and impulse radiation will be discussed. It was found from experiments that the coupling was below -10dB in the frequency range 2-7 GHz indicating good isolation between individual antennas. This ensures that maximum energy is transmitted from each individual antenna and hence diversity between antennas can be exploited.

GENERALIZED SHEET BOUNDARY CONDITIONS FOR FDTD  
REPRESENTATION OF A METAFILM IN A HOMOGENEOUS  
MEDIUM

\*This talk has been cancelled.



## DORT METHOD FOR UWB ELECTROMAGNETIC FIELDS IN INHOMOGENEOUS AND DISPERSIVE MEDIA

Yavuz, M. E., Teixeira, F. L.

ElectroScience Laboratory, The Ohio State University, 1320 Kinnear Rd, Columbus, OH, USA

The *decomposition of the time-reversal operator* method (DORT under its French acronym) provides a simple and robust algorithm for detection and localization of point-like, well-resolved scatterers in disordered media by exploiting the invariance of the Maxwell's equations under time-reversal (TR) [C. Prada and M. Fink (1994), *Wave Motion*, 20, 151-163]. However, in lossy and dispersive media, this invariance is broken and additional attenuation and phase shift occur on the signals propagating in such media. Therefore, a compensation has to be applied to obtain a performance similar to the lossless (nondispersive) case. In this work, we first study the effects of frequency dispersion on the eigenvalue and eigenvectors of the time-reversal operator (TRO) and on the subsequent selective focusing using the associated eigenvectors. Having a better understanding of the TRO behavior under these conditions, we apply the full time-domain DORT method to ultrawideband (UWB) electromagnetic (EM) signals in both dispersive and inhomogeneous media under limited aspect antenna configurations. The frequency dispersion is modeled using an *inhomogeneous N-species Lorentzian* media (which can be reduced to a Debye media as a particular case) where UWB signals undergo frequency dependent attenuation. To compensate for the losses, a time-dependent filtering approach previously employed for homogeneous media [M. E. Yavuz and F. L. Teixeira (2005), *IEEE Geosci. Remote Sensing Lett.*, 2(2), 233-237] is extended to inhomogeneous random media. Since attenuation undergone depends on each particular realization (of a random medium with known statistical properties), filters adapted for random media are obtained using the ensemble averages. Although exact compensation can not be achieved, the overall performance is close to that of the non-dispersive case for weak background fluctuations where Born approximation holds. Finally, a previously proposed alternative numerical compensation algorithm based on a synthetic modification of the medium dispersive characteristics [P. Kosmas and C. M. Rappaport (2005), *IEEE Trans. Microwave Theory Tech.*, 53, 2317-2323] is assessed and compared against the time-dependent filtering approach. The TRO is explicitly obtained via finite-difference time-domain simulations (FDTD). Random medium models are based on inhomogeneous soil models with spatially fluctuating random permittivities with Gaussian distribution. Impenetrable point-like targets are considered as primary scatterers.

ELECTRIC TWEEZERS: EXPERIMENTAL STUDY OF POSITIVE DIELECTROPHORESIS BASED POSITIONING AND ORIENTATION OF A GOLD NANOROD

Edwards, B.E.<sup>1</sup>, Evoy, S.<sup>2</sup>, Engheta, N.<sup>1</sup>

<sup>1</sup>Dept. of Electrical and Systems Engineering, University of Pennsylvania, Philadelphia, PA 19104, USA

<sup>2</sup>Dept. of Electrical and Computer Engineering and National Institute for Nanotechnology, University of Alberta, Edmonton, AB T6G 2V4, Canada

The manipulation of individual micrometer-sized objects has been the focus of significant research efforts over the last few years. We first briefly review a method that we had analyzed earlier to arbitrarily move and orient a prolate conductive particle such as a gold nanorod in the region between a set of electrodes using positive dielectrophoretic forces. Each electrode is approximated as a set of sources, namely an unknown point charge and induced dipole. Imposing constraints on the electric field at the location of the particle and requiring self-consistency uniquely determines the sources. They can then be subsequently used to determine the set of electrode voltages that creates an electric field that will produce the prescribed orientation and force on the particle. Compared to the idealized single medium geometry in this derivation, the experimentally realizable geometry in our current work requires both a substrate to support the electrodes and a fluid to suspend the particle. Here, we discuss the electrostatic consequences of these complications. We demonstrate an experimental apparatus that implements the theory and discuss its parameters and constraints. The drag coefficients of a gold nanorod are determined by sequentially applying a constant force both parallel and perpendicular to its axis and observing the resulting motion. With the drag coefficients in hand, the velocity rather than force can be prescribed, and the rod is directed to accurately move at oblique angles to its orientation. The rod is in a constant state of unstable equilibrium and requires negative feedback to maintain a fixed position. This is most easily done by computer. We demonstrate that this can be automated and program a nanorod to travel over a complex path.

PHYSICAL INTERPRETATION OF ELECTROMAGNETIC FIELDS  
REFLECTED AT A FREE SPACE CHIRAL MEDIA INTERFACE

Bahar, E.

University of Nebraska-Lincoln, Electrical Engineering Department,  
WSEC 209N, Lincoln, NE 68588

Biological materials usually possess some degree of chirality. Conventional solutions for electromagnetic fields in chiral media are the right and left circular polarized waves. To provide a full wave (rigorous) basis for the analysis of general scattering problems, Generalized Fourier Transforms are derived, Maxwell's equations are converted into Generalized Telegraphist's Equations for chiral media, on imposing exact boundary conditions at rough interfaces. They account for diffuse scattering in non specular directions, as well as coupling between the different species of the circular polarized waves. Reflection coefficients at a free space-chiral medium interface are expressed in matrix form, both in terms of circular (C) and linear (L) polarized waves:

$$E_r^C \equiv \begin{pmatrix} E_r^R \\ E_r^L \end{pmatrix} = \begin{pmatrix} R^{RR} & R^{RL} \\ R^{LR} & R^{LL} \end{pmatrix} \begin{pmatrix} E_i^R \\ E_i^L \end{pmatrix} \equiv R^C E_i^C$$

$$E_r^L \equiv \begin{pmatrix} E_r^V \\ E_r^H \end{pmatrix} = \begin{pmatrix} R^{VV} & R^{VH} \\ R^{HV} & R^{HH} \end{pmatrix} \begin{pmatrix} E_i^V \\ E_i^H \end{pmatrix} \equiv R^L E_i^L \quad (1)$$

in which the subscripts  $i$  and  $r$  denote incident and reflected and the superscripts  $C$  and  $L$  denote circular and linear. The relationships between the circular and linear polarized fields are also expressed in matrix form as follows;

$$E_i^C = \begin{pmatrix} E_i^R \\ E_i^L \end{pmatrix} = A E_i^L, \quad A \equiv \begin{pmatrix} 1 & -j \\ 1 & j \end{pmatrix} \quad E_r^L = \begin{pmatrix} E_r^V \\ E_r^H \end{pmatrix} = A^{-1} E_r^C \quad (2)$$

Thus the relationship between  $R^C$  and  $R^L$  is given by

$$R^L = A^{-1} R^C A \quad (3)$$

When the degree of chirality is small  $|k_1 \beta_1|^2 \ll 1$ , to first order in  $k_1 \beta_1$ , the linear like polarized reflection coefficients  $R^{VV}, R^{HH}$  are the same as for the achiral case, however the linear cross polarized reflection coefficients are (to first order).

$$\frac{1}{2} j k_1 \beta_1 T_{10}^V T_{01}^H \tan^2 \theta_1 \begin{pmatrix} 0 & 1 \\ -1 & 0 \end{pmatrix} \equiv \begin{pmatrix} 0 & R^{VH} \\ R^{HV} & 0 \end{pmatrix} \quad (4)$$

in which the transmission coefficients for the vertically and horizontally polarized waves are  $T_{10}^V, T_{01}^H$  (across the interface in both directions). They are obtained from the circular like polarized scattering coefficients (3). Thus chirality impacts primarily upon the eight quasi off diagonal terms of the Mueller Matrix (consistent with the experimental observations). Physical interpretation of the scattering mechanism at a free space – chiral media interface and the specific dependence of the Mueller Matrix elements (due to chirality) upon frequency and angle of incidence are given in (4).

B/F1

Session B/F2, 08:35 – Fri.

**ROUGH SURFACES AND  
INTERFACES**

Co-Chairs: E. Bahar, M. Moghaddam

B/F2

RADAR CROSS SECTION FOR COMPOSITE GAUSSIAN OR PEARSON-MOSKOVITZ TYPE RANDOM ROUGH SURFACES BASED ON THE TWO SCALE UNIFIED FULL WAVE APPROACH

Bahar, E.<sup>1</sup>, Paul Crittenden<sup>2</sup>

<sup>1</sup>University of Nebraska-Lincoln, Electrical Engineering Department, WSEC 209N, Lincoln, NE 68588-0511

<sup>2</sup>Air Force Institute of Technology, Department of Mathematics and Statistics, WPAFB, OH

A composite two scale model of rough surfaces is considered using superpositions of Gaussian or Pearson-Moskovitz type surface height spectral density functions. The full wave backscatter cross sections of the random rough surfaces are expressed as weighted sums of two cross sections. The first, associated with the larger scale component of the rough surface is reduced by a factor related to the smaller surface height characteristic function. The second, associated with the smaller scale component of the rough surface, accounts for slope modulation by the larger scale surface. Unlike the conventional hybrid perturbation/physical optics solutions, the unified full wave approach used here is not restricted by the small scale Releigh parameter  $\beta = 4k_0^2 \langle h_s^2 \rangle \ll 1$ , (where  $k_0$  is the free space wave number and  $\langle h_s^2 \rangle$  is the mean square height of the small scale surface) nor are two cross sections added in an ad hoc manner.

The total composite surface height spectral density function is decomposed in a smooth, continuous manner, into larger and smaller scale surface height spectral density functions. Thus the distinction between the smaller and larger scale spectral density function is not characterized by a discrete spacial wave number where spectral splitting is assumed to occur. Furthermore the Pearson-Moskovitz spectral density function is not truncated abruptly in order to make the mean square slope of the larger scale surface finite.

The ratio of the mean square height of the smaller scale surface and the mean square height of the total surface  $r = \langle h_s^2 \rangle / \langle h^2 \rangle$  can be varied from zero to unity. Thus, in the limit  $r = 0$ , the total composite surface is regarded as a large scale surface (associated with the physical optics solution) or in the limit  $r = 1$  as a small scale surface (associated with the small slope, original full wave solution). In order to ascertain the stationarity of the solutions for the entire range  $0 \leq r \leq 1$  of the variational parameter, the norm of the error over the backscatter angles is plotted as a function of the variational parameter  $r$ . It is shown that the unified full wave solutions for the polarization dependent scatter cross sections are stationary over a very wide range of the variational parameter  $r = \langle h_s^2 \rangle / \langle h^2 \rangle$ . For rough soil surfaces over slowly undulating fields for example, the decomposition of the composite rough surface into larger and smaller scale surfaces may not be very difficult to ascertain. However in the general case of scattering from composite rough surface this is not obvious a priori. The examination of stationarity over the variational parameters  $r$  in the two-scale full wave solutions, provides a very useful guide in determining the appropriate spectral splitting of composite rough surfaces.

ESTIMATION OF MODULATION TRANSFER FUNCTION FROM  
DIRECT NUMERICAL SIMULATIONS OF RANGE-RESOLVED  
BACKSCATTER FROM OCEAN-LIKE SURFACES

Toporkov, J.V., Sletten, M.A.  
Naval Research Laboratory, Washington DC

Modulation transfer function (MTF) has been a useful and established tool in interpreting radar images of ocean surface. As the name suggests, the concept of MTF arises from the desire to relate the observed variations in radar image intensity (backscatter cross section) to the large-scale waves present on the surface in a simple, linear fashion. Under certain conditions (intermediate incidence angles, moderate sea states) such a linear dependence appears to be a reasonable assumption, with MTF relating the amplitudes of the same-frequency radar image and surface harmonics.

Usually, MTF is derived analytically using the approximate scattering models. There have been attempts to evaluate MTF from experimental data, but such efforts are typically hindered by the need to have rather accurate measurements of the surface profile. In contrast, studies of surface scattering through direct numerical simulations automatically provide the benefit of detailed surface information. In this work, we use large Monte Carlo ensembles of simulated range-resolved surface backscatter realizations (originally generated to study statistical properties of the clutter) to estimate the complex radar MTF.

In our simulations, the electromagnetic part of the problem is solved exactly using a first-principles boundary integral equation technique. Surfaces are generated as realizations of Gaussian random process with Pierson-Moskowitz spectrum; their non-Gaussian counterparts with non-linear hydrodynamic interactions introduced through Creamer transform are considered as well. With simulations limited to a 2D space, MTF is calculated by cross-correlating Fourier components of the backscatter power with the complex spectrum of the corresponding surface profile. The incidence angles are 60 and 85 degrees (i.e. 30 and 5 degrees grazing), and both VV and HH returns at a 3-cm wavelength (X-band) are investigated. Estimated MTFs are compared to the predictions of closed-form analytical expressions based on the 2-scale, tilted Bragg concept. Another comparison that tests a different set of simplifying assumptions uses an approximate scattering model (e.g. G. S. Brown, 1978) to calculate backscatter from each Monte Carlo surface realization. MTF is then evaluated by cross-correlation technique in the same way this was done for the clutter ensemble with exact scattering solution.



ON THE USE OF SAMPLING THEOREM IN THE METHOD OF  
MOMENT FOR SURFACE SCATTERING SIMULATIONEllen X. Huang, Adrain K. FungWave Scattering Research Center, Department of Electrical Engineering,  
University of Texas at Arlington, UTA Box 19016 Arlington, TX  
76019-0016

The method of moment(MoM) is a numerical procedure for solving the equation

$$Lf = g \quad (1)$$

where  $L$  is a continuous linear operator,  $f$  is the unknown function to be determined and  $g$  is a known excitation. In essence, the procedure converts the linear equation into a matrix equation and determines the unknown function in the form of a set of samples of the function through matrix inversion. It is well known that the sampling theorem states that to completely represent a function, one requires a minimum of two samples per wavelength, when basis function is the Sinc function. Thus, by choosing the Sinc function as the testing and basis function in MoM implementation, we should have the smallest possible size for the matrix. In this paper, the Sinc-Galerkine MoM has been developed and the number of the unknowns has been discussed. The formulations for the unknown current of 2-D rough surface for both VV and HH polarization have been developed based on the Sinc-Galerkine procedure. Then backscattering coefficients of VV and HH polarization have been further computed by calculated unknown current respectively. To test the above stated approach, we calculate the scattering coefficient from 2-D rough surface with a Gaussian distribution. The standard point matching approach is also used so that comparisons can be made between the two results. By comparing these numerical calculations with the IEM model, it is found that to achieve the same degree of accuracy, the number of unknowns used in the point matching method is an order of magnitude more than when the Sinc function is used as the basis function. This reduction in matrix size is specially significant in a three dimensional surface scattering problem, because we shall be able to reduce the matrix size by two orders of magnitude.

## BACKSCATTERING ENHANCEMENT OF SURFACE PLASMONS FROM MULTILAYER ROUGH SURFACES

Chih H. Kuo, Mahta Moghaddam

Radiation Laboratory, Department of Electrical Engineering and Computer Science, The University of Michigan, Ann Arbor, Michigan, USA, kuoch@umich.edu and mmoghadd@eecs.umich.edu

Backscattering enhancement is a phenomenon in rough surface scattering which manifests itself as a well-defined peak in the backscattering direction and finds a number of interesting applications in remote sensing and optical probing of metal-coated dielectrics. In the small roughness regime, backscattering enhancements are induced by the excitations of surface plasmons along a certain path followed by their retracing the same path in the reverse direction. In the scattering from multilayer rough surfaces, only a few studies in the mechanisms of backscattering enhancements due to surface plasmons have been reported over the past decades. In the past works, the analysis of the scattering physics of the process has focused on the development of small perturbation methods to the second order and other even orders. In this paper, an exact solution to the two-dimensional scattering from multilayer rough surfaces based on extended boundary condition method (EBCM) and scattering matrix approach is developed. The proposed solution in the paper accurately accounts for all orders of scattering and multiple bounces due to wave interactions between rough interfaces. Bistatic scattering coefficients are obtained by incoherently averaging the power computed from the Floquet modes in the scattering directions. The Floquet modes resulting from the EBCM analysis are then used to form and investigate the mechanism of backscattering enhancements. Numerical simulations are performed on a dielectric slab deposited with a silver film and the results are compared against the analytical SPM solution to two-rough-interface rough surface scattering. The emphasis is placed on the investigation of how layered rough interfaces affect the phenomenon of backscattering enhancement.

## ELECTROMAGNETIC SCATTERING FROM A BURIED CYLINDER IN LAYERED MEDIA WITH ROUGH INTERFACES

Chih H. Kuo, Mahta Moghaddam

Radiation Laboratory, Department of Electrical Engineering and Computer Science, The University of Michigan, Ann Arbor, Michigan, USA, kuoch@umich.edu and mmoghadd@eecs.umich.edu

An exact solution to scattering from a cylinder buried arbitrarily in layered media with rough interfaces based on extended boundary condition method (EBCM) and scattering matrix technique is developed. The reflection and transmission matrices of a rough interface as well as an isolated single cylinder are constructed using EBCM and recursive T-matrix algorithm, respectively. The cylinder/rough surface interactions are taken into account by applying the generalized scattering matrix technique. The scattering matrix technique is used to cascade reflection and transmission matrices from individual systems (i.e., rough surfaces or cylinders) in order to obtain the scattering pattern from the overall system where a cylinder is embedded in layered rough surfaces. Bistatic scattering coefficients are then obtained by incoherently averaging the power computed from the resulting Floquet modes of the overall system. In numerical simulations, the bistatic scattering coefficients are first validated by comparing the simulation results with the existing solutions which are the limiting cases including scattering from two-rough-interface rough surfaces without any buried object and from a buried cylinder beneath a single rough surface. The simulated results are in good agreement with those of limiting cases. Subsequently, the numerical simulations of scattering from a buried cylinder in layered rough surfaces are performed to investigate the relative importance and sensitivity of various physical parameters of layered rough surfaces to incoherent scattering coefficients. The emphasis is placed on how layered rough surfaces affect the overall scattering pattern of a buried cylinder. Results show layered rough interfaces can significantly alter the scattering behaviors of a buried cylinder.

AN ENHANCED AND ROBUST METHOD FOR INVERSION OF  
SUBSURFACE PROPERTIES OF LAYERED MEDIA WITH ROUGH  
INTERFACES

Tabatabaenejad, A., Moghaddam, M  
Radiation Laboratory, Department of Electrical Engineering and Com-  
puter Science, University of Michigan

A Newton-type inversion algorithm formerly applied to our forward model of two-layer dielectric structures with rough interfaces has been able to retrieve a few of the involved unknowns: real part of the dielectric constant and statistical characteristics of the random profile, in the case of a single rough surface, and real parts of the dielectric constants and separation of layers, in the case of double rough surfaces. To fully invert the two-rough-layer forward model, in general, nine unknowns must be retrieved. To increase the number of retrieved unknowns, we applied various methods including the Simplex Method and Simulated Annealing. Results show that a combination of these two methods is not only able to increase the number of retrieved unknowns from three to four in the case of a single rough surface, which is a complete inversion, and also in the general case of double rough surfaces, but also allows for a significantly larger tolerance on the a-priori estimate of the unknowns. In this work, we present quantitative results for this improvement. The choice of the cost function used in the optimization process is key in obtaining correct estimates and convergent algorithms. We use a different cost function that allows robust convergence to the correct values. We also examine the stability of the inversion algorithm, with respect to the measurement noise present in data. The inversion algorithm will be applied to the problem of estimating subsurface soil properties using the data from a tower-based radar system. These data consist of measurements of the backscattered wave for different incidence angles at center frequencies of 137 MHz and 435 MHz.

STATISTICS OF TRAVEL TIMES AND INTENSITIES OF TWO  
FIRST ARRIVALS OF SHORT PULSES BACKSCATTERED BY A  
ROUGH 3-D SURFACE

Fuks, I.M.<sup>1</sup>, Chamotskii, M.I.<sup>1</sup>, Godin, O.A.<sup>2</sup>

<sup>1</sup>Zel Technologies, LLC, NOAA/Environmental Technology Laboratory, Boulder, CO, USA

<sup>2</sup>CIRES, University of Colorado, NOAA/Environmental Technology Laboratory, Boulder, CO, USA

We consider backscattering of short pulses from the statistically rough surface at normal incidence in the geometrical optics limit, when only specularly reflecting points contribute to the backscattered signal. This paper extends the results obtained for 2-D surface in (I. M. Fuks and O. A. Godin, *Waves Random Media*, **14**, 539-562, 2004) to the 3-D case. The rough surface assumed to be spatially homogeneous and statistically isotropic with a Gaussian probability density function (PDF) of roughness heights and slopes. Statistical properties of travel times and intensities of the two first (i.e., earliest) arrived pulses are investigated.

Two specific cases are studied: a spherical wave front and a collimated incident beam. First signals from the rough surface return to the source location earlier than from the mean plane by time interval  $O(2\sigma/c)$ , where  $c$  is the velocity of wave propagation, and  $\sigma$  is r.m.s. of surface roughness. For a spherical wave front, we assume a point source located sufficiently far from a rough surface, and show that the PDFs  $w_1(\tau)$  and  $w_2(\tau)$  of the deviation  $\tau$  of the travel time (normalized by  $2\sigma/c$ ) of the first and the second arriving pulses from the travel time in the absence of roughness are functions of a single dimensionless parameter  $T$ ,  $T = \gamma_0^2 H / (\sigma\sqrt{2\pi})$ , where  $\gamma_0^2$  is the variance of the rough surface slope, and  $H$  is the source altitude. Our analytical approach is applicable only in the limiting case  $T \gg 1$ . For a collimated beam with a plane wave front, quantity  $B = \gamma_0^2 S / \sigma^2 (2\pi)^{3/2}$ , where  $S$  is an illuminated area on the surface, replaces parameter  $T$ ; both  $T$  and  $B$  are proportional to the average number of specularly reflecting points in the area significant for scattering. For a spherical wave front,  $S = O(H\sigma)$ .

For a spherical wave, PDFs  $w_1(\tau)$  and  $w_2(\tau)$  have the following explicit forms:

$$w_1(\tau) = \tau\varphi_s(\tau) e^{-\varphi_s(\tau)}, \quad w_2(\tau) = \varphi_s(\tau) w_1(\tau), \quad \varphi_s(\tau) = T e^{-\tau^2/2}.$$

On average, the travel times of the first and second arrivals decrease as parameter  $T$  increases, with the average travel time shift  $\tau$  being proportional to  $\sqrt{\ln T}$ . The time delay between the first and the second arrivals is inversely proportional to  $\sqrt{\ln T}$ . The joint PDFs of travel times and intensities of the first two backscattered pulses are derived. This allows us to obtain the travel time PDF for signals exceeding the given intensity threshold. It is shown that travel time and the intensity are strongly correlated: on average, earlier arrivals have smaller intensities.

## NUMERICAL SIMULATION OF SCATTERING FROM BREAKING SURFACE GRAVITY WAVES IN PRESENCE OF SMALL-SCALE ROUGHNESS

Voronovich, A.G., Zavorotny, V.U.

NOAA/Environmental Technology Laboratory, 325 Broadway, Boulder, CO 80305, USA

Description of the ocean gravity waves as a weakly-nonlinear, nearly-Gaussian statistical ensemble albeit convenient often contradicts observations. Calculation of microwave backscatter from the ocean surface in the low-grazing-angle (LGA) regime based on this representation does not produce such features as sea spikes with high horizontal-to-vertical polarization ratio, or anomalous behavior of Doppler spectra registered in field observations. There are many experimental facts speaking in favor of breaking waves as a primary source of those LGA backscatter effects.

In this paper, bistatic scattering from the 1-D impedance rough surface is numerically studied. A model of the rough surface consists of two types of waves: large-scale periodic non-linear gravity waves, and random short-scale capillary-gravity waves riding atop longer waves. Evolution of the longer surface waves is modeled by a hydrodynamic code allowing temporal description of the profiles of the steep and breaking waves. The short waves are described statistically by a stationary and spatially-uniform power-law spectrum with a lower cutoff spatial frequency three times smaller than the spatial frequency of the EM wave.

The simulations proceed in three steps. First, the hydrodynamic equations for potential surface waves including surface tension but without viscosity are solved producing a temporal sequence of large-scale wave profiles. The approach used allows appearance of non-single-valued profiles. As a result, it becomes possible to follow through various stages of wave breaking: steepening, cresting, involution, and jetting. Then scattering of EM wave is calculated from those profiles. Finally, using surface fields obtained at this step as sources for the small-perturbation theory the Bragg-type scattering on the small-scale roughness is calculated and added to the cross sections caused by steep breaking waves.

Calculations have been performed for 1.0-m wavelength surface waves and 4.65-cm EM wavelength and two orthogonal polarizations for various incident and scattering angles. For backscattering regime and for the upwind, front-face incidence at grazing angles about or less than  $20^\circ$  the results evidently support observable behavior of backscatter with an expected spike-like increase of HH-pol. that exceeds VV-pol. when the surface wave is passing the cresting stage and goes into involution. Onset of jetting leads to a relative subsiding of backscatter with HH-pol. getting smaller than VV-pol. Also, for the strongly non-linear waves alone, the corresponding Doppler spectrum at HH-pol. is broader than at VV-pol.

## AZIMUTHAL DEPENDENCE OF THE MICROWAVE EMISSION FROM FOAM GENERATED BY BREAKING WAVES

S. Padmanabhan<sup>1</sup>, S. C. Reising<sup>1</sup>, W. E. Asher<sup>2</sup>  
, L. A. Rose<sup>3</sup>, P. W. Gaiser<sup>3</sup>, J. P. Bobak<sup>3</sup>  
, D. J. Dowgiallo<sup>3</sup>, M. Anguelova<sup>3</sup>

<sup>1</sup>Microwave Systems Laboratory, Electrical and Computer Engineering Department, Colorado State University

<sup>2</sup>Applied Physics Laboratory, University of Washington, Seattle

<sup>3</sup>Naval Research Laboratory, Washington, DC

WindSat, the first polarimetric microwave radiometer on orbit, and the NPOESS Conical Microwave Imager/Sounder, scheduled for launch in 2010, are both designed to retrieve the ocean surface wind vector from radiometric brightness temperatures. Measurements and model results show that the wind direction signal is only 1-3 K peak-to-peak at 19 and 37 GHz, much smaller than the wind speed signal. Therefore, quantitative knowledge of the dependence of the ocean surface emissivity on properties such as surface roughness and wave breaking is critical for wind vector retrieval. However, the azimuthal dependence of the microwave emission from breaking waves and foam has not been adequately addressed. Recently, a number of experiments have focused on the increase in microwave emission due to foam.

The Polarimetric Observations of the Emissivity of Whitecaps Experiment (POEWEX '04) was conducted during Nov. 2004 at the OHMSETT wave tank and focused on characterization of the azimuthal dependence of the microwave emissivity of foam. A wave tank was used to observe highly repeatable breaking waves as a function of both incidence and azimuth angles. Microwave radiometers at 6.8, 10.7, 18.7 and 37 GHz were suspended below the basket of a boom-lift crane and positioned to view the water surface at azimuth angles of 0°, 45°, 90°, 135° and 180° and incidence angles of 45°, 53° and 65°. The radiometers also measured emission from the roughened surface with no breaking in the field of view. The fractional area foam coverage in the field of view of the radiometers was found by analyzing bore-sighted video measurements. In-situ measurements included void fraction, bubble size spectrum, and large-scale wave field measurements from an array of pressure transducers. These measurements demonstrated several first-order similarities between the wave dynamics of the wave tank and those on the open ocean.

The increases in emissivity at all frequencies vary as a function of azimuth angle, and this variation is more significant for horizontal polarization than for vertical polarization. For the increases in emissivity measured at 6.8, 10.7, 18.7 and 37 GHz, the azimuthal variations as a percentage of the mean vary from 13% to 25% for vertical polarization and from 11% to 45% for horizontal polarization. The azimuthal averages of the increases in emissivities from POEWEX '04 measurements were also used to estimate the effects of whitecap coverage on brightness temperatures measured by a satellite radiometer. These effects were expressed as a function of wind speed using a number of empirically-based parameterizations of whitecap coverage with wind speed. These results can be used to quantify and correct spaceborne passive microwave measurements for the effect of increased surface emission due to foam.

B/F2



Session B/F3, 15:15 – Fri.

## **BROADBAND ANTENNAS**

Co-Chairs: K. Demarest, E. Topsakal



OPTICALLY CONTROLLED SEMICONDUCTOR DIELECTRIC  
 RESONATOR ANTENNAS FED WITH LOW LOSS IMAGE  
 GUIDES AT MM-WAVE FREQUENCIES

Song Lin , Suren Gigoyan , Aly E.Fathy

The ECE Department, , University of Tennessee,, Knoxville, TN, 37996

Recently, there has been an increasing interest in the use of Dielectric Resonators (DRs) as radiating elements, especially at millimeter wave frequencies. DRs have a high radiation efficiency, small size, are light weight, and simple to manufacture. DRs can be easily utilized to build antennas. In a Dielectric Resonator Antenna (DRA), various modes can be excited; however, a DRAs radiation performance depends on its shape, dielectric material, and feed structure. A cylindrical DRA is preferred for its wide operating bandwidth. It is possible to reach bandwidths up to 35 percent as in the case of a Dielectric Resonator puck with a height to diameter ratio of approximately 4. Generally, the TE<sub>01</sub> mode of a cylindrical resonator radiates like a magnetic dipole oriented along its axis, and the TM<sub>01</sub> mode radiates like an axial electric dipole. However, coupling a DR to a microstrip line in the millimeter wave range is relatively difficult. Hence, we prefer using a Dielectric Image Guide (DIG) to feed these cylindrical DRs as the DIG properties are very similar to that of the Dielectric Resonators. In this case the feed line is the DIG line, and the radiating elements are the DRs. Obviously, we can use more than one DR to build an antenna array. Hence, a smooth back-to-back transition from rectangular metallic waveguide to a DIG line has been designed and built first. The fabricated transition has been optimized to operate over the 26-40 GHz frequency range with less than 0.3 dB insertion loss for a 2 inch DIG line. The DIG material is high resistivity silicon (10000000 ohm.cm and its loss tangent is 0.00007). The insertion loss characteristics of the feed line have been measured (i.e. S<sub>21</sub>) with and without the Si DR resonators and will be reported in our presentation. The degree of coupling to the main DIG feed line can be optically controlled in this case using IR radiation. The IR incident radiation on the DRA surface creates non-equilibrium charge carriers, which diffuse during their lifetime into the bulk of the resonator material. These excited carriers spoil the Q-factor of this high resistivity DRA silicon material and lead to higher RF-absorption from the main line. Clearly, the absorption is higher when the diffusion length is larger than the height of the DRA as in the selected Si DR pucks. In this paper, we will present in detail the theoretical and measured radiation results of these DRAs as well as the advantages of optically controlling them, and novel concept for steering.

++ Prof. S. Gigoyan is a visiting Fulbright scholar at the University of Tennessee from the Institute of Radio Physics Electronics, IRPHE Ashtarak -2, Armenia 378410.

[1] S. S. Gigoyan, Y. Cassivy and Ke Wu, Design of optically controlled NRD guide components for millimeter-wave applications, Book of Abstracts ISMOT-2003, Ostrava, Czech Republic, 11-15 Oct. 2003, p. 13

[2] Low-Inertial Optically Controlled Circuits in 110-130 GHz Range Based on Dielectric Image Guides, by S. Gigoyan et al, to be presented at the IEEE Radio Wireless conference, Jan. 2006, San Diego, CA.

ENHANCING SMALL VIVALDI-ARRAY PERFORMANCE WITH  
BAFFLESDemarest, K.R., Syeda, A. K.

Center for Remote Sensing of Ice Sheets, Department of Electrical Engineering and Computer Science, The University of Kansas, Lawrence, Kansas, USA

Vivaldi notch antennas are a popular choice for wide-band arrays. These antennas have a number of attractive features, including mechanical simplicity and a surprisingly symmetric endfire radiation pattern from a flat structure. Although Vivaldi notch-antennas remain relatively unexplored from an analytical point of view, there have been a number of recent numerical parameter studies that have provided helpful guidance for designing both single elements and arrays.

One interesting property reported by these studies is that the low-frequency return loss performance of a Vivaldi element improves when it is embedded in a large, linear array of identical elements. In this case, mutual coupling effects shift the minimum operating frequency downward, thus allowing the use of shorter and narrower elements for a given bandwidth requirement. This reduction in element dimensions is attractive, since, for a given bandwidth requirement, tighter element spacings can be realized. Unfortunately, this advantage is largely lost for small arrays, because of the well-known truncation effect. As a result, the element dimensions required for small arrays tend to be larger than those required for arrays with more elements.

This paper presents a novel technique for improving the performance of small-to medium-sized arrays of Vivaldi elements. The guiding idea for this technique follows from the periodic structure viewpoint, which shows that the mutual coupling effects in an infinite array have the effect of making each element think it is radiating into an infinite waveguide. This suggests that, for small Vivaldi arrays, metal baffles can be used to emulate the coupling effect of the missing elements of the infinite array.

We will show that attaching metal baffles to the edges of small, E-plane Vivaldi arrays can significantly reduce the truncation effects, thus improving return-loss performance. Results will be presented that show small, baffled arrays of Vivaldi elements exhibit return-loss characteristics similar to infinite arrays of the same elements, while retaining essentially the same radiation patterns as un-baffled Vivaldi arrays.

## MINIATURIZATION OF PLANAR TWO-ARM SPIRAL ANTENNAS USING SLOW-WAVE ENHANCEMENTS

Yang, T., Davis, W. A.

Virginia Tech Antenna Group, Blacksburg, VA 24061-0111

The size of a spiral antenna depends on the lowest operating frequency. The radius from the center feed to the outer boundary of the spiral antenna is normally about quarter wavelength of the lowest operating frequency. Basically, fundamental limit theory on antenna size shows that the size, efficiency, gain, and bandwidth are trade-offs. Thus, the reduction of antenna size while retaining the same bandwidth causes both lower radiation efficiency and lower antenna gain. Typical approaches to reduce the antenna size are dielectric loading, slow-wave structural patterns on the radiating element, and capacitive/inductive loading. The dielectric loading method is direct and very effective for shrinking antenna size. Typically, non-magnetic dielectric materials are used with the antenna size related to the inverse of the dielectric constant. However, this loading increases the  $Q$  of the antenna structure dramatically and causes severe reflection between the boundary of the antenna structure and air, having a negative impact on the impedance bandwidth. Thus, frequency independent antennas constructed on high electrical dielectric-constant materials usually are found to be narrow band. Dielectric loading with magnetic materials can be considered, but those are generally heavy, expensive, and very lossy. Methods other than dielectric loading also increase the  $Q$ , but not as significantly. Thus, size reduction using these other methods is not as dramatically affected. The bandwidth can be maintained at a slight cost in efficiency.

In this study, we explore size reduction methods using zigzag spiral arms for the Archimedean, equiangular, and stacked equiangular spirals (the stacked equiangular having arms located in different planes in order to maximize the zigzag). Preliminary simulation results show that the zigzag Archimedean has a smaller size reduction than found with the equiangular structure. The stacked zigzag equiangular spiral shows a significant on reducing the lower end of operating frequency, though having an overall efficiency lower than the other structures.

The detail influence of size-reduction methods on return loss, antenna input impedance, radiation directivity, and axial ratio will be compared. The impact of the size reduction on the peak amplitude of the transient response for various wrapping rates and configurations of slow-wave structures will also be discussed and compared to other classic UWB antennas.

## A PHYSICS-BASED IMPEDANCE MODEL FOR A MINIATURIZED BROADBAND SPIRAL ANTENNA

Lee M., Kramer B.A., Chen C.C. , Volakis, J.L.

ElectroScience Laboratory, Dep. Electrical and Computer Engineering,  
The Ohio State University

There is a strong interest in the commercial and military sectors for small and broadband antennas. Existing commercial applications have a need for a single antenna operating in the frequency range of 825-2500 MHz (AMPS, DAB, GPS, PCS, SDARS), for example. For military applications, there is also a need to have a single aperture which permits operation in different communication bands and can also be used for imaging and guidance applications. These needs require wide band antennas, such as the miniaturized spiral antenna. Due to its broadband nature, broadband antenna miniaturization usually can not be achieved by conventional ways of port impedance tuning. Instead, more homogenous treatment across the whole antenna aperture has to be applied. Various such techniques had been developed, including dielectric material loading, distributed lumped element loading, etc. Almost all of these strategies intend to reduce the effective wavelength inside antenna geometry, thus making the antenna electrically larger. However, it has also been observed that this approach results in diminishing gain-shift return when more aggressive miniaturization is applied to a broadband antenna. To understand such behavior one has to explain the impact of miniaturization strategies on antenna impedance. This paper presents a simple physics-based working model describing broadband spiral antenna impedance as a function of frequency. Comparison between the model and the full wave simulation shows very good agreement. Further more, this model is able to include the impact of miniaturization strategies on spiral antennas. Based on this model, we are able to explain the two major issues associated with broadband spiral miniaturization, namely, the diminishing gain-shift return and the broadside gain drop at high frequency. Specifically, we model the spiral antenna as a wrapped transmission line structure in terms of wave propagation, and a continuous set of radiating loops in terms of radiation. The model shows that the slow wave situation results in unavoidable spiral antenna radiation pattern broadening. At the same time, radiation resistance shows mixed response, namely, shifting toward lower frequency but was also lowered in magnitude. The physical insight into these issues can not be provided by full wave simulation, which is also computationally heavy for a broadband spiral structure. We also show that this working model is in line with the well known small antenna limit theory. While the small antenna limit theory grandly provides a universal limitation on all radiation elements, the working model proposed in this paper provides more functional details when spiral antenna is of concern. This allows more focused solutions to the miniaturization issues to be developed.

## A DOUBLE-SIDED ROUNDED BOW-TIE ANTENNA FOR UWB COMMUNICATION

Karacolak T., Topsakal E.  
Mississippi State University

After the United States Federal Communications Commission (FCC) adopted the first Ultra Wide Band (UWB) Report and Order in February 2002, there has been a great interest for commercial UWB technologies. The most important issues in the UWB systems is to design a compact and extremely wide band antenna covering the spectrum from 3.1 GHz to 10.6 GHz. Moreover, good impedance matching characteristics, gain flatness, and phase linearity are required. In this study, we propose a double sided rounded bow-tie antenna for UWB communications.

Finite Element Boundary Integral Method (FE-BI) has been applied to the antenna for determining return loss and radiation characteristics. Finite elements have been extensively used to model open- and closed- domain electromagnetic problems in scalar form in two and three dimensions. For our case, we are employing the tetrahedral elements for the volume and triangular elements for the surface/aperture and metallic structure. Using tetrahedral elements offers higher flexibility when simulating complex structures, and mixed-order tangential vector finite elements (TVFES) guarantee tangential field continuity across element boundaries and suppress spurious modes. For validation purposes, we also simulated our design using a commercial software (HFSS).

The antenna has reasonable gain flatness above 2.5 dBi and return loss below -10 dB for the whole frequency band. It has omni-directional radiation characteristics and good phase linearity over the same frequency band. We show that the rounded bow-tie patches work better than flat ended conventional bow-ties for the UWB communications. Results regarding antenna parameters such as return loss, radiation pattern and gain will be presented.

DOUBLE-SIDED EXPONENTIALLY TAPERED SLOT ANTENNA  
(DE TSA) FOR UWB APPLICATIONS

Hood A.Z., Topsakal E.  
Mississippi State University

This paper discusses a modified version of the double exponentially tapered slot antenna (DE TSA) for use in ultra wide band (UWB) applications. In 2002 the Federal Communications Commission (FCC) opened the UWB frequencies (3.1-10.6 GHz) for commercial use. Applications for UWB technology include broadband wireless communications, which benefit greatly from increased bit rates available to higher bandwidth. Tapered slot antennas have long shown great promise for achieving wide bandwidths. [1] showed that by exponentially tapering both the inner and outer edges of the traditional Vivaldi antenna, the bandwidth and other characteristics may be greatly improved. Traditional bowtie antennas exhibit wideband properties, but lack the ability to operate over the entire UWB range. In [2], the double-sided printed bow-tie antenna was introduced with a bandwidth exceeding the required 3.1-10.6 GHz. This paper introduces a similar concept with the double-sided double exponentially tapered slot antenna.

By placing the radiating patch directly above the grounded patch and feeding the antenna with a microstrip line, the structure of the DE TSA becomes drastically smaller while allowing for larger patches. Following the equations for the tapering of the slots found in [3] a double-sided DE TSA was designed on a substrate of  $36 \times 36 \text{ mm}^2$ . The antenna is capable of operation over the UWB band and beyond, which opens it to the possibility of use in future applications. The antenna also exhibits strong directivity along its central axis, as well as above and below the E-plane, as is expected from an end-fire design. While the double-sided DE TSA does offer better performance than similar single-sided configurations, the main advantage of the antenna is its extremely compact dimensions. Results for and an optimized version of the double-sided DE TSA will be presented.

[1] Lee, J.J. and Livingston, S., Wide band bunny-ear radiating element, IEEE Antennas and Propagation Society International Symposium, pp. 1604-1607, July 1993, Ann Arbor, MI.

[2] Kiminami, K., Hirata, A., and Shiozawa, T., Double-sided printed bow-tie antenna for UWB communications, IEEE Antennas and Wireless Propagation Letters, vol. 3, pp. 152-153, 2004.

[3] Greenberg, M.C. and Virga, K.L., Characterization and design methodology for the dual exponentially tapered slot antenna, IEEE Antennas and Propagation Society International Symposium, pp. 88-91, July 1999, Atlanta, GA.



Session C1, 10:15 – Wed.

**SIGNALS AND SYSTEMS**

Co-Chairs: J. Krolik, D. Palmer



## SIMULATION OF INTERFERENCE EFFECTS FROM UWB SIGNALS TO A QPSK DIGITAL NARROWBAND SYSTEM

Idnin Pasya, Tomiki Atsushi, Takehiko Kobayashi

Wireless System Laboratory,, Department of Information and Communication Engineering,, Tokyo Denki University

This paper reports on the study of the interference effects from Ultra wide-band (UWB) sources on QPSK transmission system by simulation. The culprit UWB sources were: multi-band orthogonal frequency-division multiple-access (MB-OFDM), direct-sequence code@division multiple@access (DS-CDMA), DS spread spectrum UWB (DS-SS UWB), and additive white Gaussian noise (AWGN). The MB-OFDM and DS-CDMA were modeled based on the proposal specifications in the IEEE.802.15.3a to standardize high-speed wireless personal area networks. Average bit error rate (BER) degradation of the victim system was evaluated while verifying the desired-to-undesired signal power ratio ( $D/U$ ), where  $D$  is the transmission signals average power and  $U$  represents the power of the UWB signals average power occupying the same bandwidth. The statistical properties of the culprit UWB signals entering the victim receiver were also investigated by means of amplitude probability distribution (APD).

We proposed a modified equivalent baseband system to accelerate the simulation speed. In the proposed system, the victim system was generated in the passband domain, while the UWB signals were generated at the equivalent baseband domain to lower the sampling rate of the simulation. The simulation was carried while varying the bandwidth of the victim system from 1, 5, to 10 MHz to observed significant relations between the BER and the victimfs bandwidth.

It was found that the DS-CDMA signal at the pulse repetition frequency (PRF) shows non-Gaussian properties, degrading the BER of the victim system 3 dB worse than the AWGN one. The interference effects from the MB-OFDM signal however were nearly 3 dB lower than that of the AWGN one in the  $D/U= 10$  dB region. In a previous report, the authors pointed out that the MB-OFDM signal marked frequency peaks at every 3.2 MHz which would degrade the BER further. However, in this paper, the victim systemfs bandwidth was relatively wide, thus eliminating the difference in power between the spectral peaks. We also concluded that the average BER degradation were gradually improved with increasing bandwidth of the victim system.

## HIGH RESOLUTION UWB INDOOR LOCALIZATION SYSTEM OPERATING AT 8 AND 24 GHZ UTILIZING TIME DIFFERENCE OF ARRIVAL APPROACH

Zhang, C.<sup>1</sup>, Kuhn, M.J.<sup>2</sup>, Brandon, M.<sup>2</sup>, Fathy, A.E.<sup>1</sup>, Mahfouz, M.<sup>2</sup>

<sup>1</sup>ECE Department, University of Tennessee, Knoxville, TN 37996

<sup>2</sup>MABE Department, University of Tennessee, Knoxville, TN 37996

Currently, there is a great demand for wireless localization systems to cover numerous indoor applications such as asset tracking, surgical navigation, indoor GPS, etc. The most important feature of these systems is their accuracy, which is highly susceptible to multipath effects in an indoor environment. Generally, there are many approaches to achieve accurate localization[1]; however FMCW and UWB techniques have relatively high potential with regard to ranging resolution.

We have developed an accurate ultra wideband localization technique based on a time difference of arrival (TDOA) approach[2]. The developed method provides sub-centimeter accuracy, which is excellent for indoor utilization as compared to FMCW systems. This developed method is also compliant with FCC UWB regulations. The utilized time domain measurements suppress multipath signals and even have potential for sub-millimeter resolution. Excellent localization results for our UWB system at 8 GHz have been previously demonstrated[2].

Recently, we have extended the capability of this set-up from a two dimensional to a three dimensional localization system, and we have developed a new system operating at 24GHz. Detailed comparisons to the previously built 8 GHz system, our hardware development, optimization algorithms, and experimental results will be presented in this paper in detail.

Most of the components that comprise this system have been designed and fabricated in-house. For example, a pulse generator with an adjustable pulse width from 300 to 700ps has been developed as the source of our UWB positioning system. It can produce either Gaussian or Monocycle pulse shape signals. A broadband omni-directional patch antenna has also been designed and applied in our positioning system. The patch antenna allows the transmitter to have a small size and low cost. In addition, a novel nearly-base band UWB mixer has been developed[3] for our UWB positioning system. Details of these developments will be presented as well.

[1] Wireless local positioning, M. Vossiek, L. Wiebking, P. Gulden, J. Wieghardt, C. Hoffmann and P. Heide in IEEE Microwave Magazine, Volume 4, Issue 4, Dec. 2003, pp. 77-86.

[2] Accurate UWB Indoor Localization System Utilizing Time Difference of Arrival Approach, by Cemin Zhang, Michael Kuhn, Brandon Merkl, Aly E. Fathy and Mohamed Mahfouz, to be presented in the IEEE Radio and Wireless Symposium, Jan. 2006, San Diego, Ca.

[3] A Novel Ultra Wideband Uniplanar Subharmonic Mixer for Near-Base Band Applications submitted by Song Lin, Yunqiang Yang, Aly E. Fathy for URSI 2006 Symposium, Boulder, Co.

## STRUCTURE FUNCTION AND EMPIRICAL MODE DECOMPOSITION BASED FEATURE EXTRACTION METHOD FOR RADAR PULSE SEQUENCES

Guo Qiang<sup>2</sup>, Zhang Xingzhou<sup>1</sup>, Li Zheng<sup>2</sup><sup>1</sup>College of Information and Communication Engineering, Harbin Engineering University.<sup>2</sup>National Key Laboratory of Electronic Warfare.

**Abstract:** Modern electronic warfare faces complex and dense pulses environments, which brings a severe challenge to radar signal sorting. A new feature extraction method for radar pulse sequences was presented based on structure function and empirical mode decomposition in this paper. The 2- dimension feature information was constituted with radio frequency and time-of- arrival in this method, which analyzes the feature of radar pulse sequences for the very first time by employing structure function and empirical mode decomposition. The experiment result shows that the method can extract efficiently the frequency that of the period-change radio frequency signal in the complex pulses environment and find out a new feature for the signal sorting of interleaved radar pulse sequences. This paper provides a total new ideal to extract the new sorting feature of radar signals. Radar signal sorting is a vital part of electronic intelligence system (ELINT) and electronic support measures (ESM) processing. We can analyze and extract the parameters of radar emitte signals only based on sorting. Therefore, signal sorting is a key technology to electronic countermeasures. With all kinds of complex-systems radars emerging and pulse's density increasing, the current low-efficiency method (e.g. histogram[1-4], clustering[5-7], etc.) based on five parameters which include time-of-arrival (TOA), radio frequency (RF), pulse width (PW), direction of arrival (DOA) and pulse amplitude (PA) cannot adapt to the complex-variety and high-density pulses environment in modern electronic warfare. It urgently demands use of the current instantaneous pulse parameters to look for the new sorting feature so that we can obtain a new sorting way. According to variant characteristics of instantaneous pulse parameters for radar emitte signals, a feature extraction method for the radar pulse serial signal based on structure function and empirical mode decomposition (EMD) was presented. It can extract agile frequency of the period-change RF signal (e.g. sine regulation) from radar pulse sequences containing complex-variety feature. Thus, the sorting of this kind of signals is possible. The validity of the feature extraction method was demonstrated by simulation experiment.

## ERROR VARIANCE ESTIMATION IN BAYESIAN REFRACTIVITY FROM CLUTTER INVERSION

Caglar Yardim<sup>1</sup>, Peter Gerstoft<sup>2</sup>, William S. Hodgkiss<sup>2</sup>, Ted Rogers<sup>3</sup>

<sup>1</sup>Electrical and Computer Engineering Department, University of California, San Diego

<sup>2</sup>Marine Physical Laboratory, Scripps Institution of Oceanography, University of California, San Diego

<sup>3</sup>Atmospheric Propagation Branch, SPAWAR Systems Center, San Diego, CA

## Error Variance Estimation in Bayesian Refractivity from Clutter Inversion

A common occurrence in low altitude sea-borne radar applications is ducting. Its effects can be calculated using the modified index of refraction (M-profile). An approach for estimating M-profiles is Refractivity From Clutter (RFC). In a heavily ducted environment, there is strong interaction with the sea surface and sea clutter is much higher than it would be in a standard atmosphere. Therefore, radar clutter returns can be a rich source of information about the environment the radar is operating in. RFC uses this clutter return to estimate the modified refractivity profile.

The inversion problem is formulated in a Bayesian framework. A likelihood formula is defined using the radar clutter return and a non-informative prior and a range-independent M-profile is used for simplicity. Maximum a posteriori solutions are calculated by use of a genetic algorithm (GA) while Bayesian minimum mean square error estimates and other necessary multi-dimensional Bayesian integrals are calculated using a hybrid genetic algorithm Markov chain Monte Carlo (GAMCMC) sampler. An electromagnetic split-step fast Fourier transform parabolic equation propagation model is used as a forward model. The posterior probability distributions of the unknown duct parameters are estimated. Then they are used to calculate propagation factors and coverage diagrams, which can be incorporated into radar performance predictions.

The likelihood depends on the probability distribution of the errors. The errors are assumed to be Gaussian distributed with zero mean and a full covariance matrix. Often, the errors are assumed to be independent, identically distributed with constant variance. However, this actually is not an accurate model in RFC. The error variance changes with range and errors can also be correlated depending on the propagation conditions. Based on the observed statistics of the errors, various methods of obtaining the covariance matrix will be presented. Their effects on the overall inversion results will also be discussed.

STRUCTURE OF COHERENCE BETWEEN MAGNETIC FIELDS  
AT ACE AND GOES-10

Thomson, D.J.  
Queen's University.

The presence of persistent periodic components in earth's ionosphere and magnetosphere have been reported for decades but have remained controversial. Here I show evidence that they are forced by the normal modes of the sun and describe some of the reasons for the controversy.

First, coherences computed between the  $Y$  and  $Z$  (duskward and poleward) components of the magnetic field at the ACE spacecraft are found to be highly coherent with the  $hn$  and  $hp$  ( $\approx$  East and North) components of the magnetic field on the GOES-10 geosynchronous satellite out to the common Nyquist frequency of  $\approx 8mHz$ . (The radial components appear to be less coherent.) This coherence is easily detected using multitaper methods and, on single blocks of several days duration, it is typical to have more than 50% of the estimates above the nominal 90% point with particularly high coherences in the  $3mHz$  band associated with solar  $p$ -modes. AS a specific example, the magnitude-squared-coherence (MSC) between ACE  $Z$  and GOES  $hn$  in Jan. 1999 exceeded 0.94 between  $\sim 2800$  and  $3300\mu Hz$ , significant at over  $7\sigma$ . Canonical coherences between the two pairs of components at ACE and GOES are even higher. Despite the presence of such high coherences on individual blocks of a few day's duration, simple calculations of the long-term average coherence give low values. There appear to be three distinct reasons for this: First, the ratio of peak-to-background spectrum at ACE has a pronounced two cycle/year dependency that is 180 degrees (3 months) out-of-phase with the usual Russell-McPherron dependency of geomagnetic "disturbances" Second, the phase of the coherences computed at different times vary. Third, as one should expect, the coherences between ACE and GOES shifted by one cycle/day ( $11.57\mu Hz$ ) are commonly higher than coherences at the same frequency. Thus, taking data segments too short to resolve a few  $\mu Hz$  give particularly unreliable coherences.

An explanation for these observations is that, in the solar  $g$ - and  $p$ -mode bands, the phase estimates imply propagation at nearly the speed of light (that is the fast plasma mode) but, above the  $p$ -mode band, propagation drops to the Alfvén speed. The velocity of propagation in a plasma depends critically on the plasma density, so the varying density of the solar wind modulates the phase shift seen between ACE and GOES. The modal signals are also coherent with solar surface velocity measured by the GONG network, pointing unequivocally to a solar source.

## INVESTIGATION OF USING FERROELECTRIC MATERIALS IN HIGH POWER FAST RF PHASE SHIFTERS FOR CHARGED PARTICLE ACCELERATORS

Joshua Wilson<sup>1</sup>, Yoon Kang<sup>2</sup>

<sup>1</sup>University of Tennessee, Knoxville

<sup>2</sup>Spallation Neutron Source Project, Oak Ridge National Laboratory, MS-6474, Oak Ridge, TN 37831, U.S.A.

A fast ferroelectric phase shifter is being investigated for high-power RF vector modulation. Such a device could be used in charged particle accelerators, allowing vector control of the RF power delivered to accelerating RF cavities. This will save construction and installation cost by reducing number of klystrons; allowing many cavities to be powered by a single high-power klystron, while maintaining control over the input to each cavity. A vector modulator is constructed using two of these phase shifters connected to a quadrature hybrid junction. By varying the phases of these shifters independently, one can control amplitude and phase of the output signal. Ferromagnetic materials have previously been developed for high-power phase shifters in accelerators, but the response of these devices tends to be slow since it is difficult to change the bias magnetic field quickly.

Bulk ferroelectric materials, particularly those based on barium-strontium titanate compounds, have shown promise in high-power applications because of their low loss tangent and high dielectric strength. Phase shifting is affected by changing the permittivity through application of a bias electric field. Such materials have already been investigated for use in fast phase shifters at X-Band frequencies [1]. Several different compositions of barium-strontium titanate compounds are tested at frequencies from 100 MHz to 2 GHz that could be used for future large-scale accelerator projects employing superconducting RF cavities. The ratio of barium versus strontium in the composition is varied from sample to sample. This allows an investigation of the tradeoffs involved between dielectric strength, loss tangent, tunability, and relative permittivity. Since ferromagnetic materials have also been investigated for this application, a comparison is made between phase shifters employing ferromagnetic materials and those employing ferroelectric materials. Both qualitative and quantitative comparisons are presented.

Since ferroelectrics are by nature nonlinear dielectric compounds, the effects of nonlinearity on the propagation of the high-power RF signal are of concern. Harmonic generation and shock waves could be produced if care is not taken. Preliminary research on the effect of these nonlinearities is conducted through computer simulation. The simulations give rough estimates of the amount of distortion, aiding the evaluation of the feasibility of this phase shifter concept.

[1] V.P. Yakovlev, O.A. Nezhevenko, and J.L. Hirshfield, Fast X-Band Phase Shifter, Advanced Accelerator Concepts: Eleventh Workshop, 2004

\* SNS is managed by UT-Battelle, LLC, under contract DE-AC05-00OR22725 for the U.S. Department of Energy.



Session D1, 15:15 – Thurs.

**ELECTRONIC AND PHOTONIC  
DEVICES**

Co-Chairs: J. Bernhard, F. Zhao

D1

## UHF AND L-BAND 4H-SiC RF BIPOLAR TRANSISTORS

F. Zhao<sup>1</sup>, I. Perez-Wurff<sup>1</sup>, J. Torvik<sup>1</sup>, B. Van Zeghbroeck<sup>1,2</sup>

<sup>1</sup>Boulder Advanced Technology Center, Advanced Power Technology, Boulder, CO 80301, USA

<sup>2</sup>Department of Electrical and Computer Engineering, University of Colorado, Boulder, CO 80309, USA

4H-SiC BJTs are promising RF power devices for radar, avionics and communication applications due to their ability to handle larger bias voltage and power density compared to their silicon counterparts, because of the 10 times larger breakdown field of SiC. The combination of these performance advantages with the superior thermal conductivity of SiC leads to compact and rugged RF power amplifiers for high power level and long pulse applications. Researchers at Advanced Power Technology have made significant progress towards developing high power RF 4H-SiC BJTs, and in this paper we will describe devices with potential for high power UHF and L-band operations.

UHF high power amplification was demonstrated using 4H-SiC BJTs fabricated on a conductive substrate with optimized design. Devices with the  $f_T/f_{MAX}$  of 2.5/2.4 GHz and blocking voltage larger than 200 V without junction termination were operated in class A. Under pulsed conditions at 450 MHz a maximum output power of 215 W was achieved with a power gain of 7.5 dB, corresponding to a power density of 4.13 W/mm.

4H-SiC BJTs with L-band performance were designed and fabricated on a semi-insulating substrate which completely removes the effect of the parasitic capacitance of the base-collector pads. A record  $f_T/f_{MAX}$  of 7/5.2 GHz was obtained. In class A operation at 1 GHz, devices exhibited 10 dB of power gain with less than 0.1 dB pulse droop and a peak power density of 2.3 W/mm under pulsed conditions, and 8 dB power gain at a power density of 1.6 W/mm under CW conditions. The RF performance remained practically unchanged from room temperature up to 75°C and the power gain decreased by slightly 1 dB at 125°C.

\* This work was supported in part by NIST/ATP.

## A NOVEL UNIPLANAR SUBHARMONIC MIXER FOR NEAR BASEBAND UWB APPLICATIONS

Song Lin , Yunqiang Yang , Aly E.Fathy

The ECE Department., University of Tennessee., Knoxville,TN,37996

An ultra wideband uni-planar sub-harmonic mixer1 has been designed for ultra-wideband applications. This mixer is designed to operate at RF frequencies ranging from 8 to 12 GHz. The mixers IF frequency is nearly base-band as it covers an extremely wide range from 0.1GHz to 2GHz. Using short pulses as the IF signal would obtain some advantages over conventional narrow band radars, especially for ranging applications. The LO frequency is adjustable from 4.9 GHz to 5.1 GHz.

The sub-harmonic mixer uses an anti-parallel diode pair to generate a non-linear conductance waveform at twice the frequency of the applied LO signal. Therefore, the required LO frequency is half that of the RF signal. This mixer also employs a low-pass filter, a narrowband-pass filter, a wideband-pass filter, and radial line stubs to sustain high isolation between various ports over the ultra wide band operating range. This design was implemented using a uni-planar microstrip line structure to facilitate on-chip design and fabrication.

The fabricated unit was experimentally evaluated, and the measured results agree well with the simulated ADS results. The ultra wideband mixer has an SSB conversion loss of less than 13 dB over a wide range of 8 to 12 GHz and requires only 7 dBm LO drive level. The designed mixer has excellent LO to RF isolation, where the measured LO to RF isolation exceeded 40 dB within the LO frequency range of 4.9 GHz to 5.1 GHz. The developed unit was successfully used to build an ultra-wide band receiver2, 3 for see thru wall applications. The design and analysis of the mixer circuit, using the non-linear harmonic balance method, and the measurement results of the fabricated unit, including the detection of pico-second narrow pulses, will be presented in detail in this paper.

### Reference:

- [1]. "A 140-170-GHz low-noise uniplanar subharmonic Schottky receiver" by Gauthier, G.P.; Raskin, J.-P.; Rebeiz, G.M.; MTT, IEEE Trans. on Vo. 48, Issue 8, Aug. 2000 pp.1416 1419
- [2]. "Ultra-wideband radar Ultrawideband and Ultrashort Impulse Signals", by Immoreev, I.; Ziganshin, E.; 2004 Second International Workshop 19-22 Sept. 2004, pp.211 213.
- [3]. "Development of SAR-Based UWB See Through Wall Radar System" presented by Y. Yang, at IEEE-MTT 2005 Symp. See Thru Walls Workshop, Long Beach, CA.

## SIC HIGH EFFICIENCY WIDEBAND POWER AMPLIFIERS

Kanamaluru, S., McGinty, F., Samay, S.

Sarnoff Corporation, 201 Washington Road, Princeton, NJ 08543-5300

The Joint Tactical Radio System (JTRS) program of the United States Department of Defense (DoD) is to develop a family of software programmable radios that function from 2 2800 MHz, and are designed to provide reliable multi-channel voice, data, imagery, and video communications - and eliminate communications problems caused by "stovepipe" legacy systems. The radios support a number of legacy (e.g., FM) and advanced (e.g., Wideband Networking Waveform, a.k.a., WNW) waveforms. The radios are of different form factors, ranging from handheld versions with up to 5W RF output to rack-mounted versions with more than 100W RF output.

Many JTRS radios, especially the small form factor (SFF) versions will have a single RF power amplifier (PA) that supports a very wide bandwidth, typically exceeding several decades. Moreover, the SFF radios operate using batteries. The battery operation places a premium on power efficient sub-systems of the radio, primarily the PA, to extend mission operational time. The high efficiency requirement for the SFF radio PA is in addition to the other stringent requirements required of all JTRS PAs, namely linearity, wide bandwidth, and very low spurious and harmonics.

Highly efficient power amplifiers are currently available, and have been designed for narrowband niche applications such as mobile base stations and DoD narrow band radios. The design of wideband power amplifiers is a challenge, especially when coupled with stringent linearity requirements. Typically, Class A amplifiers offer the highest linearity albeit, with reduced efficiency. Classes AB, B, C, D, and F offer increasing efficiencies with corresponding decrease in linearity. Classes AB and B amplifiers offer a compromise between efficiency and linearity when operated in a push-pull mode. Class B push-pull amplifiers offer a theoretical efficiency of 78.5% (at saturation) and have the additional benefit of reducing all even order modes. Further, these amplifiers provide broader bandwidth than single ended amplifiers. The use of a linearizer provides an additional degree of control over the linearity of the power amplifier module. These linearizers provide a pre-distorted signal to the power amplifier input, such that the amplifier output is linear.

Sarnoff Corporation is currently developing a 20W High Power Amplifier (HPA) as a Line Replaceable Unit (LRU) for the JTRS radios. Our HPA utilizes silicon carbide (SiC) HEMTs in a Class AB Push-Pull configuration, to achieve high efficiency, linearity, and wide bandwidth. Preliminary measured results show that more than 50% power added efficiency (PAE) can be achieved for multi-octave bandwidth. Inter-modulation distortion (IMD) less than 20-dBc for up to P1dB of the PA is achieved without the use of any linearizers. Additional design details and measured results of the HPA, including the linearizer will be presented at the conference.

## TWO TRANSFORMER MATCHING OF LASER DIODES FOR INCREASED RF DRIVE EFFICIENCY

Kim, E.M.<sup>1</sup>, Hu, Y.<sup>2</sup>, Lumori, M.L.D.<sup>1</sup><sup>1</sup>University of San Diego, 5998 Alcalá Park, San Diego, CA 92110<sup>2</sup>Lightwave Solutions, 8665 Miralani Drive, San Diego, CA 92126

Efficient RF signal excitation of semiconductor laser diodes is becoming critical in Cable Television (CATV) transmission due the increased bandwidth demand of current and future broadband video and data content. In order to transmit higher bandwidth content with the required signal quality, each fiber optic transmitter delivers signal to smaller numbers of subscribers. This transmission architecture requires the use of larger numbers of semiconductor laser diode transmitters that are driven by 75 Ohm RF broadband high power amplifiers. The RF output of each broadband amplifier is divided among large numbers of transmitters. In order to drive the maximum number of transmitters per 75 Ohm RF power amplifier, each laser diode transmitter must be efficiently driven.

Semiconductor laser diodes typically exhibit dynamic resistances of 6 to 8 Ohms. In order to more closely match the  $S_{22}$  of 75 Ohm RF broadband high power amplifiers, Distributed Feedback (DFB) laser diodes include a series 25 Ohm resistor built in its laser diode package. For better impedance match to a 75 Ohm RF power amplifier, circuit designers typically use a series 35 to 40 Ohm resistor in series with the packaged 25 Ohm resistor and semiconductor laser diode to yield an acceptable  $S_{11}$  of the laser drive circuit to the 75 Ohm RF power amplifier. Unfortunately, using the internal 25 Ohm series matching resistor of the laser diode package results in drive power loss that reduces the RF efficiency of the laser diode package.

RF signal drive efficiency has been increased by using two commercially available broadband RF transformers in series with ratios of 1.5:1 and 4:1 in series with a 6.2 Ohm resistor to drive a coaxially packaged laser diode without an internal resistive matching element. The use of two series matching transformers has resulted in decreasing required RF drive power by 6 dB over drive circuits with the 25 Ohm series matching resistor. The resulting laser diode and its matching network show substantially improved  $S_{11}$  over resistive matching (with 25 Ohms) with flat broadband frequency response characteristics.

Session E1, 10:15 – Wed.

**HIGH-POWER  
ELECTROMAGNETICS, NOISE  
AND INTERFERENCE**

Co-Chairs: I. Kohlberg, C. Ropiak





ASPECTS OF RANDOM-LAY  
MULTICONDUCTOR-CABLE PROPAGATION WHICH ARE NOT  
STATISTICAL

Baum, Carl E.  
University of New Mexico

The interaction of electromagnetic fields with complex electrical and electronic systems gives us a very difficult or even intractable problem to fully analyze. Part of the problem lies in the very description of the system itself which can have various uncertainties (e.g., wire location, joint corrosion, etc.). Two copies of the same system type (aircraft model, ship model, etc.) may have significant differences in their responses. How, then, should one approach the interaction analysis in such cases?

Many practical multiconductor transmission lines can be considered as random-lay cables in which the wires assume various positions in the transmission-line cross section. This paper considers some of the properties of propagation on such structures. In particular some aspects of such propagation are deterministic in nature. Such conclusions are based on low- and high-frequency considerations, and symmetry. Furthermore, reciprocity and energy conservation place restrictions on the allowable statistical distributions.

One approach to this problem is statistical in nature. One makes certain parameters of the problem (position coordinates, impedance values, etc.) random variables, and from this attempts to find distribution functions for the electromagnetic response parameters (voltages, currents, fields). This has been applied with some success to cavities, including mode-stirred chambers and related system response.

There has been some attempt at a statistical description for the response of random non-uniform multiconductor transmission lines (random NMTLs or RNMTLs). This is the subject of the present paper. As we shall see, there are certain aspects of this problem which are deterministic rather than statistical.

Here we consider the physics of the problem to obtain constraints on RNMTL response. After summarizing the general product-integral formulae, various constraints are imposed. These include reciprocity and conservation of energy. There are also special cases for low- and high-frequency response. Then some implications of geometrical symmetry are explored.

## SYMMETRY IN LOW-IMPEDANCE MAGNETIC ANTENNAS

Baum, Carl E.

University of New Mexico

A previous related paper [C.E. Baum, Compact, Low-Impedance Magnetic Antennas, Sensor and Simulation Note 470, 2002] gives the basic geometry of the segmented-loop antenna. Several possible geometries were considered, including the case of a four-loop array fitting in a rectangular parallelepiped. The symmetry provides equal currents (at low frequencies) in the four loops.

Not considering the connection near the coordinate origin to the source, this loop structure has three symmetry planes:  $x=0$ ,  $y=0$ ,  $z=0$ . We can also note that the three coordinate axes are also two-fold rotation axes. If we constrain  $a = b$  then there are two additional symmetry planes:  $x = y$ . Also the  $z$  axis becomes a 4-fold rotation axis and we now have four two-fold axes;  $x$ ,  $y$ , and bisectors of those two axes. In the present paper we extend the previous results to include the geometry near the coordinate origin. This is followed by the inclusion of some of the pulse-power equipment.

Now let us introduce other conductors in the loop geometry. This will aid in the inclusion of the pulse-power equipment. An interesting possibility considers the loop bisectors. Except for the small region near the coordinate origin, the 4-loop array has three symmetry planes, as discussed previously. The currents are symmetric with respect to the  $z = 0$  plane, making the magnetic field perpendicular to this plane on the plane (except near the origin). Thin conductors on this plane which carry no net current do not interfere with the loops. For there to be no current (net) the voltages between the plus junction and neutral, and minus junction and neutral must balance.

A differential Marx generator is appropriate for inclusion with the neutral conductors. Taking such conductors as a metal tube we have the two halves (+ and -) parts on opposite sides of the tube. Each represents a source connected to the junctions. Note that the Marx columns are approximately parallel to the neutral tube, and connect to this tube at some distance away from the junctions. They also have a source impedance to be included in the calculations.

PERFORMANCE AND SURVIVABILITY OF COMBINED RANDOM AND STATIC TELECOMMUNICATION NETWORKS IN ELECTROMAGNETIC INTERFERENCE BACKGROUNDS

Kohlberg, I.

Associates, Inc., Reston, VA, 20190

Integrating data networks into a large system that generates varied types of information at different bit rates is of increasing importance to both the civilian and military infrastructures. A similar, but drastically scaled down version of integrating different types of radio systems from ELF to SHF satellite links and land lines, occurred during the Cold War. At that time the physical integrity of the nodes was a serious consideration, as well as being able to communicate through nuclear stressed propagation backgrounds. Required information rates were, however, extremely low by today's standards. The location of nodes and links were, however, known at all times, as were the EMC hardening levels necessary to achieve a desired Probability-of-Survival between a pair of command posts. Forming integrated telecommunication systems is different today. A major difference between then and now is that relatively few nodes were used then, compared with the thousands of sensor and communication nodes used in today's integrated systems. For example, ad-hoc wireless mobile networks that originate, receive, and relay messages between themselves without a relay tower that is typical of a common cellular system, can be a key component of large information systems. The positions of the nodes are not fixed; they are random. Their positions are not controlled and many of the nodes could end up in configurations that cause destructive electromagnetic interference. This weakens the integrity of the entire system. This paper deals with quantifying the interference conditions that cause breakup of a random network into isolated clusters, and the effect this breakup has on the non-random part of the integrated system. Analytical tools are developed to assess the survivability and performance of a large combined system. The theoretical tools are based on random graph theory and percolation theory. These theories show that the survivability of a random network increases when nodes have sufficient link coupling to support the creation of a network spanning cluster.

## DYNAMICS OF POWER AND TELECOMMUNICATIONS RECOVERY FOLLOWING A HEMP INSULT

Kohlberg, I. , Clark, J.<sup>1</sup> , Morrison, P. <sup>2</sup><sup>1</sup>Kohlberg Associates, Inc., Reston, VA 20190<sup>2</sup>Telcordia<sup>3</sup>SAIC

Today's electric power grid relies on public data networks for a small fraction of its real-time data requirements. This dependence is expected to grow substantially in the near future. While public data networks may be more efficient and cost-effective for power companies under normal operating conditions, it is not clear that this level of reliance on real-time data provided by public data networks reduces the combined susceptibility of power and telecommunications infrastructures. A mathematical model describing the coupled dynamics between the power and telecommunication infrastructures following an attack on the U.S. from a high-altitude nuclear detonation is developed which incorporates experience-based analytical models of telephone network recovery. We address the question of whether or not these dynamically coupled infrastructures will recover from a HEMP attack. Solution of the developed non-linear equations identifies a scenario we call negative reinforcement. This is the case where the power grid and supporting telecommunication networks both collapse due to their mutual interdependence, whereas they would not collapse if they were not dynamically coupled. The same theory that predicts negative reinforcement also predicts conditions for the opposite case, mutual recovery. This is the case where both infrastructures recover when they are dynamically coupled. The interdependency equations show there are four dimensionless parameters that determine whether the combined systems will recover or collapse: the fraction of telecommunication equipment required to provide a positive growth of power, the fraction of telecommunication equipment at the beginning of the joint power-telecomm recovery process, the fraction of power available at the beginning of the joint power-telecomm recovery process, and another dimensionless parameter defined in the equations. Illustrative examples are rendered that depict negative reinforcement and mutual recovery.

Session F1, 13:35 – Wed.

## **ATMOSPHERIC PROPAGATION**

Co-Chairs: E.R. Westwater, K. Chamberlin



PROPAGATION MEASUREMENTS IN THE COASTAL OCEANIC  
EVAPORATION DUCT AT 45 GHZ

Hampton, J. R., Jones, S. D., Merheb, N. M. , Paunil, D. E.  
Johns Hopkins University Applied Physics Laboratory, 11100 Johns  
Hopkins Road, Laurel, MD 20723-6099

This paper presents results from a series of experiments that were conducted to measure the effect of evaporation ducting on propagation path loss at 45 GHz. The tests were performed in February and June of 2005 off the Mid-Atlantic coast near Ocean City, Maryland. Testing involved transmitting a tone from a research vessel (RV) and measuring the signal strength of the tone at several receivers positioned along the coast in high-rise hotels, ranging in height from 19 to 50 meters. Path loss, which was computed as a function of distance between the RV and the various receiver locations, was estimated by computing the FFT of the received signal and examining the amplitude of the appropriate frequency bins containing the tone energy. By calibrating the receivers appropriately, it was possible to map the FFT magnitudes of the tones to actual received power levels, which, when compared to the known transmit power, provided a straightforward means of estimating the path loss. This process was repeated as the RV moved along a relatively straight course beginning close to shore (about 4 km) and continuing out to about 55 km at its furthest point. Data was collected during a total of eight days, four in February and four in June.

In addition to measuring signal strength, meteorological data was also collected on the RV to help characterize the evaporation duct height and to produce refractivity height profiles, which were used to identify the presence of surface and elevated ducts. The evaporation duct height was inferred from measured air and sea temperature, relative humidity, wind speed, and atmospheric pressure. The refractivity profiles were obtained from measurements made by rocketsondes launched from the RV. The meteorological data were collected periodically during the course of the experiment. In the February tests, the evaporation duct heights were observed to vary between about 3 and 9 meters, and no significant surface or elevated ducts were present. During the June tests, the opposite conditions were observed negligible evaporation ducting, but occasional pronounced surface and elevated ducts.

The paper presents plots of measured path loss versus over-water path length. In order to facilitate the interpretation of these results, reference curves are superimposed on these plots showing free space path loss and path loss due to the refractivity effects of a standard atmospheric model. The impact of ducting on path loss is readily observed by comparing the measured path loss with the reference curves. The February 2005 results show that evaporation ducting reduces path loss by 50 dB or more relative to a standard atmosphere. It is shown that this is equivalent to more than doubling the potential communications range. The corresponding data from the June tests shows significantly less path length extension, presumably due to the near total absence of evaporation ducts during the June collection period. Further testing is ongoing at the same frequency to more thoroughly examine the seasonal impact of evaporation ducting on path loss. This study addresses the impact of evaporation ducts on propagation at a frequency for which there is little data in the published literature.

REFRACTIVITY PROFILE STATISTICS RELATED TO PROPAGATION ASSESSMENT OF COASTAL CITIES OF IRAN IN THE VICINITY OF THE PERSIAN GULF

J. Goldhirsh

Johns Hopkins University, APL

Statistics associated with ducting and non-ducting profiles were examined for three coastal cities, located in the vicinity of the Persian Gulf; namely, Bushehr, Bandar Abbas and Cha Bahar. The results were compiled from a database of pressure, temperature and dew point measured from approximately 1000 radiosondes during the spring-summer of 1973 and winter of 1974 by the U.S. Air Force (Ko et al., "Refractivity Profiles for the Persian Gulf," Technical Report STD-N-522, Applied Physics Laboratory, Johns Hopkins University, Laurel, MD Sept 27, 1987.) Modified refractive index-height profiles were calculated from these radiosonde measurements, and cumulative density distributions of duct heights and duct slopes were subsequently determined for both bi-linear and tri-linear surface-based ducts. Non-ducting profiles were also statistically examined in terms of K-Factor and layer-heights. The layer-height for the non-ducting profile was assumed to correspond to the first significant height level of the radiosonde measurement, above which, the profile was assumed to have a refractivity-height slope corresponding to that of a standard atmosphere. The likelihoods of propagation conditions such as ducting, superrefraction, subrefraction and extreme subrefraction were determined for each of the coastal locations. Typical or "most-probable" profiles were generated for bi-linear, tri-linear ducts and non-ducting cases for both spring-summer and winter periods. This is the first time profiles have been determined for the Persian Gulf such that duct-heights or layer-heights were correlated with slopes of the modified refractive index below them. For example, Bushehr, the most northern of the above mentioned cities near the middle latitude of the Persian Gulf, showed for the spring-summer period that the most-probable bi-linear duct had a height of 180 m and a correlated duct slope below it of  $-125$  M/km down to the surface. The slope above the duct-height was assumed to be standard. This contrasts with the most-probable bi-linear duct for the winter period, for which the duct-height was 100 m and the duct slope below it was  $-25$  M/km. The most-probable non-duct profile during the winter period was found to have a K-Factor of 1.35 from the surface up to a layer-height of 95 m. Based on 247 radiosondes measurements for Bushehr during the spring-summer period, ducting occurred 92% of the time. This compared to 21% of the time during the winter relative to 92 radiosondes. Of the ducting cases during the spring-summer period, 69% were of the bi-linear type and 31% were tri-linear. A comparative description of similar types of propagation related statistics for the three coastal locations will be presented.



CHARACTERIZATION OF THE MEASUREMENT UNCERTAINTY  
AND STABILITY OF A MINIATURIZED WATER VAPOR RA-  
DIOMETER BASED ON MMIC TECHNOLOGY

F. Iturbide-Sanchez<sup>1</sup>, S. C. Reising<sup>1</sup>, R. W. Jackson<sup>2</sup>  
, S. Padmanabhan<sup>1</sup>

<sup>1</sup>Microwave Systems Laboratory, Electrical and Computer Eng. Dept.,  
Colorado State University, Fort Collins, CO 80523

<sup>2</sup>Laboratory for MM-Wave Devices and Applications, Electrical and  
Computer Eng. Dept, University of Massachusetts, Amherst, MA 01003

A Miniaturized Water Vapor Radiometer (MWVR) based on Monolithic Microwave and Millimeter-wave Integrated Circuit (MMIC) technology has been developed, fabricated and tested at the University of Massachusetts Amherst and Colorado State University. The MWVR is designed to profile the water vapor in the troposphere using four frequencies in the vicinity of the 22.235 GHz water vapor resonance.

MMIC technology has provided the capability to reduce the volume, weight and cost of instrumentation for remote sensing applications. As a consequence, MMIC-based radiometers are excellent candidates for deployment on small, light Unmanned Aerial Vehicles (UAVs) or to realize networks of significant numbers of remote sensing instruments. In addition to reductions in mass, volume and cost, MMIC technology tends to decrease the power consumption of microwave radiometers, both by increasing component power efficiency and by reducing power requirements of heating/cooling systems to maintain internal temperature stability.

The MWVR is a Dicke radiometer in which gain calibration is achieved both by external calibration, i.e. tipping curves and viewing an ambient microwave absorber load, and by internal calibration, i.e. a two-point calibration internal to the radiometer. MMIC-based radiometers can be implemented in small volumes and with low power consumption compared to waveguide-based or connectorized component radiometers. Therefore, maintaining stable internal temperature tends to be easier for these low-power, low-volume radiometers.

Radiometric sensitivity ( $NE\Delta T$ ) is commonly used to characterize the measurement precision of a microwave radiometer. However, the uncertainty of brightness temperature measurements depends not only on radiometric sensitivity but also on other factors, such as accuracy and stability of internal/external calibration reference sources, algorithms to combine internal and external calibration, and the stationarity of gain variations between successive calibrations. The stability and measurement uncertainty of the MWVR are evaluated under field measurement conditions using tipping curves and ambient microwave absorber calibrations performed over long time durations and observed on each of MWVR's four frequency channels.

Finally, the feasibility of ground-based network operation is considered, using low-mass, low-volume radiometers to retrieve 3D estimates of the water vapor in a given atmospheric volume using tomographic inversion techniques. A network consisting of MWVRs performing coordinated scanning of the troposphere would have spatial resolution determined both by vertical profiling and by antenna beamwidth considerations.

## TOWARDS A DIAGNOSTIC AND PROGNOSTIC LITTORAL RADIO FREQUENCY PROPAGATION PRODUCT

Robert E. Marshall

Naval surface Warfare Center, Dahlgren, VA

The diurnal characteristics of the thermodynamic structure of the coastal atmospheric boundary layer lead to spatio-temporal refractivity structures in the littorals. Daytime heating of the land surface potentially creates low-level circulations that alter the vertical distribution of temperature and humidity to approximately 50 kilometers offshore. With offshore winds, stable surface layers created onshore at night due to radiational cooling transition from thermodynamically stratified surface layers to well mixed layers approximately 100 kilometers from the shoreline. Complex coastline shape and tidal exchanges that alter littoral sea surface temperature fields will impose spatially inhomogeneous characteristics on these diurnal effects. For a littoral navy attempting to maintain a cooperative engagement capability consisting of multiple RF sensors and communication systems, the ability to diagnose and forecast evolving coastal propagation fields is essential.

This paper will present the results of initial work to demonstrate the spatio-temporal structure of RF propagation in the littorals using high-resolution numerical weather prediction (NWP) modeling. Validation efforts with high resolution Wallops Island 2000 Microwave Propagation Measurement Experiment data will be presented.

NWP enjoys a nearly 75-year history recently dramatically driven by the rapid advances in computing technology. This has facilitated the ability to resolve the smaller scale atmospheric boundary layer processes that create anomalous refractivity fields. Remote sensing of land and water surface characteristics that strongly influence the thermodynamic structure of the atmospheric boundary layer have also improved. These developments over the last decade have created the potential for NWP technology to quantitatively diagnose and forecast complex littoral refractivity fields.

Initial validation efforts indicate that NWP provides, at the least, a competent situational awareness of littoral anomalous RF propagation. Suggested improvements that potentially would lead to a quantitative anomalous propagation prognostic capability include a more robust and dynamic sea surface temperature field (SST), an examination of stable boundary layer parameterization schemes, and improved land surface characterization and parameterization.

DATA COLLECTION, ANALYSIS AND MODEL VALIDATION OF  
LOW-ALTITUDE PROPAGATION FOR VHF MOBILE RADIO

Chamberlin, Kent<sup>1</sup>, Barrios, Amalia<sup>2</sup>, Jenkins, Josh<sup>1</sup>

<sup>1</sup>University of New Hampshire, Dept. of Electrical Computer Engineering

<sup>2</sup>Atmospheric Propagation Branch, SPAWAR Systems Center San Diego

The Advanced Propagation Model (APM) is a terrain and atmosphere-sensitive radio propagation model that was developed by the Navy. Validation studies of the APM, where APM predictions are compared against measured data, have shown close agreement in some cases with lesser agreement in others. The objective of this study presented here is to provide additional validation data for the APM, and to focus in particular on the effects of atmospheric ducting.

To meet study objectives, a data collection site was selected where refractive index profile data were routinely measured, where atmospheric ducting would be a predominant propagation mechanism in the event that ducting occurred, and where atmospheric ducting would be likely to occur. A site that meets these criteria is in the vicinity of Albany, New York, and that is where the data presented here were collected. The approach used to measure VHF signal strength over a range of conditions was to install a calibrated receiver and GPS in a vehicle, and then travel repeatedly in the region identified to be appropriate for data collection. Using this approach, each collection effort provided thousands of data points consisting of measured signal strength as a function of receiver position. Those data points were subsequently compared against estimates provided by the APM to assess accuracy.

Data were collected over a range of weather conditions and at different times during the day. Attempts were made to collect some of the data at times most likely to coincide with atmospheric ducting conditions, although the existence of those conditions could not be confirmed until after the measurements were made. As it turned out, ducting conditions did not exist during any of the times that data were collected for this study. Consequently, the primary significance of this work is to provide additional validation data for the APM and to document a baseline for normal-propagation signal levels along with a methodology for performing future work in this area in the event that further exploration of APM sensitivity to the refractive index profile is pursued.

GROUND-BASED                      PASSIVE                      MILLIMETER-  
AND SUBMILLIMETER-WAVE OBSERVATIONS OF THE ARCTIC  
ATMOSPHERE

Cimini, D.<sup>2</sup>, Westwater, E. R.<sup>2</sup>, Gasiewski, A. J.<sup>2</sup>  
, Klein, M.<sup>2</sup>, Leusky, V.<sup>2</sup>, Dowlatshahi, S.<sup>1</sup>

<sup>1</sup>CIRES, University of Colorado, Boulder

<sup>2</sup>ETL, NOAA, Boulder

During March-April 2004, the Environmental Technology Laboratory (ETL) of the National Oceanic and Atmospheric Administration (NOAA) conducted the Arctic Winter Radiometric Experiment - Water Vapor Intensive Operational Period (WVIOP2004), at the Department of Energy Atmospheric Radiation Measurement (ARM) Programs site in Barrow, Alaska. During the WVIOP2004, a new instrument, developed at NOAA/ETL, was deployed for the first time, the multi-channel polarimetric Ground-based Scanning Radiometer (GSR). The GSR operated continuously for a month, collecting observations at twenty-five channels in the micro- and millimeter-wave spectrum (from 50 to 380 GHz), plus one infrared channel (10 mm). All the channels were pointing simultaneously in the same direction and continuously scanned the atmosphere in elevation down to about 19 deg, both sides. Thus, the GSR provided simultaneous information on the spectral and angular features of the cloudy Arctic atmosphere. The set of frequencies was selected for the simultaneous retrieval of atmospheric temperature profile, water vapor content, cloud liquid path, and cloud depolarization ratio. Particularly, the millimeter- and submillimeter-wave channels are very sensitive to low water vapor content and allow for accurate observations even in the extremely dry and cold conditions typical of the Arctic. Moreover, window channels (e.g. 90 and 340 GHz) show a large sensitivity to Arctic clouds over an extended range of liquid water content. In addition, the depolarisation ratio at 340 GHz and the possibility of radiometric ice water path retrievals are investigated. In summary, an overview of GSR measurements under a variety of conditions will be presented, together with a comparison with colocated active and passive observations, as well as simulations based on in situ balloon-borne soundings.

COMPARISONS OF MEASUREMENTS AND FORWARD MODEL CALCULATIONS OF MILLIMETER- AND SUBMILLIMETER-WAVE BRIGHTNESS TEMPERATURES FOR AN ARCTIC ATMOSPHERE.

Ed R. Westwater<sup>1</sup>, Domenico Cimini<sup>1</sup>, Vinia Mattioli<sup>2</sup>, Albin J. Gasiewski<sup>3</sup>, Marian Klein<sup>1</sup>, Vladimir Leuski<sup>1</sup>, Sally Dowlatshahi<sup>4</sup>

<sup>1</sup>Cooperative Institute for Research in Environmental Sciences, University of Colorado/NOAA, Boulder, Colorado, 80305

<sup>2</sup>Dipartimento di Ingegneria Elettronica e dell'Informazione, Università di Perugia, 06125 Perugia, Italy

<sup>3</sup>Environmental Technology Laboratory, NOAA, Boulder, Colorado 80305

<sup>4</sup>Science and Technology Corporation, Boulder, Colorado 80305

In a companion paper in this digest (Cimini et al, 2006), an overview is given of the Arctic Winter Radiometric Experiment - Water Vapor Intensive Operational Period (WVIOP2004) that was conducted near Barrow, Alaska. During the WVIOP2004, the multi-channel polarimetric Ground-based Scanning Radiometer (GSR) was deployed for the first time. In addition, the Radiometrics Corporation's Microwave Radiometric Profiler (MWRP) was also operated. The major goal of the experiment was to compare measurements of water vapour during cold (-20 to -40 deg C) and dry (Precipitable Water Vapor less than 5 mm) conditions. A variety of in situ data were available, including observations of temperature, pressure, and humidity profiles from radiosondes that carried Vaisala RS90 and chilled-mirror humidity sensors. During clear-sky conditions, comparisons of measured and calculated brightness temperatures can be made using radiosonde data inserted into absorption and radiative transfer models. For our analysis, an infrared radiometer from the MWRP was used to determine clear conditions. In addition to the calibration techniques that are described by Cimini et al.(2006), we also present a quality control method that was required because of radio frequency interference that was sometimes present in the data. Calculations of brightness temperature from five absorption models are compared with measurements: Liebe-1987, Liebe-1983, Rosenkranz-1998, Rosenkranz-2003, and Liljegren-2005. Data are taken at 7 GSR frequencies in the 50 to 56 GHz region, 7 GSR channels near 183.31 GHz, and 7-MWRP channels in the 50 to 58.8 GHz region. We also compare calculations with measurements taken by the dual-polarized GSR channels at 89 and 340 GHz. No one model is superior to the others at all frequencies, although the latter two more recent models show the best overall agreement.

Reference: Ground-based passive millimeter- and submillimeter-wave observations of the Arctic atmosphere, D. Cimini, E. R. Westwater, A. J. Gasiewski, M. Klein, V. Leuski, S. Dowlatshahi, this digest. (National Radio Science Meeting, University of Colorado at Boulder, 2006).

## MAXIMIZING GROUND STATION DOWNLOAD CAPACITY FOR LEO SATELLITES USING GENETIC ALGORITHMS

William C. Barott, Mary Ann Ingram, Paul G. Steffes

Georgia Institute of Technology, School of Electrical and Computer Engineering, Atlanta, GA

We present several techniques for maximizing the contact time between a low earth orbiting (LEO) satellite and a ground station array of electronically steered antennas. Such arrays will benefit EESS applications, promising a decreased cost and increased reliability as compared to ground stations consisting of large dish antennas. Because of their low-cost design, these arrays will enable the construction of a distributed downlink network for efficiently retrieving the ever-increasing amount of EESS science data.

The optimization for maximum contact time is necessary because the distance between a ground station and a LEO satellite is not constant throughout a pass; the signal strength incident on a ground station can vary by more than 10dB while the satellite is in view. By taking advantage of the scan loss properties of the electronically scanned fixed antennas, the array is arranged so that the aggregate gain of the array results in a received signal strength that is very close to the threshold value for demodulation, regardless of the distance to the satellite.

Genetic algorithms were chosen as the optimization method. Three optimization models will be considered:

- 1) Electronic scanning in the elevation direction and mechanical scanning in the azimuth direction: The antenna boresight directions are optimized to minimize the elevation angle at which a signal is acquired.
- 2) Total electronic scanning with fixed antennas: The boresight direction of each antenna is optimized to maximize the contact time per day by using the probability density function of the satellites position as well as the ground stations location.
- 3) Electronic scanning with mechanical repositioning: The boresight directions are optimized prior to each pass. The array is fixed and electronically scanned for the duration of a pass.

Results will be presented for the application of these models to an array of Space-fed Lens antennas that is designed to receive X-band data from the satellite SAC-C. It will be shown that by properly orienting the antennas in the array, the contact time with the satellite is greatly increased as opposed to alternative arrangements. Additionally, under certain conditions, one array can receive data from several satellites simultaneously, further reducing the cost-per-link of the ground station.

AN INVESTIGATION OF A NOVEL RADAR FOR IONOSPHERIC  
DISTURBANCES USING A GLOBAL 3-D FDTD MODEL OF THE  
EARTH-IONOSPHERE WAVEGUIDE

Jamesina Jean Simpson, Allen Taflove

EECS Dept., McCormick School of Engineering, Northwestern University,  
Evanston, IL 60208, USA

We report a finite-difference time-domain (FDTD) computational solution of Maxwell's equations (A. Taflove and S. C. Hagness, *Computational Electrodynamics: The Finite-Difference Time-Domain Method*, 3rd. ed. Norwood, MA: Artech House, 2005) to model a novel radar for ionospheric disturbances. Specifically, we study ionospheric anomalies, such as the local lowering of the effective ionospheric height above Los Angeles. Such anomalies have been hypothesized to exist prior and during earthquakes (Hayakawa, M. and Fujinawa, Y. (Eds): *Electromagnetic Phenomena Related to Earthquake Prediction*, Terra Scientific Publishing Company, Tokyo, Terrapub, 1994.), for example, and their understanding is also important for naval communication systems (Ferguson, J. A., *Computer Programs for Assessment of Long-Wavelength Radio Communications*, Version 2.0, Space and Naval Warfare Systems Center, Tech. Doc. 3030, May 1998.). Using our novel extremely low frequency (ELF: 3 - 300Hz) radar (J. J. Simpson and A. Taflove, "A novel ELF radar for major oil deposits," *IEEE Geoscience and Remote Sensing Lett.*, in press), we investigate the detectability of the ionospheric disturbance and its properties.

The FDTD technique employed in this study enables a direct, full-vector, three-dimensional (3-D) time-domain Maxwell's equations calculation of round-the-world ELF propagation accounting for arbitrary horizontal as well as vertical geometrical and electrical inhomogeneities and anisotropies of the excitation, ionosphere, lithosphere, and oceans. Our entire-Earth model grids the annular lithosphere-atmosphere volume within 100 km of sea level by following lines of latitude and longitude (J. J. Simpson and A. Taflove, "Three-dimensional FDTD modeling of impulsive ELF propagation about the Earth-sphere," *IEEE Trans. Antennas and Propagation*, vol. 52, pp. 443-451, Feb. 2004). The nominal lateral resolution is 40 x 40 km at the equator. Subgridding is used to refine the radial grid resolution in the lithosphere near the Earth's surface to 1.25 km, a factor of 4 times finer than the nominal radial resolution of 5 km used in the atmosphere and deeper within the lithosphere.





Session F2, 13:15 – Thurs.

**PROPAGATION AND  
SCATTERING FROM VEGETATION**

Co-Chairs: S. Saatchi, K. Sarabandi

## EFFECTS OF TREES ON PATH LOSS IN A VEGETATED RESIDENTIAL ENVIRONMENT - ANGULAR SPECTRAL APPROACH

Torrico, S.A.<sup>1</sup>, Lang, R.H.<sup>2</sup><sup>1</sup>Comsearch, 19700 Janelia Farm Boulevard, Ashburn, VA 20147<sup>2</sup>The George Washington University, Department of Electrical Engineering, Washington, DC 20052

Future wireless communication systems require a more precise prediction of the propagation loss between the transmitter and the receiver to improve the capacity of their systems. These systems are expected to have the base-station transmitters located close to the surrounding rooftops so that propagation takes place over the buildings. When the transmitter and/or the receiver is in a vegetated residential environment, then it is important to understand the effects of trees and buildings on the propagation loss in order to maximize the throughput of the system.

The aim of this work is to improve the approach presented by Torrico and Lang [2005 IEEE AP-S International Symposium and USNC/URSI National Radio Science Meeting, pp. s017p02u, July 3-8 2005], by taking into account the off-angle attenuation effects on the incoherent scattered fields produced by the trees. As in Torrico and Lang, the incoherent intensity produced by multiple trees/houses is added to the coherent intensity in order to predict more accurately the propagation loss between a base-station transmitter and a mobile receiver in a vegetated residential area. The vegetated residential area is modeled by parallel rows of houses/buildings each with an adjacent tree canopy. A row of houses/buildings is modeled as a half plane absorbing screen that is perpendicular to the ground. The tree canopy is modeled as an ensemble of leaves and branches all having prescribed location and orientation statistics. The shape of the tree canopy adjacent to each row of buildings is modeled as an elliptical cylinder.

The total field after the  $n$ th-row of trees and buildings is found by adding the diffracted field from the half-plane for the  $n$ th-row of buildings and the scattered field from the canopy of the  $n$ th-row of trees. The diffracted field from the half-plane of the  $n$ th-row depends on the total field at its aperture and is found by employing the Kirchhoff-Huygens technique. The total field at its aperture consists of two parts: the incident field from the previous aperture attenuated by the effective canopy medium and the scattered field from the preceding tree canopy. The scattered field from the  $n$ th-row of trees is obtained by treating the canopy by the distorted Born approximation. The total propagation loss is then computed by repeating this procedure from the first to the last aperture. The analysis is simplified by employing a transverse spectral representation of the field quantities. It is assumed that only forward scattering is important and that only single scattering within each tree canopy contributes. Results of these calculations will be presented in order to characterize the effects of trees on the propagation loss in a vegetated residential area.

MODELING AND SIMULATION OF NEAR-EARTH WAVE PROPAGATION IN PRESENCE OF A TRUNCATED VEGETATION LAYER

DaHan Liao, Kamal Sarabandi

The Radiation Laboratory, The University of Michigan, Ann Arbor, Michigan, U.S.A.

In our studies, we are currently in the process of assembling a physics-based propagation model to facilitate accurate prediction of signal path-loss among the nodes of an unattended ground sensor (UGS) network deployed in a natural environment. In a previous paper [Liao and Sarabandi, 2005], the problem of VHF wave propagation in the presence of a vegetated-terrain was treated by replacing the physical medium with an effective homogeneous two-layer medium and then applying the asymptotic dyadic Greens function to compute the radiated field distribution of an electric-dipole with the assumption that the vegetation layer is infinite in extent. In practice, the effects of any discontinuity in the vegetation layer would have to be included to accurately model the path loss between the transmitter and receiver. The geometry of a related canonical problem can be visualized if the vegetation layer is truncated in one of its two infinite dimensions in other words, in this modified problem, the ground is covered by a semi-infinite dielectric slab. An exact solution to this problem can be found through a full-wave numerical technique such as FDTD; however, for near-earth propagation problems in which the computational domain is large and the wave energy spreads out to the receiver at grazing-angles, a full-wave analysis is rather difficult to implement in an efficient and straight-forward manner.

To the best of our knowledge, the propagation effects of a truncated vegetation canopy have been analytically examined only by Tamir through a ray-tracing approach [Tamir, 1977]; while Tamir's solution is simple to construct, its accuracy has not been fully verified. In this work, we seek out to formulate a semi-exact, analytical solution to the same problem by making use of the equivalence principle; specifically, the field at an observation point located in the far field of a truncated vegetation canopy is solved by performing a surface-field integration over the vertical, fictitious 2-D plane containing the truncation facet. Since the solution contains limits of integration that are infinite, the stationary phase approximation is applied as needed to achieve computationally-efficient solutions. It is seen that for large receiver heights, a very efficient full 2-D stationary phase approximation can lead to accurate results; however, for an observation point located in the vicinity of the ground, in order to correctly capture the Norton waves emanating from the equivalent sources situated on the plane of integration close to the ground, the modified approach in the form of a 1-D stationary phase approximation augmented with numerical integration is more appropriate.

Liao, D.H., and K. Sarabandi (2005), Near-Earth Wave Propagation Characteristics of Electric Dipole in Presence of Vegetation or Snow Layer, *IEEE Trans. Antennas and Propagat.*, 53, page numbers not yet been assigned.

Tamir, T. (1977), Radio Wave Propagation Along Mixed Paths in Forest Environments, *IEEE Trans. Antennas and Propagat.*, 25, 471-477.

## COHERENT MODEL FOR VHF SCATTERING FROM FORESTS ON MULTILAYER ROUGH GROUND

Mahta Moghaddam, Alireza Tabatabaenejad  
University of Michigan, EECS, Ann Arbor, MI 48109

In this paper we present a coherent scattering model for a forest situated on top of a layered ground. The ground layers are separated by rough interfaces of arbitrary depth and dielectric constant. Scattering from forests has been studied extensively by several researchers in the past 20 years, but in all known studies the ground under the vegetation canopy has been assumed to be a single rough surface. With the recent interest and prospects for availability of radar data at the VHF band, the validity of a single rough surface model for the forest floor has to be revisited. Due to the large depth of penetration at VHF, the waves can travel well into the ground surface and scatter from subsurface layers, even for dense forests. Furthermore, realistic forests include a mix of multiple tree species, which is generally not taken into account in previous works. Here, we start from an existing coherent model for a single species forest on a single ground surface, which solves for the scattering coefficients using the distorted Born approximation. The layered ground with rough interfaces is then incorporated using a solution we have developed based on the small perturbation model that takes into account multiple interactions between the interfaces. First we consider a three-layer (two-interface) subsurface, although the solution can be extended to more layers. The first-order interaction of the vegetation, which in the new model consists of several layers of discrete random media, with all rough interfaces is included in the solution. Although multiple interactions between vegetation layers and between vegetation and soil layers are disregarded, the forward scattering matrix for each random layer is used to modify the wave propagation hence the distorted Born approximation. Comprehensive simulation results are presented, and sensitivity of the backscattering coefficients to the vegetation type and density, frequency range, and ground layering properties is evaluated. The results of this study directly impact the analysis of data obtained from low frequency radar systems on tower, airborne, and prospective spaceborne platforms.

## INTERFEROMETRIC AND POLARIMETRIC SCATTERING CHARACTERISTICS OF FOREST CANOPIES

Sassan Saatchi

Jet Propulsion Laboratory

Mapping forest types and estimating their structural attributes is the first step to understanding the distribution of forest above ground biomass and carbon content in tropics. Synthetic Aperture Radar (SAR) backscatter and interferometric measurements at low frequency (L- and P-band) over tropical forests have shown longer penetration in forest canopy and higher sensitivity to forest stem volume and biomass. In this study, we present a physically based model approach in simulating the foliage penetration and scattering of various forest structural components. Extinction coefficient along the forests vertical structure controls SAR polarimetric and interferometric measurements. By using the wave theory approach and the structural data collected from field surveys, the heterogeneity of forest canopy is included in the model by introducing analytical expressions for the crown size and shape, gap geometry, and the canopy roughness. Radar measurements collected at a site in neotropical forest of La Selva in Costa Rica were used to examine the performance of the model and to analyze its behavior in terms of forest structural parameters such as basal area, height, vertical distribution of leaf area, and the above ground biomass. Once the significance of structural parameters and their contributions to the extinction coefficient are determined, the model results were used to test the hypothesis that radar backscatter and interferometric cross-correlation respond to different aspects of vegetation structure. Can interferometric measurements at low frequencies recover the vertical structure of the forest canopy? Comparison with field and radar measurements is used to provide quantitative tests of the hypothesis and the sources of uncertainties.

Keywords: SAR, Backscatter, Interferometry, Forest Structure

AN ANALYTICAL APPROACH TO THE MEAN FIELD PROBLEM  
OF STATISTICALLY PERIODIC DISTRIBUTIONS OF INFINITELY  
LONG CYLINDERS

Cuneyt Utku, Roger H. Lang

George Washington University, Dept. of Electrical and Computer Engineering, 801 22nd St. NW, Washington, DC 20052

Remote sensing from agricultural crops has been an area of research for a long time. Unlike natural vegetation canopies, agricultural canopies like corn are generally aligned in rows. This aligned row structure of the canopy sometimes poses problems in interpreting the data acquired by remote sensing instruments. Several studies have been made in modeling the effects of the row structure of the canopy, however, the general tendency is to use simple models that ignore these effects. Studies that consider the row structure either idealize the canopy and assume it to be periodic or investigate the effects by Monte Carlo simulations. This study is an attempt to develop analytic tools to analyze such canopies with row structures.

In order to analyze and understand the effects of row structure on the mean field, we consider a simple canopy of randomly distributed infinitely long cylinders. In this canopy model, an ideal canopy is a two dimensional periodic lattice with each cylinder placed at a lattice point. A real canopy, on the other hand, is a disordered canopy where the cylinders are randomly displaced from their ideal canopy positions. It is assumed that the probability densities of the displacements of the cylinders are identical and are nonzero over a finite region  $R$ . We will refer to such a random distribution of cylinders as statistically periodic. Analytical expressions are derived for the propagation of the mean field through this statistically periodic distribution based on the Foldy approximation. In this approach however, we do not assume a uniform distribution in conjunction with the Foldy approximation as is generally done in the literature. In the presentation we will show that under the Foldy approximation, the mean field experiences a periodic dielectric medium. Furthermore, the shape of the dielectric is identical to the shape of the region  $R$ , and the dielectric permittivity is determined by the distribution properties. The ability to construct an equivalent periodic problem for the statistically periodic problem of the mean field is of great value since there is a rich literature on periodic structures.

Analytical results are compared with Monte Carlo simulations for a finite section of statistically periodic distributions of infinite cylinders. The results show excellent agreement in most cases. A discussion of the possible limitations of the analytical results will be given.

Session F3, 15:15 – Thurs.

## **RADIOMETRY**

Co-Chairs: A. Gasiewski, V. Zavorotny





## EXPERIMENTAL RESULTS FROM A SPECTRAL SCANNING TECHNIQUE FOR PASSIVE REMOTE SENSING OF SOIL MOISTURE

McIntyre, E.M.<sup>1</sup>, Gasiewski, A.J.<sup>2</sup>, Klein, M.<sup>3</sup>,  
Leuski, V.<sup>3</sup>, Weber, B.L.<sup>1</sup>, Irisov, V.<sup>4</sup>

<sup>1</sup>Science and Technology Corporation, Boulder, Colorado

<sup>2</sup>NOAA Environmental Technology Laboratory, Boulder, Colorado

<sup>3</sup>CIRES University of Colorado, Boulder, Colorado

<sup>4</sup>Zel Technologies, Boulder, Colorado

Global scale use of microwave hardware in industrial, business, and consumer electronics is rapidly increasing the terrestrial anthropogenic interference encountered by passive remote sensors of soil moisture at C-band, including the JAXA AMSR-E sensor on the NASA EOS Aqua satellite and the WindSat sensor on the U.S. Navy's Coriolis satellite. To facilitate continued accurate passive remote sensing of soil moisture and other microwave environmental observables, the NOAA Environmental Technology Laboratory (ETL) has developed a C-band frequency-scanning spectrometer for use within its Polarimetric Scanning Radiometer (PSR) system. The spectrometer observes emissions between 5.8 and 7.5 GHz within step-tunable 10 and 100 MHz bandwidths selectable to within 3 MHz precision. The spectrometer is integrated within the 4-subband C-band radiometer scanhead, PSR/CX, and used successfully for several airborne soil moisture mapping missions within the past 6 years.

In 2002, Gasiewski et al. developed an algorithm for interference mitigation for use with ETL's PSR/CX C-band radiometer based on chi-squared statistical analysis of brightness temperature spectra observed in parallel C-band subbands. A similar algorithm was implemented for use with the new C-band spectrometer to provide estimates of upwelling brightness temperatures with mitigation of anthropogenic radio frequency interference. The algorithm also quantifies the spectral distribution and intensity of such interference.

The NOAA/ETL spectrometer has been used to collect data during four recent experiments, including the 2004 Soil Moisture Experiment (SMEX) over Arizona and Mexico, the 2004 Antarctic AMSR-E Sea Ice Experiment (AASI), one flight over the NASA Wallops Flight Facility in Virginia, and two separate high-altitude experiments on the NASA Johnson Space Centers WB-57F aircraft over Texas. During each experiment the spectrometer was rapidly swept to observe emissions in eighteen 100 MHz-wide subbands. Experimental results to be presented are based on the performance of the mitigation algorithm with respect to raw brightness temperatures observed in these eighteen subbands. A summary of instrument hardware, algorithm implementation, and results of recent experiments will be discussed.

## NOAA POLARIMETRIC SCANNING RADIOMETER MEASUREMENTS OF SNOW COVER PROPERTIES IN THE COLORADO ROCKY MOUNTAINS

Stankov, B. B.,<sup>1</sup> Gasiewski, A. J.,<sup>1</sup> Cline, D.,<sup>2</sup>  
, Weber, B. L.,<sup>3</sup> Wick, G. A.,<sup>1</sup> Klein, M.,<sup>4</sup>

<sup>1</sup>NOAA Environmental Technology Laboratory, Boulder, CO USA

<sup>2</sup>NOAA/NWS/ National Operational Hydrologic Remote Sensing Center, Chanhassen, MI, USA

<sup>3</sup>Science and Technology Corporation and NOAA/ETL, Boulder, CO, USA

<sup>4</sup> NOAA/ETL - University of Colorado CIRES, Boulder, CO USA

The 2002, 2003A, and 2003B field campaigns of the Cold Land Processes Experiment (CLPX) were multi-institutional studies designed to both provide improved understanding of cryospheric processes and to support the design of an advanced cryospheric observation system. These campaigns involved one of the most intensive snow sampling efforts undertaken, and used as the primary airborne sensor the NOAA Environmental Technology Laboratorys Polarimetric Scanning Radiometer (PSR). The PSR was operated over three sites within the Colorado Rocky Mountains in February 2002 on board the NASA DC-8 aircraft and again in February and March 2003 on board the NASA/WFF P-3B to obtain the first high-resolution (150-500 m) airborne multiband microwave imagery of snowpack. The PSR is the first operational airborne conical imaging radiometer system and provides a unique means of simulating what a future NASA cryospheric satellite could observe. Such spaceborne snowpack data will ultimately improve techniques for monitoring and prediction of hydrological runoff and storage, avalanche danger, and regional weather and climate trends. The PSR also provides snow emissivity data for NOAA and NPOESS retrieval algorithm development

In this paper we present the PSR multiband microwave polarimetric snow images over the three CLPX mesocell study areas (MSAs) in the AMSR-E bands for 21 flights spanning two seasons. Conditions included drought, normal snowpack, and spring snowmelt. The brightness temperatures are related to the physical snowpack quantities, particularly snow water equivalent (SWE). Comparisons of the PSR/A-derived SWE estimates compare favorably with in situ measurements, Gamma SWE observations, and AMSR-E retrievals after correction for grain size. A conclusion is that snow grain size is of great importance in retrieval algorithms based on 18 and 37 GHz data. We also use the PSR CLPX data set to study relationships between land cover type and snow brightness spectra to establish the principal modes of brightness variation caused by snowfall. Emissivity depressions of up to 70-75 percent were observed for fresh snowfall at 89 GHz horizontal polarization, but are highly sensitive to snowmelt state. New algorithms tailored to use information from a broad suite of microwave channels are discussed.

## SEASONAL MEASUREMENTS OF SOIL MOISTURE USING A STATIONARY L-BAND RADIOMETER

Zavorotny, V.U.<sup>1</sup>, Gasiewski, A.J.<sup>1</sup>, Zamora, R.J.<sup>1</sup>, McIntyre, E.M.<sup>2</sup>, Leuskiy, V.Y.<sup>B</sup>, Irisov, V.G.<sup>4</sup>

<sup>1</sup>NOAA/Environmental Technology Laboratory, Boulder, CO

<sup>2</sup>Science and Technology Corporation, Boulder, CO

<sup>3</sup>CIRES/University of Colorado, Boulder, CO

<sup>4</sup>Zel Technologies LLC, Boulder, CO

Currently, soil moisture (SM) is a key variable in both drought assessment and understanding the impact of the boundary layer on climate and biological processes, including deforestation and convection development. Knowledge of SM will improve streamflow forecasts for flooding in the short term, and for water supply and agricultural irrigation in the long term. A spaceborne remote sensing system that provides wide-area measurements of SM over both the U.S. and other continents for drought, weather, and climate studies is urgently needed. Along with the current planned satellite systems for SM measurement the development of systems with watershed-scale spatial resolution should also be pursued.

For these reasons, the NOAA Environmental Technology Laboratory has designed and built an L-band (1.4 GHz) Tower Soil Moisture Radiometer (TSMR) for continuous and unattended SM measurements. The TSMR uses a standard (15 dB) gain horn antenna at horizontal polarization. The TSMR was mounted onto an external carriage at the top of the 300-m tall ETL Boulder Atmospheric Observatory (BAO) tower. *In situ* SM measurements were performed in the center of TSMR antenna footprint using two stations located 10 m apart with time-domain reflectometer (TDR) probes at each station installed at 5, 10 and 15 cm depth. Measurements of SM using both sets of instruments have been performed during a period from June 2004 to September 2005. The objective of the long-term experiment is to demonstrate the retrieval of the seasonally changing SM from measured soil radiometric brightness temperatures by validating it with *in situ* SM measurements.

In this paper, we present an analysis of results of seasonal microwave SM measurements. Theory predicts deeper penetration to the soil of L-band signals compared with commonly used remote sensing microwave bands, and initial results from the experiment indicate useful sensitivity to subsurface SM content. We also analyze how SM retrieval are affected by presence of surface snow during winter and various stages of grassy vegetation during spring and summer seasons.

## GEOSTATIONARY PASSIVE MICROWAVE SENSOR SIMULATION

Gasiewski, A.J.<sup>1</sup>, Weber, B.L.<sup>2</sup>, Voronovich, A.G.<sup>1</sup>  
, Schneider, T.L.<sup>1</sup>, Smith, D.F.<sup>2</sup>, Stankov, B.S.<sup>1</sup>  
, Bao, J.W.<sup>1</sup>, Klein, M.<sup>3</sup>

<sup>1</sup>NOAA Environmental Technology Laboratory, 325 Broadway R/ET1, Boulder, CO, USA 80305-3328

<sup>2</sup>Science and Technology Corporation, 325 Broadway R/ET1, Boulder, CO, USA 80305-3328

<sup>3</sup>CIRES University of Colorado, 325 Broadway R/ET1, Boulder, CO, USA 80305-3328

Passive microwave sounding and imaging from geosynchronous orbit was first studied in the mid-1970s, although initial proposals using microwave channels below 220 GHz required prohibitively large antennas. Studies during the early 1990s suggested that antenna size and costs could be significantly reduced while retaining good spatial resolution by using key submillimeter-wavelength water vapor and oxygen bands. It was with this notion that the Geosynchronous Microwave Sounder Working Group (GMSWG) was convened to develop a model for a practical submillimeter-wave geosynchronous microwave (GEM) sounder and imager. The current GEM concept is based on a 2-3 meter Cassegrain reflector antenna and fast-scanning sub-reflector. GEM will be capable of either intensively observing specific areas near severe weather or obtaining synoptic information over an extended environment.

During the mid-1990s an alternate means of geostationary microwave imaging and sounding using aperture synthesis was proposed. Aperture synthesis relies on precision measurements of the coherence function in an aperture plane made using a set of receivers and correlators, along with subsequent application of a Fourier transform to obtain the angular radiation field. As implemented in geostationary orbit the system would require no moving components to synthesize an image of the radiation field across the Earth's disk, albeit with tradeoffs in sensitivity, spectral coverage, and spaceborne hardware complexity. The JPL GeoSTAR concept is based on implementing this technique at the two primary AMSU bands (50-57 and 183 GHz).

In order to assess the operational capabilities of each of these systems for forecasting applications NOAA/ETL has embarked on a set of observation system simulation experiments (OSSEs) using the two (real and synthetic aperture) concepts. In this talk we present the status of our OSSEs with a focus on forward radiative transfer modeling studies of upwelling radiation fields from a simulated landfalling hurricane. Discussed will be the information content of the simulated imagery and the potential for using such imagery to drive regional numerical weather prediction models using direct radiance assimilation.

## HIGH-RESOLUTION AIRBORNE PASSIVE MICROWAVE SEA ICE MAPPING IN SUPPORT OF AMSR-E CALIBRATION AND VALIDATION

Klein, M.<sup>1</sup>, Gasiewski, A.J.<sup>2</sup>, Stankov B.B.<sup>2</sup>

, Leuski, V.<sup>1</sup>, Irisov, V.<sup>4</sup>, D. Cavalieri<sup>3</sup>, Markus, T.<sup>3</sup>, Comiso, J.<sup>3</sup>

<sup>1</sup>NOAA/ETL - CIRES/University of Colorado, 325 Broadway, Boulder, Colorado 80305

<sup>2</sup>NOAA/ETL, , 325 Broadway, Boulder, Colorado 80305

<sup>3</sup>NASA Goddard Space Flight Center

<sup>4</sup>Zeltech Inc., , 325 Broadway, Boulder, Colorado 80305

During 2003 and 2004 three sea ice campaigns took place in Arctic and Antarctic polar regions in support of the AMSR-E instrument calibration and validation. The prime objectives of these experiments was to establish statistical relationships between the sea ice parameters derived from the new AMSR-E sea ice algorithms and the same parameters derived from the Polarimetric Scanning Radiometer (PSR) covering different geographical areas and different seasons. The parameters of interest include sea ice concentration, temperature for both hemispheres, and snow depth on sea ice. A secondary objective was to evaluate the performance of two sea ice algorithms under different conditions and in both polar regions.

The NOAA Environmental Technology Laboratory (NOAA/ETL) supported these experiments by deploying the PSR/A and PSR/CX scanheads flying on the NASA Wallops P-3B and the Naval Research Laboratory (NRL) P-3 674 aircraft. The Arctic campaign was based in Fairbanks, Alaska during March 2003, and included 7 sorties covering a variety of sea ice conditions. The Antarctic campaign occurred in two phases, the first being in in September of 2003 and second in October 2004. Overall four data sorties in the vicinity of Antarctic Peninsula were flown. A single Sea of Okhotsk sortie was based out of Yokota AFB, Japan in January of 2003.

Sea ice brightness temperature spectral variation due to different phenomena such as the sea ice concentration anisotropies, ice snow cover, and first-year ice versus multi-year ice were observed. Sample brightness temperature maps for microwave channels from 6 to 89 GHz from the experiments will be presented.



Session G1, 07:55 – Wed.

**GROUND AND SPACE BASED  
RADIO BEACONS**

Co-Chairs: A. Komjathy, F. Kamalabadi





## LOCALIZED THREE-DIMENSIONAL IONOSPHERIC TOMOGRAPHY WITH GPS GROUND RECEIVERS

Lee, J., Kamalabadi, F., Makela, J.

Department of Electrical and Computer Engineering, University of Illinois at Urbana-Champaign, 1406 West Green St. Urbana, IL 61801-2918

This paper evaluates the performance of two different reconstruction techniques for localized 3D tomographic imaging of the ionosphere with high spatial resolution. The total electron content (TEC) values are derived from dual-frequency measurements obtained from GPS satellites by ground-based receivers. Ionosonde observation data is used to construct *a priori* vertical profiles modelled using Chapman functions. The altitude range of interest is 100km to 800km, with voxel sizes at most about 30 km in altitude.

Two regularization algorithms are used for tomographic image reconstruction: Tikhonov and Total Variations (TV). The methods have different norm minimizations of the penalty constraint: quadratic and  $l_1$ . The TV method is used because it generally better preserves jump discontinuities in the image and is more resistant to noise. By contrast, Tikhonov or quadratic regularization tends to oversmooth image structures. However, a closed-form solution of the TV method does not exist, and so performance depends heavily on numerical optimization techniques, which is non-trivial to implement because the inverse problem is both ill-posed and ill-conditioned.

The algorithms are demonstrated using real and simulated GPS TEC measurements from actual observation geometry centered in Southern California. We demonstrate the successes and limitations of these techniques under quiet mid-latitude conditions. The resulting reconstructions reasonably determine the shape of the ionospheric profile. The limitations, such as artifacts near voxels with no ray path information, are directly related to the sparseness and nonuniform distribution of the GPS ray paths. Some methods addressing this are discussed. We also apply regularization parameter-selection methods to demonstrate their applicability in our study.

OBSERVATIONS OF STORM ENHANCED DENSITY (SED) OVER  
NORTHERN EUROPE AND AMERICAN LONGITUDE SECTORS

M. J. Colerico<sup>1</sup>, A. Coster<sup>1</sup>, J. Foster<sup>1</sup>  
, W. Rideout<sup>1</sup>, F. Rich<sup>2</sup>, J. M. Ruohoniemi<sup>3</sup>

<sup>1</sup>MIT Haystack Observatory, Off Route 40, Westford, MA 01886-1299

<sup>2</sup>AFRL, 29 Randolph Rd, Hanscom AFB, MA, 01731-3010

<sup>3</sup>Applied Physics Lab, 11100 Johns Hopkins Rd, Laurel, MD, 20723-6099

Storm enhanced density (SED) is formed by the large scale transport of plasma which occurs during geomagnetically active conditions. The forces underlying this transport are thought to be associated with electric field driven coupling processes which penetrate into both mid and equatorial latitudes. Its effects are evident in the redistribution of low latitude ionospheric plasma into mid-latitudes and its impact on equatorial electrodynamics during magnetically disturbed conditions. SED occurrence can also impact communication and navigation systems. SED is characterized by large gradients in electron density over a few degrees latitude and longitude. For some time now, SED has been observed in the American longitude sector appearing in global GPS TEC maps as plume-like structures of greatly enhanced TEC values. In this paper, we present the first examples of SED over Northern Europe as seen in global TEC maps during various seasonal and solar cycle conditions. Most of the observed cases of SED, but not all, which develop over Northern Europe continue to propagate westward over the American sector. Correlated DMSP ion drift measurements indicate the presence of the sub-auroral polarization stream (SAPS). A comparison is presented between the American and Northern European sector SED occurrences addressing the latitude and magnitude of the base of the SED plume. The results indicate that the SED strengthens as it propagates westward between European and American longitudes. Comparison between northern hemisphere Super-Darn convection maps and the TEC maps highlight the correlation between the westward propagation of the SED plume and the convergence of the two cell convection pattern.

## MAGNETIC CONJUGACY OF STORM ENHANCED DENSITY

Anthea J. Coster<sup>1</sup>, Marlene Colerico, John Foster  
, Bill Rideout, Fred Rich, Brandon Taylor

<sup>1</sup>MIT Haystack Observatory, Off Route 40, Westford, MA 01886

<sup>2</sup>Air Force Research Lab, AFRL/VSBXP, Hanscom AFB, MA 01731

<sup>3</sup>University of Texas at Austin, Applied Research Laboratory, Austin,  
Texas 78713

The SED is the plume-like structure of greatly enhanced TEC values (greater than 50 TEC units) that extends from east coast up across the continental US into Canada. SED is associated with large gradients and high ion flux values. It is typically observed between 17:00 and 23:00 UTC over the eastern US coast during moderate to severe geomagnetic storms. SED is associated with large gradients and high ion flux values. It is typically observed between 17:00 and 23:00 UTC over the eastern US coast. In this talk, we will address the magnetic conjugacy of SED.

The Madrigal database at MIT Haystack Observatory now contains total electron content (TEC) data with an unprecedented combination of global spatial coverage and high temporal resolution. Data from more than 2000 GPS receivers distributed world-wide are being incorporated into the daily 2005 TEC maps. This database has allowed for long term statistical studies of the presence of SED.

In this paper, we present statistics of SED plumes observed during multiple storms during the 2000-2005 time period. The location, size of gradients, and time evolution of multiple SED events has been statistically characterized using an automated gradient analysis tool. Examples of magnetically conjugate SED plumes over northern Europe and the American longitude sectors, and the associated southern hemisphere SED observations, will be discussed. Inter-hemispheric comparisons of the TEC magnitude of the observed SED events at the base, as well as within the plume, will be presented. The results also include observations of magnetically conjugate sub-auroral polarization streams (SAPS) which accompany the SED events using DMSP ion drift measurements.

## SOME FEATURES OF THE TEC BEHAVIOR OBSERVED UNDER DISTURBED CONDITIONS

Araujo-Pradere, Eduardo, Fuller-Rowell, Tim  
CIRES-Univ. of Colorado and , SEC-NOAA

To understand and eventually model the ionospheric Vertical Total Electron Content (VTEC) behavior under quiet and disturbed conditions is of great importance for communications and navigation. In this work, Global Position System (GPS) data from the Continuously Operating Reference Stations (CORS) network have been used to obtain the ionospheric Vertical Total Electron Content values over the continental USA, corresponding to a series of 10-day storm periods with good seasonal coverage. The VTEC values have been extracted using the Data Assimilation Algorithm for Ionospheric Imaging package, a Kalman filter based code that is the basis of SECs US-TEC model. The storm response of the VTEC was extracted from the data as a ratio to the quiet periods preceding the storms, and sorted as a function of latitude and a storm index defined as the integral, or filtered, ap over the previous 33 hours. When studying the 10-day periods we found consistent features from storm to storm, but these features are more apparent when separating the data between the driven phase of the storm, when the integral of ap is rising, and the recovery to the storm, when the integral of ap is declining. The driven phase shows, for these storms, a positive phase for the mid latitude region when CONUS is in the right time sector, while the recovery shows a negative phase. The existence of the positive phase over CONUS at the beginning of the storm period seems to be related to the timing of the peak of the perturbation; a positive phase will be observed when the peak of the perturbation occurs near midnight UT.

## AUTOMATED DETECTION OF SED PLUMES USING GPS TEC DATA

Brandon Taylor<sup>2</sup>, Anthea Coster<sup>1</sup>, Bill Rideout<sup>1</sup><sup>1</sup>MIT Haystack Observatory<sup>2</sup>Applied Research Laboratory

The effects of Storm Enhanced Density (SED) structures with high level of and sharp changes in total electron content (TEC) must be compensated for in order to ensure stability of trans-ionospheric communications. The MIT Haystack Observatory's Madrigal database contains a collection of TEC data from the world-wide GPS receiver network (<http://madrigal.haystack.edu/madrigal/index.html>). This collection offers a new tool for identifying and studying these SED structures. With over 10 years of continuous GPS TEC data that will soon be available on the database, an automated system for detecting when these SED structures are present will greatly assist in the study of them. Two Matlab methods that will be made available on the Madrigal server at MIT Haystack Observatory will provide such a system. The first method downloads and formats the GPS TEC data over a specified time period and allows the user to specify binning parameters. The second method accepts this formatted data and returns a structure characterizing any detected SED structures. This program not only offers an indication whether an SED structure exists, but also returns information about its location and magnitude which can be used to study the movement and evolution of the SED structure in time. A detailed discussion of the algorithm used to identify the presence of an SED structure is presented. Additionally, comments are made about the limitations of these Matlab methods and possible adjustments that users could make to customize the algorithms function. A few days in which SED structures were known to exist were analyzed to offer some indication of the utility of these methods.

SCINTILLATION OF TRANSIONOSPHERIC GPS SIGNALS AT  
ASCENSION ISLAND: SPACED RECEIVER OBSERVATIONS  
DURING SOLAR FLARES

Linda Habash Krause<sup>1</sup>, Luke Haywas<sup>1</sup>, Keith L. Groves<sup>2</sup>  
, Theodore L. Beach<sup>2</sup>

<sup>1</sup>United States Air Force Academy , Department of Physics

<sup>2</sup>Air Force Research Laboratory, Space Vehicles Directorate

Measurements of severe ionospheric scintillation of L1 and L2 GPS signals obtained by two ground-based receivers during periods of significant solar activity are presented. Two Ashtech  $\mu Z$ -12 12 channel dual frequency receivers were located on Ascension Island, separated by 87 m and oriented primarily along the E-W direction. Data used for this study were acquired from 8 March 2002 until 17 March 2002, a period encompassing relatively little geomagnetic activity but a significant amount of solar activity. Differential pseudoranges between a single receiver and multiple satellites were examined in a time series; by comparing the temporal occurrences of scintillation activity, a map of Line-Of-Sight irregularities within the ionosphere could be systematically reconstructed as a function of time. For example, such an irregularity map produced for 8 March 2002, during which several C-class flares occurred, revealed significant patches in these irregularities: the simultaneous measurements taken by a single receiver of the GPS signals from six satellites indicated drastically different levels of scintillation as a function of time, thus providing observations of distinct spatial structure. Maps generated from the data taken by the second receiver using the signals from the same satellites provided further information regarding the structure, especially in altitude, of these irregularities. Finally, using the techniques outlined in previous studies, we were able to reconstruct the zonal velocity of the irregularity pattern. These techniques will be helpful in the analysis of ionospheric irregularities during a ground campaign used to augment upcoming ionospheric satellite experiments, including the United States Air Forces Communications/Navigation Outage Forecasting System (C/NOFS) and the FalconSAT-2 and FalconSAT-3 missions.

TEC, L-BAND SCINTILLATION AND ZONAL PLASMA DRIFTS  
MEASURED BY THE BRAZILIAN GPS RECEIVER NETWORK

Muella, M. T. A. H.<sup>1</sup>, de Paula, E. R.<sup>1</sup>, Kantor, I. J.<sup>1</sup>  
, Fedrizzi, M.<sup>2</sup>, Rodrigues, F. S.<sup>3</sup>, de Rezende, L. F. C.<sup>1</sup>  
, Kintner, P. M.<sup>4</sup>

<sup>1</sup>National Institute for Space Research, Aeronomy Division -  
INPE/DAE, So Jos dos Campos, SP - Brazil

<sup>2</sup>National Oceanic Atmospheric Administration, Space Environment  
Center - NOAA-SEC, Boulder, CO - USA

<sup>3</sup>Cornell University, Earth and Atmospheric Sciences, Ithaca, NY, USA

<sup>4</sup>Cornell University, School of Electrical and Computer Engineering,  
Ithaca, NY, USA

In the present days, a chain of 32 Global Positioning System (GPS) receivers operates in the Brazilian territory. Since September 1997, in a collaborative project involving the Aeronomy group from National Institute for Space Research (INPE) and the Space Plasma Physics group from Cornell University, a network of twelve single-frequency GPS receivers was established for the purpose of monitoring nighttime amplitude scintillations at the L1 frequency (1.575 GHz). Also, a network of twenty dual-frequency GPS receivers operated by the Brazilian Institute for Geography and Statistic (IBGE) has been used for total electron content (TEC) measurements. The scintillation monitors (SCINTMON) developed by Cornell University have been in routine operation and have provided an excellent database used as a tool for ionospheric studies, such as, the latitudinal-longitudinal morphology of ionospheric irregularities, their changes and responses due to geomagnetic disturbances and, dynamics of equatorial and low-latitude F region irregularity zonal drifts. The dual-frequency GPS receivers have been used to generate storm time maps of total electron content dynamics. The signatures of ionospheric F region irregularities on TEC measurements and GPS performance degradation investigations have also been performed in the Brazilian region. In this work, the GPS TEC and scintillation receivers network will be described, and some relevant observational results for the past seven years (1998-2005) of operation will be present and discussed. The long-term intention with respect to the scintillation, TEC and ionospheric drifts observations is to characterize its statistical properties, temporal dependence, dynamics and its effects on GPS link performance within the Brazilian longitude sector. It will allow the developing of scintillation models to provide a prediction of scintillation activity and to quantify the potential for navigational degradation, especially during periods of elevated solar activity and geomagnetically disturbed conditions.

L-BAND SCINTILLATIONS ON THE WAAS SIGNAL MEASURED  
FROM HALEAKALA VOLCANO: INSIGHTS GAINED FROM  
COLLOCATED RADIO AND OPTICAL MEASUREMENTS

Jonathan J. Makela<sup>1</sup>, Brent M. Ledvina<sup>2</sup>, Jason D. Readle<sup>1</sup>  
, Michael C. Kelley<sup>3</sup>, Paul M. Kintner<sup>3</sup>, Thomas L. Gaussarian<sup>2</sup>

<sup>1</sup>University of Illinois at Urbana-Champaign, Department of Electrical  
and Computer Engineering

<sup>2</sup>University of Texas at Austin, Applied Research Laboratories

<sup>3</sup>Cornell University, School of Electrical and Computer Engineering

Utilizing the signals transmitted by the Global Positioning System (GPS) satellite network provides a simple method to estimate irregularity structuring in the F-region ionosphere. Measurements of the power received from each GPS satellite by a single-frequency receiver located atop the Haleakala Volcano on Maui, HI have been recorded since the beginning of 2002. Beginning in August of 2004, measurements of the received signal power from a Space Based Augmentation System (SBAS) geostationary satellite called a Wide Area Augmentation System (WAAS) satellite have also been recorded. From these signal power measurements it is possible to study the scintillations and irregularity structures due to the overhead passage of ionospheric irregularities. These irregularities are typically associated with the equatorial spread-F phenomenon, although evidence exists for the passage of irregularities not associated with this phenomenon. The difference between the GPS satellites and the SBAS satellite is that the former move with respect to the Earth, while the latter are fixed. The lack of motion in the Earth's reference frame simplifies the interpretation of the scintillations on the SBAS signals. Several case studies of scintillations are presented. On several occasions, these scintillations occurred during times when both the moon and sun were below the horizon and the skies were clear. This allows us to compare the scintillation measurements to airglow depletions observed using a collocated imaging system. The data collected by the imaging system places the one-dimensional scintillation data into a broader two-dimensional spatial context and allows conclusions to be drawn as to the spatial structure of the irregularities with respect to the larger-scale airglow depletions.



## PHASE SCREEN RECONSTRUCTION FROM SPACE BASED RECEIVERS

Paul A. Bernhardt, Carl L. Siefring

Plasma Physics Division, Naval Research Laboratory, Washington, DC 20375

Space-to-ground transmissions are the most common use of radio beacons for ionospheric scintillation studies. Ground based reception from an orbiting beacon samples the scintillated wave front from a satellite beacon at many locations along its orbit. From the point of view of data analysis, ground transmissions to a receiver in low earth orbit (LEO) are preferred because the satellite receiver can sample the distorted spherical wave generated for a single point source. Inverse diffraction can be applied to the sampled complex amplitude to provide an estimate of the phase screen equivalent of the refractive index structures associated with ionospheric irregularities. The primary limitations for ground to space studies of the ionosphere are (1) the availability of radio beacons on the earth's surface and (2) the cost of putting a dedicated scintillation receiver in space. The constellation of ground beacons that comprise the French DORIS network is available for ionospheric studies. These beacons radiate 10 Watts at 401.25 MHz and 2036.25 MHz. These frequencies are ideal for UHF scintillation studies with an S-Band reference. To test the utility of the DORIS system for ionospheric scintillation studies, the Naval Research Laboratory is flying the Scintillation and Tomography Receiver in Space (CITRIS) instrument on the Air Force STPSAT1 satellite. This satellite will be launched into an 35 degree inclination orbit at 560 km altitude. Simulations of radio diffraction by equatorial bubbles have demonstrated that the CITRIS data will provide global estimates of the phase distortion structures in the ionosphere responsible for radio scintillations. The phase screens reconstructed from the CITRIS data may be used to estimate the scintillation effects at frequencies in the VHF to L-Band range.

## COMPARISON OF CHAMP AND DIGISONDE PLASMA FREQUENCIES AT JICAMARCA, PERU

McNamara, L.F.Boston Collge Institute for Scientific Research

Ionospheric plasma frequencies at the altitude of the CHAMP satellite have been deduced from ionosonde true-height profiles for Jicamarca, Peru, and compared with the in situ measurements made by CHAMP.

All Jicamarca ionograms for the interval September 2001 to August 2002 were considered. The ionograms were hand-scaled, since indiscriminate use of autoscaled values is not recommended. The hand-scaled ionograms were filtered by the authors program QualScan, which scans the scaled ionogram traces (virtual height vs. plasma frequency) for acceptability using a rule-based system.

A satellite-ionosonde coincidence was defined as the sub-satellite point being less than 250 km from the ionosonde, and the CHAMP observation being within 15 minutes of an ionogram sounding. The ionogram filtering by QualScan, together with the spatial and temporal coincidence requirements, but mainly the latter, reduced the number of relevant Digisonde ionograms to 142 (from the original 27,000). This number was further reduced to 100 after visual inspection of the 142 ionograms, to exclude doubtful traces affected by weak ionosonde echoes and spread F.

The differences between the plasma frequencies have been found to be well within the uncertainties associated with the ionosonde profiles, confirming the validity of the CHAMP measurements. For satellite-ionosonde separations of less than 250 km, and for satellite altitudes below the peak of the F2 layer, the average discrepancy between the two plasma frequencies was 0.25 MHz or 4% (N = 198). For the most reliable ionosonde measurements, the average discrepancies reduced to 0.18 MHz or 1.7%, with a standard deviation of 0.16 MHz or 1.5% (N = 75). Most of the ionograms were recorded between about 10 and 20 LT.

Given the validity of the CHAMP plasma frequencies, corresponding ionosonde and CHAMP observations were then used to support the practice of extending the ionosonde profile above hmF2 by assuming a Chapman layer with a constant scale height equal to that of the lower side of the F2 layer peak. The average discrepancy for CHAMP passes above the peak of the F2 layer is 0.22 MHz or 2.6%, and the standard deviation is 0.8 MHz or 13.3% (N = 95). Most of the data points were for local times between 03 and 09LT, when foF2 is low and hmF2 is usually less than 400 km.

DETECTING IONOSPHERIC-SEISMIC SIGNATURES DURING  
THE SUMATRA EARTHQUAKE EVENT USING GROUND AND  
SPACE-BORNE GPS MEASUREMENTS

Attila Komjathy, Byron Iijima, Lawrence Sparks , Anthony Mannucci

NASA Jet Propulsion Laboratory, California Institute of Technology

It has been known for decades that perturbations of the ionosphere can arise in response to solid Earth motions. A large variety of isolated ionospheric observations have identified such disturbances, but very few systematic investigations of the solid Earth-ionosphere coupling have ever been performed. A better understanding of this coupling is not only of inherent scientific interest; it can also be exploited to advance our understanding of the physics of solid Earth events.

Recent developments in ionospheric remote sensing, in particular, the advent of techniques that use the Global Positioning System (GPS), provide an unprecedented capability for detecting, monitoring, and characterizing ionospheric disturbances on a routine basis. As a means of assessing the state of the ionosphere, GPS measurements of ionospheric total electron content (TEC) offer several advantages over prior methods: simultaneous coverage encompassing a large spatial domain, continuous coverage in time, and high temporal resolution. Thus, networks of GPS receivers provide an important new means of systematically studying the ionospheric response to solid Earth motions. Measurements of ionospheric perturbations generated by solid Earth events are potentially powerful signals for Earth science research.

In our paper, we describe a new algorithm we developed to process individual GPS stations to extract ionospheric perturbations caused by Traveling Ionospheric Disturbances (TIDs). We applied this algorithm to extract ionospheric signatures at the 0.1 TECU level caused by the December 26, 2004 Sumatra Earthquake event. We demonstrate that multiple satellites using several GPS stations separated by about 1500 km show the seismic-ionospheric signatures consistent with the propagation velocities of Rayleigh waves, coupled with acoustic and gravity waves. We found a peak-to-peak variation of the ionospheric TEC caused by the tsunami at the 0.2 TECU level.

We also demonstrate the seismic-ionospheric signatures are present in the space-borne GPS measurements. We use a modified version of our new algorithm to process GPS occultation data. We compare the ionospheric signatures caused by the tsunami using ground and space-based GPS measurements.

G1

9

Session G2, 12:55 – Wed.

## **RADIO & RADAR TECHNIQUES**

Co-Chairs: F. Lind, J.D. Sahr



## INCOHERENT SCATTER WITH THE AMISR PROTOTYPES

Heinselmann, C.J., Valentic, T.A., Kelly, J.D.

SRI International, 333 Ravenswood Ave., Menlo Park, CA 94025

The first face of the Advanced Modular Incoherent Scatter Radar (AMISR) is presently under construction at the Poker Flat Research Range north of Fairbanks, Alaska. This system, a phased-array radar for ionospheric studies, has been under development for the National Science Foundation for several years and that development has progressed in a staged manner with several prototype systems fielded and tested at different geographic locations. The first panels of the system were field tested near SRI's facility at the Big Dish above the Stanford University campus in California. Subsequent system testing occurred at the Jicamarca Radio Observatory in Peru, near Gakona in Alaska, and at the Poker Flat Research Range.

As the name implies, the full AMISR systems will have sufficient sensitivity to probe the ionospheric plasma via incoherent scattering of radio waves. These initial prototype AMISR systems, however, were not expected to have sufficient sensitivity to make incoherent scatter measurements at scientifically interesting time scales. The Stanford deployment, for example, consisted of just two out of the 128 total panels that make up a nominal radar face. Roughly speaking, the sensitivity of AMISR (signal to noise ratio of the return) scales as the square of the number of panels assembled, so the two panels at Stanford had a sensitivity approximately 0.02 % that of a full face. Those panels were, however, sufficient to validate aspects of the design via tropospheric wind measurements.

A threshold for practical incoherent scatter measurements with integration times of less than an hour lies around the sixteen panel mark. The processing of data from such long time series requires the careful removal of many sources of interference (e.g. range-aliased satellite returns or aircraft in antenna side lobes) but it is practical. This presentation will show results from such processing and, more importantly, will extrapolate those results to the expected sensitivity of the full AMISR system.

## AN INVERSE-THEORETIC APPROACH TO INCOHERENT SCATTER RADAR PARAMETER ESTIMATION

Romina Nikoukar<sup>1</sup>, Farzad Kamalabadi<sup>1</sup>, Michael Sulzer<sup>2</sup>,  
Erhan Kudeki<sup>1</sup>, Sixto Gonzalez<sup>2</sup>

<sup>1</sup>University of Illinois at Urbana-Champaign, Urbana, IL

<sup>2</sup>National Astronomy and ionosphere center, Arecibo, PR

We present an inverse theoretic approach to the estimation of ionospheric parameters from incoherent scatter radar data. The method consists of removing the range smearing of ionospheric autocorrelation function across the range via a set of 1-D deconvolutions, and performing nonlinear least-squares fitting on retrieved autocorrelation functions. Unlike full-profile analysis, which attempts to estimate ionospheric parameters at all altitudes simultaneously, the new method estimates the parameters at individual altitudes, and hence reduces the burden of computation significantly. Moreover, due to dimension reduction of search space, this approach prevents the least-squares routines from obtaining suboptimal estimates, and therefore it provides more reliable estimation results than full-profile techniques. Additionally, while this approach yields comparable computational cost to height-by-height analysis method, it performs superiorly in terms of the resolution of estimated parameter grid. Further computational efficiency can be obtained by considering only variances of lag-profile error estimates and ignoring the correlations, causing correlation between parameters across altitudes. Thus, in order to maintain high speed of computation, and while achieving high accuracy, we utilize two amplitude modulated pulses in F-region incoherent scatter radar experiments. These two pulses are designed so that they permit to obtain more precise deconvolved lag-profiles. The coding scheme also decreases the correlations between lag-estimate errors. This reduction in correlation justifies using only variances of the error in nonlinear least-squares fitting routines. Application of the proposed method on simulated and actual data, obtained by transmitting these amplitude modulated pulses in an F-region experiment, conducted at Arecibo Observatory, shows a reduction of about 50% in errors of estimated parameters.



## FULL-PROFILE ANALYSIS OF JICAMARCA INCOHERENT SCATTER TOPSIDE DATA

Rodrigues, F. S., Hysell, D. L.

Cornell University, Earth and Atmospheric Sciences, 2122 Snee Hall,  
Ithaca - NY 14853

An experiment employing alternating codes has been used at the Jicamarca Radio Observatory for incoherent scatter observations of the topside ionosphere since 2000. This experiment allows the simultaneous measurement of electron density, electron and ion temperature, and ion composition for altitudes up to about 1300 km during high solar activity. During periods of low solar activity, however, the sensitivity of this experiment decreases noticeably, and an alternative mode for topside observations becomes necessary.

As an alternative to the alternating code experiment, we are developing a new topside experiment which employs a long uncoded pulse together with a full-profile analysis [Holt et al., 1992; Lehtinen et al. 1996] for inversion of the ionospheric parameters. The long-pulse transmission scheme increases the sensitivity of the measurements, and the full-profile analysis mitigates the distorting effects of the 2-D long-pulse ambiguity function.

Topside observations using a 1.5 ms long uncoded pulse have been made at Jicamarca showing that reasonable autocorrelation functions (ACFs) can be measured up to 1600 km. In support to the long-pulse experiment, L/R circularly polarized double-pulse transmissions are interleaved with the long-pulse, allowing simultaneous measurements of ACFs at lower altitudes ( $< 450$  km) along with Faraday rotation measurements for absolute electron density calibration.

A forward mathematical model of the long-pulse measurements has been developed for the numerical inversion of the ionospheric parameters. This model takes into account the effects of the radar ambiguity function. For the inversion process, we use a Levenberg-Marquadt algorithm which searches for altitude profiles of the ionospheric parameters that best fit the long-pulse measurements. Following Holt et al. [1992], we used a linear combination of B-Spline basis functions to represent the altitude profiles. Regularization techniques have also been used to constrain our search for the parameter profiles.

We have tested our inversion algorithm with simulated data, and the results show that it is possible to invert electron density, electron and ion temperature, and composition (2 ions: O<sup>+</sup> and H<sup>+</sup>, or 3 ions: O<sup>+</sup>, H<sup>+</sup> and He<sup>+</sup> if  $T_e = T_i$  is assumed) profiles simultaneously. Simulations were run with noise added, with flat profiles as initial guesses, and considering that ionospheric parameters below 450-km are known from the double-pulse measurements.

We will present topside measurements made with the long-pulse experiment and discuss details and results of our algorithm for full-profile analysis of the new experiment. Details include a derivation of the full error covariance matrix for the full-profile inversion algorithm.

## THE MIDAS-MOBILE SOFTWARE RADAR SYSTEM

Lind, F.D., Erickson, P.J., Marchese, J.R. , Rideout, W.J., Holt, J.M.

MIT Haystack Observatory, Route 40, Westford, MA 01886 USA

Recent advances in software radio technology have laid the basis for the development of software radio systems which can be used to make multi-role radio science observations. Software radio systems for radio science have somewhat different requirements and characteristics from those applied to communications or defense. In particular there is an emphasis on the coherence of the receiving systems (global stability in time and frequency) and a much greater tolerance for latency in the signal processing. These properties lead directly to radio science systems where the coherent voltage level representation of RF energy is transmitted over high speed computer networks and processed using parallel supercomputing techniques. Traditional radio science systems observe the environment using a variety of techniques including active radar, passive radar, scintillation, tomography, interferometric imaging, and spectrum monitoring. Modern software radio systems can implement these techniques in a common framework where the primary differences are in the antennas used and the software chains used for signal processing and data analysis.

At MIT Haystack Observatory we have developed the MIDAS-Mobile system (Millstone Data Acquisition System). MIDAS-M is a software radar platform designed to operate as a flexible multi-role radio science instrument for making observations of the near space environment. Seven MIDAS-M nodes have now been constructed as part of the Intercepted Signals For Ionospheric Science project (ISIS). Testing is ongoing and initial deployment of the ISIS Array will occur over the next year with the primary focus of early experiments being on multistatic active and passive radar observations of the mid-latitude ionosphere. I will discuss the MIDAS-Mobile system design and its place in an overall software radar architecture. I will also show examples of data for a variety of signal types and discuss plans for early experiments involving both coherent and incoherent scatter radar applications.

## A MID-LATITUDE BISTATIC INCOHERENT SCATTER RADAR SYSTEM

P. J. Erickson, F. D. Lind, J. M. Holt

Atmospheric Sciences Group, MIT Haystack Observatory, Westford,  
MA 01886 USA

A new Millstone Hill / Green Bank Bistatic Incoherent Scatter project currently under way will create a bistatic mid-latitude incoherent scatter radar (ISR) system on the east coast of North America. The system uses the Millstone Hill UHF ISR system at MIT Haystack Observatory in Massachusetts with its 150 foot and 220 foot antennas as the transmitter site and the 140 foot radio telescope at the Green Bank, West Virginia National Radio Astronomy Observatory facility as the receiver site. Green Bank is located at mid-latitudes in close proximity to Millstone Hill (approximately 450 km south and 900 km west), and the ionospheric fields of view of instruments at both sites overlap well. The bistatic incoherent scatter configuration will allow studies of E region thermosphere/ionosphere coupling and F region flows near sub-auroral polarization streams in the dusk sector. Significantly enhanced bistatic link sensitivity to E region coherent backscatter will also serve as a UHF diagnostic of mid-latitude electric field structuring during geomagnetically disturbed events.

The core platform for the remote Green Bank site, denoted MIDAS-Mobile, is a high performance software radio system designed to be easily portable and capable of operation as a flexible, high coherence data acquisition, signal processing, and analysis platform. This instrumentation has been developed through the Intercepted Signals for Ionospheric Science (ISIS) project. The installation of ISIS node 001 at Green Bank/NRAO is the first field deployment for the ISIS array and will enable both bistatic incoherent and coherent scatter observations.

We will discuss project plans, describe expected system capabilities, and present initial results.

PULSE-LEVEL INTERFERENCE AND METEOR PROCESSING OF  
ARECIBO ISR DATA

C.-H. Wen, D. J. Livneh, J. F. Doherty, J. D. Mathews  
Communications and Space Sciences Laboratory, The Pennsylvania  
State University, University Park, PA 16802

The Arecibo 430MHz incoherent scatter radar (ISR) has been used to observe the ionosphere for many decades. Issues have included interference, clutter, meteor returns, and limited real-time signal processing capability. We report application of newly developed interference and meteor processing techniques to 36 hours of pulse-by-pulse voltage-level ISR data from 22/23 March 2004. These observations were made using a 13-baud Barker code and a 10 msec inter-pulse period (IPP) over a 60-540 km altitude range. Interference processing includes signals from other radar systems as well as returns from aircraft and satellites. Meteor returns, characterized as Barker code ambiguity functions at large Doppler shift, are treated as unwanted signals cluttering the ISR results. We present signal processing techniques to remove signals from other radar systems and to separate meteor signals for further analysis to provide useful information for the meteor-related research. This report updates that of C.-H. Wen et al. (*J. Atmos. Solar-Terr. Phys.*, **67**, 1190-1195, 2005).

Observed signals from other radar systems are usually impulsive. We utilize this characteristic to design a nonlinear filter using order statistics to detect and remove the interference. We divide each IPP into several sectors in each sector we compare the maximum and 4th maximum signals. If the ratio exceeds an empirical threshold, we declare interference detection and remove it. For meteor signals, a FFT-based filterbank is utilized to detect and separate the meteor return from the incoherent scatter return. Each filter of the filterbank is a frequency shifted Barker decoder corresponding to different Doppler speeds ranging up to 60 km/sec in 1 km/sec increments. The filter with the maximum impulsive response identifies the correct Doppler speed enabling an energy estimate of that signal that can then be returned to a zero Doppler-shift complex signal that is then subtracted from the original data. The meteor range, speed, and energy are retained for further analysis. Before and after results for the 22/23 March 2004 data set are presented. We note that this processing yields the cleanest E-region ISR results we have ever observed. Further processing of this data reveals 100-540 km quasi-periodic wave structure with a period near 1 hour that lasts through the entire 36 hour data-set. Meteor results are also given.

RETRIEVING METEOR INFORMATION FROM INCOHERENT  
SCATTER DATAGeorge, R.C.<sup>1,2</sup>, Sulzer, M.<sup>2</sup>, Janches, D.<sup>3</sup><sup>1</sup>UC Berkeley<sup>2</sup>Arecibo Observatory<sup>3</sup>NorthWest Research Associates Inc/CoRA Div.

On an effort to monitor the seasonal and inter-annual trends of the sporadic micrometeor activity over Arecibo, Puerto Rico we are developing algorithms that retrieve meteor information from data collected for incoherent scatter studies of the ionosphere. At Arecibo, the 430 MHz radar transmits in many different modes and although they are not best suited for meteor studies, basic parameters such as daily rates, and altitude and velocity information can be obtained. In this manner we can maximize the observing time without the crucial need of requiring specific meteor experiments in an already over-scheduled national facility. We present preliminary results from a meteor search using the coded-long pulse (CLP), power (PWR), and Multiple Radar Auto-Correlation Function (MRACF) modes that are used primarily for studying the E and F regions. For the first mode results of a similar search were already published (Sulzer, Atmos. Chem. and Phys, 4, 947-954, 2004). We have also determined and presented here that meteor information can be obtained from the latter two modes. Processing the PWR mode was successful, but using another algorithm or fitting technique would be beneficial to increase the frequency resolution. The MRACF mode works well for strong signal return meteors, but it is not yet efficient to obtain meteor information from weaker meteors where ambiguous situations can occur. This last mode is based on the simultaneous transmission of 8 pulses, each one separated by 100 kHz. Interestingly, the return amplitude of each pulse relative to the other seem to change randomly for each returned radar inter pulse period or IPP and does not seem to be correlated to the amplitude relation of the transmitted pulses. We believe this variability offers new insight on the nature of the head-echo and speculation on its origin will be discussed.

## OPTIMAL APERTURE SYNTHESIS RADAR IMAGING

D. L. Hysell<sup>1</sup>, J. L. Chau<sup>2</sup><sup>1</sup>Cornell University, Ithaca, NY USA<sup>2</sup>Jicamarca Radio Observatory, Lima, Peru

Radar imaging techniques have been used to investigate coherent backscatter from ionospheric plasma irregularities at Jicamarca and elsewhere for more than ten years. Radar targets of interest include irregularities produced by equatorial spread  $F$ , the equatorial electrojet, 150-km echoes, meteor trails, and mesospheric echoes. The sought after images are related to spaced-receiver data through an integral transform, but direct inversion is generally impractical. Optimal inversion of the data is instead performed using information theory and Bayesian statistics to utilize all available a priori and a posteriori information. The most important constraint on the images, other than the radar data themselves, is the fact that images are positive semidefinite. This reduces substantially the space of possible solutions to be considered. Regularization of the data using an entropy-based metric enforces this constraint while also favoring images with a high likelihood of occurrence. There is also a presumption that the images are, in some sense, smooth. Finally, images are expected to be consistent with the data only to the degree required by the confidence limits of the data. The imaging algorithm used at Jicamarca (called MaxEnt), derived from radio astronomy, implements the principles outlined above. It was improved recently by 1) incorporating the antenna radiation pattern in the a priori probability and 2) estimating and including the full error covariance matrix in the constraints. The new algorithm will be tested using new 28-baseline electrojet data from Jicamarca and compared with less computationally intensive algorithms useful in real-time applications. Methods of validating the images will be discussed.

THE DYNASONDE THREE-DIMENSIONAL PROFILE INVERSION ALGORITHM NEXTYZ: AN INSTRUMENT TO INVESTIGATE MID-SCALE MORPHOLOGICAL FEATURES OF THE IONOSPHERE (SPORADIC LAYERS, PRECIPITATION, GRAVITY WAVES ETC.)

N.A. Zaboltn<sup>1</sup>, J.W. Wright<sup>1</sup>, G.A. Zhabankov<sup>2</sup>, L.Ye. Zaboltna<sup>1</sup>

<sup>1</sup>CIRES, University of Colorado at Boulder, Box 216, Boulder, CO, 80309 USA

<sup>2</sup>Institute of Physics, Rostov State University, Stachki Ave., 192, Rostov-on-Don, 344091 Russia

Electron density profile inversion from digital ionogram data has been re-considered in our previous publications from the viewpoints of new possibilities and of modern requirements. The Dynasonde data processing system (DSND) provides accurate information for every echo, of not only group range but also about its direction of arrival (among other physical parameters), thus yielding three-dimensional distributions of apparent echolocations. A contemporary PC processes this information quickly enough using a multiple ray tracing technique, to obtain parameters of a quite sophisticated three-dimensional model of the local electron density distribution (the so-called Wedge-Stratified Ionosphere). The WSI model characterizes the vertical N(h) profile together with its horizontal gradients and general tilts. This approach has been implemented in the NeXtYZ ("Next Wise") algorithm that inaugurates a new generation of ionospheric electron density inversion procedures.

Ionogram traces can often be characterized as belonging in one or the other of two broad groups: those that describe an essentially continuous (not necessarily vertical) structure, and "fragments" that describe parts of sufficiently intense lateral structures. The first group yields the natural product of NeXtYZ, the WSI parameters and calculated 3-D positions of reflection points for each of the echoes used in that part of the inversion process. In addition, when traces of the second type are present, and provided that WSI parameters from the first group are fully available, ray tracing is performed for echoes in traces of the second type. In this way, NeXtYZ represents accurately all significant ionospheric structures in the local three-dimensional space. It is a useful instrument in research aimed at studies of auroral precipitation, gravity waves and the notoriously intense equatorial structures.

AN INEXPENSIVE DUAL-FREQUENCY GNSS RECEIVER FOR  
USE IN DENSE NETWORKS THAT REMOTELY SENSE TEC AND  
SCINTILLATIONS

Brent M. Ledvina<sup>1</sup>, Todd E. Humphreys<sup>2</sup>, Mark L. Psiaki<sup>2</sup>  
, Thomas L. Gaussarian<sup>1</sup>

<sup>1</sup>Applied Research Laboratories, University of Texas at Austin, Austin,  
TX 78713

<sup>2</sup>Sibley School of Mechanical and Aerospace Engineering, Cornell Uni-  
versity, Ithaca, NY 14853

A new GNSS/GPS receiver is being developed for use in dense networks that remotely sense ionospheric properties. Its suitability for this application derives from its low cost and its enhanced signal tracking abilities. Networks of such receivers will be useful for investigating scintillations, the development and evolution of the associated irregularities, storm-enhanced density, and plasma flow dynamics. This receiver exploits two new technologies in order to provide performance that is superior to that of existing TEC and scintillation monitors. The first technology is the new civilian signal that is about to appear on the GPS L2 frequency. This signal allows civilian receivers to track dual-frequency signals more reliably than current civilian dual-frequency receivers and at a lower cost. Increased reliability comes about because the new signal is not encrypted. An unencrypted signal allows a tracking loop to maintain lock during power fades that are 20 dB deeper than those through which current dual-frequency receivers can maintain lock. The new signal contributes to the cost reduction of the receiver because unencrypted tracking is simpler and because the new L2 civilian signals spread spectrum bandwidth is 10 times narrower than the current L2 signal. A narrower spectrum permits the use of simpler hardware. The second enabling technology is a new type of tracking loop that has been specially designed to maintain lock in the presence of strong signal amplitude and phase fluctuations. The tracking loop uses an extended Kalman filter that automatically adapts loop bandwidth to optimally trade off measurement errors vs. signal dynamics at varying signal power levels. The performance advantage of these technologies is demonstrated using data recorded during equatorial scintillations and using a hardware GPS simulator.



## FIRST LIGHT ON A 3-RECEIVER DISTRIBUTED PASSIVE RADAR SYSTEM

Melissa Meyer, Andrew Morabito, Zachary Berkowitz , John Sahr

University of Washington, Electrical Engr. Dept., Box 352500, Seattle, WA 98195-2500

Distributed, passive radar is emerging as a powerful yet affordable technique in geophysical remote sensing. The Manastash Ridge Radar (MRR) is one such instrument, and until recently it consisted of two receive stations tuned to the FM radio band. In July 2005, we added a third receiver to the MRR network, making the radar multistatic. We will discuss some new scientific opportunities this multistatic architecture affords; particular challenges of deploying and maintaining the three-receiver network; and show some data collected simultaneously on the three receivers.

The MRR now routinely collects commercial FM broadcasts from two to three stations in both Seattle and Spokane, Washington. Scattered signals from plasma density irregularities are received atop Manastash Ridge in central Washington State. The three-receiver system allows us to simultaneously monitor slightly different fields of view in the sub-auroral latitudes of southwestern Canada. With this information we can study the meso-scale properties of phenomena that cause the irregularities, such as the SAPS. Also, we can perform experiments on flow angle and aspect angle sensitivity, and more precisely estimate velocity vectors, within scattering volumes by taking advantage of illumination from multiple angles and frequencies (different FM stations).

Challenges associated with these experiments include proving that the scattering volume detected on each “radar station” is the same. Interferometry proves useful here, and the multiple frequency signals can help to reduce ambiguity in azimuth bearing estimates.

We were fortunate to have the three-receiver MRR system running for the mid-September 2005 solar flare activity and related geomagnetic storms. We will present some of the data we obtained during these events, and show preliminary results from the newly enabled analysis techniques mentioned above.



Session G3, 13:35 – Thurs.

**IONOSPHERIC SPACE WEATHER  
AND FORECASTING**

Co-Chairs: J.C. Foster, T. Fuller-Rowell

G3

## PLANETARY DYNAMICS OF IONOSPHERE STORMS

Andrey Lyakhov , Mikhail Nikitin

Institute of Geospheres Dynamics, Leninskij pr-kt 38m korp.1, Moscow,  
119334, RUSSIA

Ionosphere storms have been studied for more than 40 years using ionozondes and incoherent scattering radars. Meanwhile, some morphological features and underlying physics still remain unclear. EISCAT measurements have shown that TEC is collinear to the NmF2 values. To study not only temporal but also spatial properties of the ionosphere storms we use global TEC data in the same manner as the ionozonde measurements. Namely, for any point we calculate 28 day running median for each hour -  $\overline{TEC}$ . Then the deviation is determined as  $\delta TEC = (TEC_{ij} - \overline{TEC}) / \overline{TEC}$ . When  $\delta TEC$  exceeds 40% over the median value it is considered as the positive disturbance, and when it is less than 60% of the median value it is prescribed to negative disturbance. Years 1995-2004 have been processed. The results of morphological analysis explain the uncertainties in the data of the European ionozonde network. Under westward movement the zone of the positive disturbance may change its shape into the narrow structure and pass between ionozondes.

Very interesting fact is that during strong magnetic storms the coverage of the positive storms significantly increases the same for the negative storms in the mid-latitude region. Negative storms in the mid-latitude region only accompany the positive storms. In the auroral region clear but narrow negative storm is generated under magnetic disturbance.

Generally negative disturbances come to the midlatitudes from the North, traveling westward. Meanwhile, another class of disturbances exists, when the negative zone appears at the subequatorial latitudes (20N) and then moves to the midlatitudes. The rate of movement for the latter is 2-3 times larger than for the classical disturbances produced in the auroral zone.

Results of statistical spatio-temporal analysis are reviewed.

## IONOSPHERIC IMAGING DURING MAJOR STORMS AND THE IMPLICATIONS FOR DISCOVERING PHYSICAL DRIVERS OF THE IONOSPHERE

Bust, G.S.<sup>1</sup>, Mitchell, C.N.<sup>2</sup>, Yin, P.<sup>2</sup>

<sup>1</sup>Applied Research Laboratories, The University of Texas at Austin (ARL:UT), University of Texas at Austin

<sup>2</sup>Department of Electronic and Electrical Engineering, University of Bath, UK

Two four dimensional (4D) ionospheric imaging techniques have been used to study the vertical dynamics of the storm-time ionosphere at mid-latitudes. In both techniques GPS dual-frequency observations are used to produce electron density distribution with a 4-D tomography inversion technique. The Multi-instrument Data Analysis System (MIDAS) uses only GPS, while GPS, as well as data from other sensors are used in the 3DVAR objective analysis algorithm Ionospheric Data Assimilation Three Dimensional (IDA3D). The advantage of GPS for physical studies of the ionosphere is that the data are available all of the time during and since the recent solar maximum - all storms can be studied and compared.

For this study, these two algorithms have been used to explore the mid-latitude response to three major ionospheric storms that occurred in: (i) 15 July 2000, (ii) 30 Oct 2003 and (iii) 20 Nov 2003. The characteristics of all three storms in terms of TEC, F region heights (hmF2) and electron densities (NmF2) have been compared. We analyzed the TEC and hmF2 as a function of universal time (UT) and different longitudinal sectors across Europe and the USA. We have also analyzed the characteristics and evolution of these storms with latitude. The use of two independent techniques, with different underlying assumptions, for inverting the same GPS data gives confidence in the resulting images and their unexpected physical results in terms of the changes in ionospheric morphology.

Here, we report the results of our observations and analysis of the dramatic uplifts of F2 layer heights have been observed in mid-latitude ionosphere over Europe and the USA for all three storms. We discuss the dependence of these uplifts on longitudinal sector, latitude, universal time and changes in the Interplanetary Magnetic Field (IMF) - in particular the southward turning (Bz component). We also discuss how the 4D imaging observations can be used to help in the understanding of what physical mechanisms are responsible for the TEC changes with heights, such as neutral winds, electric fields and photo-ionization effects.

## MAJOR STORMS OF 2000-2005 AS OBSERVED BY THE RADIO PLASMA IMAGER AND THEIR SONIFICATION

Briea, P.<sup>1</sup>, Galkin, I.A.<sup>1</sup>, Reinisch B.W.<sup>1</sup>, Song, P.<sup>1</sup>, Green, J.L.<sup>2</sup><sup>1</sup>University of Massachusetts Lowell, Center for Atmospheric Research<sup>2</sup>NASA Goddard Space Flight Center

The Radio Plasma Imager (RPI) on NASAs IMAGE mission is continuously monitoring plasma wave natural emissions in the magnetosphere and plasmasphere of the Earth using high-sensitivity passive-mode reception between 3 and 1200 kHz. The 14.2 hour elliptical orbit of the IMAGE spacecraft with the perigee at 1200 km and the apogee altitude at 7.2 RE gives an excellent opportunity to record a variety of signatures pertaining to the processes in the solar-terrestrial system. Even outside the plasmasphere, the RPI can capture a detailed record of the solar type III radio bursts often associated with an elevated explosive activity on the Sun such as the coronal mass ejections (CME) that often accompany the solar flares. When inside the plasmasphere, RPI observes the whistler-mode radiations that reflect dynamics of the energetic particle streams via the particle-wave interaction mechanism. Finally, passive mode RPI spectrograms can be inspected for signatures of the upper-hybrid resonance and gyrofrequency harmonics, providing means of obtaining local measurements of the plasma density and the Earths magnetic field strength along the orbit. Thus, the RPI passive reception mode has a good potential for space weather applications, providing within a single frame of observation a set of identifiable signatures belonging to important events associated with the storm activity in the Sun-Earth system. We have developed a sonification technique that translates the RPI spectrograms to sound indicating intensity and frequency range of the received radiation. This paper presents several case studies of the major storms during 2000-2005 observed by the RPI instrument, including the Tax Day storm of 2002, the Halloween storm of 2003, the Bastille Day storm of 2000, and a recent sequence of solar flares in September 2005. The identified RPI signatures recorded during these events are compared to observations made by other space weather instruments.

## SUB-AURORAL ELECTRIC FIELD EFFECTS ON THE MID-LATITUDE IONOSPHERE

Foster, J.C.<sup>1</sup>, Coster, A.J.<sup>1</sup>, Colerico, M.<sup>1</sup>, Rideout, W.<sup>1</sup>, Rich, F.J.<sup>2</sup>

<sup>1</sup>MIT Haystack Observatory, Westford, MA 01886 USA

<sup>2</sup>Air Force Research Lab, Hanscom AFB, MA

Magnetospheric electric fields and ionosphere-magnetosphere feedback contribute strongly to the formation of ionospheric space weather effects over populous mid-latitude regions during severe geomagnetic disturbances. Electric fields often appear in regions of low ionospheric conductivity equatorward of auroral electron precipitation. Currents driven into the sub-auroral ionosphere from the disturbed ring current put into play a sequence of M-I coupling and feedback mechanisms with dramatic consequences for the electric fields and particle populations of the Plasmasphere Boundary Layer (PBL). The Sub-Auroral Polarization Stream (SAPS) defined by Foster and Burke [EOS, 83(36), 393, 2002] refers to the broad, persistent, poleward-directed electric fields which drive sunward plasma convection at sub-auroral latitudes in the evening local time sector. Observations of subauroral plasma convection with DMSP satellites and the Millstone Hill incoherent scatter radar, have been used to characterize SAPS phenomenology at low altitudes ( $\leq 1000$  km) in the coupled inner-magnetosphere / ionosphere system.

The effects of SAPS in the ionosphere and magnetosphere can be spectacular - including Storm Enhanced Density (SED) plumes of greatly enhanced ionospheric total electron content (TEC), erosion of the dusk-sector plasmasphere, and the formation of sunward-reaching plasmasphere drainage plumes. These features constitute significant space weather effects and an understanding of the global nature of the coupled upper-atmosphere systems which drive them is needed to model or predict their occurrence and severity. The inward extent of the SAPS electric field overlaps the outer plasmasphere on field lines mapping to the high-density cold plasmas equatorward of the ionospheric trough. We use ground-based GPS propagation data to produce two-dimensional maps depicting the evolution of the SED features as they are carried from their low-latitude source to the cusp ionosphere and across the polar caps.

Penetrating electric fields and storm positive-phase disturbances combine to produce greatly elevated TEC in the dusk-sector PBL. This solar-produced ionization constitutes the source plasma for the SED plumes which are carried to higher latitudes in the SAPS flow. Ground-based radio-propagation data provide a means of monitoring these phenomena over large portions of the globe.



## AN EXAMINATION OF THE VARIABILITY AND CORRELATIONS IN THE TOPSIDE IONOSPHERE

T W Garner<sup>1</sup>, B T Taylor<sup>1</sup>, T L Gaussiran II<sup>1</sup>

, M R Hairston<sup>2</sup>, R W Coley<sup>2</sup>

<sup>1</sup>Applied Research Laboratories, University of Texas at Austin, Austin, TX

<sup>2</sup>W Hanscom Center for Space Science, Univeristy of Texas at Dallas, Richardson, TX

In order to understand the global response of the ionosphere to space weather events, it is important to examine the inherent variability of the ionosphere and the correlations associated with this variability. This paper examines both the variability of the topside ionosphere and the correlations between the different distributions of the observations. For this study, the existing database of electron density observations from the Defense Meteorological Satellite Program (DMSP) is used. These observations have been taken for nearly a complete solar cycle from 1995 to 2005 with some earlier observations. The measurements are taken over all geographic latitudes and longitudes every four seconds along the satellite orbit. However, the data exist in four local time regions at mid and low latitudes. In total, over eighty million data points are included in this statistical study.

The topside electron densities, when binned by F10.7 cm solar radio flux and geomagnetic latitude, obey a lognormal distribution. These distributions can be characterized by three parameters: a scale parameter related to the median density, a location parameter related to the minimum observable density, and a shape parameter related to the width of the tail of the distribution. These parameters are calculated from the data and are presented. Finally, linear correlation coefficients can be constructed from these distribution functions, which represent the overall correlation in the variability of different ionospheric regions. Since each data bin has a different number of data points, sample distributions using the statistical parameters are constructed for a 20000 point distribution. During geomagnetic storms, these correlations provide insight into the ionospheric response in data sparse regions.

## MODELING THE F2 TOPSIDE AND PLASMASPHERE FOR IRI

Nsumei, P.<sup>1</sup>, Reinisch, B. W.<sup>1</sup>, Huang, X.<sup>1</sup>  
, Bilitza, D.<sup>2</sup>, Gallagher, D. L.<sup>3</sup>

<sup>1</sup>Center for Atmospheric Research, University of Massachusetts Lowell, 600 Suffolk St., Lowell MA 01854

<sup>2</sup>Raytheon ITSS, GSFC Code 632, Greenbelt MD 20771

<sup>3</sup>NASA Marshall Space Flight Center, Space Science Dept., SD50, Huntsville, Alabama 35812

Empirical models are an important tool for the study of the different geospace regions from Earth to sun, providing the user with easy access to a synthesis of most or all reliable measurements from ground and space for specific parameters and regions. This paper describes a new effort to develop a coherent model of the topside F2 layer and the plasmasphere with the goal to improve the representation of the topside electron density in the IRI model and to extend the IRI description into the plasmasphere. An  $\alpha$ -Chapman function with a continuously varying scale-height, dubbed a vari-Chap function, is used to describe the topside F2 vertical electron density profile  $N(h)$  that seamlessly connects the ionosphere with the plasmasphere. While the Chapman (neutral) scale-height  $H(h)$  varies only slowly near  $h_mF2$ , it increases rapidly at the  $O^+$  to light-ion transition height. A hyperbolic tangent function is suitably representing this variation. New plasmasphere density profile data from the IMAGE/RPI measurements and topside profiles from the ISIS topside sounders are used to construct a continuous profile from  $h_mF2$  to several RE altitude. A large number of ISIS-2 topside profiles have recently become available through the TOPIST-processing of the digitized ISIS-2 ionograms. We represent these profiles in terms of vari-Chap functions using a scale-height function that is specified by three parameters: the height  $h_T$  and scale-height  $H_T$  of the  $O^+$  to  $H^+$  transition and a shape factor that controls the gradient of  $H(h)$  at the transition height. These parameters show a systematic variation with latitude. The task of matching the topside profiles to the RPI measured profiles in the plasmasphere and polar cap is under development.

DAY-TO-DAY VARIABILITY IN DAYTIME, VERTICAL EXB  
DRIFT VELOCITIES AT TWO CLOSELY SPACED, LONGITUDE  
SECTORS

Anghel, A.<sup>1</sup>, Anderson, D.<sup>1</sup>, Chau, J.<sup>2</sup>, Yumoto, K.<sup>3</sup>

<sup>1</sup>Univ. of Colorado/CIRES, NOAA/SEC, Boulder, Colorado

<sup>2</sup>Radio Observatorio de Jicamarca, Instituto Geofísico del Perú, Lima, Peru

<sup>3</sup>Space Environment Research Center, Kyushu University, Japan

A recent study has quantitatively established the relationship between the vertical daytime ExB drift velocity in the ionospheric F region and the DH values measured by two magnetometers in the South American (west coast) longitude sector. Magnetometer H component observations from Jicamarca (0.8 N. dip lat.) and Piura (6.8 N. dip lat.) in Peru and daytime, vertical ExB drift velocities measured by the Jicamarca Unattended Long-term Ionosphere and Atmosphere (JULIA) radar have been used to establish this relationship. The magnetometer observations and the JULIA 150 km echo ExB drift measurements were obtained for the period between January, 2001 and December, 2004. It has also been demonstrated that the DH vs ExB drift relationships derived in the Peruvian longitude sector can be applied in the Philippine longitude sector to provide realistic ExB drift velocities that, for quiet days, compare favorably with the Fejer-Scherliess, climatological ExB drift model. In the Philippine sector, magnetometers located at Davao (125.4 E. geog. long., 1.4 S. dip lat.) and Muntinlupa (121.0 E. geog. long., 6.3 N. dip lat) provided the daytime DH values that were used to infer the vertical ExB drift velocities at this longitude. Expanding on these studies, this investigation now examines the day-to-day variability in vertical ExB drift velocities in both the Philippine and Indonesian longitude sectors. Between January, 2001 and December, 2004, there are over 450 geomagnetically quiet days ( $A_p \leq 10$ ) and more than 230 geomagnetically disturbed days ( $A_p \geq 20$ ). Magnetometer observations from Davao and Muntinlupa in the Philippines and from Yap (138.5 E. geog. long., 10 N. dip lat.) and Biak (136.0 E. geog. long., 9.70 S dip lat.) in Indonesia provide the DH-inferred ExB drift velocities for these quiet and disturbed days. Specific questions that will be addressed are: 1.) How do the DH-inferred ExB drift velocities compare between the two longitude sectors on a day-to-day basis, 2.) How do the quiet-day average ExB drift velocities compare with the Fejer-Scherliess climatological model, 3.) For disturbed days, are the magnitudes of the prompt penetration electric fields in the Philippine sector consistent with the observations in the Indonesian sector? The impact of these results on Space Weather, low latitude, theoretical and operational ionospheric models will be discussed.

## UPPER ATMOSPHERE MODIFICATION UNDER THE MOVEMENT OF THE NORTH MAGNETIC POLE

Andrey Lyakhov<sup>1</sup> , Timothy Fuller-Rowell<sup>2</sup>

<sup>1</sup>Institute of Geospheres Dynamics

<sup>2</sup>CIRES University of Colorado , and NOAA Space Environment Center, , Boulder, CO.

The North Magnetic Pole (NMP) rate of movement has more than doubled in the last 30 years, reaching a velocity of around 40 km/year in 2001. This fact may indicate the possible approach of a polarity reversal. Since 1970 the NMP moved directly from the American Arctic sector towards the Russia coast. At the current rate, extrapolation predicts it's position will be somewhere near Severnaya Zemlya (approximately 80N, 100E) by 2050. In this paper we investigate the likely consequences of the NMP shift on the structure of the ionosphere and thermosphere.

The reasons for this work are clear. The present state of the upper atmosphere is the result of the dynamical balance between solar energy input and the energy flux from the magnetosphere. The latter obviously depends on the magnetic pole position. The movement of the auroral oval towards midlatitudes implies the balance between solar radiation and auroral precipitation will change significantly at a given location. Simulations of the impact have been performed using a coupled thermosphere-ionosphere model (CTIM), to investigate the impact of the change in NMP position from its known location in 2000 to its predicted position in 2050. CTIM allows the study of the impact within the context of the self-consistent interaction between the ionosphere and thermosphere. Results are presented for all seasons. The simulations indicate that the structure of the upper atmosphere will change significantly. The current classification of the "polar" and "mid-latitude" ionosphere will be lost. The polar ionosphere would merge with the mid-latitudes and the auroral zone (under magnetic disturbances) will reach to the Chinese border. The configuration of the neutral winds will also change thus modifying the response of the mid-latitude ionosphere to geomagnetic storms. The interaction of solar and magnetosphere-driven wind fields will become more complex and will alter the transport of internal energy, affecting the global temperature structure and neutral composition.

The possible consequences on radio communications and space weather will also be discussed.





Session G4, 08:35 – Fri.

## **DATA ASSIMILATION**

Co-Chairs: B. Wilson, L. Scherliess





## INCORPORATING VIRTUAL HEIGHT PROFILES INTO THE IONOSPHERE DATA ASSIMILATION THREE DIMENSIONAL (IDA3D) ALGORITHM

T W Garner, G S Bust, S Kilpatrick

Applied Research Laboratories, University of Texas at Austin, Austin, TX

After total electron content measurements from ground-based GPS receivers, observations from the global network of digisondes and ionosondes are the most abundant source of ionospheric data. These instruments emit a radio pulse at a given frequency and measure the reflection time of the pulse. Traditionally, the reflection time  $\tau$  is reported as a virtual height  $h' = c\tau/2$ . Since digisondes emit a series of pulses at different frequencies, a virtual height profile is constructed as a function of the emission frequency. This profile can be inverted into an electron density profile as a function of altitude. These profiles or the peak values of the profiles are usually reported to the publicly-available data centers. Presently, ionospheric data assimilation and analysis algorithms use the inverted electron density values derived from digisondes and ionosondes. However, the usage of derived densities goes against the spirit of objective analysis algorithms.

In general, objective analysis (OA) algorithms (data assimilation models contain an OA module) attempt to manipulate the observed data as little as possible. Instead, the background specification is transformed into the quantity and location of the measurement. The difference between the observations and the transformed background values is the innovation vector. Hence, the innovation for a point measurement of electron density is the difference between the measurement and the background electron density interpolated to the measurement location. Similarly, the innovation for a slant TEC measurement is the difference between the measurement and the background electron densities integrated along the GPS ray path. This study presents the first attempt to incorporate virtual height measurements into an OA algorithm rather than the inverted densities.

## VALIDATION OF THE 4D IMAGING ALGORITHM IDA3D

Bust, G.S., Garner, T.W., Taylor, B.

Applied Research Laboratories, The University of Texas at Austin  
(ARL:UT), University of Texas at Austin

Recently, several new methods have been developed to specify and/or predict ionospheric electron densities over large spatial and temporal regions. These methods have applicability both towards Space Weather modeling and forecasting, and towards helping in the understanding of what physical phenomena is responsible for the observed electron densities. Some of these algorithms are true data assimilation models that combine data directly with first principle models. Other algorithms, such as 4D ionospheric imaging algorithms, more directly use the data to specify or image the electron density. In order for these new imaging techniques to be useful they must be validated against independent data sets. This is particularly true when 4D imaging results are used to constrain first principle models and assist in determining what is the underlying physics. For such cases it is necessary that an accurate estimate of the error on the imaging be provided.

In this presentation we present the current status of our continuing validation of the 4D ionospheric imaging algorithm Ionospheric Data Assimilation Three Dimensional (IDA3D). In order to validate IDA3D we have selected analysis days that represent solar minimum and maximum conditions; summer, winter and equinox; and low and high geomagnetic activity levels. We compare the IDA3D results to climatology and to first principle ionospheric models. As independent data sets we use incoherent scatter radar (ISR) observations of electron densities, in-situ observations of electron density from the CHAMP satellite, and total electron content (TEC) observations from TOPEX. We analyze the accuracy of IDA3D both through direct comparisons with the independent data, and through a skill score calculation that measures the relative improvement IDA3D provides over climatology.

The skill score is defined as

$$S = 1.0 - \frac{\langle |\vec{D} - \vec{T}| \rangle}{\langle |\vec{M} - \vec{T}| \rangle}. \quad (1)$$

Where  $\vec{D}$  is the array of metric values output from IDA3D,  $\vec{T}$  is the independent measurements of the metric that serve as "truth", and  $\vec{M}$  is the array of climate predictions of the metric values. The skill is a function of time in the sense that every time IDA3D is improved a new skill score is generated. The values of the skill score range from 1.0 for when the data assimilative model is perfect (that is agrees with the measurements), to 0.0 when the data assimilative model is no better than the climate predictions, to negative infinity as the data assimilative model does much worse than climate.

We will present results of how well IDA3D estimates electron density and TEC in terms of an absolute measure of error and the relative skill score for the different days described above. This analysis of the accuracy of IDA3D is a first step towards fully quantifying the error on imaging algorithms.

## INITIAL VALIDATION STEPS FOR THE USTEC IONSOPHERIC NOWCAST SYSTEM

C. F. Minter<sup>2</sup>, E. A. Araujo-Pradere<sup>2</sup>, D. S. Robertson<sup>B</sup>,  
P. S. J. Spencer<sup>B</sup>, T. J. Fuller-Rowell<sup>2</sup>, A. R. Jacobson<sup>4</sup>,  
R. Moses<sup>4</sup>, D. M. Susczynsky<sup>4</sup>

<sup>1</sup>Cooperative Institute for Research in Environmental Sciences, University of Colorado

<sup>2</sup>NOAA - Space Environment Center

<sup>3</sup>National Geodetic Survey, NOS/NOAA

<sup>4</sup>Los Alamos National Laboratory

Initial validation for the United States Total Electron Content (USTEC) nowcast system has been underway. USTEC provides 4-dimensional total electron content maps over the continental United States. MAGIC the analysis version of USTEC is evaluated in using two different methods. The first examines forecast error growth with time through differential validation. In this method, error growth, obtained from the difference between the actual and expected observation, asymptotes to a final value with time, indicating a type of upper bound on the error of the system. The upper bound for this method indicates an error within 2 to 3 TECU over the United States. The second method uses ionosphere imaging data assimilation software with total electron content data from the Fast Onboard Recording of Transient Events (FORTE) satellite to evaluate the combined error level of the MAGIC and FORTE systems. The MAGIC/USTEC software uses ground-based GPS observations to model the 4-dimensional variations in the electron density of the ionosphere. The FORTE satellite detects the arrival time vs. frequency for a broadband (pulse) VHF signal from a transmitter at Los Alamos. The resulting group-delay measurements can be used to estimate the TEC along the raypath. Because of the relatively low frequencies involved, raypath bending effects are significant and have been corrected using a numerical integration raytrace algorithm. The RMS errors between the FORTE and MAGIC solutions is about 2.872 TECU using all the FORTE observations and 60 GPS stations in MAGIC. This value can be reduced to 1.659 TECU if FORTE observations with high ( $\geq 55$  degrees) elevation angles and low ( $\leq 60$  TECU) TEC values are chosen to mitigate numerical errors from the raypath bending calculation. Increasing the number of GPS stations in the MAGIC solution to 133 reduces these numbers to 2.705 TECU and 1.148 TECU respectively.

DIGISONDE TECHNOLOGIES IN SUPPORT OF IONOSPHERIC  
DATA ASSIMILATION

Galkin, I.A., Khmyrov, G.M., Reinisch, B.W.  
, Huang, X, Kozlov, A.V., Kitrosser, D.

University of Massachusetts Lowell, Center for Atmospheric Research

Ionospheric data assimilation techniques have gone a long way since the 1980s when the space weather prediction systems started to rely on real time ionospheric conditions derived from ionospheric HF sounding data. Next generation assimilative models based on Kalman filtering impose new requirements on the real-time data suppliers. The University of Massachusetts Lowell digisonde group has expended a considerable development effort in recent years to meet the requirements and provide reliable and seamless source-to-destination performance of ionosonde networks. This paper describes the status of the digisonde networking as an example for any modern ionosonde network and discusses its evolution in light of recent technology trends in distributed sensor networks. In order to quantify uncertainty of the electron density profiles provided to the assimilation models, the ionogram scaling algorithm ARTIST is currently augmented to automatically determine the uncertainty for an appropriate set of anchor points using the time of measurement, ionosonde location, and spread F characteristics, and obtain the inner and outer boundaries that enclose the profile by modifying the profiles Chebyshev coefficients so that the boundary fits the uncertainty intervals on the anchor points. Special attention is paid to automated and unattended operations of the sensor network components, including the digisonde itself, the data ingestion servers, the Digital Ionogram Database (DIDBase) and the Drift Database (Drift-DB), and the Automated Data Request Execution Subsystem (ADRES) designed to manage incoming requests for verified ionospheric data. The paper discusses lessons learned from the ADRES operations in support of calibration/validation campaigns for space borne UV profile measurements.

PRINCIPLES OF EFFECTIVE IONOSPHERIC DATA ARCHIVING  
AND WEB SERVICET.W. Bullett<sup>2</sup>, N.A. Zabolin<sup>3</sup>, J.W. Wright<sup>3</sup>, L.Ye. Zabolina<sup>3</sup><sup>1</sup>Air Force Research Laboratory, Space Vehicles Directorate, Hanscom  
AFB, MA, USA<sup>2</sup>NOAA, E/GC 325 Broadway, Boulder, CO, 80305-3328 USA<sup>3</sup>CIRES, University of Colorado at Boulder, Box 216, Boulder, CO,  
80309 USA

Modern advanced digital ionosondes produce abundant and diverse information about the current state of the ionosphere. For each sounding session (an "ionogram") it includes several tens of standard ionospheric parameters, an estimation of the local three-dimensional distribution of electron density, vector velocities, irregularity characteristics, trace-classified ionogram data in the form of echo tables (up to several thousand entries), etc., with attached error estimations. This information must also be accompanied by software/hardware configuration parameters or "metadata" comprising several tens of numerical and string values. The correct and modern way to handle such datasets is to use relational database technologies for storage and retrieval.

A central archival storage equipped with a relational DBMS enables data analysis from broad geographic areas (and even globally), to compare data from different locations, and to review long time series of data. Quite sophisticated scientific problems may be posed and solved this way. An example on the frontier of Dynasonde diagnostics technology is the discovery of a positive correlation between the Anomalous Attenuation (AA) of ionospheric radio echoes caused by multiple scattering, and small-scale irregularity amplitude deduced by the Phase Structure Function method. Another example is an investigation of statistical properties of radio echoes for various geographical locations that reveals both ionospheric state indications and peculiarities of hardware operation.

A relational DBMS supports straightforward ways to create and support a web service, providing easy access to data for the scientific community and for customers with both small and large data demands. Customers perceive effective operation of DBMS web services that offer: (1) customer-defined type and format of the data provided; (2) data availability both in near-real-time and in retrospect; (3) no specialized software for access: only internet browser needed for interactive sessions; (4) an XML-based (SOAP) interface for automated requests; (5) effective data mining and visualization tools; (6) data re-processing on-line, when required; (7) free access for individual customers after automated registration.

Visit <http://www.ngdc.noaa.gov/stp/IONO/Dynasonde/> to exercise an operating prototype of a central repository/web service offering these features for existing Dynasondes.

## INCOHERENT SCATTER RADAR BASED EMPIRICAL MODELS

Zhang, S.-R.<sup>1</sup>, Holt, J. M.<sup>1</sup>, van Eyken, A. P.<sup>2</sup>,  
McCready, M.<sup>3</sup>, Amory-Mazaudier, C.<sup>4</sup>, Fukao, S.<sup>5</sup>, Sulzer, M.<sup>6</sup>

<sup>1</sup>MIT Haystack Observatory

<sup>2</sup>EISCAT Association

<sup>3</sup>SRI International

<sup>4</sup>CNRS Centre for the Study of Earth and Planets Environments

<sup>5</sup>Kyoto University Research Institute for Sustainable Humanosphere

<sup>6</sup>NAIC Arecibo Observatory

This paper presents an overview of empirical ionospheric models developed from long-term incoherent scatter radar observations at 7 sites. These include local models for Sondrestrom, Millstone Hill, and Arecibo radars, respectively, in America longitudes, local models for EISCAT Svalbard and mainland radars and for St. Santin radars in Europe, and local models for the Middle and Upper atmosphere radar at Shigaraki in Asia. These models cover a height range largely between 100-600 km, with exceptions for Millstone Hill for up to 1000 km, and for Shigaraki for starting from 200 km. Developed also are a regional model over Millstone Hill area based on the radar's steerable antenna measurements spanning 32-55° geographic latitudes and a regional model for the America sector incorporating local models for the three NSF UAFs and Millstone Hill regional model. These models produce variations in electron density, ion and electron temperatures, as well as ion parallel drifts for some radars, as a function of height, local time and season with dependence on solar and magnetic activities.

In addition to models for the scalar parameters, a new high-latitude convection model is produced based on line-of-sight velocity measurements provided by the Millstone Hill extra-wide coverage experiments and by Sondrestrom compscan experiments. The convection model has a dependence on Interplanetary Magnetic Fields (IMF) components Bz and By and its variations with season are also identified. The convection can be also driven by an alternative set of parameters, Kp index and the IMF By direction. Future plans for new ISR-based models will be briefly discussed.

## JPL/USC GAIM: A REAL-TIME GLOBAL IONOSPHERIC DATA ASSIMILATION MODEL

Brian Wilson<sup>1</sup>, Lukas Mandrake<sup>1</sup>, George Hajj<sup>1</sup>, Chunming Wang<sup>2</sup>, Xiaoqing Pi<sup>1</sup>, Byron Iijima<sup>1</sup>

<sup>1</sup>Jet Propulsion Laboratory

<sup>2</sup>University of Southern California

We are in the midst of a revolution in ionospheric remote sensing driven by the illuminating powers of ground and space-based GPS receivers, new UV remote sensing satellites, and the advent of data assimilation techniques for space weather. The University of Southern California (USC) and the Jet Propulsion Laboratory (JPL) have jointly developed a Global Assimilative Ionospheric Model (GAIM) to monitor space weather, study storm effects, and provide ionospheric calibration for DoD customers and NASA flight projects. GAIM is a physics-based 3D data assimilation model that uses both 4DVAR and Kalman filter techniques to solve for the ion & electron density state and key drivers such as equatorial electrodynamics, neutral winds, and production terms. GAIM accepts as input ground GPS TEC data from 1000+ sites, occultation links from CHAMP, SAC-C, IOX, and the coming COSMIC constellation, UV limb and nadir scans from the TIMED and DMSP satellites, and in situ data from a variety of satellites (C/NOFS & DMSP). GAIM ingests multiple data sources in real time, updates the 3D electron density grid every 5 minutes, and solves for improved drivers every 1-2 hours. Since our forward physics model and the adjoint model were expressly designed for data assimilation and computational efficiency, all of this can be accomplished on a single dual-processor Unix workstation.

GAIM density retrievals have been validated by comparisons to vertical TEC measurements from TOPEX & JASON, slant TEC measurements from independent GPS sites, density profiles from ionosondes & incoherent scatter radars, and alternative tomographic retrievals. Daily JPL/USC GAIM runs have been operational since March 2003 using 100-200 ground GPS sites as input and TOPEX/JASON and ionosondes for daily validation. A prototype real-time GAIM system has been running since May 2004. RT GAIM ingests TEC data from 80+ streaming GPS sites every 5 minutes, adds more TEC for better global coverage every hour from hourly GPS sites, and updates the ionospheric state every 5 minutes using the Kalman filter. We plan to add TEC links from COSMIC occultations and UV radiance data from the DMSP satellites, when they become available, to the daily and RT GAIM runs. Our presentation will include results from numerous validation case studies, including profile validation using ISR data, and more than a year of TOPEX/JASON validation statistics. Customers are currently evaluating the accuracy of JPL/USC GAIM 8220;nowcasts8221; for ray tracing applications and trans-ionospheric path delay calibration.





Session G/H1, 13:15 – Fri.

**METEOR PHYSICS**

Co-Chairs: Y. Dimant, J.D. Mathews



## METEORIC HEAD ECHOES: THEORETICAL PRODUCTION RATES AND REQUIRED LEVELS FOR DETECTION

ReVelle, D.O.

Los Alamos National Laboratory

Small and generally quite high velocity meteoroids interacting with the upper and middle atmosphere lose their initial kinetic energy by producing heat, light, ionization, dissociation, diffuse waves, ablation and fragmentation debris, etc. The instantaneous and remnant ionization produced can be readily detected by both classical and large aperture radar systems. It has been a long standing problem that the instantaneous part of the ionization is difficult to interpret theoretically even though the standard range time plots available from classical meteor radars have consistently shown that the slope of the electromagnetic signal return is from a moving ball target whose velocity is consistent with the instantaneous meteor velocity. Recently, Janches and ReVelle (2005) have developed a set of single-body meteor entry relations to theoretically predict the instantaneous ionization levels (neglecting recombination effects at lower atmospheric heights where the atmospheric densities are much larger) as well as the prediction of the levels required for ground-based detections of this ionization. It was determined that the predicted detection threshold is a function of the depth of penetration of the meteors with smaller values required at progressively higher end heights. In order to achieve this required level an assumption had to be made regarding the absolute level of ionization in the gas cap volume in front of the meteor. We have attempted to bound this problem by assuming that the required level of ionization in the gas cap should fall between the synoptic, naturally occurring values prevailing in the ambient undisturbed atmospheric column (at the corresponding D, E or F region heights) and an upper limit produced by the intense meteor-atmosphere interaction and assumed to correspond to a 0.10 percent ionization level. Surprisingly, naturally occurring, ionospheric background levels were found sufficient to determine the required level of ionization necessary at quite large Knudsen numbers for ground-based radar detection of the instantaneous ionization levels produced theoretically. In this talk we will examine these predictions in more depth to try to better understand the full implications of these new predictions.

## VELOCITY AND MASS BIASES IN HPLA HEAD ECHO DATA

Sigrid Close<sup>1</sup>, Patrick Colestock<sup>1</sup>, Meers Oppenheim<sup>2</sup><sup>1</sup>Los Alamos National Laboratory, Space and Remote Sensing Sciences<sup>2</sup>Boston University, Center for Space Physics

High-power large-aperture (HPLA) radars provide a unique capability for characterizing the meteoroid population. HPLA radars are best-suited for detecting the meteor head echo, which is the radar return from the plasma immediately surrounding the meteoroid and moving at approximately the meteoroid velocity. Classical meteor radars, in comparison, are best suited for characterizing the specular trail, which is the reflection from the quasi-stationary plasma behind the meteoroid. The meteoroid population detected by HPLA radars differs from meteoroids detected using classical radars. For example, HPLA radars primarily detect sporadic meteoroids, even during shower periods, and the particles tend to be smaller and less massive than those seen by classical radars. Also, HPLA radars show a higher average velocity relative to classical data. For example, the ALTAIR and Arecibo data puts the average speed near 55 km/s. One possible explanation for this difference lies in the radar selection effect. Specifically, it has been posed that HPLA radars are more sensitive to the high-velocity meteoroid population, since the ionization probability scales with the velocity (to some power). This presentation addresses the possible biases in HPLA data by examining data collected by the ALTAIR system.

First, we review the dependence of head echo signal-to-noise (SNR) and radar-cross-section (RCS) on meteoroid mass and velocity. Second, we identify and model this radar selection effect. Finally, we apply this selection effect to our HPLA data in order to determine any possible biases in our detected meteoroid mass and velocity distributions. Our results can potentially be applied to all HPLA data.

ELECTROMAGNETIC SCATTERING  
FROM METEOR-GENERATED SPHERICAL PLASMAS WITH FI-  
NITE PRESSURE: PLASMA WAVE RESONANCES AND PLASMA  
GRADIENT EFFECTS

Patrick Colestock, Sigrid Close

Los Alamos National Laboratory, Space and Remote Sensing Sciences

The plasmas that are created at the heads of meteors descending into the upper atmosphere present clear RCS signatures for determining the speed and mass of the projectile. In particular, the size of the critical layer where the incident wave frequency is equal to the plasma frequency, coupled with the knowledge of the mean free path for ionization, can be used to infer the mass. However, both geometric and dielectric properties of the plasma can affect the RCS, and these must be taken into account when interpreting the scattered radiation. Although scattering from spherical reflecting layers is well understood (i.e. Mie scattering) even in the presence of plasma inhomogeneities, the potential for exciting electron plasma waves in the underdense region of the plasma can radically affect the RCS. These electrostatic, longitudinal waves are coupled to the incident transverse waves through the density gradient and the resulting resonances, known as Tonks-Dattner resonances, and give rise to new bands of absorption not present in a cold plasma. The full scattering cross-section is developed as a series of spherical harmonics where the surface impedance of the plasma plays a crucial role in determining the scattering. For the general case, this impedance is found by a numerical integration of the wave equations, but for many cases of practical interest, WKB analysis is adequate. We present the analysis of the warm plasma boundary value problem and derive an expression for the RCS. The implications for the interpretation of RCS data for meteor head echoes will be given.

## HIGH RESOLUTION METEOR OBSERVATIONS USING THE 50MHZ JICAMARCA RADAR

Meers M. Oppenheim<sup>1</sup>, Jorge L. Chau<sup>2</sup>, Elizabeth N. Bass<sup>1</sup><sup>1</sup>Center for Space Physics, Boston University, 725 Comm. Ave, Boston MA 02215<sup>2</sup>Jicamarca Radio Observatory, Instituto Geofisico del Per, Apartado 13-0207, Lima 13 - Peru

High-power, large-aperture (HPLA) radars frequently observe two types of signals resulting from meteors. First, they measure head echoes, short duration echoes with large Doppler shifts created at the leading edges of ablating meteoroids. Later, they may detect non-specular trails, echoes which persist for a period lasting from a few 100ms to over 10minutes. These occur only in a limited altitude range and only if the radar wave is propagating nearly perpendicular to the geomagnetic field. In July, 2005 we recorded many hours of measurements using the large 50MHz antenna at the Jicamarca Radio Observatory near the magnetic equator in Peru. These observations were made with the shortest possible pulse period (sub-microsecond) for this radar in order to give us the maximum time and range resolution. The radar was configured to return separate signals from three sections of the radar, allowing us to use interferometry to locate the positions and velocities of the echoes within the beam.

These measurements immediately revealed two interesting features of such observations. First, as in the highly resolved ALTAIR measurements, they typically showed distinct head echoes followed by a short period of little to no signal, and then were sometimes followed by a non-specular trail signal lasting for up to many minutes. These measurements strongly suggest that the gap between head and trail echoes will appear in nearly all observations with sufficient time and range resolution. Second, these measurements show a dramatic difference in the frequency and altitude range of non-specular echoes between daytime and nighttime. During nighttime, meteors generate far more non-specular trails over a far broader altitude range than during daytime.

In this talk, we will discuss these measurements and present statistics generated from thousands of head echoes and trails. We will compare our results to earlier observations. Additionally, we will interpret these observations in terms of both earlier theories of non-specular meteor trails and the recent theoretical work of Oppenheim and Dimant (presented at this meeting).

## APPARENT EFFECT OF METEOR TRAILS ON THE FORMATION AND EVOLUTION OF E REGION FIELD-ALIGNED IRREGULARITIES

Mathews, J.D.<sup>1</sup>, Malhotra, A.<sup>1</sup>, Zhou, Q.H.<sup>2</sup><sup>1</sup>Penn State University<sup>2</sup>Miami of Ohio

Mid latitude E region plasma irregularities have been studied using the MU radar (34.9 degrees N, 131.6 degrees E, geomagnetic latitude 25.0 degrees N). Interest was renewed in the study of mid-latitude E-region plasma instabilities and irregularities with the report of quasiperiodic structuring of these irregularities by Yamamoto et al. [1991] using the MU radar. An explanation for these quasiperiodic striations observed initially in the post sunset period and later even in the post sunrise period stills remains elusive. We report here the first results from the study of the effect of meteor trails, particularly as revealed in range spread trail echoes (RSTE), on these field-aligned irregularities. Using radar data collected from the summer of June 2001 and analyzing the data on both pulse by pulse basis and on an averaged scale we show that range spread trail echoes play a significant role in the formation and development of Quasi Periodic Echoes and in some cases might be mistaken as the actual striations itself. We also provide the first known report of Low Altitude Quasi Periodic Echoes observed by the MU radar. The aspect sensitivity of both the quasiperiodic echoes and the range spread trail echoes is also discussed.

## References:

Yamamoto, M., S. Fukao, R. F. Woodman, T. Ogawa, T. Tsuda, and S. Kato, Mid-Latitude E region field aligned irregularities observed with the MU radar, *Journal of Geophys. Res.*, 96, 15,943, 1991

Zhou, Q. H., J. D. Mathews, and T. Nakamura, Implications of meteor observations by the MU radar, *Geophys. Res. Lett.*, 28, 1299-1402, 2001.

MODELING LARGE RADAR OBSERVATIONS OF METEORS  
AND THE ELECTROJETLars Dyrud<sup>1</sup>, Meers Oppenheim<sup>2</sup>, Erhan Kudeki<sup>3</sup>, Yakov Dimant<sup>2</sup><sup>1</sup>Center for Remote Sensing, Fairfax, VA<sup>2</sup>Center for Space Physics, Boston University<sup>3</sup>University of Illinois

To understand high-power large-aperture (HPLA) radar observations of meteors and the resulting atmospheric effects, we constructed a model that follows meteor evolution from ablation and ionization to head echo formation and through non-specular trail reflections. As a meteor enters the Earth's atmosphere, the particle heats up and atoms begin boiling off the surface in a process known as ablation. A fraction of the ablated particles ionize upon collision with a neutral constituent, converting the tens of km/s linear velocity into a hot plasma distribution. Radar reflections from this initial meteor plasma are known as head echoes and have Doppler shifts and range rates of tens of km/s. The hot meteor plasma rapidly thermalizes producing a column of enhanced ionization in the E-region ionosphere. In the past, we conducted plasma simulations demonstrating that these meteor columns are unstable to the growth of Farley-Buneman gradient-drift (FBGD) waves that become turbulent and generate large B-field aligned irregularities (FAI). These FAI result in radar reflections called non-specular meteor trails. We have updated our model to include the effects of winds and background electric fields as they polarize meteor trails, and if they are strong enough, produce electrojet irregularities in the background plasma. This model incorporates existing meteor physics together with knowledge we gained from the simulations, such as instability physics and anomalous diffusion. The result is a model that follows the physics of the meteor interaction with the atmosphere from entry and ablation, to ionization, thermal expansion and instability generated FAI. We display the results in the form of simulated RTI images of meteor reflections, allowing for direct comparisons with observations. Comparing results from this model with large radar observations of head echoes and non-specular trails shows that we can reproduce many of the observed features, such as the general altitude profile and duration of head echoes and non-specular trails. For example, when neutral winds or electric fields are included in our model, the same model predicts both short duration ( 1 second) and long duration meteor trails (several minutes) depending upon the characteristics of the meteoroid and atmosphere. The addition of a background E-field or wind also reproduces a commonly observed non-specular trail feature we call an extended tail where the delay time between head echo and non-specular reflection at the lower altitude portion of the trail increases as the meteor gets lower in the atmosphere. Finally, we have added to our model predictions of where electrojet echoes occur in the background ionosphere when driven by external electric fields. We present results which show the need to modify IRI collision frequencies with altitude in order for our model to simultaneously reproduce meteor and electrojet echo height distributions.



## METEOR TRAILS IN THE E-REGION IONOSPHERE: DIFFUSION AND ELECTRIC FIELDS

Y. S. Dimant<sup>1</sup>, M. M. Oppenheim<sup>1</sup>, L. Dyrud<sup>1</sup>, G. M. Milikh<sup>2</sup>

<sup>1</sup>Boston University

<sup>2</sup>University of Maryland, College Park

Meteoroids penetrating the Earth's atmosphere frequently leave behind trails of dense plasma in the region between 130km and 75km. Low-power, small-aperture radars detect many of these trails as specular echoes when the trail lies perpendicular to the radar line-of-sight. Upper atmospheric scientists use these radars to monitor winds between 85 and 105 km altitude and solar system scientists use them to estimate the population of small particles in the solar system. High-power, large-aperture (HPLA) radars observe short duration signals, traveling with the ablating meteoroids, called head echoes and long duration signals, persisting for a relatively long time in a broad altitude range, called non-specular echoes. We have argued that non-specular echoes result from radar signals scattered from turbulent electron density irregularities generated by plasma instabilities, which in turn are driven by strong electric fields developing during the trail ambipolar diffusion. Obtaining accurate quantitative predictions for the diffusive evolution and fields generated by these trails within the magnetized ionosphere has proven difficult. In this talk, we will present a refined quantitative model of the fields and density evolution which accounts for both the geomagnetic field and the background plasma. Combining our theory with radar observations of specular and non-specular echoes should yield useful information about meteor trails and the surrounding atmosphere.

Using both simulations and 2-D analytical theory, we can accurately model trail evolution for trails at a broad range of altitudes and initial plasma densities. Both simulations and theory show that at altitudes above 94km, meteor trails initially become highly anisotropic due to the different diffusion rates for electrons and ions. With time, however, the trail diffusion becomes nearly isotropic due to its interaction with the background plasma. The transition from anisotropic to isotropic diffusion takes place when the plasma trail density remains much larger than the background plasma. This may help explain unexpected results of some radar observations of specular echoes.

Ambipolar diffusion of trails leads gives rise to polarization electric fields, which may drive plasma instabilities and generate electron density irregularities visible to radars as non-specular echoes. During the trail evolution, when the trail diffusion becomes more isotropic, the electric field may drop below the level necessary to drive instabilities. This is of importance for interpretation of non-specular trails.

At the equatorial and high-latitude E-region electrojets, a strong external DC electric field perpendicular to the magnetic field frequently occurs. This field polarizes a highly conducting meteor trail resulting in substantial spatial redistribution of the electric potential around the trail. A simplified 3D analytical theory shows that the total electric field in the near-trail region may be drastically amplified, which may help explain long-lived non-specular echoes.

## UNDERSTANDING THE NEAR-EARTH MICROMETEOR ENVIRONMENT USING RADAR MEASUREMENTS

Janches, D.<sup>1</sup>, Chau, J.L.<sup>2</sup>, Heinselmann, C.<sup>4</sup>,  
Erickson, P.J.<sup>5</sup>, Palo, S.E.<sup>3</sup>

<sup>1</sup>NWRA, CoRA Div., USA

<sup>2</sup>Jicamarca Radio Observatory, Lima, Peru

<sup>3</sup>Dept. of Aerospace Engineering, University of Colorado, USA

<sup>4</sup>SRI International, Palo Alto, USA

<sup>5</sup>MIT Haystack Observatory, Westford, Ma, USA

We discuss initial results from an effort to model the annual micrometeor influx into the Mesosphere/Lower Thermosphere (MLT) atmospheric region based on very precise meteor head-echo radar observations. The principal goal of this effort is to construct a new and more precise sporadic meteoric input function needed for the subsequent modeling of the atmospheric chemistry of the meteoric material and the origin and formation of metal layers in the MLT. Modeling this function requires precise knowledge of the meteor directionality, velocity distributions, mass flux and diurnal and/or annual variability of the sporadic micrometeoroid environment. The model is constructed based on meteor radar observations obtained with the 430 MHz dual-beam Arecibo (AO) radar in Puerto Rico and the 50 MHz Jicamarca (JRO) radar in Peru. We also compare the modeled fluxes with observations from Sondrestrom and Millstone-Hill radars, thus utilizing the entire NSF ISR chain. The observed meteors are produced by particles with sizes between one to a few hundred microns in radii. The particle size and mass distributions are derived from very precise measurements of meteor velocity and deceleration and assuming meteoroid shape and bulk density. The observed results show that these radars, and probably every other high power/large aperture radar, only detect an Apex-centered dust population with no strong evidence of additional meteoroid populations with other radiant distributions. We also show that in order to explain the diurnal and seasonal variability of the meteor rate detected at AO an atmospheric filtering effect must exist which seem to be produced by the early and higher ablation of micrometeors, which enter the atmosphere at low elevation angles. These particles probably reach high temperature at higher altitudes and deposit some or all their material before they penetrate deep into the MLT region. Furthermore, we present specular meteor trail measurements from the quasi-all-sky meteor radar system installed in 2001 at the geographic South Pole. The diurnal and seasonal variability of the meteor flux observed over the South Pole indicate that most of the activity occurs during the Antarctic summer around a very concentrated region of the sky in elevation and azimuth. These results agree with previous Arctic meteor observations and suggest that most of the flux is concentrated around the ecliptic plane.

CHARACTERIZATION AND ASTRONOMICAL IMPLICATIONS  
OF METEOR-HEAD ECHOES OBSERVED OVER JICAMARCA

Chau, J. L., Woodman, R. F., Galindo, F. , Condor, P.

Radio Observatorio de Jicamarca, Instituto Geofísico del Perú, Lima

We present a summary of the observations of meteor-head echoes obtained with the high power-aperture Jicamarca 50 MHz radar. Our observations are limited to few hours around sunrise when the echoes from equatorial electrojet (EEJ) irregularities are weak or absent. We give a description of the technique that allows us to get estimates of the radial velocities, direction of arrival (using interferometry), absolute geocentric velocities, absolute geocentric decelerations, etc. We also present our latest development related to the detection of meteors and their characterization, including manual selection of events. Three different experiments have been performed since November 2001: coded long pulse, uncoded long pulse, and short pulses. The advantages and disadvantages of these experiments, as well as their optimal processing are discussed. For example, we find that for detection of meteors even under strong EEJ uncoded long pulses should be used, although, range determination is poor.

Results for observations made since 2001 on campaign basis are presented. Our observations consistently show that the distribution of the meteors with respect to the Earth's frame of reference is clustered around the Apex, within +/-10 degrees transverse to the Ecliptic and no more than a few degrees in heliocentric longitude in the Ecliptic plane. We also show the consistent discrepancy between the velocity obtained from range versus time and the Doppler velocity. Finally, we present special cases that require careful analysis, for example events with non-constant decelerations, and if time permits we will show preliminary results of inferred orbits based on our interferometric observations, including the very fast meteors with hyperbolic orbits.

## A COMPARISON OF AUTOMATED-SEARCH METEOR RESULTS FROM RADAR OBSERVATIONS AT TWO LOCATIONS

S. J. Briczinski<sup>1</sup>, J. D. Mathews<sup>1</sup>, D. D. Meisel<sup>2</sup>, C. J. Heinselman<sup>3</sup><sup>1</sup>Communications and Space Sciences Laboratory, The Pennsylvania State University, University Park, PA 16802<sup>2</sup>Department of Physics and Astronomy, SUNY Geneseo, Geneseo, NY 14454<sup>3</sup>SRI International, Menlo Park, CA 94025

The automated FFT periodic micrometeor searching algorithm developed by Mathews et al. [An update on UHF radar meteor observations and associated signal processing techniques at Arecibo Observatory, *JASTP* **65** (2003) 1139-1149] has now cataloged over 33,000 separate sporadic meteor events seen with the 430 MHz Arecibo Observatory radar over 30 hours of observation time. An additional 30 hours of meteor data were taken in July and August 2005 using the 1290 MHz Sondrestrom incoherent scatter radar. The Sondrestrom radar was run in two modes to observe sporadic meteors. In the first mode, the radar beam was pointed at zenith to mimic conditions at Arecibo. In the second mode, the radar beam was pointed due east at a 60 degrees zenith angle. The second configuration was chosen as an attempt to maximize the meteor flux rate and is an observation condition not possible using the Arecibo radar. The searching algorithm was run on data sets from both radars. We present and compare sporadic meteor parameters (i.e. altitudes, velocities, decelerations) from both facilities while considering the resultant insights into the head-echo scattering process at 430 MHz versus 1290 MHz. We also use the observation parameters to determine mass distributions and orbit parameters. Additionally, the Perseid meteor radiant was tracked at Sondrestrom. We present the orbit parameters of the Perseid meteor shower as a contrast to the parameters from presumed sporadic meteor events. The statistics obtained from the shower are compared to published results from the ALTAIR radars [Close et. al. Analysis of Perseid meteor head echo data collected using the Advanced Research Projects Agency Long-Range Tracking and Instrumentation Radar (ALTAIR), *Radio Sci.* **35** (2000) 1233-1240].

## COMPARISON OF TIDAL RESULTS OBTAINED WITH METEOR RADARS WITH NON-INTERFEROMETRIC AND INTERFEROMETRIC CAPABILITIES

Lau, E.M.<sup>1</sup>, Iimura, H.<sup>2</sup>, Avery, S.K.<sup>1</sup>  
, Avery, J.P.<sup>3</sup>, Palo, S.E.<sup>2</sup>, Makarov, N.A.<sup>4</sup>

<sup>1</sup>University of Colorado, Cooperative Institute for Research in Environmental Sciences (CIRES), U.S.A.

<sup>2</sup>University of Colorado, Department of Aerospace Engineering, U.S.A.

<sup>3</sup>University of Colorado, Department of Electrical and Computer Engineering, U.S.A.

<sup>4</sup>Institute for Experimental Meteorology, Scientific Production Association TYPHOON, Russia

Until recently the remoteness and harsh environment of the polar regions limited our understanding of the dynamics of the upper atmosphere over these regions. Over the last decade some instruments have been installed at the Amundsen-Scott station at the South Pole. Optical instrument measurements first revealed the existence of a faint nonmigrating semidiurnal tide in the mesosphere-lower thermosphere (MLT) over the South Pole. This nonmigrating semidiurnal tide was found to propagate in the westward direction with a zonal wavenumber one. Surprisingly at that point the migrating semidiurnal tide was not discerned from the measurements as it had been at lower latitudes; this behavior has since been explained by physical principles. A meteor radar installed in the mid 1990's that operated for over one year revealed that the nonmigrating semidiurnal tide was stronger during the austral summer and almost disappeared during the winter. The nonmigrating semidiurnal tide was measured to have an amplitude of  $\sim 20$  m/s during the summer. A similar behavior was observed for the migrating diurnal tide but with significantly smaller amplitudes. One limitation of that meteor radar was the lack of vertical resolution so all returns were assumed to come from a height of 95 km.

A new meteor radar started operating in 2001 at the South Pole station with the goal of helping in the understanding of the horizontal wind field dynamics over the Antarctic continent. This new meteor radar includes a system similar to the one installed in the mid 1990's (COBRA system) and another one that has interferometric capabilities and thus can resolve the altitude of the wind measurements associated with each meteor trail (MEDAC system). The tidal results of the COBRA and MEDAC systems are compared. It is found that the nonmigrating semidiurnal tide results obtained with the COBRA system could be underestimated by about 20% due to the lack of altitude resolution.

## METEOR ARRAY GEOMETRY PERFORMANCE BASED ON THE CRAMER-RAO BOUND

Chunmei Kang, Scott E. Palo

Department of Aerospace Engineering and Sciences, Department of Aerospace Engineering and Sciences

Interferometric techniques commonly used in all-sky meteor radar systems to determine the position of the meteor in the sky. Essentially, interferometric techniques use the phase information recorded from different receiving antennas to estimate the elevation and azimuth of the meteors. Prior efforts have been made to determine an antenna geometry that improves the performance for meteor system. For example, Hocking and Thayaparan (1997) used four antennas typically spaced by 1.5 to 3 wavelengths to locate the meteors. Jones (1992) and Hocking (1997) presented an antenna geometry using a 5 element array with minimum antenna spacing of 2 wavelengths to estimate the direction of arrival (DOA) of the meteors. By spacing the antennas more than 1 wavelength apart, these array geometries were successful in reducing the coupling effect between the antennas. However, it is not clear if these arrays can be improved or are optimal without a metric for comparison. One metric for performance is the Cramer-Rao bound (CRB), which is the minimum variance that can be obtained for any unbiased estimator. The CRB is only dependent upon the array geometry and the unknown parameters of elevation and azimuth angles. In this work, we derive the CRB for the azimuth and elevation angle given a planar array with arbitrary sensors and multiple temporal measurements from each sensor. Several array geometries are studied all of which utilize 5-antennas. These are the cross-array, T-array and the L-array. For all of these geometries the elevation angles can be estimated more accurately at a high elevation angle and the azimuth angles are determined less accurately. Our analysis shows that, at a fixed elevation angle cone, the cross-array has the worst performance in estimating the azimuth and elevation angle compared with the other two arrays. L-array shows better estimation accuracy than the cross array except for a few azimuth-elevation angles. T array also performed better than the cross-array at all azimuth and elevation angles. Increasing the number of temporal samples from each antenna will improve the estimation accuracy of azimuth-elevation angles. Our study shows that using 50 samples will improve the estimation performance by 20dB, while increasing from 50 to 100 samples will improve the estimation performance by an additional 5dB. The CRB study can be helpful in designing arrays with optimum DOA estimation ability, based on the array geometry DOA estimation algorithm can be developed to achieve this CRB. Simulation results using the DOA method proposed by Jones indicates that at an elevation angle of 30 degree, the variance of the estimated azimuth-elevation angles will meet the CRB at a signal to noise ratio of 15dB with 10 samples and at a signal to noise ratio of 4 dB with 100 measurements.

Session G/H2, 07:55 – Sat.

**PLASMA INSTABILITIES AND  
WAVES**

Co-Chairs: Y. Dimant, M. Oppenheim

G/H2



## DENSITY STRUCTURES PRODUCED BY NONLINEAR ULF ELECTROMAGNETIC WAVES IN THE MAGNETOSPHERIC PLASMA

Streltsov, A.V.<sup>2</sup>, Lotko, W.<sup>1</sup>, Ganguli, G.<sup>2</sup>,  
Rudakov, L.I.<sup>3</sup>, Mithaiwala, M.<sup>4</sup>

<sup>1</sup>Dartmouth College, Hanover, NH 03755, USA

<sup>2</sup>Naval Research Laboratory, Washington, DC 20375, USA

<sup>3</sup>Icarus Research Inc., Bethesda, MD 20824, USA

<sup>4</sup>NRC-NRL Postdoc, Washington, DC 20375, USA

Results from a numerical study of the nonlinear interaction between ultra-low-frequency shear Alfvén waves, slow MHD waves, and the high-latitude auroral ionosphere are presented. The goal of this study is to investigate the role of magnetic field-aligned currents carried by shear Alfvén waves in the formation and spatiotemporal development of density structures in the low-altitude auroral magnetosphere and the ionosphere. Interest in this problem is motivated by ground-based radar and satellite observations of field-aligned ion flows and density cavities, extended along the ambient magnetic field and localized across it, in conjunction with discrete auroral arcs and intense field-aligned currents. The study is based on a reduced, two-fluid MHD model describing shear Alfvén and slow MHD waves in the cold, low-altitude magnetospheric plasma. Coupling between these two MHD modes occurs due to (a) the finite plasma compressibility, and (b) the nonlinear  $\mathbf{j} \times \mathbf{B}$  term in the ion momentum equation. Another important nonlinear effect included in the model is active ionospheric boundary conditions (ionospheric feedback mechanism). Numerical simulations of the model equations have been performed in a two-dimensional, axisymmetric, dipole geometry of the ambient magnetic field with realistic parameters of the ambient field and the background plasma. Simulations show that ULF Alfvén waves generated in the equatorial magnetosphere or in the plasma sheet boundary layers carry significant amount of the electromagnetic power to the low-altitude magnetosphere and indeed modify plasma density there. This variation of the plasma density feeds back on the dynamics of the waves. Simulations also show that another important physical effect responsible for formation of intense electromagnetic and plasma structures in the ionosphere and low-altitude magnetosphere is the ionospheric feedback mechanism.

## BOUNCE RESONANT INSTABILITIES OF KINETIC ALFVEN WAVES ON AURORAL FIELD LINES

Lysak, R. L., Song, Y.

School of Physics and Astronomy, University of Minnesota

Recent observations from the FAST satellite as well as a number of sounding rocket missions have shown two distinct modes of auroral electron acceleration: the classic inverted-V signature consisting of a beam broad in pitch angle but narrowly confined in energy, and a lower energy, field-aligned acceleration that has been attributed to kinetic Alfvén waves. A non-local theory of the interactions of auroral electrons with these waves has been developed, and used to describe this Alfvénic acceleration process. However, observations indicate that these two acceleration mechanisms often co-exist, suggesting that Alfvénic acceleration can occur on field lines with a quasi-static potential drop. The presence of this parallel potential drop leads to several new populations of auroral electrons. Cold ionospheric electrons are reflected back to the ionosphere. In addition, electrons of appropriate energy and magnetic moment can be trapped between this potential drop and their magnetic mirror points. Calculations indicate that trapped electrons of a few hundred electron volts have bounce periods of 1-5 seconds, comparable to the period of waves in the ionospheric Alfvén resonator, a structure produced by the gradients in the Alfvén speed above the auroral ionosphere. This suggests that a bounce resonant instability may occur that would excite waves in the resonator that could play a role in the acceleration of low-energy field-aligned electrons. Such bounce resonant waves would have perpendicular scales comparable to the electron inertial length, which enhances the trapping of these waves in the ionospheric resonator. A non-local kinetic theory including trapped electrons has been developed to determine what role such bounce resonance plays in the auroral acceleration process.

## GENERATION OF AN ALFVENIC WAVE RESONATOR IN THE MAGNETOSPHERE\*

Manish Mithaiwala<sup>1</sup>, Gurudas Ganguli<sup>2</sup>, Leonid Rudakov<sup>3</sup><sup>1</sup>NRC-NRL Postdoc<sup>2</sup>NRL Plasma Physics Division<sup>3</sup>Icarus Research Inc.

It is known that whistler waves, through reflection at the lower-hybrid resonance, can form a resonator<sup>1</sup>. We find that in a multi-ion species environment, such as the Earth's magnetosphere, the bi-ion rotation<sup>2</sup> (cutoff) frequency and Buchsbaum (resonance) frequency are important for the propagation and evolution of Alfvénic waves near the ion-cyclotron frequency. The physics of the reflection process between Alfvénic and whistler mode waves is similar. Here we show that Alfvénic waves with ( $k_{\perp} \gg k_z$ ) can be captured by a magnetic cavity to form a strongly localized Magnetospheric Resonator which can interact with the electrons over a long time period and can lead to both energization and loss of the electrons, and as known, couples to the ions. This possibility would have important consequences for the evolution of the ring current and radiation belts during storms and substorms. A novel feature of this approach is that the Alfvénic waves can be generated by a ring distribution of one of the ion species. Ring ion distributions are known to form when the solar wind interacts with the magnetosphere or a comet interacts with the solar wind, and by the release of chemicals in the magnetosphere. This type of instability is in contrast to the usual temperature anisotropy instabilities invoked for the generation of ion-cyclotron waves, as this is a reactive instability, and therefore presents unique questions pertaining to the absolute versus convective growth of these waves and the loss of these waves through tunneling out of the resonator.

\* Work supported by ONR

1. Thorne, R. M. and Kennel, C. F. JGR 72, 857.
2. Ganguli, G. and L. Rudakov. Phys. Plasmas 12. April 2005.

## MF/HF RADIO EMISSIONS FROM THE AURORAL IONOSPHERE AND THEIR CONNECTIONS TO PLASMA INSTABILITIES

LaBelle, J.

Department of Physics and Astronomy,, Dartmouth College, Hanover,  
New Hampshire, USA

Among the possible consequences of ionospheric plasma instabilities is transport of energy out of the local plasma in the form of electromagnetic radiation. The observation of electromagnetic emissions from auroral ionosphere strongly suggests that this process plays a role there. At medium and high frequencies (MF/HF), three types of radio emissions of auroral origin are observed: auroral hiss, MF-burst, and roar. There is strong evidence that auroral roar and much auroral hiss arise from plasma instabilities; that is, from collective processes in the plasma which result in conversion of free energy stored in plasma particles into the observed electromagnetic radiation. The amount of energy emitted in electromagnetic radiation is small compared to that stored in the plasma particles, but sufficient knowledge of the generation mechanism implies that these radiations may be used to diagnose ionospheric conditions using passive ground-based measurements. Some examples of these diagnostic methods will be discussed. The connection of the MF-burst emissions to plasma instability is less well understood. However, based on elementary considerations of wave intensity and frequency range, some constraints can be placed on the generation mechanism, and two or three possible mechanisms have appeared in the literature. A brief review suggests that some of these warrant deeper consideration. In conclusion, the generation of MF/HF radio emissions of natural auroral origin has a close connection to ionospheric plasma instabilities, and observations of these radio emissions from ground-based and spacecraft-borne sensors can play a significant role in identifying and understanding the plasma instabilities occurring in the Earth's ionosphere and magnetosphere.

## SIMULATION AND THEORY OF BUNEMAN INSTABILITIES IN INHOMOGENEOUS AND TIME-VARYING SPACE PLASMAS

Newman, D. L., Goldman, M. V., Sen, N.

Center for Integrated Plasma Studies, University of Colorado at Boulder, 390 UCB, Boulder CO, 80309-0390

Buneman instabilities and their kinetic variants (which include ion-acoustic instabilities) occur when the relative drift between electrons and ions exceeds a threshold value. Thus, these are *current-driven* instabilities that can play a key role in the evolution of current sheets. For example, in recent 3-D simulations of magnetospheric reconnection (J. F. Drake et al., *Science*, **299**, 873, 2003) electron holes produced by Buneman instabilities were observed inside the reconnection current sheet.

To illustrate the fundamental linear and nonlinear stages of Buneman-like instabilities driven by currents that vary in space and/or time, we will present and interpret the results from a series of electrostatic Vlasov-based simulations for a range of plasma conditions, including the degree of ion and electron magnetization. First, we consider 1-D simulations in which an initially current-free plasma is driven by a weak electric field. The current is observed to increase linearly until the Buneman threshold is exceeded ( $v_d \approx 2v_e$ , where  $v_d$  and  $v_e$  are the electron drift and thermal velocities, respectively), after which the Buneman-unstable waves grow and saturate through trapping and electron hole formation. Subsequent electron heating coupled with a decrease in the electron drift (due to momentum exchange with ions) results in the plasma no longer being Buneman-unstable, until the electric field again causes the current to exceed the *new* Buneman threshold in the hotter plasma.

In 2-D simulations with strongly magnetized electrons and differing ion magnetization states, a current sheet (localized perpendicular to  $\mathbf{B}$ ) can either be imposed as an initial condition or driven by an inhomogeneous parallel electric field. If the current in the center of the sheet exceed the Buneman threshold, linearly unstable waves described by non-sinusoidal *global* eigenfunctions in the direction of the current inhomogeneity (i.e., *velocity shear*) begin to grow. The form of these eigenfunctions can be determined using a *Mathieu function* analysis for weak shear with a time-independent sinusoidal velocity profile, and numerically for stronger shear and other profiles. The nonlinear evolution is dominated by electron holes that in some cases are preferentially localized to particular regions of the shear profile. Such localization has also been found in related simulations in which the electrons are weakly magnetized.

MULTIPLE ION VLASOV SIMULATIONS OF THE LOWER  
BOUNDARY OF THE AURORAL UPWARD CURRENT REGION

Main, D. M.<sup>1</sup>, Newman, D. L.<sup>1</sup>, Ergun, R.<sup>2</sup>

<sup>1</sup>Center for Integrated Plasma Studies, University of Colorado, UCB  
390

<sup>2</sup>Laboratory for Atmospheric and Space Physics, 1234 Innovation  
Drive, Boulder, Colorado 80303-7814

The upward current region is characterized by a strong anti-earthward ion beam with complimentary earthward travelling electrons. There is usually a density depression known as the auroral cavity associated with the anti-earthward ion beam along with the associated auroral lights at low altitudes caused by the earthward travelling electrons “showering” the upper atmosphere at about 100 km. At the interface between the upper ionosphere and the auroral cavity (between  $\sim 3000 - 6000$  km), spacecraft (s/c) measurements indicate that there is usually a strong, localized parallel and perpendicular electric field (on the order of 100 to 500 mV/m). Using the electric field measurements together with the distribution functions measured from the FAST s/c, we have modelled this interface, known as the lower boundary, as a BGK double layer (DL) (Ergun et al., *phys. plasmas*, **9**, 3695-3704, 2002). We then evolve the BGK DL in an open boundary 1-D Vlasov simulation. We have also run simulations using a 2-D magnetized Vlasov simulation with both open and periodic boundary conditions. In 1-D we show that the dominant instability occurs when the slow  $H^+$  acoustic beam mode and the fast  $O^+$  acoustic beam mode couple (Bergman and Lotko, *JGR*, **91**, 7033-7045, 1986). Both  $O^+$  and  $H^+$  have been accelerated through the same potential drop and thus have different beam velocities in the auroral cavity. The linear growth of the  $O - H$  instability saturates by trapping of the  $H^+$  which then leads to  $H^+$  phase space holes which propagate anti-earthward up the field line. These ion holes have electric field signatures that are similar to observations. In particular, the size of the holes are consistent with the holes observed by FAST. The ion holes are still seen in 2-D along with strong Bernstein waves in related periodic simulations. The Bernstein waves form after the  $H^+$  holes have formed. There is also a shock type structure which forms in the simulation and propagates toward, and eventually interacts with, the DL. Once the shock type structure hits the DL, the strength of the DL weakens but the DL remains stable. The shock type structure that we see in the simulation may partially explain at least one FAST observation of a parallel electric field which cannot be explained by using a static BGK model. We conclude then that these simulation results are consistent with many features of the auroral cavity that have been observed using the FAST s/c: a strong density depression between the ionosphere and auroral cavity, a strong ion beam persistent for the entire simulation run, ion holes, Bernstein waves and a DL that is stable for the length of the simulation with no signs that it is becoming unstable.

REDUCED VLASOV SIMULATIONS OF TRANSITION LAYERS  
AND ASSOCIATED STRUCTURES IN THE IONOSPHERE: EF-  
FECT OF FINITE ION MAGNETIZATION

Naresh Sen, Martin V. Goldman, David L. Newman  
University of Colorado

The existence of *transition layers* (including *laminar double layers*) in the downward current region of the ionosphere is observationally well established by satellites such as FAST. Associated with the transition layers are nonlinear structures such as phase-space electron holes, and waves at the hydrogen ion cyclotron frequency and its harmonics. In order to understand the interactions between the double layers, holes and waves, we perform electrostatic Vlasov-based simulations in two spatial dimensions. The phase-space dynamics parallel to the geomagnetic field  $\mathbf{B}$  is typically very complex and is therefore modeled using the full Vlasov equations. The perpendicular magnetized ion dynamics are modeled by a *reduced* algorithm, using a ring of modes in the transverse velocity plane. The radius  $v_{\perp}$  of the ring is proportional to the nominal perpendicular thermal velocity. The simulations are initialized with counterstreaming Maxwellian distributions of strongly magnetized electrons and finitely magnetized ions, each drifting at their respective thermal velocities. In order to seed the double layer, a charge-neutral density depression is introduced at the midpoint in the direction parallel to  $\mathbf{B}$  and uniform perpendicular to it.

Simulation results indicate a turbulent double layer developing at the location of the initial density depression, and producing electron phase-space holes (bipolar in the parallel electric field) that are localized in both dimensions and propagate away from the double layer. These have been seen in previous 2-D simulations. The new feature resulting from the finite ion magnetization is the appearance of diagonal wave fronts in the perpendicular electric field. These are ion Bernstein waves resonantly driven by the electron holes. This identification is corroborated by the power spectrum of ion density fluctuations, which indicate ion waves with wave vector approximately perpendicular to the magnetic field oscillating near the ion cyclotron frequency and its harmonics, in agreement with kinetic theory and consistent with observations. Thus the present simulation results suggest a mechanism, that of resonant excitation of the waves by electron holes, that provides an explanation for the observations, although other mechanisms may play a role as well. The present simulations will be compared with previous simulations with unmagnetized and strongly magnetized ions.

## NONLINEAR EVOLUTION OF E REGION PLASMA WAVES AND THEIR CONSEQUENCES.

J-P St-Maurice<sup>1</sup>, J. Drexler<sup>2</sup>, D. Hysell<sup>2</sup><sup>1</sup>ISAS, U of Saskatchewan<sup>2</sup>Cornell University, Ithaca, NY

Using a recent intermittency formulation of E region irregularity theory we argue that Farley-Buneman waves break down into blobs and holes to produce echoes that behave the same as if the structures were elliptical hard targets moving at the ion-acoustic speed in a direction that is rotated away from the electron  $\mathbf{E} \times \mathbf{B}$  drift direction. This description explains qualitatively why the spectral width is smallest and the power greater in the direction where the phase velocity is greatest. At high latitudes, however, the rotation is limited by the necessary growth of large aspect angles in the later stages of evolution of the structures. The growth of nonzero aspect angles has several consequences. For one thing, it leads to electron heating by the wave fields. Other interesting consequences are found when ambient and/or gradient-drift induced gradients are affecting the growth of 1- to 10-m size structures: for example, when gradients are unfavorable to growth, the growth phase undergoes two separate stages of evolution while a sudden change in the threshold speed is taking place. By contrast, when extending this idea to low latitudes, we find that the nonlinear growth of large aspect angles does not have to take place. This means that, even when not considering the nonlocal effects due to altitude variations, blobs and holes that evolve from large scale gradient-drift waves can undergo very large rotations, with furthermore a very clear contrast between holes and blobs electric fields and densities. This in turn introduces pronounced asymmetries in type I irregularities, particularly when conditions are extreme enough to cause type I irregularities to be seen along the vertical.



## A THEORY OF FARLEY-BUNEMAN WAVE STABILIZATION: DE-COHERENCE

Bahcivan, H.<sup>1</sup>, Hysell, D.L.<sup>2</sup><sup>1</sup>Center for Geospace Studies, SRI International<sup>2</sup>Earth and Atmospheric Sciences, Cornell University

We propose a new mechanism for the stabilization of primary Farley-Buneman waves. Wave stabilization occurs due to spatial decoherence of the primary wave with the EXB drifting electron fluid parcels driving the instability.

Many of the previous studies invoking mode coupling arguments of wave stabilization assumed a uniform background flow and calculated separately the effect of nonlinear drifts on the evolution of the waves. Our description of the wave-background interaction is one where the nonlinear mode coupling processes disrupt the electron flow through fluctuating EXB drifts making it nonuniform in space and time. Such fluctuations are attributed to the secondary ion acoustic structures generated through mode-coupling. A plane Farley-Buneman wave on such nonuniform background will be observing and interacting with a mixture of background flow patches convecting at different velocities. When this happens, the wave loses resonance with the background flow. We term this picture as wave decoherence.

A modified fluid equation for electrons is introduced that takes into account a model nonuniform and fluctuating background electric field representing the above picture. A single parameter directly enters into the system of equations describing this interaction: the spread or the mean square value of the turbulent electron flow after the mean flow velocity is subtracted. The new theory predicts a modified anisotropy factor, albeit through a collisionless process in contrast to previous works invoking anomalous electron collisions. The predicted anomalous anisotropy factor is complex and does not have a simple analytical solution. Numerical solutions of the new dispersion relation predict a reduced wave phase velocity and growth rate as the turbulent spread increases.

## PLASMA INSTABILITIES IN IONOSPHERIC DENSITY GRADIENTS FROM 120-200 KM ALTITUDE

Lars Dyrud<sup>1</sup>, Meers Oppenheim<sup>2</sup>, Joshua Semeter<sup>2</sup><sup>1</sup>Center for Remote Sensing, Fairfax, VA<sup>2</sup>Center for Space Physics, Boston University

We present recent plasma simulations showing the effects and evolution of gradient drift type instabilities at a broad range of ionospheric altitudes (from 120-200 km) and parameter regimes. This work is motivated by several recent observations such as those by the Sondrestrom Radar which observed narrow field aligned filaments of enhanced density extending from approximately 100-200 km altitude (Semeter et al., JGR 2005). These density gradients are approximately 10-200 km wide in the transverse to B direction, and have a peak density as high as 10 times that of the background ionospheric density. Additionally, these simulations likely apply to various HF backscatter regimes, including those of ionospheric patches and or the structuring responsible for cusp backscatter (Moen et al., JGR 2002). To examine the stability of such density gradients when immersed within plasma convection, we conducted a number of 2-D (plane perpendicular to the magnetic field) hybrid plasma simulations of enhanced density columns. We will present results from these simulations at various altitudes from 120-200 km, and discuss the implications. These simulations show a relatively rapid development (of the order of seconds) of gradient drift type instability waves. For parameters near 200 km altitude, and convection velocity of 600 m/s plasma columns are unstable to waves with a wavelength of about 10-20 m. For gradients near 115 km, we see the development of strong polarization fields and rapid structuring at 5-10 meter wavelengths. All of the instabilities simulated are strongly non-linear, due to the background gradients, and will influence the evolution of the medium scale plasma through processes such as a greatly enhanced anomalous diffusion.

Session G/H3, 12:55 – Sat.

**ACTIVE EXPERIMENTS**

Co-Chairs: P. Bernhardt, W. Sayles



THE EFFECT OF HF-WAVE INTERACTIONS WITH THE AU-  
RORAL IONOSPHERE ON THE GENERATION OF UNUSUALLY  
BRIGHT ARTIFICIAL AIRGLOW

Gerken, E.<sup>1</sup>, Kagan, L.<sup>2</sup>, Starks, M.<sup>3</sup>, Kelley, M.<sup>4</sup>, MacDougall, J.<sup>2</sup>

<sup>1</sup>Center for Geospace Studies, SRI International, Menlo Park CA 94025

<sup>2</sup>Department of Physics and Astronomy, University of Western Ontario,  
London Ontario N6A 3K7

<sup>3</sup>Air Force Research Laboratory/VSBXI, Hanscom AFB, MA 01731

<sup>4</sup>School of Electrical and Computer Engineering, Cornell University,  
Ithaca NY 14853

At mid-latitudes, in general, only the 630.0 nm oxygen line is bright enough to unambiguously detect in HF-induced artificial airglow, with rare cases of detectable 557.7 nm emissions (Bernhardt et al., *J. Geophys. Res.*, **94**, 9071, 1989). However, if a sporadic E-layer (Es) develops, then the heating HF wave interacts with dense plasma at much lower altitudes and brighter 557.7 nm emissions (up to 100 R) are observed (Djuth et al., *Geophys. Res. Lett.*, **26**, 1557, 1999; Kagan et al., *Phys. Rev. Lett.*, **85**, 218, 2000). In the case of patchy Es, the 557.7-nm airglow induced presents a footprint of the Es horizontal structure (Kagan et al., *Phys. Rev. Lett.*, **85**, 218, 2000). Unlike the mid-latitudes, the nighttime E-layer at high latitudes is either created by auroral precipitation which is associated with strong ionospheric absorption and bright auroral emissions, or is in the form of thick slabs of ionization (a so-called cusp- or C-type Es). In the March 2004 HAARP optical campaign, very bright (4 kR) green line airglow emissions were observed in kilometer-scale patches between auroral arcs during E-layer conditions (Pedersen and Gerken, *Nature*, **433**, 498, 2005). The single most surprising feature of these airglow patches observed in the presence of aurora is their brightness. At 4 kR, these patches are above the naked eye threshold and are comparable to dim visible aurora. Since the airglow height for this observation is unknown, two mechanisms for the generation of such bright airglow are possible based on the ionospheric conditions at the time. One possibility is that the bright airglow was caused by a nonlinear interaction of the HF-wave with an overdense cloud of ionization centered near 120 km (a so-called cusp- or C-type Es) whose thickness was of about an order of magnitude higher than that observed at Arecibo and therefore the HF waves deposited significantly more power. The second possible mechanism is that the bright airglow resulted from heater beam focusing by underdense sporadic ionization patches produced by auroral precipitation near 100 km altitude. We present our observations of artificial airglow in the presence of aurora and discuss both possible generation mechanisms.

## ACTIVE PERTURBATION OF PLASMA IRREGULARITIES ASSOCIATED WITH CHARGED AEROSOLS IN THE MESOSPHERE

Chen Chen, W.A.Scales

Bradley Department of Electrical and Computer Engineering, Virginia Polytechnical Institute and State University

Recently, experimental observations have shown that Polar Mesospheric Summer Echoes PMSE may be modulated by radio wave heating the irregularity source region with a ground-based ionospheric heating facility. In the first experiments, the strength of the PMSE was observed to be reduced upon turning on the radio wave heating and there was ultimate recovery of the PMSE upon turning the radio wave heating off. Subsequently, it was predicted and verified that an overshoot effect may occur during the recovery period. During this period after the radio wave turn-off, the PMSE strength may be enhanced over the undisturbed level. It is clear from past investigations that the temporal behavior of PMSE during ionospheric heating shows promise as a diagnostic for the associated dust layer. For investigating this temporal behavior, this work describes a new model that incorporates both finite diffusion time effects as well as dust charging. The model utilizes fluid ions described by continuity and momentum equations, electrons whose behavior is determined from quasi-neutrality, and charged dust described by the standard Particle-In-Cell PIC method. The model has been used to investigate temporal behavior of electron irregularities during electron temperature enhancement associated with radio wave heating. The model predicts that the temporal behavior of the irregularities depends on the ratio of the electron-ion ambipolar diffusion time to the dust particle charging time  $\tau_{\text{dif}}/\tau_{\text{chg}}$ . The results indicate that typically for  $\tau_{\text{dif}}/\tau_{\text{chg}} \ll 1$ , an overshoot occurs during turn-off of the radio wave heating. This is the regime of previous models which incorporated Boltzmann electrons. The work also predicts that for  $\tau_{\text{dif}}/\tau_{\text{chg}} \gg 1$ , a turn-on overshoot should be observed in which there is an increase in PMSE amplitude for a short period of time before ultimate suppression of the PMSE during continued heating. Also, for sufficiently large  $\tau_{\text{dif}}/\tau_{\text{chg}}$ , the PMSE amplitude may be enhanced during the entire heating period. Due to the dependence of  $\tau_{\text{dif}}$  on irregularity scale-size, these results have important implications for observations of PMSE modification at different radar frequencies. Therefore new possibilities may exist for diagnosing the dust layer with radio wave heating which are discussed.

MEASUREMENTS OF ELECTROSTATIC AND ELECTROMAGNETIC EMISSIONS FROM HIGH POWER RADIO WAVES IN THE F-REGION OVER HAARP

Paul A. Bernhardt<sup>1</sup>, Craig Selcher<sup>2</sup>, Brent Watkins<sup>3</sup>,  
Shin Oyoma<sup>3</sup>, Bill Bristow<sup>3</sup>, John Hughes<sup>3</sup>, Craig Heinselmann<sup>4</sup>

<sup>1</sup>Plasma Physics Division, Naval Research Laboratory, Washington, DC 20375

<sup>2</sup>Information Technology Division, Naval Research Laboratory, Washington, DC 20375

<sup>3</sup>Geophysical Institute, University of Alaska, Fairbanks, AK 99775

<sup>4</sup>SRI International, Menlo Park, CA 94025

In February 2005, high power radio wave experiments were conducted to diagnose the HF heating of the ionosphere over HAARP. The experiments used ground diagnostics to detect the nonlinear wave interactions in the F-Region. The measurement approach used three simultaneous radio/radar techniques. For stimulated electromagnetic emissions (SEE) that radiate from the modified plasma the Stimulated Ionospheric Electromagnetic Radio Receiver Array (SIERRA) was set up in a five receiver array extending from Fairbanks in the north to Valdez and Cordova Alaska in the south. Enhanced ion and plasma lines were observed using the eight-panel version of the Advanced Modular Incoherent Scatter Radar (AMISR). Backscatter from the heater induced field aligned irregularities was monitored by the Super Dual Auroral Radar Network (SuperDARN) in Kodiak Alaska. Many types of HF transmission modes were scheduled for the radio/radar Measurements with HAARP operations. The results of these experiments have provided an integrated view of simultaneously produced photons (electromagnetic waves), plasmon (plasma waves), phonons (ion sound waves), and density irregularities. The observations have been used to validate theories on high power wave interactions in the F-Region. The HAARP simultaneous radio measurement (SRM) campaign yielded several new discoveries and observations including (1) duty cycle dependence of Doppler spread of SuperDARN backscatter, (2) spatial dependence of relative downshifted maximum (DM) and broad upshifted maximum (BUM) SEE intensities, and (3) the first enhanced ion and plasma lines recorded at UHF at the HAARP site. The results of these experiments are explained using mode conversion of the electromagnetic pump wave to generate electrostatic waves, parametric decay of the pump and electrostatic waves to generate frequency shifts, Bragg scatter of the radar signals and mode conversion to yield radiated electromagnetic waves.

## GENERATION OF VLF WAVES IN THE IONOSPHERE WITH COHERENT MULTIPLE-SITE EXCITATION

Wong, A. Y.<sup>1</sup>, Wei, E.<sup>1</sup>, Pau, J.<sup>1</sup>, Pilling, S.<sup>2</sup>, Dave Boyd<sup>1</sup>, Corpuz, A. R.<sup>2</sup>, Bick, C.<sup>2</sup><sup>1</sup>HIPAS Observatory, Two Rivers, AK 99712<sup>2</sup>University of California, Los Angeles, 1-129 Knudsen Hall, m. s. 154705, Box 951547, Los Angeles, CA 90095-1547

HIPAS and HAARP are two radiating facilities in the Arctic region. The distance between these two radiating facilities is 287 km, which is on the order of the ELF/VLF wavelengths. The electrojet in the E region of the ionosphere above each facility can be modulated to radiate ELF/VLF waves via HF heating. These two facilities are link together to transmit HF heating power in a manner that can enhance the efficiency of excitation of ELF/VLF by both low frequency modulations and high frequency beam interactions. The electrojet radiates electromagnetic waves at its modulation frequency in the ELF/VLF band and thus becomes a wave source. When both HIPAS and HAARP are radiating with amplitude modulation (AM) at the same ELF/VLF frequency, the wave sources formed above the two sites become coherent. Coherent excitations by these two facilities can create constructive interference which is sensitive to the phase difference between these two sources. Density irregularities, or striations, generated by high power radio frequency heating, can be modeled as a vertical conducting surface in ionospheric region directly above each radiating facility. Since a conducting surface reflects electromagnetic waves, ELF/VLF waves will be reflected and will propagate within the ionospheric region between HIPAS and HAARP in a manner dependant upon the reflection coefficient of the surfaces. The multiple reflections between these two wave sources above HIPAS and HAARP create the equivalent of a large antenna source for ELF/VLF signals. Generalization of this result to N sites for ELF/VLF excitation could imply that it is more advantageous to distribute a given amount of power among N sites as opposed to a single site concentration.



## IONOSPHERIC MODIFICATION AND ELF/VLF WAVE GENERATION BY HAARP

Nikolai G. Lehtinen, Umran S. Inan

STAR Lab, Electrical Engineering, Stanford University, Stanford, CA 94305, USA

HAARP is a high-power HF transmitter facility which after an upgrade to 3.6 MW power scheduled in 2006 will have an effective radiated power of the order of 2 GW in 2.8–10 MHz range. Facilities such as HAARP are used to study various effects of powerful HF radiation throughout all regions of ionosphere. The powerful emission at 3 MHz causes a significant modification of electron distribution at altitudes of 70–120 km. With modulation at (for example) 2 kHz applied to the HF carrier, the periodic changes in conductivity of the ionosphere modulate the subauroral electrojet currents and lead to emission of ELF/VLF waves into the magnetosphere, which then propagate to a point geomagnetically conjugate to HAARP. In this paper, we report the preliminary results of a fully kinetic model of the nonlinear heating by the HF signal, and the generation of the ELF/VLF signals via the modulation of such heating, with specific application to the parameters of the HAARP facility.

To calculate the modified electron distribution, we use a time-dependent solver of the kinetic equation with harmonically varying electric and static geomagnetic fields. The non-Maxwellian distribution obtained in this way can be characterized in terms of effective electron temperature defined by the average electron energy. The calculated changes in the effective electron temperature as a function of altitude show some similarities with Maxwellian models with static heating, but also display new features such as nonlinear saturation of the effective temperature at high HF power levels. The electron distribution obtained from the kinetic solver is used to find the conductivity for both HAARP HF radio wave and a low-frequency (approximated as DC) electric field. The modulated DC conductivity results in the modulation of the electrojet current, while the HF conductivity affects losses during the HF wave propagation. Since the modification of ionosphere affects the propagation of the HAARP radio wave itself, the power flux is calculated self-consistently together with the solution of the kinetic equation at each altitude. We pay specific attention to the highly nonlinear dependence of electrojet modulation on the applied HF power, and the effects of the geomagnetic field.

## LONG-DISTANCE DETECTION OF ELF WAVES GENERATED VIA MODULATED HF HEATING OF THE AURORAL ELECTROJET

Moore, R. C., Inan, U. S., Bell, T. F.

STAR Laboratory, Stanford University, Stanford, CA 94305

The High-frequency Active Auroral Research Program (HAARP) HF transmitter in Gakona, Alaska robustly generates electromagnetic ELF/VLF signals via modulated heating of the lower ionosphere. ELF/VLF signals produced in this manner propagate to large distances in the Earth-ionosphere waveguide with relatively low attenuation. Between 0800 and 1200 UT on February 11, 2005, the HAARP HF transmitter modulated the auroral electrojet currents, generating ELF waves alternately at 575 and 2125 Hz, each for 60 minutes at a time. Each of the ELF signals produced were detected at an ELF/VLF receiver 35 km from the HAARP facility. The ELF/VLF receiver at Midway Atoll, located in the middle of the Pacific Ocean at a distance of 4500 km from the HAARP facility, detected the 2125 Hz transmission between 1100 and 1200 UT. This 4500 km ground distance separation between the ELF signal source and the receiver constitutes the largest distance at which HAARP-generated ELF/VLF waves have been detected to date. In this paper, we quantitatively assess the characteristics of the ELF/VLF source region using an Earth-ionosphere waveguide propagation model with realistic electromagnetic parameters together with the observed properties of the ELF signals detected both in the near field and in the far field. Near field measurements are used to calculate the relative excitation magnitudes and phases of a set of effective Hall and Pedersen dipoles, the radiation from which is shown to be consistent with far field observations for radiated power levels on the order of several tens of Watts. In addition, our results suggest that a single dipole located between 60 and 85 km altitude cannot accurately model the polarization ellipse observed in the far field at Midway Atoll, despite the 4500 km distance between the signal source and the receiver. This observation underscores the importance of the Earth-ionosphere waveguide mode-excitation process as it relates to a distributed body of radiating currents such as that present above the HAARP HF heater array.

TERRESTRIAL  
FLASHES OBSERVED ON BATSE/CGRO AND ELF/VLF RADIO  
ATMOSPHERICS

GAMMA-RAY

This talk has been moved to Session H/G3, page 294.

## HIGH VOLTAGE ANTENNA IN MAGNETOSPHERIC PLASMA

Bibl, K., Paznukhov, V., Galkin, I. , Cheney, G.

Center for Atmospheric Research, 600 Suffolk St., Lowell MA 01854

We present the results of measuring capacity and radiation resistance of a large VLF antenna in magnetospheric plasma. This experiment was performed with the RPI instrument onboard of the IMAGE satellite using a specially developed program, which was run during three orbit passes in the fall of 2004. Measurements were made when the satellite was near its perigee both inside and outside of the plasmasphere. Using the RPI observations in other modes made simultaneously with the antenna experiment, we were also able to measure local plasma and electron gyro frequencies. Results were very successful in showing the dependence of the antenna capacity and radiation resistance on surrounding electron density. It is demonstrated that at high electron density (inside the plasmasphere) antenna capacity increases by about 70

In this experiment we measured the current and voltage on the transmit antenna during the transmissions made with different tuner settings. Because the RPI instrument was not specifically designed for such operation and the actual antenna capacity was not known, the tuning of the antenna was not a trivial task. Namely, in order to change the tuner settings, the operating frequency had to be changed as well. However, dependence of the measured antenna parameters on the operating frequency (between 13 and 20 kHz) was shown to be insignificant when this frequency was small compared to the electron gyro frequency and the plasma frequency. Analysis of the antenna-tuner equivalent circuit showed that the magnitude of antenna current also depends on the parameters of the tuner circuit. Therefore, in order to compare the antenna current values obtained with different tuner settings we had to derive certain normalization factor. When the current in the antenna is corrected by this factor there is still less current in the antenna when the antenna is radiating. The additional correction factor represents the effect of the inductor loss resistor and radiation resistance. Taking into account these corrections we get a rather smooth picture of the amplitude of the antenna current as a function of capacity and time (or location on the orbit). Making use of RPI-measured local plasma and electron gyrofrequencies it was possible to obtain a clear picture of the change of the antenna capacity with the plasma frequency. We are currently studying the dependence of antenna radiation resistance on the electron gyro frequency.

Session H1, 13:15 – Wed.

**LABORATORY EXPERIMENTS  
AND DUSTY PLASMAS**

Co-Chairs: W. Amatuucci, E. Bering, and R. Merlino



HIGH POWER ELECTRODELESS PLASMA PROPULSION USING  
NONLINEAR HELICON WAVES

Winglee, R. M., Ziemba, T., Prager, J.

, Roberson, B. R., Stobie, N., Carscadden, J.

Univ. of Washington, Dept. Earth and Space Sciences, Seattle, WA  
98195-1310

Helicon plasma propulsion systems are a recent development in plasma propulsion that uses high intensity rf helicon (whistler waves) to create the plasma. Such systems have several advantages. They are electrodeless and therefore not subject to erosion at high power operation. Helicons are known to create high density plasmas so that for a fixed thrust level, helicon plasma propulsion system can be very compact. In this paper we discuss results of the High Power Helicon (HPH) being developed at the University of Washington. This system can be operated over at least two orders of magnetic in power which adds to its versatility. At high power ( 100 kW) it operates in a non-linear wave regime where the wave field intensity is comparable to the background field required to support the whistler waves. This regime enables the creation of very dense plasmas at  $10^{21} \text{ m}^{-3}$  with high specific impulse of 2000 s for argon and even higher Isp for lighter gases at nearly 100 percent gas efficiency. At these density and energies the plasma can be considered high beta so that detachment issues from the guide magnetic field is not a problem. The high beta characteristics of the systems also facilitate the usage of magnetic nozzles to provide a highly focused plasma stream with the bulk of the plasma thermal energy converted to directed beam energy. This ability to focus the plasma stream aids in the overall power efficiency of the system and leads to other applications beyond a simple thruster, including beamed plasma propulsion systems.

## THE HELICON DISCHARGE IN THE VASIMR EXPERIMENT

Jared P. Squire<sup>1</sup>, V. T. Jacobson<sup>1</sup>, T. G. Glover  
, G. E. McCaskill<sup>1</sup>, F. C. Chang-Diaz<sup>2</sup>, F. W. Baity<sup>3</sup>  
, M. D. Carter<sup>3</sup>, R. H. Goulding<sup>3</sup>, R. D. Bengtson<sup>4</sup>  
, E. A. Bering, III<sup>5,6</sup>, M. Brukardt<sup>5</sup>

<sup>1</sup>Muniz Engineering Inc, Advanced Space Propulsion Laboratory, Ad Astra Rocket Company, Houston, TX, USA

<sup>2</sup>Advanced Space Propulsion Laboratory, Ad Astra Rocket Company, Houston, Texas, USA

<sup>3</sup>Oak Ridge National Laboratory, Oak Ridge, Tennessee, USA

<sup>4</sup>Physics Department, University of Texas at Austin, Austin, Texas, USA

<sup>5</sup>Physics Department, University of Houston, Houston, Texas, USA

<sup>6</sup>ECE Department, University of Houston, Houston, Texas, USA

The Advanced Space Propulsion Laboratory (ASPL) of the Ad Astra Rocket Company is performing research on the Variable Specific Impulse MagnetoPlasma Rocket (VASIMR). The VASIMR is a high power, > 10 kW, radio frequency (RF) driven magnetoplasma rocket, capable of very high exhaust velocities, > 100 km/s. In addition, its unique architecture allows in-flight mission-optimization of thrust and specific impulse to enhance performance and reduce trip time. The ASPL's experimental research focuses on three major areas: helicon plasma production, ion cyclotron resonant frequency (ICRF) acceleration and plasma expansion in a magnetic nozzle. A flexible four-magnet system, with a 1.3 Tesla maximum magnetic field strength, is used to study axial magnetic field profile shape effects. Power generated at 13.56 MHz with over 20 kW is used to perform helicon plasma source development. A 2 to 4 MHz RF transmitter capable of 10 kW is coming online for ICRF experiments. The primary diagnostics are: gas mass flow controllers, RF input power, Langmuir probes, retarding potential analyzers (RPA), microwave interferometers, neutral pressure measurements, plasma light emission and spectroscopy.

Helicon research has focused on operation with hydrogen, deuterium, and helium. Others are also being explored as well, nitrogen and argon. Optimization studies have been performed with the magnetic field axial profile shape, gas flow rate, gas tube geometry, RF frequency and antenna geometry. High performing discharges have been found for deuterium where the plasma source performance (ion current per kW) is proportional to the applied magnetic field at the helicon antenna. The present capability of our plasma source is a steady state plasma flux of about  $410^{20}$  /s or almost 80 A of ion current. The operating frequency of the helicon discharge is now several times the lower hybrid frequency, which raises interesting questions regarding the role of the lower hybrid resonance in helicon operation. These high-density plasmas have enabled exciting ICRF experiments that will be discussed in a companion paper by *Brukardt et al.* This paper will highlight the primary results in the development and evaluation of the helicon plasma source.



## ION CYCLOTRON RESONANCE HEATING IN THE VASIMR

Michael S. Brakardt<sup>1</sup>, Edgar A. Bering III<sup>1</sup>, Franklin R. Chang-Diaz<sup>2</sup>, Jared P. Squire<sup>2</sup>, Timothy W. Glover<sup>2</sup>, Verlin Jacobson<sup>2</sup>

<sup>1</sup>University of Houston, Department of Physics, Houtson TX 77204-5005

<sup>2</sup>Advanced Space Propulsion Laboratory, AdAstra Rocket Company, 13000 Space Center Blvd, Houston TX, 77059

The production of upward moving ion conics and ion heating are significant features in auroral processes. It is believed that ion cyclotron heating plays a role in these processes, but laboratory simulation of these auroral effects is difficult due to the fact that the ions involved only pass through the acceleration region once. In the Variable Specific Impulse Magnetoplasma Rocket (VASIMR) we have successfully simulated these effects. The current configuration of the VASIMR uses a helicon antenna with up to 20kW of power to generate plasma then uses an RF booster stage that uses left hand polarized slow mode waves launched from the high field side of the resonance. The current setup for the booster uses 2Mhz to 3Mhz waves with up to 1.5kW of power. This is similar to the ion cyclotron heating in tokamaks, but in the VASIMR the ions only pass through the resonance region once. The rapid absorption of ion cyclotron waves has been predicted in recent theoretical studies and these theoretical predictions have been confirmed with several independent measurements. The ion cyclotron resonance heating (ICRH) should show an increase in ion velocity perpendicular to the magnetic field. This increase should take place in the resonance region where the ion cyclotron frequency is equal to the frequency on the injected RF waves. Downstream of the resonance region the perpendicular velocity boost should be converted to axial flow velocity through the conservation of the first adiabatic invariant as the magnetic field decreases in the exhaust region of the VASIMR.

## MESOSPHERIC AEROSOL PARTICLE DETECTORS

Sternovsky, Z.<sup>1</sup>, Robertson, S.<sup>2</sup>, Knappmiller, S.<sup>2</sup>, Horanyi, M.<sup>1</sup>

<sup>1</sup>LASP, University of Colorado, Boulder, CO 80309-0392

<sup>2</sup>Physics Department, University of Colorado, Boulder, CO 80309-0390

Two instruments have been developed to detect charged aerosol particles in the mesosphere. The first is a flat charge collecting graphite surface on the skin of the rocket that has returned data in several sounding rocket campaigns. The collection surfaces have permanent magnets behind them to provide shielding from electrons. Some of the probes also have an electrical bias to repel light positive ions. Two probes, one with and one without an electric bias have been launched in January 2005 from Esrange, Sweden, as a part of the MAGIC campaign. The probes have detected a distinct layer of aerosols at around 82 km altitude. The second instrument has been developed to detect charged, sub-visible aerosol particles in the upper atmosphere. The instrument is designed to fly on a sounding rocket and has a 30 square centimeter entrance slit. Venting ports are placed lower on the detector in order to let the air out and reduce pressure buildup inside the detector. The air sample flows between four pairs of graphite electrodes biased symmetrically with increasing bias potentials. Electrons, light ions, cluster ions and heavy charged aerosol particles of both polarities are collected mass-selectively on the electrodes that are connected to sensitive electrometers. Direct Simulation Monte Carlo (DSMC) codes have been used to optimize the supersonic airflow within and around the instrument. A laboratory prototype of the instrument has been fabricated and calibrated using low energy ion beams. The instrument is scheduled for launch in the summer of 2007 from Andoya, Norway. These in-situ measurements are planned to coincide with the Aeronomy of Ice in the Mesosphere (AIM) mission. Acknowledgement: The project is supported by NASA.

## POTENTIAL ERRORS IN ELECTRON DENSITY MEASUREMENTS IN THE PRESENCE OF DUST.

Barjatya, Aroh, Swenson, Charles M.  
Utah State University

We report on electron density observations made simultaneously with Langmuir and impedance probe techniques on a common sounding rocket platform as it passed through dusty plasma. Discrepancies between the observations of the two instruments are the subject of this paper and raise concern with Langmuir probe techniques for dusty plasmas. The NASA Sudden Atom Layer (SAL) campaign was an experiment to investigate the presence of charged dust within and/or around a sporadic metal layers in Earth's mesosphere. The SAL rocket passed through a sporadic sodium layer at 94 km, accompanied by a sporadic E layer at 92.5 km. An onboard dust detector observed a 5 km thick positively charged dust layer starting at 90 km. This work presents the data from three other instruments: an electric field probe, a DC Langmuir probe, and a RF impedance probe. The impedance probe data is analyzed using Balmain's theory of a short antenna in a cold magnetoplasma to determine absolute electron density, and to which the DC fixed bias Langmuir probe data is normalized giving relative electron density. The payload skin potential is observed relative to a floating sphere, which was a part of the E-field probe. The three datasets indicate a case of payload surface charging when the rocket passed through the dust layer. We first discuss the rocket wake effect through a 3-dimensional direct simulation Monte Carlo method. A circuit model is then used to hypothesize possible vehicle charging scenarios attributed to the presence of the dust layer. We conclude that triboelectric charging from the neutral dust present in the layer may have played a role in the charging of the payload.

## ROCKET MEASUREMENTS OF ICY DUST PARTICLES OBSERVED IN THE POLAR SUMMER MESOSPHERE

Phillip. A. Webb<sup>1</sup>, Richard. A. Goldberg<sup>2</sup>, W. Dean Pesnell<sup>2</sup>  
, Henry D. Voss<sup>3</sup>

<sup>1</sup>UMBC/GEST, Goddard Space Flight Center, Greenbelt, MD 20771, USA

<sup>2</sup>NASA/Goddard Space Flight Center, Greenbelt, MD 20771, USA

<sup>3</sup>Taylor University, Upland, IN 46989, USA

The two Black Brant payloads flown during the DROPPS (Distribution and Role of Particles in the Polar Summer Mesosphere) rocket program were launched during early July, 1999 from Andøya Rocket Range (ARR), Norway. The purpose was to investigate the polar summer mesosphere, particularly polar mesospheric summer echoes (PMSE) and their possible relationship to noctilucent clouds (NLC). Both DROPPS payloads included front mounted side by side Particle Impact Detector (PID) charge and mass telescopes. Computer simulations have shown that the PID telescopes have the potential to detect atmospheric ice particles within the mesosphere having dimensions of a few nanometers. Ice particles of nanometer size are believed to be responsible for PMSEs through the process of scavenging. Evidence for this process is suggested by the presence of an electron biteout observed in the same region as the observation of nanometer size particles at an altitude of ~82-87 km over Andøya during the first DROPPS launch sequence. Evidence for this dusty plasma was observed independently by several instruments aboard the DROPPS payload.

We have previously presented results from the longer PID charge telescope that indicated two possible particle distributions differing by mean particle size. Due to the different geometries of the PID telescopes (primarily, that the charge telescope is longer than the mass telescope) each PID telescope collects a different portion of the nanometer sized PMSE particle distribution. When compared to the previous PID charge telescope results, the PID mass telescope results allow the true PMSE particle size distribution to be estimated. This talk will introduce the new findings from the shorter PID mass telescope and the comparison to the previous PID charge telescope. By comparing PID observations with the computer simulations we can obtain information concerning the properties of the PMSE particles, including their rocky core size, ice mantle thickness and distribution. This paper discusses the results of this analysis.

## OBSERVATION OF RESISTIVE DRIFT ALFVEN WAVES IN A HELICON PLASMA

Earl Scime

West Virginia University

We will present three dimensional electromagnetic wave frequency and amplitude measurements of low frequency instabilities observed in the expansion region of a magnetized helicon plasma. The wave is localized to the vicinity of the largest plasma density gradient and appears only at low neutral pressure. The wave amplitude grows rapidly with increasing magnetic field strength (and the wave frequency downshifts with increasing magnetic field strength), consistent with previous helicon source experiments. Because the waves arise in a plasma that satisfies the requirements for growth of resistive drift Alfvén waves

$$1.0 \gg \beta > (\nu_e/\omega_{ce}) > (m_e/M_i) \quad (1)$$

we have compared the measured wave frequencies to expectations for resistive-drift Alfvén waves. The observed wave is a transverse electromagnetic wave and the wave frequency is consistent with expectations for a resistive-drift Alfvén wave. With increasing magnetic field strength, the wave amplitude increases and eventually the plasma becomes unstable. A theoretical model of the resistive drift Alfvén instability, developed by Mikhailovskii will be shown to accurately predict the measured wave frequency dependence on magnetic field strength. Other helicon research groups have suggested that similar low frequency waves observed in their experiments result from the resistive drift instability. Because these measurements are of electromagnetic and not electrostatic waves, we suggest that the relatively high beta of helicon sources actually places this wave in the drift-Alfvén regime. Because of the large amplitude of these waves, it is possible (as suggested by others) that these waves could be responsible for reduced plasma confinement in helicon sources at large magnetic field strengths. We also note that because the wave appears under the same conditions as a spontaneously generated electric double layer, other researchers have suggested that similar observations may provide evidence of ion-ion streaming instabilities created in the double layer and not resistive drift waves. We will also compare our measurements to expectations for an ion-ion streaming instability.

GENERATION OF SPIKY POTENTIAL STRUCTURES ASSOCIATED WITH MULTI-HARMONIC ELECTROSTATIC ION CYCLOTRON WAVES

Kim, S. H.<sup>1</sup>, Merlino, R. L.<sup>1</sup>, Ganguli, G. I.<sup>2</sup>

<sup>1</sup>Dept. Physics and Astronomy, University of Iowa, Iowa City, IA 52242

<sup>2</sup>Plasma Physics Division, US Naval Research Laboratory, Washington, DC 20375

A common feature of electric fields observed on satellites in the earth's auroral region is their spiky, repetitive nature. These spiky electric field structures appear as either unipolar or bipolar pulses in high resolution time domain waveforms of the potential difference between pairs of spheres deployed from the spacecraft. Time domain waveforms of three different hydrogen-cyclotron wave events observed with the S3-3 satellite [Temerin et al., Phys. Rev. Lett. 43, 1941, 1979] showed examples of both narrow spectral features at a frequency just above the local hydrogen-cyclotron frequency and spiky, bipolar structures with a repetition frequency just above local hydrogen-cyclotron frequency. Data obtained from the Fast Auroral Snapshot (FAST) satellite in the upward current northern auroral region showed a multi-harmonic EIC spectrum with corresponding spiky structures in both the perpendicular and parallel electric field waveforms [Ergun, et al., Geophys. Res. Lett. 25, 2025, 1998; Gavrishchaka et al., Phys. Rev. Lett. 85, 4285, 2000]. Spiky electric field structures have also been seen on the Viking satellite and on Cluster. The production of coherent, spiky electrostatic potential structures, similar to the spiky electric field structures that have been observed in the earth's auroral region is investigated experimentally. These structures are associated with coherent multi-harmonic electrostatic ion cyclotron (EIC) waves in a current-free plasma. A multi-harmonic EIC spectrum is produced when broadband electrostatic noise, launched into the Q machine plasma from an antenna, propagates through a spatially localized region of parallel (to B) ion flow with a gradient in the direction transverse to B [Kim et al., Phys. Plasmas 11, 4501, 2004]. The spiky potential waveforms result from a linear combination of coherent multi-harmonic EIC waves, when the harmonics have comparable amplitudes and are phase-locked.

Work supported by the US Dept. of Energy

THE MODEL OF SECONDARY EMISSION FROM SPHERICAL  
DUST GRAINS AND ITS COMPARISON WITH EXPERIMENTS

Ivana Richterova, Zdenek Nemecek, Jana Safrankova , Jiri Pavlu

Charles University, Faculty of Mathematics and Physics, Prague, Czech  
Republic

Dust grains in the space are charged by various processes and finally reaches an equilibrium state. The most important charging processes are the attachment of ions and electrons of the ambient plasma, photoemission by the solar UV radiation, and secondary electron emission. In this contribution, we present a new numerical model that provides a realistic description of the secondary emission process from small spherical samples of different materials. For a comparison of model results with laboratory simulations, we have chosen the metals as well as nonconducting materials. The fact that results of numerical modeling are in a very good agreement with measurements suggests that the model can be used for considerations on the dust charge under different conditions in the space. We discuss the model assumptions and the behavior of thue secondary and backscattered electrons in detail.

DUST CHARGING: ELECTRON AND ION FIELD EMISSIONS IN  
LABORATORY SIMULATIONS

Jiri Pavlu, Jana Safrankova, Zdenek Nemecek  
, Ivana Richterova, Martin Jerab  
Charles University, Faculty of Mathematics and Physics, Prague, Czech  
Republic

Almost one percent of our galaxy consists of dust grains; objects of different shapes with a size distribution from micro to nanometers. In the space, a number of processes leads to their charging. Among them, the photoemission and electron and ion attachments are dominant. On the other hand, processes like electron or ion field emissions can limit the total grain charge.

Our laboratory simulations of dust grain charging are performed inside a quadrupole trap where a single dust grain can be held and exposed to electron and/or ion beams for several days. This experimental approach allows us to separate individual charging process. A secular frequency of the grain motion in the trap makes possible to measure the charge-to-mass ratio and to calculate the grain surface potential. In this contribution, we survey results of our experiments with a special attention to an influence of electron and ion field emissions on dielectric and gold grains.



Session H/G1, 08:35 – Wed.

## **RADIATION BELT**

Co-Chairs: J. Albert, J. Bortnik

H/G1

## CONTRIBUTION OF LIGHTNING WHISTLERS TO THE PLASMASPHERIC HISS SPECTRUM

James Green<sup>1</sup>, Shing Fung<sup>1</sup>, Scott Boardsen<sup>2</sup>  
, Leonard N. Garcia<sup>3</sup>, Xi Shao<sup>4</sup>, Robert F. Benson<sup>1</sup>

<sup>1</sup>NASA/Goddard Space Flight Center, Greenbelt, MD

<sup>2</sup>L3 Communications, Government Services, Inc., Largo, MD

<sup>3</sup>QSS Group, Lanham, MD

<sup>4</sup>Department of Astronomy, University of Maryland, College Park, MD

The long-standing issues surrounding the origin of plasmaspheric hiss, especially with regard to lightning whistlers, and their contributions to slot-region electron losses will be explored using observations from the Dynamics Explorer-1 (DE) and IMAGE spacecraft. DE and IMAGE are polar orbiting satellites with plasma-wave receivers that measure low-frequency equatorial electromagnetic emissions (below about 0.3 kHz), plasmaspheric hiss (0.3-3 kHz), and VLF ground-transmitter radiation (10-50 kHz) within the plasmasphere. Since whistler-mode waves have field-line like trajectories, or are completely field-aligned when traveling in plasmaspheric density ducts, only polar orbiting missions are able to survey their entire spatial domain and provide a unique perspective that cannot be obtained from equatorial missions. In this study, plasmaspheric hiss has been identified as having the same frequency and spatial distribution as the electromagnetic wave observations over the range of 330 Hz to 3 KHz within the plasmasphere. Geographic control of plasmaspheric hiss, along with similar local time and seasonal variations between the distribution of lightning and hiss within the plasmasphere, are compelling indicators of a lightning origin. From an exhaustive analysis of wave observations from DE and IMAGE it is found that, over a significant portion of the wave spectrum, the distribution of the broad-band hiss intensity is similar to the distribution of lightning: stronger over continents than over oceans, stronger in the summer than in the winter, and stronger on the dayside than on the nightside. Simultaneous observations of lightning by the TRMM satellite and by IMAGE show that the plasmaspheric whistler-mode spectrum can extend up to frequencies greater than 50 kHz over regions of lightning. These frequencies far exceed what has been considered the upper frequency of the hiss spectrum of 3 kHz. This investigation supports lightning as the dominant source for plasmaspheric hiss, which has been regarded as the primary agent for creating the slot region in the radiation belts.

## SOURCES OF PLASMASPHERIC HISS

Meredith, N. P.<sup>1</sup>, Horne, R. B.<sup>1</sup>, Horsfall, D.<sup>1</sup>, Thorne, R. M.<sup>2</sup>

<sup>1</sup>British Antarctic Survey, Cambridge, UK

<sup>2</sup>University of California, Los Angeles, USA

There are two theories for the origin of plasmaspheric hiss; lightning generated whistlers and wave turbulence in space. Here we analyze CRRES wave data together with the global distribution of lightning to test both theories. Using the entire CRRES wave database we split the data into seven frequency bands between 0.1 and 5 kHz, and analyze the region  $2.0 \leq L \leq 3.5$ . The data are selected for high density and low electron cyclotron harmonic wave activity to ensure it lies inside the plasmasphere. At each point, the CRRES observations are mapped along the field to the ionosphere. Wave power peaks in the frequency range  $0.2 \leq f \leq 0.5$  kHz, and for  $f \leq 1$  kHz, is independent of lightning flash rate at the foot of the field lines (within a semi-circle of radius of 1000 km equatorward) over 4 orders of magnitude. Wave power increases with magnetic activity for all frequencies. There is no evidence for increased wave power when the footprints are over land compared to water. Conversely, for  $f \geq 1$  kHz, there is a tendency for wave power to increase with flash rate, and wave power increases after 1800 MLT. The data suggest that wave turbulence, not lightning whistlers, is the main source of wave power below 1 kHz, which is traditionally defined as plasmaspheric hiss. Wave power above 1 kHz is related to lightning whistlers, and traditionally known as MR whistlers. Since hiss power is orders of magnitude higher than for  $f \geq 1$  kHz, hiss should dominate the loss of electrons in the region  $2.0 \leq L \leq 3.5$ .

## EVOLUTION OF LIGHTNING-GENERATED MAGNETOSPHERICALLY REFLECTING WHISTLER WAVES INTO AN INCOHERENT NOISE BAND

Bortnik, J., Thorne, R.M.

Dept. Atmospheric and Oceanic Sciences, Rm. 7115, Math Sciences Bldg., UCLA

We use a numerical method to simulate the frequency-time ( $f - t$ ) spectrogram as it would be observed at any location in the magnetosphere, that results from a lightning discharge at any given latitude on Earth. We model the lightning discharge as a short, vertical current channel with a double exponential return-stroke current, and then calculate the radiated wave power at the bottomside of the ionosphere (100 km). The wave power is then translated to the topside of the ionosphere (1000 km) using latitude and frequency dependent trans-ionospheric damping factors. Using a two-dimensional ray tracing code we then calculate the trajectories of 5330 whistler rays that effectively sample the lightning strikes frequency spectrum and latitudinal spread about the source, and then use these so-called “sample rays” to create 120 million interpolated rays, each weighted with a measure of energy according to its frequency and injection latitude. This energy is progressively attenuated along the rays trajectory using a Landau damping calculation with realistic suprathermal electron fluxes [Bell *et al.*, 2002]. A detection area is defined in the plasmasphere, and rays that cross this area are used to construct the  $f - t$  spectrogram representative of what would be observed on a satellite located in that region. We investigate the role that the lightning source latitude, observation location, and plasmaspheric electron density structures have on the appearance of the simulated  $f - t$  spectrograms and focus specifically on the formation of the low-frequency incoherent noise band towards the end of the magnetospherically reflected whistlers lifetime, which may be related to plasmaspheric hiss. We also recap open questions and suggest future directions of research associated with hiss.

## MODELING TERRESTRIAL VLF TRANSMITTER EFFECTS ON TRAPPED ELECTRON POPULATIONS

Starks, M.J.

Space Vehicles Directorate, Air Force Research Laboratory, Hanscom AFB, MA, USA

As the number of satellites in low earth orbit continues to increase, renewed interest has arisen in using very low frequency (VLF) radio waves to mitigate the damaging effects of enhanced radiation belts created, for example, by strong solar activity. An analysis by Abel and Thorne (*J. Geophys. Res.*, **103**, A2, 2385-2396, 1998) showed the importance of ground-based VLF transmitters to loss mechanisms in the inner belt and slot region of the magnetosphere. At the time, only rough, averaged estimates of contributions from eight powerful terrestrial VLF transmitters could be used in the calculation.

As the Air Force Research Laboratory Space Vehicles Directorates end-to-end wave-particle interactions code has matured, it has become possible to directly simulate the electron depopulation process from transmitter to radiation belt in a unified way. Modern codes estimate the antenna patterns from terrestrial VLF transmitters and their subsequent coupling into the ionosphere. Three dimensional ray tracing computes to where the transmitted power travels, and incorporates changes in intensity due to geometric divergence and Landau damping. Wave-particle interaction codes then use the resulting three-dimensional wave field to compute diffusion coefficients, particle lifetimes, and ultimately electron distributions in the radiation belts.

With these tools, we have modelled the same group of terrestrial VLF transmitters assumed in Abel and Thorne (1998) and computed electron diffusion coefficients and lifetimes for comparison. We have then updated the model to use the set of transmitters existing today and estimated the effects on particle distributions resulting from changes in the ground-based transmitter network. These simulations will eventually lead to similar analyses involving proposed transmitters located in space.

DIFFUSION OF ENERGETIC ELECTRONS BY TERRESTRIAL  
VLF TRANSMITTERSAlbert, J. M.

Air Force Research Lab

The effect of terrestrial VLF wave transmitters on energetic electrons trapped on geomagnetic field lines is of great scientific and increasingly, practical interest, as documented by recent studies by Abel and Thorne [J. Geophys. Res., 103 (A2), 2385, 1998] and Inan et al. [J. Geophys. Res., 108 (A5), 1186, 2003]. With this motivation, a large scale ray tracing effort has been underway at the Air Force Research Laboratory to compute the three dimensional distribution of their wave power within the plasmasphere, as presented by Starks et al. [this meeting]. With this information, it is possible to estimate the rate of electron pitch angle scattering and loss via precipitation into the atmosphere. After identifying cyclotron resonant wave particle resonances, quasilinear pitch angle diffusion coefficients can be evaluated; these are simplified by the narrow frequency range of the waves, though they still depend strongly on the orientation (wavenormal angle) of the waves. Magnetospheric reflection of the waves is automatically taken into account. The diffusion coefficients are then combined with diffusion rates for other, natural, wave sources as well as Coulomb collisions, and used in a bounce-averaged pitch angle diffusion equation to determine the evolution of the particle population over time. This approach is well suited to studying the sensitivity to details of the initial particle distribution, cold plasma density and associated geomagnetic conditions, and wave transmitter characteristics. Proposed additional, dedicated transmitters, both ground and space based, can be modeled and studied as well. Future plans include the incorporation of Landau damping of the propagating waves, nonlinearly triggered emissions, and related dynamical phenomena.

EXCITATION OF SINGLE AND MULTI-HOP WHISTLER-MODE  
VLF SIGNALS WITH THE SIPLE STATION, ANTARCTICA VLF  
TRANSMITTER

Gibby, A. R., Carpenter, D. L., Inan, U. S. , Jira, C. F.  
Space, Telecommunications, and Radioscience Laboratory, Stanford  
University

Data from the Siple Station VLF wave-injection experiments are used to assess the conditions under which very low frequency signals from the transmitter located at Siple Station, Antarctica, are received at the conjugate station at Lake Mistissini, Quebec, in the 1986 operating year. The purpose of the study is to begin to quantify the statistical occurrence of the growth, amplification and emission triggering processes and their dependence on geophysical conditions. This year (1986) was the final period in which Siple was operated year-round and this study is the first methodical review of this data. The 1986 data show that days of strongest Siple activity tended to coincide with days of strong, often multi-hop whistler activity on paths with endpoints within a few degrees of the Siple latitude. They also tended to coincide with days of strong natural noise band activity propagating on paths within a similar range of Siple's location. These results confirm the results of previous studies. In addition, the data from the receiver at Siple Station were reviewed for the occurrence of multi-hop propagation of Siple signals. The conditions for multi-hop reception were observed less frequently than the conditions for single-hop reception, and multi-hop reception at Siple coincided with reception at Lake Mistissini in every case. Finally, the response to a frequently transmitted, diagnostic format was studied on a few of the most active transmitting days in the period. This format was transmitted four times every hour, containing a variety of ramp, staircase, and continuous pulses at a number of frequencies. Study of the response to this format allows the exploration of the short-term variation of reception activity.



## RAPIDLY MOVING SOURCES OF UPPER-BAND ELF/VLF CHORUS NEAR THE MAGNETIC EQUATOR

Manuel Platino

STAR Laboratory, Stanford University

Multiple simultaneous wideband [Gurnett et al., 2001] measurements on the Cluster spacecraft of upper band chorus emissions near the magnetic equator (at magnetic latitudes between -20 deg. and 10 deg. and  $L$  shells ranging between  $L = 4$  and  $L = 5$ ) are used to deduce the properties of the compact source regions of ELF/VLF chorus emissions. The frequency differences exhibited by the same chorus emissions observed on different spacecraft are interpreted [Inan et al., 2004] in terms of a differential Doppler shift, using a simple model involving rapidly moving sources traveling at speeds comparable to the parallel resonant velocity of counterstreaming gyroresonant electrons. These observations are used to determine the location and size along the Earth's magnetic field lines of the source of the chorus. These frequencies and time differences are interpreted as a direct consequence of the rapid motion of highly localized source regions of chorus. In this paper, we examine the previously presented model of rapid motion of sources of chorus, extending the calculations to a 3D space, using measurements of the four Cluster spacecraft. These calculations of source location and velocity as a function of frequency indicate that chorus sources extend over approx. 6000 km along the field lines. The emitted chorus waves at the source, are assumed to have a wide range of wave normal angles, but the rays reaching the spacecraft seem to be the ones with lower angles (with some exceptions). The ranges of velocity obtained vary in frequency around values ranging from  $0.01c$  to  $0.04c$ .

## FAR- FIELD RADIATION OF LINEAR ANTENNAS IN AN ANISOTROPIC PLASMA

Huang, X., Reinisch, B. W., Song, P.

Center for Atmospheric Research, University of Massachusetts Lowell,  
600 Suffolk St., Lowell MA 01854

Assuming a sinusoidal current distribution on a linear antenna immersed in a uniform anisotropic plasma and ignoring the effect of a plasma sheath, an accurate expression for the stationary radiation field is derived using the Greens function method. We avoided the usual plane wave approximation for the calculation of the asymptotic field, and the resulting spherical waves have an index of refraction that is different from the plane wave solution and varies with the propagation angle. The relation of between the refractive indices of the plane and spherical waves is derived. All expressions are valid for any point in all eight regions of the cold plasma CMA diagram, except that the resonance and cutoff phenomena are not discussed. One important result is a significant difference in the radiation cones for some CMA regions between our general solution and the plane wave approximation. The analysis gives the polarization, the radiation pattern, and the radiation resistance including solutions for whistler mode frequencies. The analysis is performed for any given frequency-dependent plasma parameter and any antenna length (the short antenna is a special case in the discussion) and antenna orientation with respect to the magnetic field (parallel and perpendicular orientations are special cases). The two solutions for the anisotropic case merge into one wave for  $Y = fB/f_0$  (the medium becomes isotropic), and reduce exactly to the well known free space solution for  $X = (fp/f)^2$ . The effect of the plasma sheath is ignored in the derivations but its effect on the far-field is discussed.

Session H/G2, 13:15 – Thurs.

**IONOSPHERIC EFFECTS OF  
LIGHTNING – I**

Co-Chairs: E. Gerken, V. Pasko



## RESULTS FROM STEPS 2000: WHY DO ONLY SOME STORMS PRODUCE TLES?

Lyons, W.A.<sup>1</sup>, Andersen, L.M.<sup>1</sup>, Nelson, T.E.<sup>1</sup>  
, Cummer, S.A.<sup>2</sup>, Jaugey, N.C.<sup>2</sup>, Huffines, G.R.<sup>3</sup>

<sup>1</sup>FMA Research, Inc., Yucca Ridge Field Station, Fort Collins, CO 80524

<sup>2</sup>Duke University, Dept. Electrical and Computer Engineering, Durham, N.C. 27708

<sup>3</sup>University of Northern Colorado, Dept. of Earth Sciences, Greeley, CO 80639

During the Severe Thunderstorm Electrification and Precipitation Study (STEPS), we addressed two basic questions. First, what are the characteristics of those positive cloud-to-ground strokes (+CGs) which produce transient luminous events (TLEs)? The vast majority optically confirmed TLEs over High Plains storms were associated with large charge moment change events (DMq), exceeding thresholds of several hundred C km, substantially larger than the DMq for "normal lightning. This finding is entirely consistent with present theoretical models of sprite ignition at 75 km due to conventional breakdown. The second question addressed why not all mesoscale convective systems (MCSs) produce TLEs, or if they do, do so only for certain stages in their life cycle. The parent +CGs occurred mostly in the storms stratiform region. Updated analyses for Lightning Mapping Array data confirm most parent +CGs removed charge from relatively low altitudes (3 to 5 km AGL.) Analyses of 1500 TLEs and their parent MCSs yields some clear criteria. The cloud top canopy must be  $\geq 20,000$  sq. km at the 50C level, and the coldest temperature must be at least -55C. The peak reflectivity somewhere in the parent storm must exceed 55 dBZ. This requirement for a very tall and also intense storm initially seems at odds with the known environment of TLE parent CGs. Yet the emerging conceptual models of TLEs within trailing stratiform regions suggest the overall picture is consistent with what is known about MCS internal structures and circulations. A case study of an MCS will be used to illustrate the updated sprite/MCS model.

## SPRITE IMAGES AND SPECTRA WITH HIGH TIME RESOLUTION

H. C. Stenbaek-Nielsen<sup>1</sup>, M. G. McHarg<sup>2</sup>, T. Kammer<sup>1</sup>

<sup>1</sup>University of Alaska, Fairbanks, AK 99775, USA

<sup>2</sup>US Air Force Academy, Colorado Springs, CO 80840, USA

A sprite campaign fielding a large aperture imaging spectrograph and a high speed imager was conducted from the Langmuir Laboratory, Socorro, New Mexico, in June and July 2005. The spectrograph slit was orientated vertically to provide height resolved spectra. The spectra were recorded on a digital intensified CCD capable of 1000 frames per second, i.e. millisecond time resolution, but the best spectra were recorded using a frame rate of 300 per second. The images cover a wavelength range of about 170 nm within the spectrographs range from 450 nm to 900 nm. Most of the data were obtained in the range from 640 to 810 nm. The estimated spectral resolution is 2 nm. The observed spectra are dominated by molecular nitrogen emissions. It is uncertain if any nitrogen ion lines are present. The high speed images were made at 10,000 frames per second gated at 50 micro seconds per frame. At this frame rate we are resolving streamer development only hinted at in our earlier millisecond resolution images. The observations show a bead, presumably the streamer head, propagating downward at approximately  $7 \times 10^6$  m/s for 1,500 microseconds. The emissions from the bead are followed 800 microseconds later by emissions from the entire sprite column. We see evidence for branching of the streamer tips in several cases. Beads propagating upward are also observed with the streamers transitioning into more diffuse emissions. Previous work (Pasko and Stenbaek-Nielsen, GRL, 29(10), 2002) indicates this transition region is related to the local dielectric relaxation time. Examples of elves and halos exhibit a much more complex temporal development than envisioned based on the earlier millisecond observations.

## SUBMILLISECOND VIDEO AND ELECTROMAGNETIC OBSERVATIONS OF TLE DEVELOPMENT AND STRUCTURE

Cummer, S. A.<sup>1</sup>, Jaugey, N. C.<sup>1</sup>, Lyons, W. A.<sup>2</sup>, Nelson, T. E.<sup>2</sup>, Gerken, E. A.<sup>3</sup>, Taylor, M. J.<sup>4</sup>, Pautet, D.<sup>4</sup>, Bailey, M.<sup>4</sup>

<sup>1</sup>Department of Electrical and Computer Engineering, Duke University, Durham, North Carolina, USA

<sup>2</sup>FMA Research, Inc., Yucca Ridge Field Station, Ft. Collins, Colorado, USA

<sup>3</sup>Center for Geospace Studies, SRI International, Menlo Park, California, USA

<sup>4</sup>Center for Atmospheric and Space Sciences, Utah State University, Logan, Utah, USA

During the 2005 summer observation campaign at Yucca Ridge, Colorado, numerous instruments aimed at observations of high altitude optical emissions driven by lightning. Included in this set were a flexible intensified high speed camera (Vision Research Phantom 7.1) and wideband magnetic field sensors (0.1 Hz to 30 kHz, built by QUASAR, Inc.) that were employed in an effort to probe the details of the connection between the low altitude lightning processes and high altitude transient luminous events (TLEs). The low frequency sensitivity of the magnetic field sensors enabled measurement of the continuing lightning current that is involved in many of the complex sprites but that can be difficult to detect by other means, while the high speed video gave precise timing of TLE onset and features relative to the driving lightning processes below.

A total of 76 TLEs were captured on high speed video during this campaign; 10 were halos or elves without sprites, and 66 were sprites, many of which were also accompanied by halos and elves. Sprites were imaged between 5000 and 10000 frames per second on 13 August 2005 during a storm that was as close as 250 km from the camera. The combination of proximity and camera speed revealed a detailed view of the spatial and temporal development of the sprites observed on this night. Some new features were also seen; for example, it appears that at least some sprite beads with persistent optical emissions form when a downward streamer head collides with an adjacent, preexisting streamer channel. We also analyze a variety of different mesospheric optical emissions, from time resolved elves and halos to complex, long duration sprite sequences.

HIGH TIME RESOLUTION ANALYSIS OF THE LIGHTNING-  
SPRITE RELATIONSHIP

Li, J.<sup>1</sup>, Cummer, S. A.<sup>1</sup>, Jaugey, N.<sup>1</sup>  
, Lyons, W. A.<sup>2</sup>, Nelson, T. E.<sup>2</sup>, Gerken, E. A.<sup>3</sup>

<sup>1</sup>Department of Electrical and Computer Engineering, Duke University,  
Durham, NC 27708

<sup>2</sup>FMA Research, Inc., Yucca Ridge Field Station, Ft. Collins, CO 80524

<sup>3</sup>Center for Geospace Studies, SRI International, Menlo Park, California,  
94025

Through simultaneous measurements of high altitude optical emissions and the magnetic field produced by sprite associated lightning discharge, previous studies have uncovered many aspects of the relationship between these phenomena. However, few data sets have acquired both of these measurements with the millisecond or faster time accuracy and resolution on which many sprite-associated phenomena occur. In this paper, we report results of the coordinated analysis of high and regular speed sprite video and wideband (0.1 Hz to 30 kHz) magnetic field measurements made simultaneously at the Yucca Ridge Field Station and Duke University during the June through August 2005 campaign period. The absolute time accuracy and precision of all instruments has been verified on the order of 10 microseconds, and the intensified high speed video was acquired at rates between 1000 and 10000 frames per second. These data thus enable a close examination with high time resolution of the link between low altitude lightning processes and high altitude sprite processes.

We report results of analysis of the connection between lightning charge transfer and sprite initiation delay and altitude, specifically comparing sprites that initiate rapidly after the lightning return stroke to those that are delayed as long as hundreds of milliseconds. We similarly investigate the relationship of lightning charge transfer characteristics and general sprite morphology and duration. On one observation night (4 July 2005), a large mesoscale convective system produced many sprites that were part of complex TLE sequences that included optical emission elements that appear well after any return stroke and initiate at apparently relatively low altitudes. The connection between these elements and the complex temporal structure of the underlying lightning flash as observed with the magnetic sensors is discussed.



## EFFECTS OF PHOTOIONIZATION ON SIMILARITY PROPERTIES OF STREAMERS AT VARIOUS PRESSURES IN AIR

Liu, N, Pasko, V. P.

CSSL Laboratory, Department of Electrical Engineering, Penn State University

Similarity relations [e.g., Roth, *Industrial plasma engineering*, Vol. 1, 1995, p. 306] represent a useful tool for analysis of gas discharges since they allow to use known properties of the discharge at one pressure to deduce features of discharges at variety of other pressures of interest, at which experimental studies may not be feasible or even possible. In addition to traditional design of glow discharge tubes, similarity relations have been successfully applied to understanding of streamer discharges in air at several atmospheres, which are used for triggering of combustion in spark ignition engines [Achat et al., *J. Phys. D: Appl. Phys.*, 25, 661, 1992; Tardiveau et al., *J. Phys. D: Appl. Phys.*, 34, 1690, 2001], and also for analysis and interpretation of streamer discharges in sprites occurring at very low air pressures in altitude range 40-90 km in the Earth's atmosphere [e.g., Liu and Pasko, *JGR*, 109, A04301, 2004]. Streamer discharges similar to those documented in sprites [Gerken and Inan, *IEEE Trans. Plasma Sci.*, 33, 282, 2005, and references therein] have been observed in point-to-plane discharge geometry in laboratory experiments at near ground pressures [Pancheshnyi et al., *Phys. Rev. E*, 71, 016407, 2005; Briels et al., *IEEE Trans. Plasma Sci.*, 33, 264, 2005]. Understanding of the physical processes which lead to the observed departures from similarity relations at different pressures in these experiments represents an important problem, resolution of which would synergistically benefit understanding of streamers in both systems (i.e., due to generally relaxed requirements on time resolution of imaging systems needed for studies of sprite streamers, and easy repeatability of discharges in high pressure laboratory experiments). In this talk we report results from a streamer model developed in [Liu and Pasko, *JGR*, 109, A04301, 2004; *GRL*, L05104, 2005; *J. Phys. D: Appl. Phys.*, in review, 2005] as applied to propagation of positive streamers at various pressures in air in a point-to-plane discharge geometry. We directly compare our results with recent experiments at atmospheric and near atmospheric pressures in air reported in [Pancheshnyi et al., 2005; Briels et al., 2005]. The modeling results emphasize that the quenching of singlet excited states of molecular nitrogen emitting photoionizing radiation is responsible for non-similar behavior of streamers at pressures higher than several Torr. Our modeling results agree with recent experimental work [Pancheshnyi et al., 2005; Briels et al., 2005] showing that streamers have more and thinner channels and branch more frequently at higher (i.e., near atmospheric) pressures than at lower pressures. The results also demonstrate importance of accounting for effects associated with electrode geometry for interpretation of experimental studies on similarity properties of streamers at various pressures. One of the major unsolved problems in current sprite research is the observed initiation of sprites by very weak lightning discharges [e.g., Hu et al., *GRL*, 29, 1279, 2002]. It has been proposed that meteoric dust particles in the mesosphere and stratosphere may be involved in the formation of sprites [Zabotin and Wright, *GRL*, 28, 2593, 2001]. In this talk we will also discuss the implications of the experimental results of Briels et al. [2005] and our related modeling studies for the meteoric dust theory of sprite initiation.

## TERRESTRIAL GAMMA-RAY FLASHES: STATUS AND PROSPECTS

David M. Smith, Brian W. Grefenstette  
Physics Dept. and SCIPP, U.C. Santa Cruz

**Overview:** Terrestrial Gamma-ray Flashes (TGFs) are millisecond flashes of gamma rays observed by satellites over thunderstorms. Their relation to lightning, VLF emissions, and transient luminous events is a rapidly evolving field of study at the moment. I will review the status of our knowledge of TGFs with emphasis on data from the RHESSI satellite.

**Background:** TGFs are bremsstrahlung from the highest-energy electrons accelerated by any natural process on Earth or in near-Earth space. They may play a role in atmospheric chemistry, the global electrical circuit, the evolution of charging in thunderclouds, and the population of particles in Earth's radiation belts. They were initially discovered with NASA's Compton Gamma-Ray Observatory, which de-orbited in 2000 (Fishman et al. 1994, *Science* 264, 1313).

**Specifics of the presentation:** Over 500 TGFs have been found in data from the Reuven Ramaty High Energy Solar Spectroscopic Imager (RHESSI) since its launch in February 2002. Each flash contains on the order of 30 photon counts, usually ranging from 20 keV to 20 MeV, lasts on the order of a millisecond, and is localized to approximately 1000 km. I will report on correlations (or lack thereof) between the intrinsic properties of the flashes (spectrum, duration, intensity) and contextual properties such as geographic latitude, magnetic latitude, local time, distance from the spacecraft (where accurate positions can be obtained from radio atmospherics), and terrain (inland, coastal, or deep ocean). A new exposure-corrected map will be presented and compared with lightning data. Unusual or extreme cases of TGF activity will be individually examined.

## IONOSPHERIC EFFECTS OF ELECTROMAGNETIC PULSES RADIATED BY LIGHTNING RETURN STROKES

Inan, U. S.

Space, Telecommunications and Radioscience Laboratory, , Stanford University, Stanford, CA 94305

The occurrence of a lightning discharge leads to the release of both electromagnetic and quasi-electrostatic energy, both of which are now known to produce detectable electrodynamic effects at high altitudes, in the form of elves, sprites, blue jets, and terrestrial gamma-ray flashes. While sprites produced largely by the quasi-electrostatic fields constitute the more spectacular and readily observable of Transient Luminous Events (TLEs), recent data, especially from space-borne measurements have confirmed earlier expectations that the more rapid (i.e., shorter duration) phenomena, such as elves and terrestrial gamma-ray flashes may well be much more common. This realization is particularly important, since lightning discharges of all types, positive, negative, cloud-to-ground or intracloud, are known to lead to the production of intense electromagnetic impulses (or EMPs), and the totality of high altitude effects produced by such EMPs may well be significant contributor to the state of the nighttime ionosphere on a global scale. In this paper, we present a review our current understanding of the interaction with the lower ionosphere of lightning EMPs and discuss their possible role in the production of terrestrial gamma-ray flashes as well as elves. We also discuss results of a three-dimensional model of the interaction, which allows the calculation of the effects of the static magnetic field (i.e., finite dip angle), leading to azimuthal asymmetries in rapidly expanding luminous rings of elves, which may possibly be detectable. Azimuthal asymmetries of EMP-ionosphere interaction may also have detectable implications for terrestrial gamma-ray flashes, depending on the altitude at which the gamma-rays photons are emitted.

NEGATIVE STEPPED LEADERS AS A SOURCE OF RUNAWAY ELECTRONS

Victor P. Pasko, Gregory D. Moss, Ningyu Liu

CSSL Laboratory, The Pennsylvania State University, University Park,  
PA 16802, USA

In the presence of sufficiently strong electric fields  $\sim 10E_k$  in a weakly ionized plasma, where  $E_k$  is the conventional breakdown threshold field defined by the equality of the ionization and dissociative attachment coefficients in air, a fraction of initially low energy ( $\sim$ several eV) electrons can be directly accelerated over the peak of the dynamic friction force of electrons in air and become thermal runaway electrons [Gurevich, Sov. Phys. JETP, 12, 904, 1961]. Streamers are filamentary plasmas, which are driven by highly nonlinear space charge waves. The enhancement of electric fields around tips of streamers is one of the unique naturally occurring circumstances in which fields  $\sim 10E_k$  can be dynamically produced and sustained for relatively extended periods of time. The ability of these streamer tip fields to generate runaway electrons was identified and discussed in the literature over two decades ago [Babich, Sov. Phys. Dokl., 263, 76, 1982, and references therein]. Streamers are known to act as building blocks of streamer zones of conventional lightning leaders. It is also believed that the filamentary plasma structures observed in blue jets and gigantic jets, which emanate from the tops of thunderclouds, are directly linked to the processes in streamer zones of lightning leaders. In this talk we will discuss a probable scenario of events in which non-relativistic thermal runaway electrons emitted from the tips of streamers in the streamer zones of lightning leaders can be accelerated to relativistic energies. With total potential differences on the order of tens of MV available in streamer zones of lightning leaders, it is proposed that during a highly transient negative corona flash stage of the development of negative stepped leader, electrons with energies 2-8 keV ejected from streamer tips near the leader head [Moss et al., Eos. Trans. AGU, 85(47), Fall Meeting Suppl., Abstract AE31A-0158, 2004; JGR, in review, 2005; Liu et al., 2005 Seminar Series on TGFs, SSL, UC Berkeley, February 15, 2005] can be further accelerated to energies of hundreds of keV and possibly to several tens of MeV, depending on particular magnitude of the leader head potential. It is proposed that these energetic electrons may be responsible (through the *bremstrahlung* process) for the generation of hard X-rays observed from ground and satellites preceding lightning discharges, or with no association with lightning discharges in cases when the leader process does not culminate in a return stroke [e.g., Fishman et al., Science, 264, 1313, 1994; Inan et al., GRL, 23, 1017, 1996; Moore et al., GRL, 28, 2141, 2001; Dwyer et al., GRL, 32, L01803, 2005; Smith et al., Science, 307, 1085, 2005; Cummer et al., GRL, 32, L08811, 2005; and references therein]. For a lightning leader carrying a current of 100 A, an initial flux of  $\sim 2$ -8 keV thermal runaway electrons integrated over the cross sectional area of the leader is estimated to be  $10^{20} \text{ s}^{-1}$  [Moss et al., JGR, in review, 2005], with the number of electrons accelerated to relativistic energies depending on the particular field magnitude and configuration in the leader streamer zone during the negative corona flash stage of the leader development. The duration of the negative corona flash and associated energetic radiation is estimated to be in the range from  $\sim 1 \mu\text{s}$  to  $\sim 1 \text{ ms}$  depending mostly on the pressure dependent size of the leader streamer zone.

## LIGHTNING SFERICS AND STROKE DELAYED PULSES MEASURED IN THE STRATOSPHERE: IMPLICATIONS FOR MESOSPHERIC CURRENTS

Jeremy N. Thomas<sup>1</sup>, Robert H. Holzworth<sup>1</sup>, Michael P. McCarthy<sup>1</sup>,  
Osmar Pinto, Jr<sup>2</sup>

<sup>1</sup>University of Washington, Dept. of Earth and Space Sciences, Seattle, WA, USA

<sup>2</sup>National Institute of Space Research (INPE), Sao Jose dos Campos, SP, Brazil

During the Brazil Sprite Balloon Campaign 2002-03, the vector ELF to VLF (25 Hz - 8 kHz) electric and magnetic fields driven by cloud-to-ground (CG) lightning strokes at horizontal distances of 75-600 km were measured at altitudes of 30-35 km. Electric field changes were measured for each of the 2467 CG strokes detected by the Brazilian Integrated Lightning Network, and magnetic field changes above the background noise were measured for about 35 percent (858) of these strokes. ELF pulses that occur 4-12 ms after the retarded time of the lightning sferic, which have been previously attributed to sprites, were found for 1.4% of 934 strokes examined with a strong bias towards positive strokes (4.9% or 9/184) compared to negative strokes (0.5% or 4/750). These distant lightning events drove ELF to VLF electric and magnetic fields, with large vertical electric field and azimuthal magnetic field components, that are generally consistent with ground-based measurements [Cummer et al., GRL, 25, 1281, 1998] and models [Pasko et al., GRL, 25, 3493, 1998]. However, these results disagree with results from the Sprites99 Balloon Campaign [Bering et al., Adv. Space Res., 34, 1782, 2004], in which lightning-driven electric and magnetic field changes were rare and stroke delayed ELF pulses were frequent. Bering et al. 2004 concluded that mesospheric breakdown and currents are a fundamental response to nearly all lightning strokes. Thus, the Sprites99 data disagree with the quasi-electrostatic field (QSF) model that suggests that only very large charge moment lightning (greater than about 300-1000 C-km) are capable of producing mesospheric breakdown. Since the Brazil payloads rarely measured stroke delayed pulses, the Brazil data suggest that mesospheric breakdown and currents are not a fundamental response to most CG lightning strokes. This is consistent with previous ground-based measurements [Cummer et al., GRL, 25, 1281, 1998] and a fully electromagnetic model of lightning driven-fields [Pasko et al., GRL, 25, 3493, 1998]. Thus, the Brazil results are not inconsistent with the QSF model of mesospheric current production.

## QUANTIFICATION OF VLF SIGNATURES OF LEP EVENTS

Peter, W. B., Inan, U. S.  
Stanford University

Lightning-induced electron precipitation (LEP) events are a well-established contributor to the loss of trapped radiation belt electrons at mid-to-low latitudes. The Holographic Array for Ionospheric/Lightning Research (HAIL), a set of VLF receivers deployed at high schools and colleges across the United States, is well situated geographically to quantify the precipitation induced by lightning-generated whistlers. The multiplicity of VLF paths enables us to measure the spatial extent and temporal characteristics of the VLF perturbation. Using theoretical models of lightning generated obliquely propagating (nonducted) whistler-induced precipitation; we estimate the precipitation energy flux associated with LEP events for several case studies of thunderstorms over Texas. The resulting precipitation flux is then input into a Monte Carlo simulation of the penetration of energetic electrons into the ionosphere to determine the amount of secondary ionization produced by energetic electron precipitation as a function of altitude. The secondary ionization rates, together with the ambient ionization rate, are used to obtain electron density profiles for the region disturbed by the precipitation. The Long Wave Propagation Code (LWPC) is used to model subionospheric VLF wave propagation, incorporating the D-region disturbances associated with electron precipitation. By varying the ionospheric profiles input into the LWPC model, the results can be iteratively compared to the VLF amplitude and phase perturbations measured at multiple VLF sites. The effects of 1) causative flash current; 2) trapped radiation belt fluxes and magnetospheric conditions; 3) pitch angle distribution of trapped flux (a function of the Earth's magnetic field); and 4) causative lightning flash location are all considered at varying levels of quantitative detail. We also discuss the extension of our analysis to regions outside of Texas, to estimate global loss of radiation belt electrons caused by LEP.

Session H/G3, 07:55 – Fri.

**IONOSPHERIC EFFECTS OF  
LIGHTNING – II**

Co-Chairs: E. Gerken, V. Pasko

H/G3



EARLY/FAST VLF PERTURBATIONS CAUSED BY SCATTERING  
FROM TRANSIENT LUMINOUS EVENTS

Robert A. Marshall, Umran S. Inan  
Stanford University,, Space, Telecommunications and Radioscience  
Laboratory

While early/fast type perturbations of VLF transmitter signals have been seen for many years, they have recently been explained as perturbations closely associated with transient luminous events. An ongoing debate has questioned whether the scattering observed is a forward-scattering from the large, diffuse sprite halo regions, or an isotropic scattering from the grid of sprite features. In some cases, large perturbations seen from events near the transmitter may be attributed to mode-coupling of non-propagating modes into propagating modes, caused by the scattering body. Modeling work has shown that most VLF perturbation signatures compare well to modeled perturbations caused by sprite halos, large luminous conductivity changes in the lower ionosphere caused by quasi-electrostatic heating following an intense cloud-to-ground discharge. Meanwhile, studies in Europe during collaborative sprite campaigns have shown a near one-to-one correlation between early/fast events and sprites. However, in these cases the simultaneous appearance of sprite halos is not readily apparent. In this paper, we present evidence showing that both theories may occur simultaneously. By investigating three types of events (near-transmitter, mid-path, and near-receiver), we attribute possible causes are compare each to existing models. Many historic early/fast events can only be attributed to backscatter, lending credence to the isotropic scattering theory. In other cases, early/fast events are observed when there was no sprite seen coincident with the causative cloud-to-ground discharge. Using simple analytical models for isotropic scattering for sprite-like conductive elements, we estimate the possible distance from the transmitter path at which isotropic scattering events can be seen, and compare this to observed events.

TERRESTRIAL  
FLASHES OBSERVED ON BATSE/CGRO AND ELF/VLF RADIO  
ATMOSPHERICS

GAMMA-RAY

Cohen, M.B.<sup>1</sup>, Inan, U.S.<sup>1</sup>, Fishman, G.<sup>2</sup><sup>1</sup>Stanford University<sup>2</sup>NASA Marshall Space Flight Center

During its nine year lifetime in orbit, the Burst and Transient Source Experiment (BATSE) detector, aboard the Compton Gamma Ray Observatory (CGRO) spacecraft observed a total of 74 Terrestrial Gamma-ray Flashes (TGFs). Of these, simultaneous broadband ELF/VLF data from Palmer Station, Antarctica, were found to be available for six new TGF cases in addition to two previously reported cases [Inan et al., 1996]. Analysis of temporal and directional association between radio atmospheric and TGFs reveal solid evidence of an associated radio atmospheric in three of the six events, while a fourth case exhibits evidence of magnetically conjugate source lightning. In all three cases, and with the propagation time of both gamma-rays and radio atmospheric fully accounted for, the associated sferics are found to occur 1-3 ms prior to the production of TGFs. In one of three cases with associated radio atmospheric, three consecutive gamma-ray peaks in the BATSE data are apparently linked to three consecutive radio atmospheric. In two of the six BATSE TGF cases with Palmer data, no evidence is found for any associated radio atmospheric occurring within 10-ms of the TGF event, although the presence of an active storm center in the region underneath BATSE/CGRO is confirmed by sferic activity during the 30-min period surrounding the event. For the remaining one of the six cases, no associated sferic is found to be arriving from a direction consistent with the location of the CGRO. However, an associated sferic is observed to be arriving from approximately the geomagnetically conjugate region, suggesting that this particular TGF might have been produced by a lightning flash in the conjugate region. Overall, the analysis of all six BATSE cases with Palmer data points to the possibility of different physical mechanisms generating TGFs under different conditions.

## BROADBAND VLF MEASUREMENT OF D REGION IONOSPHERIC PERTURBATIONS CAUSED BY FAST DISCHARGING LIGHTNING-EMP

Cheng, Z., Cummer, S. A.

Duke University, Electrical and Computer Engineering Department

The first experimental evidence of the impulsive direct coupling of energy released by lightning discharge to the lower ionosphere was reported in the form of early/fast perturbation on sub-ionospherically propagating very low frequency (VLF) signals. Since then, based on modeling and measurements, different mechanisms have been advanced to explain the fast sub-ionospheric VLF perturbations such as the ionization and heating associated with elves or electrical breakdown associated with sprites and halos. By comparing the broadband VLF spectra (3-25 kHz) of lightning discharges that occurred immediately ( $\leq 15$  s) after an intense lightning discharge ( $\geq 60$  kA) with the spectra of lightning discharges that were not preceded by an intense lightning discharge within approximately 60 seconds, we detect D region disturbances caused by these intense lightning flashes not only in the U.S. East Coast but also in the U.S. High Plains. The detailed electron density changes caused by the disturbances are measured by analyzing the broadband VLF propagation changes, and the perturbed electron density profiles from both regions are found to be consistent with those created by lightning-EMP when compared with theoretical predictions. In one case, the ionospheric perturbation occurred at the same time as an elve detected over the U.S. East Coast by the ISUAL satellite. This finding confirms that we are measuring lightning-EMP associated VLF perturbations. The elve-associated electron density profile is also found to be consistent with theoretical predictions. The characteristics of the lightning responsible for these perturbations has been investigated by comparing the intense causative lightning strokes to the intense non-causative lightning strokes, and it is found that the magnitude of VLF spheric spectrum of the intense causative lightning discharge is a reliable indicator of the measured perturbation strength. Our results suggest that many broadband detectable sub-ionospheric VLF perturbations are created by intense fast-discharging lightning-EMP, which can produce elves in the case of particularly intense discharges.

FDTD MODELING OF SCHUMANN RESONANCES ON EARTH  
AND OTHER PLANETS OF THE SOLAR SYSTEM

Heng Yang, Victor Pasko

Electrical Engineering Department, The Pennsylvania State University

Electromagnetic waves emitted by global lightning activity produce resonances in the Earth-ionosphere cavity. These resonances were first predicted by W. O. Schumann [Z. Naturforsch., 7a, 149, 1952] and therefore commonly referred to as Schumann resonances (SR). Because SR parameters (e.g., power, frequency and Q-factor) are mainly determined by the global lightning activity and conductivity profile in the lower ionosphere, these resonances are widely used in many remote sensing applications [e.g., Williams, Science, 256, 1184, 1992; Cummer, IEEE Trans. Antennas Propagat., 48, 1420, 2000; Roldugin et al., JGR, 109, A01216, 2004, and references therein]. In our previous study [Yang and Pasko, GRL, 32, L03114, 2005], a three-dimensional finite difference time domain (3D FDTD) model was used to solve SR problems in the Earth-ionosphere cavity under disturbed conditions associated with solar proton events and X-ray bursts. Also, a set of modeling studies had been conducted, which demonstrated a good agreement of SR parameters derived from the FDTD model with those obtained from previous well established numerical and analytical models [e.g., Sentman, JATP, 45, 55, 1983; Mushtak and Williams, JASTP, 64, 1989, 2002]. These results indicate that FDTD technique is suitable for solving realistic ELF problems in the Earth-ionosphere cavity [Yang and Pasko, 2005].

On January 14, 2005, HUYGENS probe landed on Titan, and started to explore this largest moon of Saturn. One of multiple missions of HUYGENS probe is to find if there are lightning discharges in the Titans atmosphere. It is believed that conducting properties of the Titans atmosphere are favorable for the formation of cavity for propagation of electromagnetic waves, so the existence of SR will give a support for the existence of the electrical discharges in the lower atmosphere on Titan. Meanwhile, the SR parameters are also useful in the study of the electromagnetic properties of Titans lower ionosphere. Several papers have recently been published in refereed literature, which discuss SR parameters on Titan [e.g., Morente et al., ICARUS, 162, 374, 2002; Nickolaenko et al., Planetary and Space Sci., 51, 853, 2003; Pechony and Price, Radio Sci., 39, RS5007, 2004]. In this talk, we will use our 3D FDTD model to predict the SR frequencies and Q-factors on Titan and will compare our FDTD results with those reported in the previously published papers. Besides Titan, we will also discuss SR on other planets, specifically Mars and Venus. The atmospheric conductivity profiles for these studies are derived from the previously reported ionospheric models for these planets [e.g., Pechony and Price, 2004; Molina-Cuberos et al., Adv. in Space Res., 33, 2309, 2004, and references therein].

LIGHTNING LOCATION USING SINGLE STATION ELF/VLF  
SFERIC MEASUREMENTSLe Cocq, C., Fraser-Smith, A. C.

STAR Laboratory, Stanford University, Stanford, CA 94305, USA

Most methods used for lightning location require multiple station measurements. The goal of the work reported here is to locate the source of an atmospheric, or sferic, using the measurements made at a single station with two crossed magnetic loop antennas. Both of these antennas are required to estimate the direction between the source and station, however only a clear signal from a single antenna is needed for estimating the distance between the two. The distance estimation is done using the slow-tail of the sferic. The slow-tail is the extremely low frequency (ELF) component of the sferic which arrives later than the higher frequency components. According to Wait's theory on modes and propagation of ELF radio waves, the first mode, where ELF components propagate, is characterized by a peak-shaped function. The delay between the start and peak of the function corresponds the slow-tail separation,  $t_s$ . The slow-tail separation is defined by the time delay between the start of the sferic and the peak of the first quarter cycle of the slow tail. Wait showed the relationship between distance,  $\rho$ , and  $t_s$  to be a quadratic function of the form  $t_s = (A + B\rho)^2$ .  $A$  and  $B$  vary depending on the waveguide conditions. The earth boundary of the waveguide remains relatively fixed while the ionosphere changes dramatically between day and night. Two different solutions for  $A$  and  $B$  are formulated for average daytime and nighttime propagation. The daytime solution gives a larger slope for  $\rho$  versus  $t_s^{1/2}$ , therefore distance estimation is more precise with daytime data rather than nighttime. The constants originally proposed by Wait are based on the average height of the ionosphere and curve fitting some limited data. The amount of data collected and analyzed in this work is much larger and also contains a larger range of  $\rho$ . This work supports Wait's theory that the square root of the slow-tail does vary linearly with distance, solves for new constants to better fit the large data sample, and analyzes the effectiveness of distance estimation of sferics using a single station.

## IONIC CHANNELS IN THUNDERCLOUDS

Losseva, T.V., Fomenko, A.S., Nemtchinov, I.V.  
Institute of Geosphere's Dynamics, Russian Academy of Sciences ,  
Leninsky pr. 38-1, Moscow, 119334, Russia

In the framework of the model of the corona discharge wave (Fomenko A. S., Losseva T.V., Nemtchinov I.V., *EOS Trans. AGU*, **85**(47), Fall Meet. Suppl., Abstract AE23A-0835, 2004) we study the formation and propagation of ionic channels in thunderclouds. In that model we proposed a hypothesis that the structure of a thundercloud becomes nonuniform due to corona discharge on the drops and small particles and formation of ionic channels with higher conductivity than the surrounding air. When the onset strength of corona discharge becomes smaller than the electric field strength, the corona discharge increases concentrations of ions in a small part of the cloud (a hot spot). An additional charge at opposite ends of the hot spot appears due to polarization process. The corona discharge front moves as a wave with the velocity of the order of ion drift and forms a highly conductive channel. The branching of the channel occurs in the case of nonuniform distribution of initiators.

At high electric field the long ionic channel becomes non-uniform and electron streamers are formed inside it. The channel propagates with a very high velocity corresponding to the electron drift velocity. Due to initiation of rather long streamers from the corona discharge initiators a subbreakdown regime is realized.

We describe this non-stationary problem by Poisson equation which is solved simultaneously with a simplified set of kinetic equations for ions, small charged particles and (at high electric fields) electrons, including ionization due to electronic impact, attachment and formation of positive ions. 3D numerical simulations of formation and branching of ionic channels and electron streamers interaction in the situation of high electric fields are presented.

The mechanism of propagation of electromagnetic fields (generated by lightnings) along the boundaries of highly conductive channels due to skin-effect is also considered.

Session J1, 13:35 – Thurs.

**RADIO ASTRONOMY TEACHING  
LABORATORIES AND  
INSTRUMENTS**

Co-Chairs: J. Carlstrom, R. Mutel





ASTRONOMY 121, BERKELEY'S UNDERGRADUATE RADIO  
ASTRONOMY LAB: DO IT YOURSELF, NO (ALMOST!) BLACK  
BOXESHeiles, Carl

Astronomy Department, UC Berkeley

Berkeley's Astronomy 121 lab course presents radio astronomy as a set of three technological puzzles, each of which the students must experience and understand using a minimum of black-box magic. The most basic puzzle is the heterodyne principle and its implementation with microwave and electronic devices, whose study takes up not quite half of the course time. The related topics include transmission lines, waveguides, and impedance matching; DSB and SSB mixers and phase measurements; noise power per unit bandwidth as described by temperature; and spectral analysis using Fourier techniques.

The other two puzzles are astronomical in nature. One is interferometry, using a 12-GHz two-element interferometer composed of  $\sim 1$  m diameter dishes on a  $\sim 10$  m baseline. The telescopes are computer-controlled and the students can devise scripts for automatic observing—it's just like a "real observatory", except that they write their own software. The fringe spacing of  $\sim 9'$  is ideal for accurately measuring the fringe pattern and diameter of the Sun and Moon by tracking them from rise to set and forcing the students to use Fourier analysis in a real-world experiment. The instrument is sensitive enough to see the major continuum sources such as Tau A and Ori A, and by using fringe-fitting the students measure declinations to within a few tens of arcsec. The other is single-dish radio astronomy, using a just recently-acquired prototype antenna of the Allen Telescope Array to map 21-cm line radiation, observe OH masers, and observe a strong pulsar (not yet actually accomplished with our new system).

All of these labs emphasize hands-on use of laboratory instruments and computer-controlled data taking. Students write their own software, using the IDL language, to obtain data, reduce data, and prepare them for the lab reports. Quality reports are an important part of the course, and we require the students to use LATEX.

MASSIVE RADIO ASTRONOMY SURVEYS AT ARECIBO USING  
ALFA: DATA MINING AND MANAGEMENT

James M. Cordes

Astronomy Department, Cornell University, Ithaca, NY 14853 USA

The Arecibo L-band Feed Array (ALFA) provides a seven-fold increase in survey throughput for extragalactic, galactic and pulsar surveys using the Arecibo telescope in Puerto Rico. These surveys are being conducted through large scientific consortia that are international in membership and which include substantial student involvement. Surveys have begun recently and will extend at least five years into the future. Both the astrophysical return and the day-to-day management of the large data volume demand new ways for conducting the surveys that involve students' participation in many different ways. In addition to traditional astronomical activities, these also include data mining and data archival and, thus, closer interaction with colleagues in computer science. In particular, the surveys require construction of data bases for all stages, from the data acquisition to data archival. For the pulsar surveys, which will yield the largest data volume of any of the ALFA surveys (e.g. one petabyte in about five years), we plan to archive all the raw data as well as the data products from the processing. Processing of the raw data and exploration of data products will be done through a web-based system sited at the Cornell Theory Center (CTC). In addition, a database is sited at the Arecibo Observatory that addresses the immediate needs for observations of a pre-defined grid of positions, data quality, and data transport. Data are moved to remote processing sites using inexpensive disks and then sent to the CTC for archival as well as processing. At Arecibo, the database system uses MySQL while at CTC, Microsoft Server SQL is used. Tools are being developed that allow two-way interchange between the two database systems using web services. ALFA surveys will contribute catalogs and refined data products to the National Virtual Observatory (NVO). My talk will discuss the surveys and consortia, data management and archival, some early science results, and student participation in these activities, including NVO participation.

## THE IOWA E-SRT PROJECT

Mutel, R. L.<sup>1</sup>, Spitler, L.<sup>2</sup>, Ivarsen, K.<sup>3</sup><sup>1</sup>University of Iowa<sup>2</sup>University of Bonn<sup>3</sup>University of North Carolina

The University of Iowa utilizes the Haystack Small Radio Telescope (SRT) in an advanced undergraduate laboratory course and a course in radio astronomy. We have modified the original hardware and software in several significant ways to make the system more flexible. We have created a new software control system (named e-SRT) for the SRT, and in addition made several hardware upgrades to the telescope itself.

The e-SRT software is written in the Python language using the wxWindows graphical library. The e-SRT program has a flexible, user-friendly interface and runs on Linux, MS-Windows, and Macintosh platforms. It provides a large number of enhanced features, and well as several new capabilities not available in the original Java-based software provided with the SRT. Enhanced features include better telescope motion control, enhanced continuum (strip chart) and spectral line plotting, more flexible chart control, and resizable task windows. New capabilities include a client-server architecture for efficient remote operation, support for a webcam, optional archived baseline spectra, support for optical shaft encoders, and diagnostic spectral line windows.

The hardware modifications included the development of a small 'pocket' 1024-channel autocorrelator with USB interface. This allows simultaneous spectral coverage of the entire hydrogen 21 cm band (2 MHz), compared with the original SRT receiver which was limited to 500 KHz segments. We also replaced the digital receiver with a standard superheterodyne system commonly used at professional observatories. The receiver is built on an 'open' chassis so students can examine signals as they pass from RF to IF to video modules.

BLENDING SCIENCE AND TECHNOLOGY IN THE DEVELOPMENT OF RADIO ASTRONOMY INSTRUMENTATION: THE NRAO/UVA EDUCATION INITIATIVE

Bradley, R.F.<sup>2</sup>

<sup>1</sup>National Radio Astronomy Observatory, NRAO Technology Center - Charlottesville, VA

<sup>2</sup>University of Virginia, Dept. of Electrical and Computer Engineering, Dept. of Astronomy

The desire to engage students in the development of new advanced tools for radio astronomy poses a unique challenge to educators due to the rapidly changing, multi-disciplinary nature of the technology base. The natural evolution of this process has resulted in a high degree of specialization within the science and engineering communities. However, an unfortunate consequence of such specialization is compartmentalization: a paradigm that nurtures the widening chasm between practicing scientists and engineers. A reduction in communications among the disciplines and a weakening of the overall decision-making process are both products of this trend. If allowed to continue, our field will become driven by a collection of experts whose ensemble understanding of the field lacks the far-reaching vision, strong motivation, and sound leadership necessary to accomplish the challenging tasks before us.

Reversing this trend will require a new approach to educating our students. This approach should provide a means for students at all academic levels to participate in the development of new instrumentation while not placing any student in the critical path of a major project. Activities should challenge individual students and promote integration of the disciplines while focused squarely on achieving goals at the forefront of both science and technology. We have created a project-based educational program that attempts to address these challenges.

Our instrument program is designed to blend significant amounts of modern science and technology into a unified educational experience. Student activities include project planning, management, design, fabrication, evaluation, observing, and data analysis. We integrate students into project teams that consist of scientists and engineers together with other students, yet we strive to maintain the student's individuality throughout the entire process. These teams involve people from NRAO and University of Virginia as well as collaborators from many other organizations. NRAO provides the instrument laboratory and deployment infrastructure and a wealth of practical experience from members of the research staff.

My presentation will include an overview of our instrument program, details of the radio astronomy projects, and our vision for the future.

INTERDISCIPLINARY RESEARCH & OUTREACH PROGRAMS  
AT SORAL

Christopher K. Walker  
University of Arizona

*Instrument Development Experience at SORAL*

The training of students in the development of state-of-the-art instrumentation is essential to the future of science. This is particularly true in mm/submm astronomy where technological advances are happening so rapidly. Ironically, there are only a handful of laboratories in the world where students gain hands-on experience in the design, fabrication, and fielding of radio astronomy instrumentation. Over the past decade the Steward Observatory Radio Astronomy Lab (SORAL) has served as a training ground for a number of students (both graduate and undergraduate) who have participated in the design and construction of submm-wave instrumentation for Antarctica (i.e. AST/RO) and the Heinrich Hertz Telescope (HHT) on Mt. Graham, Arizona. This work, and the astronomy that has come from it, has been a major component of 5 Ph.D. dissertations and numerous undergraduate research projects. Due to the interdisciplinary nature of radio astronomy instrumentation, SORAL attracts students from a variety of majors. Currently we have 6 graduate and 4 undergraduate researchers representing Physics, Astronomy, Optical Sciences, and Electrical Engineering. We are using SORAL as a model for developing a larger interdisciplinary program in astronomical instrumentation. Links between graduate and undergraduate programs in participating departments will be strengthened. Students participating in the astronomical instrumentation program will work toward a major in their home departments while being encouraged to seek minors in sister departments. A mentoring committee composed of faculty from participating departments will be convened for each student to help ensure sustained progress along the student's chosen research path.

*Outreach at SORAL: Student Radio Telescope*

In support of education and public outreach activities SORAL students have constructed a remotely operable, steerable, 3.5 m Student Radio Telescope (SRT) for observing the HI line in the Milky Way. The SRT has been used as an instructional tool in undergraduate courses (both major and nonmajor). Students from on and off campus will soon be able to monitor and control observations with the SRT. Unlike optical telescopes, the SRT can be used day and night, making it well suited for classroom instruction. Complementary classroom modules are being developed that will aid students in gaining a hands-on, intuitive understanding of underlying physical concepts.

## RADIO TELESCOPES IN THE UNDERGRADUATE CLASSROOM

Pratap, P., Rogers, A.E.E.R., Salah, J.E.  
MIT Haystack Observatory

MIT Haystack Observatory has been involved in bringing radio astronomy to the undergraduate classroom. To this end, we have developed a small radio telescope (SRT) kit that is currently available commercially. The SRT provides a hands-on introduction to the basics of radio telescopes. The SRT kit consists of a 2-m antenna with a digital receiver spanning the 1420 MHz line of hydrogen. There are over a 100 SRT units around the world.

Students wishing to extend their research are provided remote or local access to a 37-m telescope at Haystack Observatory. Projects on the telescope, using the 22 and 44 GHz receiver bands, are designed to take advantage of the capabilities of the telescope. The telescope has been used in projects such as classroom demonstrations, laboratory exercises and independent research projects.

Current developments in the program have focused on a VLBI-mode observing with two or more SRTs. A new digital receiver for the SRT containing a GPS timing system has been designed and tested. Early results have shown that this system is capable of detecting radio flares toward active regions on the sun.

College teachers wishing to use the Haystack resources have the opportunity to attend an NSF Chautauqua short course that is taught annually at the Observatory. This course introduces the faculty to the instrumentation and provides them with materials that they can use in the classroom. These materials along with other supporting materials for the 37-m and the SRT are available on the Haystack Observatory web site at <http://www.haystack.mit.edu>.

The SRT is now also being used in the high school classroom. Several lesson plans incorporating radio astronomy into the high school curriculum have been developed by teachers participating in a Research Experiences for teachers program.

ENGAGING UNIVERSITIES WITH THE LONG WAVELENGTH  
ARRAY

G. B. Taylor<sup>2</sup>, P.A. Henning<sup>1</sup>, N. Kassim<sup>3</sup>, W. Junor<sup>4</sup>, T. Gaussiran<sup>5</sup>

<sup>1</sup>University of New Mexico

<sup>2</sup>National Radio Astronomy Observatory

<sup>3</sup>Naval Research Laboratory

<sup>4</sup>Los Alamos National Laboratory

<sup>5</sup>University of Texas at Austin

The Long Wavelength Array (LWA) will be a new, open, user-oriented astronomical instrument operating in the relatively unexplored window from 20-80 MHz at arcsecond level resolution. With 2-3 orders of magnitude improved imaging power over current capabilities, and the ability to observe multiple fields simultaneously, the LWA will make crucial measurements of supernova remnants, gamma-ray bursts, active galaxies, and clusters of galaxies, and thereby constrain models for these diverse cosmic accelerators. Furthermore, by measuring the relaxation state of clusters, the LWA will help to constrain the cosmological evolution of both Dark Matter and Dark Energy in the universe. The LWA will provide high temporal (millisecond or better) and spatial resolution (arcsecond) to probe the transient universe at long wavelengths, and will explore the high redshift universe by detecting the earliest and most distant active galaxies.

Operated by the University of New Mexico on behalf of the South West Consortium (SWC) the LWA will provide a unique training ground for the next generation of radio astronomers. Students may also put skills learned on the LWA to work in computer science, electrical engineering, and the communications industry, among others. The development of the LWA will follow a phased build which benefits from lessons learned at each phase. Four university-based Scientific Testing and Evaluation (ST&E) teams with different areas of concentration (1. High resolution imaging; 2. Wide field imaging; 3. Ionosphere, and 4. RFI suppression and mitigation) will provide the feedback needed to assure that science objectives are met as the build develops. The ST&E teams will be distributed over the entire US, with concentrations in the SWC. In addition to informing the LWA design, these teams are expected to develop the software tools that will be essential to maximize the science return from the instrument. The ST&E teams will establish a community of universities engaged in Long Wavelength Astronomy, Ionosphere, and Space Science Research.

## COSMIC MICROWAVE BACKGROUND STUDENT LABORATORY

John E. Carlstrom

University of Chicago

We will review an undergraduate laboratory to detect and measure the temperature of the Cosmic Microwave Background (CMB) radiation. The lab was developed at the University of Chicago by the author while teaching an undergraduate special topics course on Radio Astronomy. It is now routinely conducted in the core curriculum for both science and non-science majors and as a result is performed by all freshman at the University. It is also conducted at adult education and other outreach events. The laboratory is based on a cooled, low-noise, HEMT receiver operating at 30 GHz with a  $\sim 10$  degree beam. The students measure the receiver and the sky temperature as a function of airmass and then extrapolate to zero airmass. The excess noise found at zero airmass is assumed to be the CMB background. In good weather conditions the results are accurate to about 0.5 K. The laboratory effectively reproduces the Penzias and Wilson CMB detection. The experiment purportedly is not automated; the students hold up the calibration loads, monitoring their temperatures with laboratory thermometers. They record all the data in their lab books. They also insert and remove a large reflective cone that acts like a ground screen. Through conducting several consistency checks as they conduct the experiment, the students learn how real experiments work and in particular how to know what data to trust. The students actually enjoy the laboratory and are excited to have detected 14 billion year old radiation from the early universe. An appeal of the laboratory is that it uses real research equipment. The receivers are the same ones used in the BIMA/OVRO Sunyaev-Zel'dovich Effect experiment. We will also discuss possible ways to reproduce the laboratory equipment using less costly components while still retaining the spirit of the laboratory.



Session J2, 08:15 – Fri.

**NEW INTERFEROMETRIC  
CALIBRATION TECHNIQUES**

Co-Chairs: S. Myers, M. Wright



DUAL FREQUENCY 230/690 GHZ INTERFEROMETRY AND  
PHASE TRANSFER AT THE SUBMILLIMETER ARRAYHunter, T.R.<sup>1</sup>, Zhao, J.-H.<sup>1</sup>, Liu, S.-Y.<sup>2</sup>, Su, Y.-N.<sup>2</sup><sup>1</sup>Harvard-Smithsonian Center for Astrophysics, 60 Garden St, Cambridge, MA, 02138, USA<sup>2</sup>Academia Sinica Institute of Astronomy and Astrophysics, 1 Roosevelt Road, Section 4, Taipei 106, Taiwan

The Submillimeter Array (SMA) is an eight-element radio interferometer located on Mauna Kea and designed to operate in the major atmospheric windows from 180 to 900 GHz with 2 GHz IF bandwidth in each sideband. With baseline lengths up to 500m, atmospheric instabilities can limit the phase coherence of the array, especially in the higher frequency bands. For this reason, the array was designed to support simultaneous operation of a low frequency receiver (< 350 GHz) with a high frequency receiver (> 330 GHz). The overlap region of 330-350 GHz was chosen to facilitate dual polarization measurements in the frequency range most likely to offer the highest sensitivity to dust continuum emission. At present, the array is equipped with SIS receivers covering the frequency ranges 176-250 GHz, 260-350 GHz, and 600-700 GHz. Single frequency operation has been routine in the lower two frequency bands for the past two years. In February 2005, with the completion of the IF hardware, dual receiver operation became possible. Since then we have made a number of Galactic and extra-galactic astronomical observations in dual-band mode. Facing a severe lack of gain calibrators at high frequency, we have primarily used minor planets (Ceres, Io, Callisto) or 658 GHz water masers. However, the minor planets are resolved in our extended configurations, and new calibration techniques are needed. We have begun to explore the option of using the 230 GHz receiver as a phase reference to enable improved interferometry in the 650 GHz band. We will present the current antenna and receiver performance, and our initial attempts at phase transfer. New functions have been added to the Miriad and MIR/IDL data analysis software packages for fitting and applying antenna-based phase transfer coefficients. During some of the observing sessions, good phase correlations are seen, and the phase transfer method has been demonstrated to recover images of a point source, albeit at a somewhat reduced signal-to-noise ratio. During other sessions, the method has been thwarted by unknown instrumental instabilities which are still under investigation. With the addition of the second set of 345 GHz receivers (by the end of 2006), dual-band observing at 230/345 GHz will become possible, which will allow more sensitive and more frequent testing and development of the phase transfer technique.

## INTERFEROMETRIC POLARIMETRY: CALIBRATION AND RESULTS FROM THE SMA

D. P. Marrone<sup>1</sup>, R. Rao<sup>2</sup>

<sup>1</sup>Harvard-Smithsonian CfA, 60 Garden Street, Cambridge, MA 02138, USA

<sup>2</sup>ASIAA, 645 N. A'ohoku Place, Hilo, Hawaii 96720, USA

The Submillimeter Array (SMA) is an 8-element interferometer on Mauna Kea. The array is presently equipped with single, linearly-polarized feeds in each of three bands: 183–245, 265–354, and 600–700 GHz. An experimental polarimetry system has been installed, which uses narrow-band quarter-wave plates to generate circularly-polarized feeds. Two sets of waveplates allow polarimetry in all three bands, with one set tuned to 348 GHz, and the second set tuned to 230 (quarter-wave retardation) and 690 GHz (three-quarter wave retardation) for simultaneous polarimetry in two bands. The waveplates are quartz, with low-density polyethylene anti-reflection coatings. They are mounted in motorized rotation stages under computer control, allowing rapid switching between left- and right-circular polarization (LCP and RCP) sensitivity. All four combinations of LCP and RCP on each baseline are efficiently sampled by switching the antenna polarizations in period-16 Walsh function patterns, with full cycles requiring four to seven minutes for typical integration times.

Since its installation in 2004, the polarimetry system has received extensive testing and calibration. Cross-polar contamination (“leakage”) is measured through observations of bright, linearly-polarized quasars, with the leakages and source polarization simultaneously determined. The use of a single linear feed to measure both circular polarization states fixes the relative phase of the LCP and RCP feeds (zero phase offset); with separate feeds this phase freedom corresponds to an arbitrary rotation of the sky polarization and can only be determined through observations of a source with known polarization position angle. Here we present the results of our commissioning observations. We discuss the frequency dependence of the leakages, which limits the frequency range over which each waveplate can produce reliable polarization images. Calibration observations of multiple quasars and unpolarized sources have been obtained together to provide cross checks on the derived leakages. With these data we examine calibration stability, measurement repeatability, and polarization image fidelity. Finally, we show sample science observations in all three observing bands.

ACCURATE ANTENNA GAIN CALIBRATIONS AT CM AND MM  
WAVELENGTH

Gibson, J.L., Welch, W.J  
University of California, Berkeley

In the absence of good celestial flux standards, accurate antenna gain calibration and the subsequent determination of new flux standards requires the comparison of an antenna response with that of a known reference antenna. This reference will necessarily be very small and simple, and therefore very different in response from the antenna(s) to which it is compared.

The challenge historically has been accurately to compare the response of antennas whose collecting area might differ by five orders of magnitude and whose beam patterns are very different. Interferometric, rather than total power comparison is much preferable because the measured correlations go as the square root of the collecting areas and the detection of only correlated signal makes the measurement relatively immune to variations in side-lobe response.

These advantages have motivated an experiment which has enabled us to measure the gain of a 6 meter antenna to about 1 percent accuracy at 1 cm wavelength. A similar experiment underway promises comparable results at 3 mm. Extension to 1 mm and shorter wavelengths seems feasible.

While making possible such accurate gain measurements of large antennas, various complications are introduced as well by the interferometry, and must be accounted for.

Several related methods are described that lead eventually to the accurate knowledge of a celestial flux density. Some include mechanical waveguide switches, some don't. Various ways of getting a power reference (a load at known temperature) into the system are considered. Application to the upcoming ALMA array is discussed, along with related requirements on the correlator, pointing accuracy, knowledge of the local weather conditions and other details to worry about.

## MOSAICING WITH RADIO INTERFEROMETERS: CALIBRATING THE PRIMARY BEAM

Corder, S. A.<sup>1</sup>, Wright, M.<sup>2</sup><sup>1</sup>California Institute of Technology, Division of Physics, Mathematics and Astronomy, Radio Astronomy<sup>2</sup>University of California Berkeley, Department of Astronomy, Radio Astronomy Lab

The ability of radio interferometric arrays to image sources larger than the primary beam requires the use of mosaicing techniques. Interferometers like ALMA and the newly commissioned CARMA have fields of view sufficiently small that mosaicing with multiple pointing centers is required for a large fraction of the possible science.

The quality of information gained from the combination of pointing centers depends sensitively on the knowledge of the shapes of the primary beam voltage patterns. While CARMA has the unique advantage of having multiple telescope sizes, capable of probing a large range of size scales interferometrically, special challenges result. The smallest telescopes in CARMA (diameter 3.5 m) have voltage patterns which illuminate the side-lobes of the largest telescopes (10.4 m). Characterizing the voltage pattern of each telescope is necessary for accurate imaging. The use of Gaussian fits to primary beam patterns provides imaging limited to the  $\sim 5\%$  level, even for homogeneous arrays. Calibrating the actual shape of the voltage patterns becomes important for high fidelity imaging.

In this work we discuss the initial results of the measurement of primary beam shapes at CARMA. Using low resolution holography we measure voltage patterns for each antenna within an observing sequence. The results are used to update the pointing and focus while measuring the full width half maximum (FWHM) of the voltage patterns. These measurements are used to build up a catalog which is used to characterize the voltage pattern as a function of elevation, temperature, focus and frequency. We discuss initial analysis of a comparison between images made using the voltage pattern templates and using standard Gaussian beam assumptions, highlighting improvements in image fidelity versus sensitivity decrement due to time lost in beam calibration.

## UPDATE ON FAST SWITCHING PHASE CALIBRATION FOR ALMA

M.A. Holdaway  
NRAO/Tucson

Chajnantor is a premiere sub-millimeter site, but phase stability is still a problem. 230GHz 300m baseline observations during median conditions lose half the sensitivity to decorrelation if phase errors are uncorrected. ALMA baselines will go to 19km, so we need Fast Switching and Water Vapor Radiometry (WVR) phase compensation.

Fast switching entails frequently slewing to a nearby calibrator, detecting atmospheric phases at 90GHz with high SNR, quickly slewing back to the target source while switching to the target source observing frequency, scaling the 90GHz phases to the target frequency, and applying those phases to the target source. The phase errors as a function of the distance to calibrator, the SNR on the calibrator, and the calibration cycle time are well understood.

Fast Switching places several demands on the ALMA design: Antennas slew and settle quickly (1.5deg in 1.5s). The 90GHz receiver is always ready to observe. Observing bands can be changed in 1.5s. Phase stability across observing bands must be maintained. A catalog of 10,000 - 30,000 calibrator sources is needed. Flexible choice of the calibrator (the closest brightest source) and optimal calibration details (the cycle time which maximizes efficiency) must be considered by the dynamic scheduling.

Without WVR, a switching cycle will typically be 25s: 3s spent slewing, under 1s spent on calibrator detection, and 21s spent observing the target source. Fast switching efficiency, considering decorrelation and duty cycle, will range from 0.80 to 0.90. Below 300GHz, calibration will often be done at the target frequency. Above 300GHz, calibration will usually be done at 90GHz, and an extra cross-band instrumental phase calibration sequence will be performed.

Fast switching with a cycle time of 25s will correct for phase fluctuations on time scales down to about 10s through interpolation. As fast switching cannot correct for phase fluctuations on timescales less than 10s, WVR can effectively reduce the decorrelation from residual phase errors. Fast switching and WVR can work together: WVR is designed to recover phase increments, but not the absolute phase, and hence requires some form of fast switching. WVR will increase the switching cycle time and will also reduce the decorrelation losses, thereby improving the sensitivity.

## CALIBRATING THE MWA LOW FREQUENCY DEMONSTRATOR

Colin Lonsdale<sup>1</sup>, Sheperd Doeleman<sup>1</sup>, Roger Cappallo<sup>1</sup>,  
Sean Ting<sup>2</sup>, Miguel Morales<sup>3</sup>

<sup>1</sup>MIT Haystack Observatory

<sup>2</sup>Stanford University

<sup>3</sup>Harvard-Smithsonian Center for Astrophysics

The Mileura Widefield Array (MWA) is a planned low-frequency imaging radio interferometer to be located at the Mileura Station in outback Western Australia. This location is extraordinarily radio quiet, offering unrestricted access to bands that elsewhere are generally considered lost to radio astronomy. The MWA Low Frequency Demonstrator (LFD) covers the 80-300 MHz range, and is planned to be operational by the end of 2007. The LFD consists of 500 antenna "tiles", each composed of a 4x4 array of crossed wideband active dipoles. The total physical extent of the LFD is planned to be 1.5 km.

The science goals of the array, which include studies of the Epoch of Reionization as well as Faraday rotation studies of the heliosphere, demand a high precision calibration of both the full polarization instrumental response, and the effects of the ionosphere. In this contribution, we describe new approaches to array calibration that exploit the potential of a fully digital array architecture. The signals from each of the 500 tiles are digitized at RF, and all 125,000 baselines in the array are correlated in order to preserve information over the full field of view of the antennas. Combined with the large number of bright sources on the sky at these low frequencies, the calibration system has access to an unprecedented wealth of information in the torrent of data flowing from the correlator. This data-rich environment facilitates the development of algorithms that are simple, robust, and rapidly convergent.

The calibration is achieved in a three-step process, solving first for position-independent antenna-based gains, then for ionospheric distortions, and finally for the full polarization power patterns of each antenna. The algorithms for accomplishing these calibrations are described, and the results of algorithm prototyping will be presented.



## UNIQUE DESIGN FEATURES THE MWA CORRELATOR AND DIGITAL BACKEND SYSTEMS

Miguel Morales

Harvard-Smithsonian Center for Astrophysics

The Mileura Widefield Array Low Frequency Demonstrator (MWA-LFD) is a unique proposed low frequency observatory for Epoch of Reionization, Heliospheric, and Radio Transient observations. The MWA is located in the radio quiet Mileura stie in Western Australia, and features a very large 15–40° FWHM field of view over the 80–300 MHz frequency range. The wide field-of-view gives the array a very high survey speed for cosmology applications and provides unique capabilities for time variable heliospheric and transient observations.

However, the wide field of view produces a number of unique challenges for the correlator, digital processing, and calibration backends. The ionospheric calibration must be performed in real time, with a time constant of a few seconds and different solutions across the field-of-view, and the precision of the calibration is closely related to the instantaneous visibility coverage of the array. Additionally, bright sources must be subtracted with very high precision to allow the sensitive observations of the Epoch of Reionization.

The correlator and backend systems were designed together to optimize the throughput of the digital processing chain and enable high precision and dynamic range observations. In this talk I will detail a number of unique design features of the MWA digital processing system, including the horizon to horizon correlator field of view, “topocentric” visibility coordinates to improve source subtraction, and the data rich computation paradigm. These design features take advantage of the characteristics and features of modern parallel supercomputing, both in the FPGA based correlator and the cluster computer based digital backend, and offer a direction forward for future high throughput radio digital processing systems.

## STEPS TOWARD A STREAMING RADIO TELESCOPE: AN IBOB CORRELATOR

Harp, G. R.<sup>1</sup>, McMahon, D. H. E., Wright, M. C. H.<sup>1</sup>SETI Institute, 515 Whisman Rd, Mountain View, CA<sup>2</sup>U.C. Berkeley Radio Astronomy Laboratory, Berkeley, CA

The data acquisition and imaging systems of next generation telescopes like the SKA will need to be integrated, so that the telescope produces calibrated images directly. One model for data reduction uses a priori knowledge of the target image region to determine calibration parameters and feeds back new data to improve the baseline model. The final result is an improved model of the desired source region. An important input to this processing is the primary dish beam (voltage) pattern, which must be characterized over the field of view and in the directions of strong interferers.

Our approach to these issues is to develop a 4-element hardware correlator based on the Interface Break Out Board (IBOB) designed and built by the Berkeley Wireless Research Center. This correlator provides a test bed for prototyping a streaming telescope design, as well as giving immediate measurements of voltage patterns on existing telescopes. With a 50 MHz bandwidth, this instrument is optimized for acquisition of beam patterns using interferometry on a narrow-band source (radio satellite, maser). The control system is highly flexible and self-contained. It can run as a dumb back-end processor, or interact with the telescope control system through a simple software interface. This architecture was chosen so that the correlator is easily ported to multiple observatories operating in the centimeter (ATA) or millimeter (CARMA) wavelength range. The correlator writes its output directly into MIRIAD format (at least for now). In this talk we review the system and present beam patterns and holography acquired at the Allen Telescope Array.

DEVELOPMENTS IN METHODS FOR VERY HIGH RESOLUTION  
ELIMINATION OF INTERFERENCE AT ARRAYS WITH APPLICA-  
TIONS FOR RADIO ASTRONOMY

Minkoff, J.  
ITT

Abstract Recently, a new approach for eliminating interference at arrays was presented [1,] which employs purely algebraic methods by projecting the interference, represented as vectors, into the null space of the projection operator. The interference is annihilated by transformation into the zero vector, and we denote this method as algebraic interference cancellation (AIC). The scheme was shown to be fundamentally different from conventional methods that reject interference by means of beam forming operations, but no quantitative comparison of the two techniques was made. Here a detailed quantitative comparison of AIC with beamforming/nulling (BFN) methods is presented on the basis of 1) Distortion experienced by the signals of interest in the course of rejecting interference and 2) Degradation in signal-to-noise ratio that accompanies rejection of interference, particularly for interference entering through the main beam. BFN systems operate by employing beam patterns that are deliberately distorted by placement of nulls ,for those angles corresponding to the interference directions. As is well known, attempts to apply ABF to interference entering through the main beam, within an array beam width of a signal of interest, encounter severe problems associated with degradation in signal-to-noise ratio (SNR) as well as distortion of the signals of interest, which in any case is unavoidable because of the deliberate distortion of the array beam pattern. Since beam forming plays no part in AIC operations, resolution in the elimination of interference is therefore not limited by the resolution of the array. There is no fundamental limit on the minimum — but non zero — separation between interfering sources that can be rejected and a signal of interest that can be recovered intact, in its original state, undisturbed and undistorted either by the interference or by the process of rejecting it; the practical limit is determined by receiver noise. Projection of interference vectors into the null space of the projection operator can be viewed as, at each sampling instant, forming linear combinations of the interference components over the array that sum to zero. This eliminates the interference selectively at each array element. Hence, for an M-element array after elimination of interference we have, rather than a single unavoidably distorted signal output as yielded by BFN, M interference free signal outputs, from which the transformation imposed by the null-space transformation can be removed, yielding an undistorted signal output. For an M-element array up to M -1 interference vectors can be eliminated in this manner. The results demonstrate superior performance of AIC over BFN systems both with regard to signal distortion as well as SNR degradation for interference entering through the main beam. It is shown that, depending on the number of interferers, and their proximity to, beam center, SNR degradation in in AIC can be less than that experienced in BFN by several orders of magnitude. . 1. Minkoff, J A new very high resolution interference rejection meyhod with potential for radio astronomy applications, Radio Science, Vol. 38, No. 3 1042 doi:10.1029/2002RS002841,2003, May 2003

## IONOSPHERIC CALIBRATION ISSUES FACING LOW FREQUENCY ARRAYS

Montgomery, M. H.<sup>1,2</sup>, Bust, G.<sup>2</sup>, Garner, T.<sup>2</sup>, Gaussiran, T.<sup>2</sup><sup>1</sup>Department of Astronomy, University of Texas, Austin, TX 78712<sup>2</sup>Applied Research Laboratories, University of Texas, Austin, TX 78713

Given that the magnitudes of the phase shifts introduced by the free electrons in the Earth's ionosphere vary inversely with frequency, i.e.,  $\Delta\phi \propto f^{-1}$ , it is not surprising that the ionosphere is the dominant source of such errors at low frequencies. In addition, the field of view seen by each "station" will be larger at lower frequencies, so that there can be many "isoplanatic patches" across the field of view. Thus, instead of there being just one phase shift for each station, a position-dependent phase screen for each station will be required. For arrays with long baselines ( $\sim 400$  km), these phase screens will essentially be independent of one another, meaning that there will be many free parameters per station which will need to be determined. The calibration issues associated with this situation are the most significant difficulties facing the proposed low frequency arrays, such as the LWA, GMRT, EVLA, LOFAR, and SKA.

In this talk we examine the level of calibration which will be necessary for the Long Wavelength Array (LWA) to reach its stated goals of precision. For this purpose, we use existing 74 MHz VLA data to derive an estimate for the phase screen which would be seen by each of the LWA stations (each station will consist of an array of  $\sim 256$  antennas), and we parameterize the result in terms of Zernike polynomials. In particular, we assess the number of Zernike polynomials which are needed in order for each station to reach a given accuracy in pointing, which in turn tells us about the number of free parameters per station which will be required for calibration.

Session J3, 13:15 – Fri.

**CHALLENGES AND NEW  
ALGORITHMS FOR  
INTERFEROMETRIC IMAGING**

Co-Chairs: M. Wright, S. Myers



## FULL BEAM IMAGING AT HIGH DYNAMIC RANGES

S. Bhatnagar  
NRAO

Full beam imaging at high dynamic range is required to exploit the increased sensitivity of the next generation interferometric radio telescopes under construction or being planned. At low frequencies (1GHz or less) a large fraction of the field of view will have significant amount of flux. In single pointing observations, to remove the contamination due to sources away from the centre, imaging the full field of view will be required. Similarly for mosaicking at higher frequencies, the effects of time varying Primary Beam pattern needs to be corrected for high dynamic ranges. Existing imaging and calibration algorithms explicitly assume direction independent sources of corruption and errors. At the required sensitivity, the effects of various direction dependent (image plane) effects currently limit the achievable dynamic range. Such effects can be classified as direction dependent effects which can be parameterized by apriori knowledge and effects which cannot be similarly parameterized apriori. Examples of the former kind are the polarization squint of VLA antennas, instrumental polarization across the Primary Beam, the effect of the w-term in imaging with non-coplanar arrays, etc. Effects of antenna pointing errors, non-isoplanatic ionosphere etc. are not known apriori and need to be solved for.

Straight forward inversion of the Measurement Equation (required for imaging and calibration using models of the sky) in the presence of direction dependent effects become impractically expensive. This makes it difficult to correct for such effects during image deconvolution. We have been working on developing efficient methods to correct for such effects during image deconvolution as well as develop solvers to solve for antenna based parameterized Primary Beam pattern. In this talk, I will present the progress so far, work in progress and the future plan of action.

## WIDE-BANDWIDTH IMAGING : CHALLENGES AND PROSPECTS FOR THE EVLA AND BEYOND

Rao-Venkata, U.<sup>2</sup>, Myers, S.T.<sup>1</sup>, Cornwell, T.J.<sup>3</sup><sup>1</sup>National Radio Astronomy Observatory, 1003, Lopezville Road, Socorro, NM 87801, USA<sup>2</sup>New Mexico Institute of Mining and Technology, 801, Leroy Place, Socorro, NM 87801, USA<sup>3</sup>Australia Telescope National Facility, PO Box 76, Epping, NSW 1710, Australia

Multi frequency synthesis (MFS) imaging involves gridding visibilities from different frequency channels separately to eliminate bandwidth smearing, and augmenting the deconvolution process to take into account flux variations across the observing band. The goal is to obtain a high dynamic range continuum image with minimal deconvolution errors due to spectral flux variation, while using the entire data set for increased sensitivity.

MFS imaging algorithms have so far been designed primarily from the point of view of enhanced UV coverage provided by multi channel data from relatively sparse arrays. These algorithms are reported to produce images with dynamic ranges of about 1000 to 1 and negligible deconvolution errors (within the rms noise) up to bandwidths of 25%. In addition, the Conway/Sault algorithm (currently the most advanced) assumes a relative power law spectrum between image pixels which translates into a constant spectral index across the band.

The planned EVLA bandwidths (50%) with >10000 observing channels, are much larger than before, and have been chosen to allow the production of wide-band continuum images with increased sensitivity, and dynamic ranges of over 10000 to 1. With these large bandwidth ratios, the assumption of a pure power-law spectrum often breaks, and it is not clear how well the existing algorithms will perform in terms of achievable dynamic ranges and deconvolution errors due to approximately estimated spectral flux variation.

We present an analysis and comparison of the existing algorithms along with some hybrids, from the point of view of wide-band imaging requirements of  $\sim 1\mu\text{Jy}$  rms noise and >10000:1 dynamic range from an 8 hour (E)VLA observation over a 1GHz band at L Band.



## LOW-FREQUENCY WIDE-FIELD IMAGING: FROM THE VLA TO THE LWA

Lazio, T. J. W.<sup>1</sup>, Kassim, N. E.<sup>1</sup>, Cohen, A. S.<sup>1</sup>,  
, Cotton, W. D.<sup>2</sup>, Lane, W. M.<sup>1</sup>, Perley, R. A.<sup>2</sup>, Condon, J. J.<sup>2</sup>

<sup>1</sup>Naval Research Laboratory

<sup>2</sup>National Radio Astronomy Observatory

At frequencies below 1000 MHz, the increasingly larger fields of view of radio telescopes make two effects increasingly important. First, if an interferometer is non-coplanar (as most current and future instruments are or will be) its geometry introduces phase errors and image distortions at larger radial distances from the phase center. Second, the isoplanatic patch from ionospheric phase distortions can become smaller (potentially much smaller) than the field of view, leading to defocussing throughout the field of view.

There are now a series of methods to deal with the non-coplanar nature of interferometers, most notably polyhedral imaging and the  $w$ -projection. The former tessellates the field of view into smaller areas over which the interferometer can be assumed to be coplanar; the latter projects, via a Fresnel-like kernel, the three-dimensional sampling of the interferometer onto a two-dimensional plane, which is then inverted. Imaging in the presence of ionospheric phase errors has been accomplished generally by restricting the field of view to be smaller than an isoplanatic patch or by restricting the size of the array so that the number of isoplanatic patches within the field of view is not too large. We illustrate these approaches using examples from the 74 MHz system on the Very Large Array (VLA) (maximum baseline  $\approx 35$  km) and from the 74 MHz "Pietown-link" extension to the VLA (maximum baseline  $\approx 70$  km).

The Long Wavelength Array (LWA) is an interferometer being developed for operation at frequencies of 20–80 MHz, with maximum baselines approaching 400 km. While many of the existing methods will be suitable for observing programs with the early stages of the LWA, full exploitation of its potential will require development of new wide-field imaging methods. Development of new ionospheric calibration techniques may require revisiting traditional assumptions about the configuration of interferometers.

Basic research in radio astronomy at the Naval Research Laboratory is supported by the Office of Naval Research. The National Radio Astronomy Observatory is a facility of the National Science Foundation operated under cooperative agreement by Associated Universities, Inc.

## CHALLENGES AND FUTURE DIRECTIONS FOR SUBMILLIMETER IMAGING

Crystal L. Brogan<sup>1</sup>, Mark Holdaway<sup>2</sup>, Steve Myers<sup>2</sup>

<sup>1</sup>University of Hawaii, Institute for Astronomy

<sup>2</sup>National Radio Astronomy Observatory

Submillimeter astronomy stands at the brink of new discovery space with the advent of submillimeter interferometers with subarcsecond resolution. These new instruments include the operational Submillimeter Array (SMA) and the future prospects of the Atacama Large Millimeter Array (ALMA). Along with these fantastic opportunities comes new challenges for submillimeter imaging. Among the most challenging is the need to (1) image large fields of view compared to the size of the primary beam; and (2) recover information on extended structures larger than that sampled by the shortest spacings of the interferometer. These techniques are important because many of the sources of interest are considerably larger than about 1/2 the primary beam (i.e. the field of view) of the array. For example, at 345 GHz, the FWHM primary beam of the the 6-m SMA antennas is only  $\sim 30''$ , while the beam for the 12-m ALMA antennas is a factor of two smaller yet.

In order to observe larger fields of view, multiple overlapping pointings of the desired region must be jointly imaged and deconvolved in a process known as mosaicing. The observing strategy and imaging algorithms adopted for mosaicing must take into account sampling on the sky, as well as in the  $u-v$  plane. For example, optimal (Nyquist or better) spacing of mosaic pointings is necessary to prevent aliasing artifacts in the image, while the deconvolution procedure must take into account any differences in  $u-v$  coverage (and hence in the synthesized beam of the array) between pointings. Though mosaicing naturally recovers more short spacing information than a single interferometric pointing alone, most mosaicing experiments will also require the addition of short and zero spacing information.

Image quality (fidelity) is directly linked to how completely the  $u-v$  plane is sampled. Two methods exist for recovering missing short spacing information: the addition of total power data from a single dish telescope and/or the addition of data from a closely packed array of smaller diameter antennas. The former is sometimes used for the SMA, while the latter in the form of the Atacama Compact Array (ACA) is envisioned for ALMA coupled with total power from four of the 12-m antennas. The best image fidelity is achieved when there is a high degree of overlap between the two datasets in the  $u-v$  plane. The optimal method for adding the two datasets (i.e. image or  $u-v$  plane) is still under investigation. It is clear that pointing errors and relative amplitude calibration have a significant impact and must be taken into consideration.

In this talk, we will present examples of the current state of submillimeter imaging using the SMA, and point out the limitations of the data and algorithms. Looking ahead to ALMA, and its ambitious imaging specifications (e.g. 10000:1 dynamic range, high image fidelity, full beam polarimetry), the advancements in imaging and calibration techniques necessary to realize these goals will be described along with suggested paths for algorithm development.

## INTERFEROMETRIC IMAGING OF THE MICROWAVE BACKGROUND RADIATION

Tim Pearson, for the CBI collaboration  
Caltech

The anisotropies of the cosmic microwave background radiation (CMB) provide valuable diagnostics of the condition in the early universe at about 100,000 yr after the Big Bang. The signals are very weak, a few microkelvin on scales of a few minutes of arc, and present a challenge to observers.

A number of ground-based interferometer arrays have recently been successful in measuring both the intensity and the polarization of the CMB on these scales. These include the Degree Angular Scale Interferometer (DASI, Antarctica), the Cosmic Background Imager (CBI, Chile), and the Very Small Array (Tenerife).

The CBI is a planar array of thirteen 0.9-m Cassegrain antennas on a common mount, with interferometer baselines ranging from 1 to 5 m, receiving radiation in the 26-36 GHz band. It measures linear polarization by cross-correlating the signals from antennas sensitive to orthogonal circular polarizations, and intensity by correlating antennas of the same polarization.

Images can be formed by mosaicking together observations from adjacent pointings of the telescope. Although the techniques involved are similar to those of longer baseline interferometers such as the Very Large Array, we have developed a number of techniques specialized for observations of the CMB. These include: elimination of contaminating ground radiation by projection of a common mode; elimination of foreground point sources of known position but unknown flux density by projection; and specialized techniques for polarization calibration. Gridding the data in the  $u, v$  plane provides an efficient way both to make images and to estimate the angular power spectrum of the fluctuations, which is the primary point of contact with theoretical models of the early universe.

The pattern of polarization on the sky can be separated into a divergence-free part (B mode) and a curl-free part (E mode). This is important because scalar (density) fluctuations generate only the E-mode, and detection of the B-mode will indicate the presence of contaminating foreground radiation or, more excitingly, tensor (gravitational wave) fluctuations from the epoch of inflation. We show how an interferometer is well suited for making this separation, and present images of the E and B modes in addition to images of the Stokes parameters I, Q and U. We also present maps of E and B in  $uv$  plane, which is equivalent to the multipole  $\ell$  space used in CMB theory.

## BAYESIAN INTERFEROMETRIC IMAGE RECONSTRUCTION

Benjamin D. Wandelt<sup>1</sup>, Edmund Sutton<sup>2</sup><sup>1</sup>Department of Physics, University of Illinois at Urbana-Champaign<sup>2</sup>Department of Astronomy, University of Illinois at Urbana-Champaign

I will discuss the Bayesian approach to image reconstruction from interferometric data. The Bayesian approach does not just return a "best estimate" of the image, but allows the characterization of significance of individual features in the image. Bayesian image reconstruction requires an explicit image prior. I will argue that a natural prior to use is the "multiplicity prior" which represents the image in terms of  $N$  flux units of strength  $s$ . This prior reduces to the widely studied entropy prior in the limit of large  $N$  and has several conceptual and practical advantages when the signal-to-noise ratio per pixel is near unity. The reconstructed image (Bayes estimate) is obtained by marginalizing the posterior over the parameters  $N$  and  $s$ . I will demonstrate the implementation of this Bayesian approach using Gibbs sampling. The analysis of simulated radio interferometry data (including point sources and extended emission) results in both a reconstructed image as well as an error model of the uncertainty in the image in terms of the variance per pixel, or significance of individual features. The Bayesian approach produces demonstrably better results than standard library routines. While the Bayesian approach is computationally demanding, recent advances in algorithms, the use of Monte Carlo techniques, and faster computer hardware now allow the exploration of the image posterior and bring full Bayesian image analysis within reach. Looking into the future, I will discuss the remaining challenges and new algorithms that may overcome them; the use of multiscale priors; the generalization of this work to polarimetry; and wideband imaging.

References: Wandelt, Larson, and Lakshminarayanan (2004), *Physical Review D* 70, 083511 (2004); Sutton and Wandelt (2005), *Astrophysical Journal*, submitted.

## REAL TIME IMAGING

Wright, M.C.HUniversity of California, Berkeley

In this paper, we propose to integrate calibration and imaging with DSP hardware in order to handle high data rates and make images in close to real time with radio telescope arrays, such as the SKA and ATA, with large numbers of antennas and large fields of view. We propose to use modular DSP boards with a flexible interconnect architecture which allows reconfiguration of computing resources for multiple projects. Correlators and beam formers with a high data bandwidth into computer clusters support a flexible programming environment. The system design allows radio astronomy to implement the latest technology in a cost effective and timely manner. The correlation function is computed with narrow frequency channels and short integration times so that images can be formed over a large field of view. Images can be made simultaneously in multiple regions within the field of view by integrating the output from the correlators at multiple phase centers on targets of interest, calibration sources, and sources whose sidelobes will confuse the regions of interest. The calibration can be improved by using a global model of the sky brightness and gains. RFI and time variable sources must be identified and measured so they can be correctly separated and subtracted from the data. The calibration varies across the sky due to frequency and time variations in the primary beam, instrumental polarization and non-isoplanicity. We must measure the gain variations in the directions of sources whose sidelobes corrupt the regions of interest. Calibration is made in close to real time using the model of the sky brightness distribution. The derived calibration parameters are fed back into the imagers and beam formers. Images are made simultaneously for multiple phase centers using an FFT algorithm in restricted fields of view. Sidelobes from sources outside each of the regions imaged are minimized by subtracting the model from the data before imaging. The regions imaged are used to update and improve the a-priori model, which becomes the final calibrated image by the time the observations are complete.

A NEW APPROACH TO RADIO ASTRONOMY SIGNAL PROCESSING: PACKET SWITCHED, FPGA-BASED, UPGRADEABLE, MODULAR HARDWARE AND REUSABLE, PLATFORM-INDEPENDENT SIGNAL PROCESSING LIBRARIES

Aaron Parsons<sup>1</sup>, Don Backer<sup>1</sup>, Dan Werthimer<sup>2</sup>, Mel Wright<sup>3</sup>

<sup>1</sup>University of California, Berkeley, Astronomy Dept.

<sup>2</sup>University of California, Berkeley, Space Sciences Laboratory

<sup>3</sup>University of California, Berkeley, Radio Astronomy Laboratory

Our group seeks to revolutionize the development of radio astronomy signal processing instrumentation by designing and demonstrating a scalable, upgradeable, FPGA-based computing platform and software design methodology that targets a range of real-time radio telescope signal processing applications. This project relies on the development of a small number of modular, connectible, upgradeable hardware components and platform-independent signal processing algorithms and libraries which can be reused and scaled as hardware capabilities expand. We have developed such a hardware platform and many of the necessary signal processing libraries for applications in antenna array correlation, wide-band spectroscopy, and pulsar surveys.

We present three hardware modules we have implemented for digitization, data preprocessing and packetization, and high end reconfigurable computing. Using this hardware and reusable signal processing libraries, we have developed applications in spectroscopy and antenna correlation as demonstrations of the technology and design methodology. Our implementations of a 128-million channel spectrometer with a selectable 200 MHz bandwidth and an 8-station, full Stokes, 1024 channel correlator demonstrate the agility and potential for rapid development that our system architecture and design toolflow allow. These instruments are currently deployed in a JPL SETI survey and prototype dipole array for redshifted 21cm detection of the Epoch of Reionization, respectively.

We also identify future directions for the development of this platform, such as packetization, RFI rejection libraries, and real-time imaging. These enhancements will expand the signal processing applications of this project, and introduce a new scalability in the ability to connect an arbitrary number of hardware modules into a Beowulf-like FPGA computing cluster.

## TIME-DEPENDENT INTERFEROMETRIC IMAGING OF NON-STATIONARY OBJECTS

Butala, M. D.<sup>1</sup>, Frazin, R. A.<sup>1</sup>, Kamalabadi, F.<sup>1</sup>, Kemball, A.<sup>2</sup>

<sup>1</sup>Department of Electrical and Computer Engineering, University of Illinois at Urbana-Champaign

<sup>2</sup>National Center for Supercomputer Applications, University of Illinois at Urbana-Champaign

Standard approaches to radio-interferometric image formation typically assume that the source brightness distribution has negligible time-variability over the course of the data acquisition. Nevertheless, in astronomical aperture synthesis, there are sources for which this standard assumption cannot be made, including studies of solar phenomena and relativistic jet sources in the Galaxy ("microquasars"), both of which may exhibit flux density variability within the span of a given observing run. Traditionally, several approaches have been taken to mitigate this problem, including sub-dividing the measured visibility data into snapshot time intervals, over which the standard assumption of a constant source brightness distribution has greater validity. These data segments can then be imaged separately, but at the cost of reduced image fidelity as a result of sparser u-v plane coverage and lower sensitivity in each individual interval. Furthermore, this approach does not take advantage of the fact that image at one measurement time is closely related to the image at the next measurement time.

We address this problem by formulating the image formation process as a time-dependent, or dynamic estimation problem. We investigate the effectiveness of a state-space formulation for interferometric imaging by incorporating recursive estimation and optimal filtering strategies based on the Kalman filter, which models the temporal evolution of the unknown object explicitly in the reconstruction. We assume no knowledge of the deterministic temporal evolution of the dynamic object but instead rely on a purely stochastic model. We illustrate that dynamic estimation offers the possibility of improved image fidelity in radio-interferometric imaging of objects of this type.

## IMAGING AURORAL KILOMETRIC RADIATION BURST USING A 4-STATION SPACE-BASED INTERFEROMETER

Mutel, R. L., Christopher, I.  
University of Iowa

We have used the University of Iowa's Wideband (WBD) receivers installed on ESA's four Cluster spacecraft to determine the locations of auroral kilometric radiation (AKR) bursts in the Earth's magnetosphere. The WBD receivers operate in the 125, 250, and 500 KHz bands with an effective bandwidth of 10 KHz. Each spacecraft is equipped with a single 88m dipole antenna. The source location technique involves cross-correlating the received waveforms (which are transmitted to DSN ground stations in real time) and measuring the resulting six differential time delays. The six delays overdetermine the source location, but the intrinsic narrowband nature of the emission (typically <1 KHz) dominates the delay uncertainties, which are typically  $\pm 0.3$  ms. The resulting position uncertainties are  $\sim 300$ -600 km for a typical projected baseline length of 10,000 km. The Cluster array is 2-dimensional, but the projected spatial frequency sampling is often highly anisotropic, with a ratio of 3-5:1 in the ellipticity of the restoring beam. The cross-correlated phase has not yet been successfully used to track source motion for long duration bursts, but this should be possible with careful reduction. In this paper we discuss the unique challenges to imaging bursty sources with short time durations and narrow bandwidths, as well as confusion caused by a strong likelihood of a multiplicity of spatially distinct sources at any given time. Nevertheless, we have successfully imaged thousands of AKR bursts over the period 2002-2005. We show the resulting locations as time lapse movies and compare the location to simultaneous UV imaging of the auroral oval using the IMAGE spacecraft.



## THE LONG WAVELENGTH ARRAY

Paravastu, N., Lazio, T. J. W., Polisensky, E.  
, Kassim, N. E., Weiler, K., Ray, P. S.  
, Hicks, B., Crane, P., Stewart, K. , Cohen, A. S.  
Naval Research Laboratory

Sub-arcminute resolution and sub-Jy sensitivity below 100 MHz is now being obtained on a routine basis using self-calibration or field-based calibration techniques with the 74 MHz system on the NRAO Very Large Array (VLA). The VLA 74 MHz breakthrough has inspired an emerging suite of new low frequency instruments, including the Long Wavelength Array (LWA), an electronic array planned to operate in the 20–80 MHz frequency range. It will have a collecting area approaching one square kilometer at its lowest operating frequencies and provide milliJansky sensitivity and a few arcseconds resolution across its observing band. The LWA will surpass, by 2–3 orders of magnitude, the power of previous interferometers in its frequency range, and thus open a window on one of the most poorly explored regions of the electromagnetic spectrum.

The LWA's scientific objectives include (1) Planetary and solar radio emission; (2) The three-dimensional distribution of Galactic cosmic rays and Galactic supernova remnants and pulsars; and (3) The extragalactic universe, including high-redshift radio galaxies and galaxy clusters. Because the LWA will explore such a poorly investigated region of the spectrum, the potential for new discoveries, including new classes of sources or physical phenomena, is high.

On-going design and development activities focus on the antenna and receiver chain, the station configuration, and a staged evolution of the LWA in the southwest U.S. The planned array element for the LWA is a dual polarization blade-dipole antenna, chosen primarily for its simplicity, affordability, and broadband characteristics. Electromagnetic simulations of the antenna structure predict that a minimum of 6 dB sky noise dominance will be observed over the 23–80 MHz frequency range. An LWA station will contain 256 blade-dipole elements over a 100 m diameter circular area. The arrangement of elements within the station has been designed to minimize the peak sidelobe level. The peak sidelobes are  $-17.7$  dB below the main beam. We illustrate some of this work using recent results from the prototype Long Wavelength Development Array (LWDA) being developed at the VLA site.

Basic research in radio astronomy at the Naval Research Laboratory is supported by the Office of Naval Research.



Session J/B1 07:55 – Wed.

**SUBMILLIMETER AND  
TERAHERTZ TECHNOLOGY FOR  
RADIO ASTRONOMY**

Co-Chairs: C. Walker, S. Radford

J/B1

## QUANTUM CASCADE LASERS

Albert Betz

University of Colorado, CASA, 593 UCB

Quantum cascade lasers (QCLs) are heterostructures made (in this case) from materials in the III-V semiconductor group (e.g., GaAs/GaAlAs). A heterostructure is a multiple quantum well (MQW) planar structure of alternating high and low gap materials. THz photons are emitted by these devices as electrons make transitions between sub-band states in the conduction band. A large number of repeating MQW sections are cascaded during MBE layer deposition to enhance the gain path. A single electron traveling through this composite structure under DC bias emits hundreds of identical THz photons without recombination (in contrast to a single photon per recombination in a bipolar diode laser). With the addition of optical feedback from the cleaved ends of the MQW gain region, the device acts as a laser. TM selection rules for these type II superlattices dictate that the emission emanates from the edge facet of the device (i.e., perpendicular to the MBE growth direction), with a polarization parallel to the growth direction.

The demonstration of practical quantum cascade lasers at frequencies between 2-5 THz in the last few years has filled the need for a fundamental signal source in this spectral region. Already THz QCLs have produced output powers exceeding 10 mW, linewidths less than 100 kHz, and CW operating temperatures above 100 K, although these parameters have not yet been achieved simultaneously. Nevertheless, QCLs have already been employed successfully as LOs in THz receivers using NbN HEB mixers. This talk will summarize the current state of the art in QCLs designed for LO applications, and outline development goals for the next few years.

## FREQUENCY SELECTIVE BOLOMETERS

Wilson, G.W.<sup>1</sup>, Chen, T.C.<sup>2</sup>, Cheng, E.S.<sup>2</sup>  
, Cottingham, D.A.<sup>2</sup>, Downes, T.<sup>3</sup>, Finkbeiner, F.M.<sup>2</sup>  
, Fixsen, D.J.<sup>2</sup>, Logan, D.W.<sup>1</sup>, Meyer, S.<sup>3</sup>  
, Perara, T.<sup>1</sup>, Ruhl, J.<sup>4</sup>, Sharp, E.H.<sup>2</sup>, Silverberg, R.F.<sup>2</sup>

<sup>1</sup>University of Massachusetts, Dept. of Astronomy, Amherst, MA 01003

<sup>2</sup>NASA/GSFC, Code 685, Greenbelt, MD 20771

<sup>3</sup>University of Chicago, Enrico Fermi Institute, Chicago, IL 60637

<sup>4</sup>Case Western Reserve University, Physics Dept., Cleveland, OH 44106

In recent years, substantial effort has been made to increase detector count in arrays and more efficiently use the available telescope field of view. This has resulted in a wide array of upcoming large focal plane instruments which will be operating in the mm and submm windows. In comparison, much less effort has been focused on technologies that increase the efficiency with which we use the available telescope bandwidth. Recognizing that many scientific observations in the mm and submm windows will benefit from an ability to measure continuum spectral energy distributions in sources, we have developed a detector technology tailored to allow compact, high-efficiency, multi-band photometers in a single pixel.

Frequency Selective Bolometers (FSBs) utilize a lossy frequency selective surface as the detector absorbing element. This allows the detectors to have both high in-band efficiency and near unity out of band transmission. Consequently, several FSBs may be stacked in a linear fashion to form a multi-band photometer in a single pixel. We describe recent results in modeling and measuring FSB absorption spectra as well as measurements of absolute absorption efficiencies of FSBs being built for the SPEED photometer. Overall we demonstrate good agreement between our electromagnetic models of lossy frequency selective surfaces which now allows design and iteration to take place in software rather than in hardware.

FSBs are not without their challenges. We also highlight some of the technical hurdles we have faced while coupling the optical portions of the FSB with transition-edge superconducting thermistors. We conclude by examining potential future opportunities with FSB arrays and polarization sensitive FSBs.

RECENT DEVELOPMENTS OF HOT ELECTRON BOLOMETER  
TECHNOLOGY RELEVANT FOR THZ ASTRONOMY RECEIVERS

Yngvesson, S.  
UMass/Amherst

Development of Hot Electron Bolometer heterodyne detectors for terahertz astronomy applications commenced in the early 1990s. At this stage, receivers with double sideband receiver noise temperatures of close to ten times  $hf/k$  have been demonstrated in the frequency range of 1 THz to 2.5 THz. HEB receiver systems have been installed on ground-based telescopes at the lower THz frequencies, and are ready to be launched on Herschel in 2007. This talk will review some new developments in the following areas:

The first Focal Plane Array (FPA) for a frequency above 1 THz (1.6 THz) was recently demonstrated (Rodriguez-Morales et al, IEEE Microw. Wireless Comp. Lett., 15, 191 (2005)). This FPA integrated three HEB elements and broadband MMIC IF amplifiers in a single block. The modeling of such receivers and the potential for extension of FPAs to larger numbers of elements and higher terahertz frequencies will be discussed.

Gain stability is a crucial issue for terahertz receivers as they are being employed in systems. We have performed new Allan variance and other measurements on HEB receivers with and without active stabilization of the local oscillator (a gas laser in this case), and will discuss these results and their relevance to the operation of HEB receiver systems.

Relatively few measurements have been performed on HEB receivers for frequencies above 2.5 THz, and the few that exist indicate a rather rapid increase of the noise temperature with frequency. This talk will review predictions for the HEB receiver noise temperature based on recent theoretical work (Kollberg and Yngvesson, submitted to IEEE Trans. Microw. Theory Techniques, September, 2005). The theory models quantum noise effects in HEB receivers at high terahertz frequencies, and it is shown that quantum noise will contribute more than half of the receiver noise temperature above about 3 THz.

## DEVELOPMENTS IN FREQUENCY DOMAIN MULTIPLEXING FOR LARGE ARRAYS OF TRANSITION EDGE SENSOR BOLOMETERS

Dobbs, M.A.<sup>1</sup>, Cho, H.M.<sup>2</sup>, Clarke, J.<sup>2</sup>  
, Holzapfel, W.<sup>2</sup>, Lanting, T.M.<sup>2</sup>, Lee, A.T.<sup>2</sup>  
, Lueker, M.<sup>2</sup>, Richards, P.L.<sup>2</sup>, Spieler, H.G.<sup>4</sup>

<sup>1</sup>Dept. of Physics, McGill University, 3600 Rue University, Montreal, Quebec, CANADA

<sup>2</sup>Dept. of Physics, University of California, Berkeley, Berkeley, California, U.S.A.

<sup>3</sup>Materials Science Division, Lawrence Berkeley National Laboratory, Berkeley, California, U.S.A.

<sup>4</sup>Materials Science Division, Lawrence Berkeley National Laboratory, Berkeley, California, U.S.A.

The next generation of bolometric Cosmic Microwave Background (CMB) experiments require large format arrays of 100-1000 sensors to achieve their science goals. Multiplexed readout for these systems is a key technological challenge. I'll discuss the frequency domain multiplexing technique which has been developed for deployment on the APEX-SZ, South Pole Telescope, POLARBEAR, and EBEX experiments. Presently operating systems will be described, as well as the status of new instrumentation developments.

The general structure of the system is as follows. The bolometers are biased with sinusoidal voltages of constant amplitude with frequency in the MHz range. Each bolometer within a readout module is connected in series with a resonant LC circuit so that it can be biased at a different frequency. The sky-signal changes the bolometer resistance and amplitude modulates the bolometer current such that the signal from each bolometer is transferred to sidebands adjacent to its carrier. Thus, the signals from different bolometers within a module are uniquely positioned in frequency, so they can be summed and connected through a single wire to a Superconducting Quantum Interference Device (SQUID). The comb of amplitude modulated carriers output by the SQUID device is transmitted to a bank of demodulators that mix the signals down to base-band, recovering the original sky-signal. The signals are then low pass filtered and digitized, and all outputs in the array are sampled synchronously.

One of the auxiliary advantages of this system is that it is very insensitive to vibrations. This is because the current path through the bolometers is bandwidth limited, and sky signals are modulated up at high frequency where vibrations do not manifest. The first generation frequency domain multiplexer employs primarily analog electronics, and includes a high loop gain feedback loop between a cold SQUID device and warm amplifier. We are pursuing a cold feedback architecture which will increase the system bandwidth and hence increase the channel count, and a new low power digital mux/de-mux that will greatly improve the scalability of the system.



## A 1.5 THZ SUPERCONDUCTING HETERODYNE RECEIVER FOR GROUND-BASED ASTRONOMICAL OBSERVATIONS

Jonathan Kawamura<sup>1</sup>, Raymond Blundell<sup>2</sup>, Daniel Marrone<sup>2</sup>,  
 Scott Paine<sup>2</sup>, Edward Tong<sup>2</sup>, T. K. Sridharan<sup>2</sup>,  
 John Pearson<sup>1</sup>, Jeff Stern<sup>1</sup>, Harold Yorke<sup>1</sup>,  
 Steven Lord<sup>3</sup>, Imran Mehdi<sup>1</sup>, John Ward<sup>1</sup>, Denis Loudkov<sup>2</sup>

<sup>1</sup>Jet Propulsion Laboratory, Caltech, 4800 Oak Grove Drive, Pasadena CA 91109

<sup>2</sup>Smithsonian Astrophysical Observatory, 60 Garden Street, Cambridge MA 02138

<sup>4</sup>IPAC/Caltech, 1200 E. California Blvd, Pasadena CA 91125

A heterodyne receiver designed for astronomical observations in the partially transmissive 200 micron (1.5 THz) atmospheric window has been deployed on a telescope on Cerro Sairecabur in Northern Chile. The 0.8 meter telescope, built by Smithsonian Astrophysical Observatory, is situated at an altitude of 5525 meters and has been in operation since 2002. It permits, on a regular basis, observations in three atmospheric windows between 1 and 2 THz, and provides access to the 350 microns window most of the time. The key lines of astronomical interest in the 200 micron window are CO(J = 13-12) at 1.5 THz and the fine-structure transition in singly ionized nitrogen at 1.46 THz.

In the receiver, the mixer element is a superconductive NbTiN phonon-cooled hot-electron bolometer. A small area (1 square micron) of very thin (4 nm) NbTiN film with normal metal electrical contacts is fabricated on a single-crystal quartz substrate, which is incorporated in a waveguide mount designed originally for the Submillimeter Array receivers. The mixer is mounted in a liquid helium cooled cryostat, which also houses the first stage low-noise intermediate frequency amplifier. The local oscillator is an all-solid-state chain, with a Gunn oscillator followed by power amplifiers driving a cascade of four frequency doublers. Operating at ambient temperature, the LO can provide a minimum of several microwatts of output power at the lines of interest, which is sufficient to pump the mixer optimally. The LO and signal beams are combined optically using a Martin-Puplett polarizing interferometer. Referenced to the input of diplexer, the double-sideband receiver noise temperature is about 1500 K at an intermediate frequency of 3.0 GHz and a bandwidth of 1 GHz. A digital autocorrelator is used to generate spectra. The astronomical spectra are calibrated using atmospheric transmission data taken continuously with a Fourier transform spectrometer.

The receiver was used to detect the CO(J=13-12) emission line at 1.5 THz toward Orion to verify the end-to-end operation of the mixer; since then, we have made a detection of the 1.46 THz line emission from singly ionized nitrogen.

## ANTENNA-COUPLED MICROWAVE KINETIC INDUCTANCE DETECTORS

Day, P.K.<sup>1</sup>, LeDuc, H.G.<sup>1</sup>, Mazin, B.A.<sup>1</sup>,  
Vayonakis, A.<sup>2</sup>, Gao, J.<sup>2</sup>, Kumar, S.<sup>2</sup>, Zmuidzinas, J.<sup>2</sup>

<sup>1</sup>Jet Propulsion Laboratory, Pasadena, CA 91109

<sup>2</sup>California Institute of Technology, Pasadena, CA 91125

We report on the development of microwave kinetic inductance detectors (MKIDs) coupled to planar antennas for submillimeter wavelengths. The MKID is a relatively new type of superconducting photon detector which is applicable from millimeter-wave frequencies to X-rays. Photons are absorbed in a superconductor, producing quasiparticle excitations, which change the surface reactance (kinetic inductance) of the superconductor. The changes in kinetic inductance are monitored using microwave high-Q thin-film superconducting resonators. We have demonstrated the detection of submillimeter-wave power with an MKID using a planar antenna and microstrip coupling. In our coupling scheme, power from a slot array antenna is transmitted along a niobium microstrip line to an MKID based on a quarter-wavelength coplanar waveguide transmission line resonator. The microstrip line overlaps the resonator over a short distance at its shorted end to transfer power to the resonator. We have fabricated single pixel devices that use a dual polarization antenna designed for 350GHz, as well as small arrays of single polarization devices designed for millimeter-wave frequencies. We have conducted measurements of the efficiency of these detectors using a thermal radiation source located inside the cryostat with the detector. Measurements of antenna beam-patterns and frequency response were conducted using a cryostat with a window. Because the MKID is particularly amenable to frequency-domain multiplexing, with likely detector multiplexing factors of  $\sim 10^3$  or more per cryogenic amplifier, these detectors are well suited for use in large arrays. We discuss the sensitivity of these detectors and the potential of antenna-coupled MKID arrays for ground and space-based millimeter/submillimeter imaging.

## ANTENNA-COUPLED MICROWAVE KINETIC INDUCTANCE DETECTORS

Anastasios Vayonakis<sup>1</sup>, Peter Day<sup>2</sup>, Alexey Goldin<sup>2</sup>,  
Rick LeDuc<sup>2</sup>, Ben Mazin<sup>2</sup>, Shwetank Kumar<sup>1</sup>,  
Jiansong Gao<sup>1</sup>, Chao-Lin Kuo<sup>2</sup>, Jeff Stern<sup>2</sup>, Jonas Zmuidzinas<sup>1</sup>  
<sup>1</sup>Caltech  
<sup>2</sup>JPL

Kinetic Inductance detectors are very promising for future large scale millimeter and submillimeter direct detection focal plane arrays. They can be easily fabricated, and many detectors can be frequency multiplexed through coupling to a single feedline. Microwave readout provides a lot of bandwidth per detector, allowing a large number of pixels to be read using a single cryogenic microwave amplifier and warm readout electronics. Sensitivity is now good enough for ground based imaging, and approaching the requirements for CMB-pol.

Planar antennas are also of great interest for future millimeter and submillimeter focal plane arrays. Each antenna consists of an array of  $N$  long slot antennas which are fed along their length at  $M$  points. The resulting  $N*M$  feed points are combined using a binary summing tree made of low-loss superconducting microstrip lines. The amplitude and phase of the electric field at each element of the array control the pointing and far-field beam pattern. By passively adding the electric fields of each antenna in a phase-coherent manner, we can synthesize the diffraction-limited beam. Due to its large size, the resulting array antenna produces a narrow beam pattern and can therefore be used without additional optical coupling elements. Such architecture promises a lot of advantages compared to existing systems. Compared to bolometers with extended area radiation absorbers, antenna-coupled detectors provide greatly reduced thermally active area, allowing for gains in sensitivity and response speed. Furthermore, the large sub-K feedhorn optics which comprise more than 95

## LARGE FORMAT IMAGING ARRAYS FOR THE ATACAMA COSMOLOGY TELESCOPE

Chervenak, J. A.<sup>1</sup>, Wollack, E. J.<sup>1</sup>, Marriage, T.<sup>2</sup>,  
Niemack, M.<sup>2</sup>, Staggs, S.<sup>2</sup>, Doriese, R.<sup>3</sup>

<sup>1</sup>NASA Goddard Space Flight Center, Greenbelt, MD 20771

<sup>2</sup>Princeton University, Physics Department, , Princeton, NJ 08544

<sup>3</sup>National Institute of Standards and Technology, Boulder, CO 80303

We describe progress in the fabrication, characterization, and production of detector arrays for the Atacama Cosmology Telescope (ACT). The completed ACT instrument is specified to image simultaneously at 145, 225, and 265 GHz. Its focal plane will use three 32x32 filled arrays of superconducting transition edge sensors (TES) read out with time-division-multiplexed SQUID amplifiers.

We present details of the pixel design and testing including the optimization of the electrical parameters for multiplexed readout. Using geometric noise suppression and careful tuning of device operation temperature and bias resistance, the excess noise exhibited by the TES device is balanced with detector speed for interfacing with the ACT optics. The design also accounts for practical tolerances such as transition temperature gradients and scatter that occur in the production of multiple wafers needed to populate fully the kilopixel cameras. We have developed an implanted absorber layer compatible with our silicon-on-insulator process that allows for tunable optical resistance with requisite on-wafer uniformity and wafer-to-wafer reproducibility.

Arrays of 32 elements have been tested in the laboratory environment including electrical, optical, and multiplexed performance. Given this pixel design, optical tests and modeling are used to predict the performance of the filled array under anticipated viewing conditions. Integration of the filled array with suitable optical components, a tuned backshort behind each column of 32 and a dielectric plate in front of the entire array, maximize absorption at the focal plane and suppress reflections. A mechanical design for the build of the full structure is completed and we report on progress toward the construction of a prototype array for first light on the ACT.

FREQUENCY DOMAIN MULTIPLEXED RECEIVERS FOR  
STUDYING THE SUNYAEV-ZELDOVICH EFFECT

Martin Lueker<sup>1</sup>, The APEX-SZ Collaboration<sup>2</sup>, The South Pole Telescope

<sup>1</sup>Department of Physics, University of California, Berkeley, Berkeley, CA, USA

<sup>2</sup><http://bolo.berkeley.edu/apexsz>

<sup>3</sup><http://spt.uchicago.edu>

Galaxy cluster surveys provide important constraints on models of large-scale structure formation. Surveys using Sunyaev-Zeldovich (SZ) effect should discover thousands of distant clusters. In current ground-based bolometric SZ measurements, the noise of each pixel is dominated by photon statistics. Future generations of bolometric receivers will contain hundreds to thousands of pixels in order to extend their sensitivity.

Two such SZ experiments include the South-Pole Telescope (SPT) and its predecessor, APEX-SZ. The APEX-SZ experiment will use an array of 300 superconducting transition edge sensor (TES) detectors and will serve as a test-bed for many of the technologies to be used in the SPT receiver, a 1000 TES-pixel SZ survey. Both arrays will operate at sub-kelvin temperatures, where cooling power is scarce. This is a serious concern for the larger SPT array. In order to reduce the thermal loading at the sub-kelvin stages, SPT uses frequency domain multiplexing (fMUX) to reduce the number of thermally conductive wires required by the detectors. Though the APEX-SZ receiver, with its smaller focal plane, does not currently use multiplexing, it uses a similar readout system and the same design for the warm readout electronics, superconducting quantum interference device (SQUID) arrays, and TES arrays. By using the same technologies, the APEX-SZ receiver paves the way for other large bolometer systems, such as SPT, as well as POLARBEAR, and EBEX, two experiments designed to study the polarization of the cosmic microwave background (CMB).

I describe the design and readout of the SPT receiver and the progress of APEX-SZ. Both of these receivers are presented as an example of a complete system using the frequency domain multiplexor technology.

## ELECTROMAGNETIC PROPERTIES OF FILLED PIXELATED ARRAYS

David T. Chuss, Edward J. Wollack, S. Harvey Moseley  
NASA Goddard Space Flight Center

Filled arrays of bolometers are currently being employed for use in astronomy from the far-infrared through millimeter parts of the electromagnetic spectrum. Because of the large range of wavelengths for which this is applicable, the number of modes supported by a bolometric pixel will vary according to specific application. Withington et al. (2003) have built a formalism for treating the electromagnetic properties of such bolometers by propagating the second order statistical properties of the radiation through a canonical optical system. In this work, we use this formalism to construct beam pattern images of square pixels for various ratios of  $p/\lambda$  where  $p$  is the pixel size and  $\lambda$  is the wavelength. In the low mode limit, the diffraction effects cause the beam pattern to be circular with a quadrupole dependence of Stokes  $Q$  and  $U$ . High mode cases approach the geometric limit. The polarization in these cases can be seen to trace the pixel edges. The effective size of the beam has a direct impact on the inter-pixel coupling and sets the number of independent detectors in an astronomical focal plane. This technique illustrates and quantifies the relationship between pixel size and angular resolution limits for a given wavelength and telescope. This is especially true in the limit of low  $p/\lambda$ . In this case, the diffraction due to pixelization is non-negligible for the calculation of the overall angular resolution of the telescope. In addition, for instruments that are polarization sensitive, this method also provides a quantitative method for determining the contribution of the instrument to the measured polarization.

POLARIMETER ARRAYS FOR COSMIC MICROWAVE BACKGROUND MEASUREMENTS

Thomas Stevenson<sup>1</sup>, Nga Cao<sup>1</sup>, David Chuss<sup>2</sup>  
 , Dale Fixsen<sup>2</sup>, Wen-Ting Hsieh<sup>1</sup>, Alan Kogut<sup>2</sup>  
 , Michele Limon<sup>2</sup>, S. Harvey Moseley<sup>2</sup>, Nicholas Phillips<sup>2</sup>  
 , Gideon Schneider<sup>1</sup>, Douglas Travers<sup>1</sup>, Edward Wollack<sup>2</sup>

<sup>1</sup>NASA, Goddard Space Flight Center, Detector Systems Branch, Code 553, Greenbelt, MD 20771, USA

<sup>2</sup>NASA, Goddard Space Flight Center, Observational Cosmology Laboratory, Code 665, Greenbelt, MD 20771, USA

We discuss general system architectures and specific work towards precision measurements of Cosmic Microwave Background (CMB) polarization. The CMB and its polarization carry fundamental information on the origin, structure, and evolution of the universe. Detecting the imprint of primordial gravitational radiation on the faint polarization of the CMB will be difficult. The two primary challenges will be achieving both the required sensitivity and precise control over systematic errors. At anisotropy levels possibly as small as a few nanokelvin, the gravity-wave signal is faint compared to the fundamental sensitivity limit imposed by photon arrival statistics, and one must make simultaneous measurements with large numbers, hundreds to thousands, of independent background-limited direct detectors. Highly integrated focal plane architectures, and multiplexing of detector outputs, will be essential. Because the detectors, optics, and even the CMB itself are brighter than the faint gravity-wave signal by six to nine orders of magnitude, even a tiny leakage of polarized light reflected or diffracted from warm objects could overwhelm the primordial signal. Advanced methods of modulating only the polarized component of the incident radiation will play an essential role in measurements of CMB polarization.

One promising general polarimeter concept that is under investigation by a number of institutions is to first use planar antennas to separate millimeter-wave radiation collected by a lens or horn into two polarization channels. Then the signals can be fed to a pair of direct detectors through a planar circuit consisting of superconducting niobium microstrip transmission lines, hybrid couplers, band-pass filters, and phase modulators to measure the Stokes parameters of the incoming radiation.

PAPPA (Primordial Anisotropy Polarization Pathfinder Array) is a project to validate such concepts for measuring CMB polarization in a balloon flight environment. PAPPA will consist of 32 independent polarimeters-on-a-chip based on superconducting microstrip circuits. For laboratory characterization of microstrip components, we have designed and fabricated test circuits with a planar antenna and RF choke on thin silicon cantilevers that act as waveguide probes. The design makes possible efficient coupling of radiation between waveguide and the planar circuits, and enables S-parameter measurements to be made to characterize and refine building blocks for a polarimeter-on-a-chip.





Session J/B2, 13:15 – Wed.

**FOCAL PLANE ARRAY  
TECHNOLOGY**

Co-Chairs: Y. Rahmat-Samii, C. Walker

J/B2

DIRECT DETECTION SUBMILLIMETER SPECTROSCOPY AT  
CORNELL UNIVERSITY

Stacey, G.J., Hailey-Dunsheath, S., Nikola, T.,  
Oberst, T., Parshley, S.C.

Department of Astronomy, Cornell University, Ithaca, NY 14853

We present an overview of the direct detection submillimeter spectroscopy that is the focus of our research group at Cornell University. Direct detection spectrometers provide an important complement to heterodyne receivers in the submillimeter windows. For velocity resolved profiles of Galactic sources, heterodyne systems are the receivers of choice. However, for sources with line widths that are well matched to their resolving power (e.g. external galaxies), direct detection spectrometers can provide superior sensitivity. They also can deliver very wide spectral bandwidths and/or widefield spectroscopic imaging. At Cornell, we have constructed two direct detection spectrometers, the South Pole Imaging Fabry-Perot Interferometer (SPIFI), and the redshift (z) and Early Universe Spectrometer (ZEUS).

SPIFI is an imaging Fabry-Perot that has been deployed on both the 15 m JCMT on Mauna Kea, and the 1.7 AST/RO telescope at the South Pole. Our results with SPIFI include mapping of the 370  $\mu\text{m}$  [CI] and CO(7-6) lines from several star-forming galaxies (e.g. NGC 253 and the Antenna Galaxy), and the Galactic Center. These lines trace the physical conditions of the warm neutral ISM, and are important coolants for this component. Among the more interesting results at JCMT is the discovery that much of the molecular ISM in the starburst nucleus of NGC 253 is heated by cosmic rays. SPIFI wintered over on the AST/RO telescope during the 2005 season, during which we detected the 205  $\mu\text{m}$  [NII] line from the Carina Nebula. The [NII] line is an important coolant for the diffuse ionized ISM, and (together with the 122  $\mu\text{m}$  [NII] line) is an excellent probe of gas density. This is the first (or nearly the first) detection of this line from the ground, and demonstrates the utility of Antarctic sites for THz spectroscopy.

ZEUS is a submillimeter grating spectrometer that had its first engineering run at the JCMT in March of 2005. Since it is a spectral multiplexer, ZEUS is optimized for detection of faint broad lines from point sources such as distant galaxies. Our primary goal with ZEUS is to detect the 158  $\mu\text{m}$  [CII] fine structure line emission from distant submillimeter bright galaxies. This line is typically the strongest cooling line from atomic clouds and photodissociation regions, and traces the strength of the ambient interstellar radiation field in galaxies. ZEUS can detect this line from star forming galaxies at redshifts from 1 to 4 as it is redshifted into the 350, 450, 620 and 850  $\mu\text{m}$  telluric windows. We hope to have science runs with ZEUS at the CSO and SMT in early 2006.

We finish our talk with a discussion of the prospects for a 25 m class submillimeter telescope on a high peak near the ALMA site.

This work was supported by NSF grants OPP-0094605, OPP-0338149, AST-0096881, AST-0352855, and NASA grant NGT5-50470.

## Z-SPEC: A BROADBAND MILLIMETER-WAVE SPECTROMETER

Glenn, J.<sup>1</sup>, Ade, P.A.R.<sup>2</sup>, Aguirre, J.<sup>1</sup>  
 , Battle, J.<sup>3</sup>, Bock, J.J.<sup>3</sup>, Bradford, C.M.<sup>3</sup>  
 , Dragovan, M.<sup>4</sup>, Duband, L.<sup>5</sup>, Earle, L.<sup>1</sup>  
 , Hristov, V.<sup>4</sup>, Maloney, P.<sup>1</sup>, Matsuhara, H.<sup>6</sup>  
 , Naylor, B.<sup>4</sup>, Nguyen, H.<sup>3</sup>, Wood, C.<sup>1</sup>, Zmuidzinas, J.<sup>4</sup>

<sup>1</sup>University of Colorado

<sup>2</sup>Cardiff University

<sup>3</sup>Jet Propulsion Lab

<sup>4</sup>California Institute of Technology

<sup>5</sup>Commissariat à l'Énergie Atomique, France

<sup>6</sup>Institute of Space and Astronautical Science, Japan

Z-Spec is a broadband millimeter-wave spectrometer that is designed to serve two purposes: first, to measure redshifts of extremely luminous, dusty, high-redshift galaxies (submillimeter galaxies) to probe the cosmic history of star formation and super-massive black hole growth and second to demonstrate a compact waveguide-coupled diffraction grating technology for future space-borne far infrared platforms. Z-Spec has an instantaneous band from 0.97 mm (310 GHz) to 1.54 mm (195 GHz), matched to the 1 mm atmospheric transmission window. The corresponding spectral resolution range is 250 to 400, respectively. For the redshift range  $1 \leq z \leq 3$ , two to four CO lines will be present in the band, enabling unambiguous redshift determinations. At higher redshifts, lines of [CII], [NII], and [OI] will fall within the bandpass. The broad, instantaneous bandwidth will enable simultaneous calibration of all the spectral lines, eliminating a source of uncertainty in line fluxes.

Z-Spec's spectral resolution is achieved with a compact, waveguide-coupled Rowland diffraction grating with dimensions of 62 cm by 48 cm by 3.3 cm; it is a compromise between maximum desirable resolution (800 to resolve lines of galaxies) and a realistic cryogenic volume. The feedhorn-fed grating is comprised of a parallel-plate waveguide coupled to tapered rectangular waveguides that terminate at an array of 160 bolometers. Simulations of the electromagnetic propagation in the parallel-plate waveguide, the tapered waveguides, and the coupling between them were used to optimize the resolution and end-to-end optical efficiency, two challenging aspects of the system. The expected millimeter-wave background led to bolometer design NEPs of  $4 \times 10^{-18}$  W Hz<sup>-1/2</sup>, which necessitated a 50 mK base temperature. This is achieved with an adiabatic demagnetization refrigerator backed by a <sup>4</sup>He/<sup>3</sup>He sorption refrigerator. The grating, which we have dubbed WaFIRS (Waveguide Far-Infrared Spectrometer), serves as a proof-of-concept for future far-infrared space platforms, including the 3.5-meter Japanese satellite SPICA and SAFIR.

We had an engineering run at the Caltech Submillimeter Observatory in June of 2005 and obtained spectra of a few evolved stars and the luminous infrared galaxy NGC 6240. Ultimately, we would like to observe with Z-Spec on the IRAM 30-meter telescope and the 50-meter LMT.

This work was supported in part by an NSF Career Grant and a Research Corporation Innovation Award to J.G., NASA grants NAG5-11911 and NAG5-12788, and matching funds from the University of Colorado, Boulder. L.E. gratefully acknowledges a NASA GSRP Fellowship.

## SCUBA-2 FOCAL PLANE ARRAYS

William Duncan<sup>1</sup>, Kent Irwin<sup>1</sup>, Gene Hilton<sup>1</sup>  
 , Carl Rentsiema<sup>1</sup>, Leila Vale<sup>1</sup>, Yizi Xu<sup>1</sup>  
 , Peter Ade<sup>3</sup>, Adam Woodcraft<sup>3</sup>, Dan Bintley<sup>3</sup>  
 , Rashmi Sudiwalla<sup>3</sup>, Cynthia Hunt<sup>3</sup>  
 , Mark Halpern<sup>5</sup>, Wayne Holland<sup>2</sup>, Michael MacIntosh<sup>2</sup>  
 , Anthony Walton<sup>4</sup>, William Parkes<sup>4</sup>, Camelia Dunare<sup>4</sup>

<sup>1</sup>NIST, 325 Broadway, Boulder, CO 80305, USA

<sup>2</sup>UKATC, Royal Observatory, Blackford Hill, Edinburgh EH9 3HJ, Scotland, UK

<sup>3</sup>Cardiff School of Physics and Astronomy, Cardiff Univeristy, 5, The Parade, Cardiff CF24 3YB, Wales, UK

<sup>4</sup>The Scottish Microelectronics Centre, The Kings Buildings, West Mains Rd., Edinburgh EH9 3JF, Scotland, UK

<sup>5</sup>Univerisity of British Columbia, 6224 Agricultural Rd., Vancouver, B.C., V6T 1Z1, CANADA

We describe the SCUBA-2 focal plane arrays, their construction, performance and the focal plane environment. SCUBA-2 is a submm camera designed to be operated on the James Clerk Maxwell Telescope in Hawaii. The camera will have two focal planes operating simultaneously imaging the sky at 850 and 450 microns. Each focal plane will consist of 4 sub-arrays of a total pixel count of 5120 per focal plane and 10,240 for the whole camera. A subarray is 32 columns by 40 rows. A sub-array is made of two parts, a multiplexer and a detector hybridised together by indium bump bonding (0.25 million bonds) to provide electrical, thermal and mechanical support. The multiplexer uses time division implemented with one active SQUID switch per pixel. In addition there are dummy SQUID switches to help control crosstalk. The detector array consists of pixels 1mm sq. deep etched into a silicon wafer which is an odd number of wavelengths (in silicon) thick. The front surface of the pixel is ion implanted to give 400 ohm per sq. and the back of the pixel is completely covered with the detector metalization to form a back short. To achieve thermal isolation a pixel is suspended on a 0.5 micron thick silicon nitride membrane which is 10 microns wide. The detectors are transition edge bolometers with NEP's of  $6 \times 10^{-17}$  watts/sqrt(Hz). Each pixel has a heater used to provide thermal power to help bias the pixels into the transition region. In operation, the heater power will be adjusted to compensate for the varying sky loading and hence keep the detector responsivity and array flat field constant.

## AN UPDATE ON THE PENN ARRAY RECEIVER.

Simon Dicker<sup>1</sup>, Mark Devlin<sup>1</sup>, Ben Werner<sup>1</sup>  
, Phil Korngut<sup>2</sup>, Brian Mason<sup>2</sup>, Dominic Benford<sup>3</sup>  
, Kent Irwin<sup>4</sup>, Carole Tucker<sup>5</sup>, Peter Ade<sup>5</sup>

<sup>1</sup>University Of Pennsylvania, 209 S. 33rd St, Philadelphia, PA 19147, USA

<sup>2</sup>National Radio Astronomy Observatory, Green Bank, WV 24944, USA

<sup>3</sup>Goddard Space Flight Center, Greenbelt, MD 20771, USA

<sup>4</sup>National Insitute of Standards and Technology, 325 Broadway, Boulder, CO 80303, USA

<sup>5</sup>Cardiff University, 5 The Parade, Cardiff, CF24 3YB, UK

The Penn Array Receiver is a 64 element array designed to work at 90 GHz. It will be deployed on the 100 meter Green Bank Telescope (GBT) in February of 2006. Each array element is a Transition edge sensor (TES) bolometer. No feed horns are used, instead cooled high-density polyethylene lenses and a cold (3 K) Lyot stop control the illumination of the telescope. Capacitive mesh filters act as IR blockers and define a bandpass of 86–94 GHz. The array elements are spaced by  $0.5f\lambda$  so that the sky is fully sampled in a single pointing of the GBT. This significantly simplifies the scanning patterns needed for sparser arrays. On a telescope the size of the GBT this is a significant advantage.

Each detector is expected to be background limited by the random arrival of photons. The best observing conditions at the GBT are winter nights when we expect to be able to map a 5 arcminute square of sky to  $80 \mu\text{Jy}$  in one hour at a resolution of 8 arcseconds.

The detectors are cooled to 0.25 K using a pulse tube cooler and helium sorption refrigerators. The cryogenics along with all the electronics, and the computer system have been successfully operated on the GBT. By February, detailed tests on the response of the detectors will allow us to further develop the data processing techniques needed to remove atmospheric noise from the data and beam measurements of the cryostat will confirm that the optical design is correct. We are also developing better control software to automatically bias the SQUID multiplexed readout which currently must be set up by hand.

DESERT STAR AND SUPERCAM: HETERODNE ARRAY RECEIVERS FOR THE 870 MICRON ATMOSPHERIC WINDOW ON THE HEINRICH HERTZ TELESCOPE

Christopher Groppi<sup>1</sup>, Christopher Walker<sup>1</sup>, Craig Kulesa<sup>1</sup>,  
 , Dathon Golish<sup>1</sup>, Abby Hedden<sup>1</sup>, Patrick Puetz<sup>1</sup>,  
 , Paul Gensheimer<sup>1</sup>, Christian Drouet d'Aubigny<sup>1</sup>, Shane Bussmann<sup>1</sup>,  
 , Jacob Kooi<sup>2</sup>, Arthur Lichtenberger<sup>3</sup>, Sander Weinreb<sup>2,5</sup>,  
 , Niklas Wadefalk<sup>2</sup>, Joseph Barden<sup>2</sup>, Glenn Jones<sup>2</sup>,  
 , Gopal Narayanan<sup>4</sup>, Ton Kuiper<sup>5</sup>

<sup>1</sup>University of Arizona

<sup>2</sup>California Institute of Technology

<sup>3</sup>University of Virginia

<sup>4</sup>University of Massachusetts

<sup>5</sup>NASA Jet Propulsion Laboratory

We present two heterodyne array receivers built for the Heinrich Hertz Telescope and the 870  $\mu\text{m}$  atmospheric window. These instruments have been optimized for wide-field spectroscopic imaging, in particular molecular Galactic plane surveys. DesertStar is a 7 pixel system based on discrete, tunerless mixer technology. This system saw first light in 2003, and is entering routine operation in fall, 2005. The instrument offers  $\sim 55\text{K}$  DSB receiver noise temperatures, a 2 GHz instantaneous bandwidth, and is tunable from 315-375 GHz. The LO source is a Virginia Diodes synthesizer driven planar diode multiplier chain that delivers at least 1 mW across the band. The array is flood illuminated with a large LO beam, making complicated LO diplexing unnecessary. The initial backend is a filterbank spectrometer that offers 8, 256 MHz channels and 1 MHz resolution. DesertStar will increase imaging efficiency at the HHT by more than an order of magnitude over the existing dual polarization receiver system. SuperCam is a 64 pixel array receiver, which will use integrated mixer technology. This receiver, begun in fall, 2004, has a focal plane based on 1x8 mixer modules, with integrated MMIC low noise amplifiers. Each waveguide mixer is based on the proven DesertStar design, but eight are integrated into a single block. Eight MMIC LNA modules are also mounted in the block, with an integrated bias tee and input matching network. These LNA modules offer  $\sim 30$  dB of gain, a 2-9 GHz IF, and  $\sim 5\text{K}$  noise temperature, while dissipating only  $\sim 5$  mW of heat. The mixer module is designed to use blind-mate connectors to allow easy assembly and service. Cryogenics are provided by a Sumitomo closed cycle 4K cryocooler augmented with a CTI 15K cryocooler for dedicated cooling of the IF semirigid cable. The local oscillator is a Virginia Diodes system similar to the DesertStar source, but designed for higher power and moderate-bandwidth. A waveguide LO diplexer will divide the LO into 64 beams with precisely defined optical properties and power balance. For a wide field of view, the instrument will be mounted at the cassegrain focus of the telescope. A new  $f/7$  composite secondary will be fabricated to replace the existing  $f/13.8$  secondary during SuperCam operation. A two-lens AR-coated reimaging system will then reduce the  $f/7$  telescope beam to  $f/5$  to match the focal plane. The backend will be either a 64 channel  $\times$  1 GHz/512 MHz correlator with 1024 lags per channel, or a 64 channel  $\times$  512 MHz realtime FFT system based on high speed digitizers and FPGAs. We hope to have the system ready for first light with one 1x8 mixer module in fall, 2006, with the full array completed by fall, 2007.

## COMMISSIONING OF HARP-B - A HETERODYNE ARRAY RECEIVER FOR JCMT

Bell, G.S.<sup>1</sup>, Buckle, J.V.<sup>1</sup>, Dent, W.R.F.<sup>2</sup>, Hills, R.E.<sup>1</sup>, Redman, R.O.<sup>3</sup>, Richer, J.S.<sup>1</sup>, Smith, H.<sup>1</sup>

<sup>1</sup>MRAO, Cavendish Laboratory, Cambridge, England

<sup>2</sup> UK Astronomy Technology Centre, Edinburgh, Scotland

<sup>3</sup>National Research Council of Canada, HIA, Victoria, Canada

A new receiver for the James Clerk Maxwell Telescope, with sixteen SIS mixers forming a four by four array and covering the frequency range 325 to 375GHz, has been constructed and is presently under test. It is due to be installed and commissioned on the JCMT by the end of 2005. The instrument includes a cooled quasi-optical single-sideband filter and a highly efficient arrangement for coupling the local oscillator into the mixers. There is a very complete control and monitoring system which provides full operation and (in principle) fault diagnosis from a remote location. It will be operated with the JCMT's new backend, ACSIS, which provides 1.8GHz of bandwidth on each of the 16 pixels.

The presentation will include an outline of the design, but, given that the main elements of the instrument have been described at earlier conferences, the focus here will be on the recent work on testing and commissioning the receiver. In particular it is intended that there will be discussion of which things worked well and which caused the main problems.

At the time of writing a large amount of laboratory test data has been obtained. This includes detailed measurements of the beam patterns, both in the far field and at its transform (the pupil plane in optical terms), and of the spectral purity and stability, in addition to the conventional parameters like receiver noise temperature. The highlights from these results will be shown, together with a description of the techniques used to obtain them. The experiences at the telescope will also be described, and it is hoped that it will be possible to complete the report with some results from the initial astronomical observations.



## THE 1.4 METER TELESCOPE DESIGN FOR THE Q/U IMAGING EXPERIMENT

William A. Imbriale

JPL, California Institute of Technology

This paper describes the optics design of the 1.4 meter telescope for the Q/U Imaging Experiment (QUIET) intended to image the polarization of the cosmic microwave background (CMB) with detectors at two frequencies with unprecedented sensitivity. Observing the polarization of the CMB demands exquisite sensitivity to both Q and U Stokes parameters and freedom from systematic errors. QUIET makes use of recent breakthroughs in millimeter-wave circuit packaging to enable large arrays of radiometers or polarimeters for modest cost. Modules based on IC-style packaging with waveguide inputs provide fully functional pseudo correlation polarimeters capable of detecting Q and U simultaneously. The feeds themselves are corrugated horns built up from stacked platelets, each with an array of holes, defining one groove in each feed.

This paper is follow-on to Imbriale, RF Optics Design for the Q/U Imaging Experiment, URSI 2005, which described a one and two-meter telescope design. A 1.4 meter minor axis is the largest mirror that can be accommodated on the available milling machine and will be the most cost effective prototype telescope. In addition, the window on the cryostat is now 18 cm thick, necessitating a telescope redesign to keep the rays on the main mirror from vignetting. The 1.4 meter design will accommodate 200 feeds at W-band (80-105 GHz) and 37 at Q-band (38-40 GHz). The corrugated horn feeds have a 1.4 inch (3.55 cm) outer diameter at W-band and a 3 inch (7.62cm) outer diameter at Q-band.

A side fed Cassegrainian design was selected because of its excellent cross-polarization and wide angle scan performance. An extremely large and flat field of view is realized with an angular extent of over 12 on the sky. At W-band the beam size is 0.22 degrees and at Q-band the beam size is 0.5 degrees.

## SIS FOCAL-PLANE ARRAY RECEIVER FEATURING SIDEBAND SEPARATION MIXERS

Narayanan, G., Erickson, N. R., Grosslein, R. M.,  
Deshpande, P., Fath, V.

Department of Astronomy, University of Massachusetts, Amherst, MA  
01003

A dual polarization 16-pixel heterodyne focal-plane array receiver is proposed to be built to operate in the 210 – 275 GHz ( $\sim$  1mm wavelength band) atmospheric window for use on the Large Millimeter Telescope (LMT). The LMT is a 50 m diameter millimeter-wavelength telescope being built in Mexico as a joint project between UMass and Instituto Nacional de Astrofisica, Optica, y Electronica (INAOE) in Mexico. Each pixel of the proposed focal-plane array receiver will feature SIS mixers operated in a novel sideband-separation mode with wideband low-noise IF amplifiers (4 – 12 GHz). In this paper, we will present design details, test results, and characterization of the components that make up the novel array mixer-block.

The array mixer-block is a highly integrated assembly, that has been optimized for use and integration into a  $4 \times 4$  array. The heart of each pixel in the array is mixer-preamplifier (MPA) block. The MPA is a split-block machined component, that consists of an input RF  $90^\circ$  waveguide hybrid, a dual-directional LO coupler, two SIS junctions, two hybrid IF LNAs (Low-Noise Amplifiers) with a IF 3dB  $90^\circ$  Lange coupler interspersed between the stages. Two SMA outputs from the mixer block bring out the separated upper and lower sidebands. Two magnetic coils that are used to suppress Josephson noise are also embedded in this integrated mixer-preamplifier (MPA) block. A new hybrid IF LNA with a discrete JFET followed by a MMIC amplifier has been designed, fabricated and tested. The integrated IF LNA which is well-matched to the IF output of the SIS mixer eliminates the need for wideband cryogenic isolators. The integrated implementation of the IF Lange hybrid coupler between the stages of the hybrid IF LNAs considerably eases the amplitude and phase balance requirements of components in the rest of the IF chain.

## FPGA-BASED SPECTROMETERS, BEAM FORMERS, AND CORRELATORS

Chen, H.<sup>1</sup>, Droz, P.Y.<sup>2</sup>, Parsons, A.<sup>2</sup>,  
Backer, D.<sup>2</sup>, Chang, C.<sup>4</sup>, Chapman, D.<sup>5</sup>,  
de Jesus, C.<sup>5</sup>, MacMahon, D.<sup>3</sup>, Siemion, A.<sup>5</sup>,  
Werthimer, D.<sup>1</sup>, Wright, M.<sup>3</sup>

<sup>1</sup>University of California, Berkeley, Space Sciences Laboratory

<sup>2</sup>University of California, Berkeley, Astronomy Department

<sup>3</sup>University of California, Berkeley, Radio Astronomy Laboratory

<sup>4</sup>University of California, Berkeley, Berkeley Wireless Research Center

<sup>5</sup>University of California, Berkeley

We describe the design of real-time high-bandwidth spectrometers, beam formers, correlators, and imagers based on the recent development of a unified computational platform for high-performance signal processing that has enabled the rapid implementation of these instruments within a short timeframe. The instruments are built around field programmable gate arrays (FPGAs) and thus are dynamically reconfigurable, which allows the different applications to share a common hardware base. In addition, the concurrent creation of a complete supporting design flow speeds up application development for use on the hardware platform, while platform-independent parameterized signal processing algorithms and libraries keep core designs reusable. Along with standardized interconnect hardware and abstracted data interface protocols, a single hardware setup at a given location can even be time-shared between different applications as different instruments. The ability afforded by this architecture to focus on the data processing aspects of an instrument around a fixed platform has allowed our group to develop and deploy a number of instruments—three spectrometers, a VLBI data recorder, and several different approaches at a modular, expandable correlator in the time span of less than a year. With each module capable of up to one trillion operations per second (1 Top/s) and supporting packet-switched data transfer, the platform is well-suited for use at antenna arrays, where it is advantageous to have data-processing elements with high computational density that are easily scaled and can be dynamically reallocated. We present the architectures of current applications to demonstrate the flexibility and scalability of the system for highly-parallel, high-throughput, real-time signal processing. Characteristics of the instruments addressing the needs of large arrays of antennas are highlighted.

## SPHERICAL REFLECTOR ANTENNAS WITH COMPENSATING ARRAY FEED FOR EXTREMELY LARGE NUMBER OF SCANNED BEAMS

Keyvan Bahadori, Yahya Rahmat-Samii  
University of California Los Angeles

Radar remote sensing of the atmosphere and severe storms from geostationary orbit is highly desirable due to the radar ability to simultaneously provide vertical rainfall profiles, large spatial coverage, and frequent observation. With the rapid advances in radar technology, the feasibility of developing such an instrument has greatly improved. Under NASA's Earth Science Technology Program, a novel instrument concept and the associated antenna technologies are currently evaluated for 35 GHz Doppler radar for detailed monitoring of hurricanes and severe storms from a geostationary orbit. One of the main challenges is the very large distance between radar in the geostationary orbit and cloud levels. This requires a very large antenna (28 meter) for both sensitivity and surface clutter considerations. To minimize surface clutter a horizontal resolution of 12 km or better is required. In addition, it is required to scan the beam of the antenna to cover an angular range of 4 degrees which translates into an unconventionally large number of 200 beamwidths. The operational frequency band has been chosen as the Ka-band in order to compromise between antenna size and atmospheric attenuation.

Considering the required size of antenna aperture, using electronically scanned array antenna seems to be formidable and almost impractical for this application. The first feasible candidate that comes to mind is a single or multiple parabolic reflector antennas. As it is known, parabolic reflector antennas suffer from severe limitation when the beam is scanned a large number of beamwidths. Implementing a focal plane array to compensate for off-axis performance of parabolic reflectors could also become an expensive proposition because it necessitates the usage of an array which must be capable of adaptively varying its excitation coefficients for different beam look angles. Another candidate for this design is a spherical reflector antenna which is inherently capable of scanning its beam to any desired direction without degradation of the quality of the radiation performance. However, a spherical reflector antenna with a single feed typically suffers from a significant amount of spherical aberration.

To overcome the performance degradation induced by this aberration, the utility of using planar array feeds for correcting spherical phase aberrations is investigated in this paper. Two different methodologies are developed for the array excitation coefficients determination based on phase conjugate matching and the results are compared. Using the compensating feed array, the radiation characteristics of the compensated spherical reflector are simulated for no scan and large scan cases and the results are compared with the uncompensated case to show performance improvement. To demonstrate the technological readiness of the concept, a 1.5 m breadboard model is also designed to be built for experimental measurements. In order to evaluate the effects of manufacturing errors on the reflector performance, several scenarios of errors in feed positioning and complex excitation coefficients of the compensating array feed are also modeled and their effects are simulated.

Session K1, 08:35 – Wed.

**EM INTERACTION OF UWB AND  
NARROWBAND ANTENNAS  
WITH THE HUMAN BODY**

Co-Chairs: G. Lazzi, E. Topsakal



## ON RESPIRATION-RATE ESTIMATION USING IMPULSE-BASED ULTRA-WIDEBAND (UWB)

S. Venkatesh, C. R. Anderson, N. V. Rivera , R. M. Buehrer  
Mobile and Portable Radio Research Group (MPRG), Virginia Tech,  
Blacksburg, VA 24060, USA.

The non-invasive monitoring of respiration-rate has potential applications in health monitoring, hostage rescue, triage and athletic performance monitoring. The use of impulse-based UWB signals in the robust detection of chest-cavity motion and the accurate estimation of respiration and heart-beat rates, even in the presence of physical obstructions between the subject and the UWB antennas, was demonstrated in [1]. Signal processing algorithms were developed to estimate respiration and heart rates and their accuracy was demonstrated using measurements.

The coefficient of reflectivity of air-to-dry-skin interface for electromagnetic waves in the 300-900 MHz range is about 72%. Due to this, and the high spatial resolution of UWB signals, the motion of a human body can cause observable changes to the multipath profile. It was shown that [1] the expansion of the chest cavity creates a significant variation in the measured multipath profile, which is exploited to estimate the respiration and heart rates.

A problem fundamental to the modeling of respiration and heart-rate estimation is the estimation of the frequency of a single-tone in additive-white Gaussian noise (AWGN), given discrete-time samples over a finite measurement interval. It can be shown that the algorithm derived in [1] represents the Maximum-Likelihood (ML) estimator [2] of the respiration rate, which, for large data sets and “high” signal-to-noise-ratios, approaches the Cramer-Rao lower bound. In the current work, the performance of this estimator is analyzed in UWB propagation environments, and results of the application of these methods to real measured data are presented.

Due to the time-sensitive and non-invasive nature of the aforementioned applications, the total measurement time needs to be minimized while ensuring that the respiration-rate estimate is sufficiently accurate. An investigation into the resulting trade-offs and the computation of “optimal” measurement times is also presented.

## References

- [1] S. Venkatesh, C.R. Anderson, N. V. Rivera, R. M. Buehrer, “Implementation and Analysis of Respiration-rate Estimation using Impulse-based UWB”, *To appear in the Proceedings of the 2005 IEEE Military Communications conference (MIL-COM 2005)*.
- [2] D. Rife and R. Boorstyn, “Single tone parameter estimation from discrete-time observations”, *IEEE Transactions on Information Theory*, vol. 20, no. 5, pp. 591 - 598, September 1974.

## ANALYSIS OF A FLOATING SLEEVE ANTENNA FOR LOCALIZED HEPATIC ABLATION

Converse, M.C.<sup>1</sup>, Yang, D.<sup>2</sup>, Bertram, J.M.<sup>3</sup>,  
O'Rourke, A.P.<sup>1</sup>, Webster, J.G.<sup>3</sup>, Hagness, S.C.<sup>2</sup>,  
Will, J.A.<sup>4</sup>, Mahvi, D.M.<sup>1</sup>

<sup>1</sup>Department of Surgery, School of Medicine, University of Wisconsin

<sup>2</sup>Department of Electrical and Computer Engineering, College of Engineering, University of Wisconsin

<sup>3</sup>Department of Biomedical Engineering, College of Engineering, University of Wisconsin

<sup>4</sup>Department of Animal Health and Biomedical Sciences, School of Veterinary Science, University of Wisconsin

Microwave ablation (MWA) is a promising technology for the treatment of liver tumors. MWA utilizes electromagnetic waves to heat tissue to high temperatures, thereby destroying all the cells in the heated region. The heated region ideally includes the tumor along with a 1 cm margin of normal hepatic tissue. This technology has been used successfully in both intra-operative and percutaneous approaches for primary hepatocellular carcinoma and hepatic metastasis of colorectal carcinoma. A persisting problem with the existing technology is the control of the region of microwave absorption and the heating distribution during interstitial MWA. The design of the antenna determines the shape of the energy deposition pattern and an improperly designed antenna can lead to significant power reflection and heating along the antenna.

We have designed, analyzed, and experimentally tested a novel interstitial antenna for hepatic microwave ablation. The antenna consists of a coaxial dipole antenna with a floating metal sleeve that is electrically isolated from the outer conductor of the coaxial feedline. The sleeve is used to prevent propagation of the EM wave along the outside of the coaxial feed and thereby reduce backward heating along the feedline. Simulations of the antenna suggest that this design achieves a highly localized SAR pattern that is independent of insertion depth and is well matched to normal liver tissue at 2.45 GHz. Experimental measurements of the input reflection coefficient of the antenna inserted into *ex vivo* liver tissue are in good agreement with the simulated results. *Ex vivo* liver ablation experiments demonstrate that the floating sleeve antenna achieves a highly localized ablated region in the liver.

The design process and optimized antenna design indicates that the length of the sleeve is critical to the localization of the SAR pattern. We examine the reasons for this and the importance of the electrical isolation of the sleeve from the outer conductor. We also examine the performance of the antenna when it is immersed in tissue exhibiting a range of dielectric properties. The liver is a fairly homogeneous medium but we expect some difference in the dielectric properties of the tumor into which the antenna is inserted, relative to the surrounding normal tissue. Preliminary work has also indicated changes in the complex permittivity with temperature and level of tissue desiccation. An ideal antenna design would maintain a favorable SAR pattern for a wide range of tissue permittivities.



## ABSORPTION IN HUMAN TISSUES DUE TO THE BODY-WORN UWB ANTENNAS

Maciej Klemm, Gerhard Troester

Electronics Laboratory, Swiss Federal Institute of Technology (ETH)  
Zurich

### ABSTRACT

Due to the rapid development of wireless technologies, new frequency bands in the microwave region operating at higher frequencies up to 10 GHz have been opened up. Currently, these frequencies are mainly used for wireless local networks, but their range of application extends to health support systems or consumer electronics in general. These devices may operate in the immediate vicinity of the human body, and they are a part of the so-called Wireless Body Area Network (WBAN). Ultra-wideband (UWB) technology is a promising candidate for future WBANs, due to its low-power operation.

In this paper we investigate electromagnetic energy absorption in human tissue due to the body-worn UWB antennas, between 3 GHz and 8 GHz. The aim is to examine energy absorption, depending on a composition of the human body model, and also on the antenna type. We compare results obtained for homogeneous muscle tissue model layered (skin, fat, muscle) model. Planar and cylindrical models are used, representing different part of the human body. For the layered model, thickness variations of the skin (0.5-2mm) and fat (3-20mm) are considered. Regarding UWB antennas, we consider different types of antennas, e.g. omni-directional UWB monopole and slot antennas, as well as the low-profile directional UWB antenna, designed specially for UWB WBANs applications. We investigate only very close (near-field) distances between the body and antennas, between 2 and 10 mm (reflecting realistic WBAN scenarios).

We will show that the absorption mechanism of the electromagnetic energy is differs significantly, between homogeneous and layered human body models, for frequencies between 3 and 8 GHz. This conclusion is clear when one looks at the peak SAR values (without mass averaging). However, for averaged SAR, these differences are not so pronounced, due to the averaging process. Additionally, we will present variation in the transmit transfer function of different UWB antennas, depending on the antenna type and distance to the body model. Transfer function is the most relevant parameter in characterizing UWB antennas; therefore these results are crucial for understanding of the human body impact on the performance of UWB antennas.

## ON THE CONVERGENCE CHARACTERISTICS OF MATRIX SOLVERS FOR IMPLANTABLE ANTENNAS

Topsakal E., Pvallalta J.,  
Mississippi State University

The finite element-boundary integral method (FE-BI) has been very attractive for scattering and radiation analysis of antennas. As is well-known, the final FE-BI system is complex valued, non-symmetric and partially sparse. Solution of these types of matrices is often performed using iterative solvers [1]. Research on developing solvers for such systems is still active. In this study, we consider the non-stationary Krylov subspace based iterative solvers for the FE-BI simulation of implantable antennas. Today, implantable antennas are increasingly used in medical fields. Some of the applications include cardiac pacemakers, radio frequency identification (RFID), ultra low power wireless devices for in-body monitoring, muscle stimulators, electromagnetic hyperthermia for cancer treatment etc. Numerical simulation tools that are fast and accurate are crucial in developing reliable and efficient implantable antenna systems. Solvers play an important role in the convergence characteristics and mainly determine the total solution time for a given problem. Therefore, it is very crucial to investigate and understand the convergence behaviour of these solvers.

First, we consider an implantable antenna that was designed for the 402-405 MHz Medical Implant Communications Service band (MICS). The antenna was embedded in the forearm at different locations. Then the performance of various solvers such as BiConjugate Gradient (BICG), Conjugate Gradient Squared (CGS), Quasi-Minimal Residual (QMR) and Generalized Minimal Residual (GMRES) were investigated for preconditioned and non-preconditioned cases. Incomplete LU and diagonal preconditioners were chosen for this study. Results regarding the convergence characteristics of these solvers as a function of the antenna location were obtained and will be discussed in detail.

[1] E. Topsakal, R.W. Kindt, K.Sertel and J.L. Volakis, Evaluation of the BICGSTAB(1) Algorithm for the Finite- Element/ Boundary-Integral Method, IEEE Antennas and Propagation Magazine, vol. 43, no. 6, December 2001.

Session K2, 13:15 – Wed.

**ADVANCES IN MEDICAL  
APPLICATIONS AND BIOLOGICAL  
EFFECTS OF ELECTROMAGNETIC  
FIELDS**

Co-Chairs: F.S. Barnes, T.S. Ibrahim



## A REVIEW OF THE USES OF ELECTRIC AND MAGNETIC FIELDS FOR THERAPY

Barnes, F.S.

University of Colorado at Boulder

Electric and magnetic fields are finding increasing uses in medicine. In this paper we will review some of the areas electric and magnetic fields have been shown to be of significant value and some areas where the results are more speculative. Radio frequencies are used to provide localized hyperthermia in the treatment of some cancers in conjunction with X-rays and have been shown to increase the cure rate over X-rays alone. RF fields are also being used in electro-surgery, MRI and microwave imaging. Lower frequency fields have been shown to help with the repair of broken bones some of which had not healed with other treatments for as long as five years. Both pulses and sine waves tuned to values of  $(q/m)B$  for specific ions have been used successfully and a signal to noise ratio model has been developed that seems to explain why some signals work and others do not. Recent work indicates that electric fields may be useful in the repair of spinal cord injuries, other nerves and wound healing. Additional results indicate that magnetic fields can be used to reduce pain and that electric fields can both inhibit and enhance growth.

At the present time considerable effort is going into understanding the mechanism by which electric and magnetic fields effect biological processes. Biological complexity leads to a long chain of events to get from electric or magnetic field forces on charged particle through changes in chemical reaction rates to biological or health effects. Some of this work will be reviewed along with some of our recent results on the effects of these fields on white blood cells (neutrophils). In this work we have shown that DC and low frequency electric and magnetic field can change the speed and direction that neutrophils move in a concentration gradient of a chemo attractant. For RF field exposures we measure increases in speed that exceed those that can be obtained by increasing the temperature alone. This implies that something other than heating is being sensed by these cells that form an important part of our immune system.

## SAR REDUCTION TECHNIQUES FOR IMPLANTED PLANAR INVERTED F ANTENNAS

Jaehoon Kim, Yahya Rahmat-Samii  
University of California - Los Angeles

For telemedicine applications, active medical devices require a reliable communication link between internal and external devices for exchange of useful information through a human body. To build a reliable link, compact antennas should be designed and evaluated in terms of the radiation performances of the antennas inside a human body. Furthermore, it is needed to study if the active medical devices on which the designed antennas are mounted observe the important electrical regulations such as effective radiation power and specific absorption rate (SAR), etc.

For this study, the basic spiral planar inverted F antenna (PIFA) with superstrate dielectric layers is designed to operate at the medical implant communications service (MICS) frequency band (402 - 405 MHz) for ultra low power active medical implants. The numerical computational procedures (Annex E of Std. C95.3-2002) recommended by IEEE are applied to calculate spatial-average SAR for the implanted antennas located under the skin tissue whose thickness is less than 1 cm. Based on this study, this paper mainly deals with how to reduce SAR value for the spiral PIFA using finite difference time domain simulations.

To improve the SAR characteristic of the antenna, the spiral PIFA is redesigned in two ways: by modifying the radiators shape and by changing the dielectric layers thickness. The antenna uses the uniform width (2.5 mm) planar patches for the radiator and the thickness of the dielectric layers (substrate and superstrate) is 2.5 mm. Using the relationship between the radiation principle and SAR characteristics of PIFAs, the radiator is modified to have non-uniform width patches. Additionally, the dielectric layers play an important role in determining the antennas radiation characteristics because the antennas directly contact biological tissues which are normally high dielectric and lossy materials.

## AN IMPLANTABLE ANTENNA FOR WIRELESS DATA TELEMETRY

Topsakal, E. , Pvillalta, J.  
Mississippi State University

Wireless applications are increasingly used in the healthcare industry. The medical community is realizing the benefits of wireless technology in medical telemetry, which is used, for example, to monitor patients physiological parameters (e.g., cardiac signals, blood glucose, body temperature) over a distance via radio-frequency (RF) communications between a transmitter worn by the patient and a central monitoring station. Undoubtedly, this technology delivers mobility, comfort, and higher levels of patient care. As designers develop new implanted medical devices taking advantage of RF technology to improve the quality of care for patients, antennas are key to these new systems. Although the antennas and RF system design is well understood for today's telecommunication systems, their application in medical systems offer unique challenges. One of the main issues is power consumption, for the in-body monitoring systems for instance, the antenna used for the implantable device should be able to radiate outside the body and yet the power associated with the device must comply with the radiation requirements. Increased power levels might cause heating of the tissue and consequently a permanent tissue damage. Finally, it is important to design the antenna with a minimum interference with other electronic devices inside or outside the body.

In this study, we present a microstrip spiral antenna for the 402-405 MHz Medical Implant Communications Service band (MICS). The antenna is embedded in the forearm and simulations are carried out using a robust Finite Element Boundary Integral Technique. Results regarding the antenna return loss, near and far fields will be presented for variety of antenna locations.

USING  
DECOMPOSITION AND 3D MULTI-RESOLUTION IMPEDANCE  
METHOD FOR DETERMINING TIME DOMAIN VARIATIONS OF  
CURRENTS INDUCED IN THE HUMAN RETINA WHEN STIMU-  
LATED BY AN IMPLANTED ELECTRODE ARRAY

Carlos J. Cela, Randall P. Barlow, Gianluca Lazzi  
North Carolina State University

Retinal degenerative diseases such as Retinis Pigmentosa (RP) and Age Related Macular Degeneration (AMD) progressively disable photoreceptor cells and eventually lead to blindness. Clinical studies have observed that even when photoreceptor cells are no longer active the rest of the visual pathway remains intact. Furthermore, patients have reported seeing points of light in an otherwise blank visual field when probe electrodes were used to make current flow through the Ganglion Cell Layer of the retina. Taking advantage of the fact that the spatial location of the perceived light corresponds to the physical location of the electrical stimulus in the Ganglion Cell Layer, a retinal prosthesis is being developed to stimulate the human retina in a systematic way and therefore restore a limited form of vision. The electrical stimulation of the Ganglion Cell Layer is performed using an implantable electrode array positioned inside the eye, on the retina. It is important to know the values for the current densities present around each electrode, as this information can be used to determine placement of implant, efficient electrode shapes and sizes, optimal spacing between electrodes within the array, convenient location of the current return, as well as certain aspects of safety of the implant. Further, this information would link electrode shape and position to desired current density patterns in the ganglion and bipolar cell layers and it could be used to gain a better understanding on the effectiveness of such a retinal stimulation. In this work, an arbitrary stimulus signal is decomposed using the Fourier transform and applied to the model. 3D Multi-resolution meshing scheme and the Impedance Method are used then to determine the resulting time domain waveform in the Ganglion Cell Layer. Results related to the utilization of the proposed method for electrical stimulation of the human retina in a retinal prosthesis system to restore partial vision to the blind will be presented.



## SAR EVALUATION FOR MEDICAL IMPLANTS

Dagang Wu<sup>1</sup>, Ji Chen<sup>1</sup>, David Jackson<sup>1</sup>  
, Wolfgang Kainz<sup>2</sup>, Howard Bassen<sup>2</sup>

<sup>1</sup>University of Houston

<sup>2</sup>FDA

The calculation of SAR for implanted devices exposed to electromagnetic signals is an important one for ensuring device compatibility and FCC regulation compliance. However, the accurate calculation of SAR is quite difficult when the device contains insulated wires that are embedded within the human body, and especially when such wires end in an exposed tip that is in contact with biological tissue. The pacing lead of a cardiac pacing system is a typical example.

When exposed to an external RF field (e.g., the RF signal from an MRI RF coil or gradient coil), the embedded wire acts as an antenna and consequently picks up an induced current and charge density. The induced electric and magnetic fields vary inversely with distance from the wire axis, and therefore the electric field and SAR become high at the surface of the insulation surrounding the wire. An accurate calculation of the fields and the SAR near the wire is difficult, unless a very fine mesh is used.

The problem is even worse near an exposed tip, since the insulation is removed and the conductive tip is in contact with the biological medium. Very strong electric fields typically exist near exposed conductors that have a high degree of surface curvature, such as a small tip. Hence, the local SAR will also become very large as the tip is approached. However, attempts to directly calculate the average SAR tend to produce results of questionable accuracy since the rapidly varying singular fields near the tip are typically not accounted for in the SAR calculation.

This aim of our work is to develop an accurate SAR evaluation procedure for implanted devices within a biological medium. The device will have one or more insulated wires embedded within the medium that end in an exposed tip. The tip region may have an arbitrary configuration of metal and insulation that is specified. After the SAR is calculated, further modeling will be done in order to calculate the local temperature rise throughout the medium, including regions near the wires and tip.

## RECENT DEVELOPMENTS IN TISSUE SENSING ADAPTIVE RADAR

Sill, J.M., Williams, T.C., Fear, E.C.Department of Electrical Engineering, Schulich School of Engineering,  
University of Calgary

Tissue sensing adaptive radar (TSAR) has been proposed as a method for breast cancer detection (J.M. Sill and E.C. Fear, *Electronics Letters*, **41**, 113-115, 2005). This method exploits the hypothesized difference in electromagnetic properties of healthy and malignant breast tissues (S.C. Hagness et al, *IEEE Transactions on Biomedical Engineering*, **45**, 1470-1479, 1998). TSAR involves illuminating the breast with a pulse of microwaves, recording reflections, and isolating reflections from tumors. A focusing step provides a three-dimensional map indicating the location of strongly scattering objects. Several challenges are inherent in this technique. First, an ultra-wideband signal is used, as a bandwidth of several GHz is desired for reasonable resolution, while the upper frequency is limited due to increasing attenuation in tissues with frequency. The pulse used in TSAR is a differentiated Gaussian signal with significant energy content between 1.4 GHz and 8.7 GHz. This presents antenna design challenges. Second, the reflected signal contains a dominant contribution from the skin. This reflection must be reduced to permit detection of small tumors in the breast. Finally, reflections arise from structures in the breast, such as glandular tissues. Reflections from structures other than the tumor are considered to be clutter. Effective clutter reduction is required to permit robust detection of small tumors. To date, the challenges of TSAR have been primarily investigated using finite difference time domain simulations of simple breast models. Recently, work has focussed on experimental testing of a prototype system that permits exploration of different antenna designs and algorithms for skin sensing and clutter reduction.

The prototype system consists of a tank, which contains an immersion liquid (canola oil), as well as the antenna under test (J.M. Sill and E.C. Fear, *2005 IEEE MTT-S Int. Microwave Symposium Digest*, 4 pp., , 2005). The simple breast model is cylindrical in shape, and consists of materials that mimic the electromagnetic properties of skin, fatty breast tissues and tumors. The breast model is rotated in order to represent scanning the antenna around the breast, and measurements are taken with a vector network analyzer (Agilent 8719ES, Agilent Technologies, Palo Alto, CA, USA). TSAR algorithms are applied to reflections measured at 16 antenna locations, and an image of the plane perpendicular to the axis of the breast model and containing the tumor is created. A 1 cm diameter tumor is detected with a signal-to-clutter ratio of 10 dB. The prototype system is also used to test advanced algorithms for sensing the location and thickness of the skin. Reflections are collected from a metal sheet in order to estimate the system response. This response is deconvolved from reflections observed from a sheet of the skin material. Results indicate location and thickness estimates with errors of 1.1% and 27.5%. This represents a slight improvement in location error and a significant reduction in thickness estimate error (factor of over 3.5) when compared with the previous method of skin sensing. Overall, work with the prototype system demonstrates the successful application of TSAR algorithms to experimental data and provides a test bed for evaluating improvements to the TSAR approach.

RECENT  
DEVELOPMENTS IN OPTICAL CELLULAR-LEVEL DIAGNOSIS  
AND IMAGING FACILITATED BY THREE-DIMENSIONAL FDTD  
COMPUTATIONAL ELECTRODYNAMICS MODELING

Xu Li<sup>2</sup>, Allen Taflove<sup>2</sup>, Vadim Backman<sup>1</sup>

<sup>1</sup>Department of Biomedical Engineering, Northwestern University

<sup>2</sup>Department of Electrical Engineering and Computer Science, Northwestern University

During the past decade, it has become apparent that the analysis of the elastic light-scattering characteristics of living tissue can provide valuable diagnostic information (Backman et al., *Nature*, 406:35-36, 2000). In order to fully utilize the potential of optical approaches for disease diagnosis, it is important to understand the sensitivity and mechanisms of how subcellular structural and compositional changes affect observable light-scattering signatures. This paper reviews recent developments in our groups research in optical cellular-level diagnosis and imaging facilitated by three-dimensional finite-difference time-domain (FDTD) computational electrodynamics modeling.

We first review our recent three-dimensional FDTD modeling results which show that mapping the angular dependence of the optical backscattering spectrum of micron-scale particles yields fingerprint patterns which can be sensitive to the existence of subdiffraction nanometer-scale features embedded within the particles (Li et al., *IEEE J. Sel. Top. Quant. Elect.*, in press, 2005). These calculated fingerprint patterns resemble our preliminary experimental optical backscattering data obtained from animal tissues and human colonoscopy biopsies, which suggest that alterations of the patterns can be used as a sensitive marker to detect neoplasia at an exceptionally early stage.

We next review our recent FDTD modeling results for a novel spectroscopic microscopy technique which combines spectral measurements with optical microscopy to yield nanoscale structural information beyond what conventional optical microscopy alone reveals. We first show how to computationally synthesize a conventional microscope amplitude image of an arbitrary microstructure by applying vector diffraction theory to the FDTD-calculated far field. We next demonstrate the validity of this image-synthesis technique by comparing sample computed images with actual photomicrographs. Finally, we use this FDTD image-synthesis technique as a tool to test our groups recently developed spectroscopic microscopy system, which allows simultaneous acquisition of microscope images and backscattering spectra at each pixel (Liu et al., *Opt. Lett.*, in press, 2005). Our numerical investigations reveal that the backscattering spectrum from each pixel of a cellular image can be predicted from a simple one-dimensional layered model. This supports our hypothesis that pixel-by-pixel spectroscopic microscopy provides a unique capability to isolate photons scattered by embedded localized intracellular structures. This finding is important for further improvement and validations of the spectroscopic microscope system, which may find clinical applications (especially for early-stage cancer detection) as well as utility in basic biological research.

ULTRAWIDEBAND MICROWAVE BREAST CANCER DETECTION: SPACE-TIME BEAMFORMING FOR 3-D MRI-DERIVED NUMERICAL PHANTOMS

Shakti K. Davis<sup>1</sup>, Henri Tandradinata<sup>2</sup>, Frederick Kelcz<sup>3</sup>,  
Susan C. Hagness<sup>1</sup>, Barry D. Van Veen<sup>1</sup>

<sup>1</sup>Department of Electrical and Computer Engineering, University of Wisconsin – Madison

<sup>2</sup>ZS Associates, Evanston, IL

<sup>3</sup>Department of Radiology, University of Wisconsin Hospital and Clinics, Madison, WI

Microwave imaging is a promising modality for breast cancer detection that exploits a dielectric contrast between malignant and healthy breast tissue. One microwave-based technique that has been proposed for detecting breast tumors is space-time beamforming (Bond, *et. al*, *IEEE T-AP*, **51**, 1690-1705, 2003). Beamforming is a spatial filtering technique used to synthetically focus array data. An image of the focused energy is plotted where high energy regions imply the presence of strong scatterers such as tumors.

In this paper we apply beamforming to computed backscatter data from 3-D MRI-derived numerical breast phantoms. Tissue composition in these phantoms is dependent on two factors. The first is the tissue architecture derived from an MRI which defines the spatial distribution of fatty and fibroglandular tissues in the breast. The second factor is the assignment of dielectric properties to represent the types of breast tissue. Further studies are needed to determine a definitive method for mapping the MRI intensity to representative dielectric properties, but for a given MRI we consider two possible methods. One method is a uniform mapping (UM) which linearly maps pixel intensity to a range of dielectric values. The second method that we consider is a piecewise linear mapping (PWLM) which partitions the range of MRI intensities into multiple intervals and each interval is linearly mapped to a distinct range of dielectric properties values. The PWLM is based on the assumption that fibroglandular and fatty tissues are distinct and their respective dielectric constant and conductivity may occupy non-adjacent ranges. In the non-adjacent case an interval of intermediate-intensity pixels is transformed to a transitional range (between fat and fibroglandular) of dielectric properties.

We compare the mappings from the perspective of clutter and tumor detectability using beamforming. An MRI for a patient with heterogeneously dense breast tissue is selected and we create 3-D MRI-derived numerical phantoms using the UM and PWLM. The overall span of assigned dielectric properties is held constant; however, while the UM leads to smooth transitions in the distribution of dielectric properties, the PWLM mapping may induce sharper transitions that give rise to higher levels of clutter relative to the UM. Beamformer images reflect the elevated clutter levels as a reduction in the signal to clutter energy ratio for a detected tumor.

Assumptions regarding dielectric properties distributions throughout heterogeneous breast tissue must be made in theoretical studies of any microwave imaging method. We have considered two possible distributions of the dielectric properties and we note that the PWLM leads to a more challenging detection problem.

## TABLE TOP MICRO FLUIDIC NUCLEAR MAGNETIC RESONANCE SPECTROMETER

James Stephenson, Cynthia Furse  
University of Utah

Nuclear Magnetic Resonance (NMR) spectroscopy is a powerful method for determining chemical composition, biological properties, and other interesting properties of fluids. NMR systems are typically very large and expensive due to the superconducting magnets that must be used and the liquid helium and nitrogen used to cool them. This paper describes the development of a portable NMR spectrometer utilizing small permanent magnets, microscale probes and sample capillaries for microfluidic analysis of biological fluids (blood, urine, tears, amniotic fluid, saliva, etc.) and chemical agent sensing (homeland security). The underlying design and fabrication principles in downscaling the technique will be described. The motivating factors for downscaling NMR include improvements in the signal to noise ratio, vastly smaller sample volume requirements, and reduced dependence on high performance magnets. This leads to increased sensitivity and field portability, at substantially lower cost.

The key to miniaturization is in the use of a permanent magnet assembly built from high permeability Vanadium Permendur. This permanent magnet assembly has been shown to generate a variable field through a creative implementation of ferromagnetic flux switches (3,000 - 23,000 Gauss). The development of a manufacturable process for the micro coil and capillary system is described. This process provides an effective capillary wall thickness of zero (100 percent fill-factor), which is key to maximizing the signal to noise ratio. Measurements from a prototype device show approximately 17 MHz shift in the resonant frequency of sample-filled coil for a 20 percent change in static field strength. The variation in static field strength is produced by changing the arrangement of the flux switches.

## AN IN-DEPTH LOOK AT THE ELECTROMAGNETICS OF MRI RF PROBES

Tamer S. Ibrahim<sup>2</sup>, Chad Mitchell<sup>3</sup>, Roney Abraham<sup>2</sup>,  
Petra Schmalbrock<sup>4</sup>

<sup>1</sup>School of Electrical and Computer Engineering, The University of Oklahoma, Norman, Oklahoma

<sup>2</sup>BioEngineering Center, The University of Oklahoma, Norman, Oklahoma

<sup>3</sup>Department of Radiology, Department of Radiology, Uniformed Services University of the Health Sciences, Bethesda, Maryland

<sup>4</sup>Department of Radiology, The Ohio State University, Columbus, Ohio

Human magnetic resonance imaging (MRI) is now reaching magnetic field strengths as high as 7, 8, and 9.4 tesla. Ultra high field (7 tesla) operation brings the potential for increases in signal-to-noise ratio. However along with such advantages, there are significant and technical difficulties associated with such operation. From a radiofrequency (RF) perspective, higher field strengths correspond to increased operational frequencies; an 8 Tesla coil, for example, operates at approximately 340 MHz for proton imaging. At these frequencies, the wavelengths of the electromagnetic waves produced by currents on radiofrequency (RF) coils can become significantly less than the dimensions of the human head/body. As such, designing suitable RF coils and/or RF approaches that render useful clinical and research images, as in the case when the RF fields are homogenous within the imaged subject, is technologically as well as physically difficult.

Current ultra high field volume coils share a common design criterion, which is to produce modes that are transverse electromagnetic (TEM) to the coils axis. This notion, however, is only applicable when the resonator is empty or when the load has minimal effect on the coil performance, such as the case with low field imaging. Clearly ultra high field MRI operation does not fall under these two conditions; and the associated volume coils produce hybrid modes that may differ significantly from the intended and desired TEM modes. Therefore, a combination of experimental approaches with full wave modeling is indeed required in order to analyze the behavior of loaded RF coils most especially during ultra high field operation.

In this work we explore what happens electromagnetically during ultra high field operation. Our goal is to study the extent of the deviation of the hybrid modes from the TEM modes in UHF MRI. Using experiments and numerical modeling, we will address 4 critical questions associated with these hybrid modes: 1) what kind of global (across the object to be imaged) and local polarization (at a single voxel) they possess, 2) how their corresponding coil current distributions deviate from those associated with the TEM modes, 3) how far their field distributions (excite and receive fields) differ from those associated with the TEM modes, and finally 4) how all of these issues would impact imaging.

## INDEX

## A

Abraham, R. 378  
 Adams, R.J. 41  
 Ade, P.A.R. 84, 352, 353,  
 354  
 Aguirre, J. 352  
 Akagi, J.M. 78  
 Albert, J.M. 275  
 Amari, S. 85  
 Anderson, C.R. 363  
 Anderson, D. 207  
 Andersen, L.M. 281  
 Anghel, A. 207  
 Anguelova, M. 115  
 Amory-Mazaudier, C. 218  
 Araujo-Pradere, E.A. 176,  
 215  
 Arnold, K.S. 84  
 Arslanagic, S. 59  
 Asher, W.E. 115  
 Atkins, P. 76  
 Atsushi, T. 127  
 Avery, J.P. 233  
 Avery, S.K. 233

## B

Backer, D. 330, 359  
 Backman, V. 375  
 Bahadori, K. 360  
 Bahar, E. 103, 107  
 Bahcivan, H. 245  
 Bailey, M. 283  
 Baity, F.W. 260  
 Baker-Jarvis, J. 9, 10  
 Bao, J.W. 168  
 Barba, P. 36  
 Barden, J. 355  
 Bargach, K. 34  
 Barjatya, A. 263  
 Barlow, R.P. 372  
 Barnes, F.S. 369  
 Barott, W.C. 154  
 Barrios, A. 151  
 Bass, E.N. 226  
 Bassen, H. 373  
 Battle, J. 352  
 Batzle, M. 13  
 Baum, C.E. 3, 27, 141, 142  
 Bayram, Y. 92, 93  
 Beach, T.L. 178  
 Bell, G.S. 356  
 Bell, T.F. 44, 254  
 Benford, D. 354  
 Bengtson, R.D. 260  
 Benson, R.F. 271

Bering III, E.A. 260, 261  
 Berkowitz, Z. 197  
 Bernhard, J.T. 20, 76  
 Bernhardt, P.A. 181, 251  
 Bertram, J.M. 364  
 Betz, A. 337  
 Bhatnagar, S. 323  
 Bibl, K. 256  
 Bick, C. 252  
 Bilitza, D. 206  
 Bintley, D. 353  
 Black, T. 29  
 Blundell, R. 341  
 Boardsen, S. 271  
 Bobak, J.P. 115  
 Bock, J.J. 352  
 Bogaert, I. 58  
 Bogle, A. 36  
 Bopp III, C.L. 43  
 Booth, J.C. 12  
 Bornemann, J. 85  
 Bortnik, J. 273  
 Boyd, D. 252  
 Bradford, C.M. 352  
 Bradley, R.F. 304  
 Brandon, M. 128  
 Breinbjerg, O. 59  
 Briczinski, S.J. 232  
 Bricia, P. 203  
 Bristow, B. 251  
 Brogan, C.L. 326  
 Brown, G.S. 29  
 Brukardt, M. 260, 261  
 Buckle, J.V. 356  
 Buehrer, R.M. 363  
 Bullet, T.W. 217  
 Burghignoli, P. 56  
 Bussmann, S. 355  
 Bust, G.S. 202, 213, 214,  
 320  
 Butala, M.D. 331  
 Butler, C.M. 43, 94, 95

C

Canales, N. 11  
 Canning, F.X. 41  
 Cao, N. 347  
 Cappallo, R. 316  
 Carlstrom, J.E. 308  
 Carpenter, D.L. 276  
 Carrion, J. 63  
 Carscadden, J. 259  
 Carter, M.D. 260  
 Cartwright, N.A. 25  
 Cavalieri, D. 169  
 Cela, C.J. 372  
 Cha, J. 71  
 Chamberlin, K. 151  
 Chang, C. 359  
 Chang-Diaz, F. 260, 261  
 Chapman, D. 359  
 Charnotskii, M.I. 113  
 Chau, J.L. 194, 207, 226,  
 230, 231  
 Chen, C. 250  
 Chen, C.C. 122  
 Chen, H. 359  
 Chen, J. 373  
 Chen, T.C. 338  
 Cheney, G. 256  
 Cheng, E.S. 338  
 Cheng, Z. 295  
 Chervenak, J.A. 344  
 Chevalier, M.W. 44  
 Chevalier, T.W. 44  
 Cho, H.M. 340  
 Choi, C. 5  
 Christopher, I. 332  
 Chuss, D.T. 346, 347  
 Cimini, D. 152, 153  
 Clark, J. 144  
 Clarke, J. 340  
 Clegg, A.W. x  
 Cline, D. 166  
 Close, S. 224, 225  
 Cohen, A.S. 325, 333  
 Cohen, M.B. 294  
 Colerico, M.J. 174, 175,  
 204  
 Colestock, P. 224, 225  
 Coley, R.W. 205  
 Comiso, J. 169  
 Condon, J.J. 325  
 Condor, P. 231  
 Converse, M.C. 364  
 Corder, S.A. 314  
 Cordes, J.M. 302  
 Cornwell, T.J. 324  
 Corpuz, A.R. 252  
 Coster, A.J. 174, 175, 177,  
 204  
 Cottingham, D.A. 338  
 Cotton, W.D. 325  
 Crane, P. 333  
 Crittenden, P. 107  
 Crossmann, S. 36  
 Cummer, S.A. 50, 281,  
 283, 284, 295

## D

Davis, B. 11  
 Davis, S.K. 376  
 Davis, W.A. 4, 121  
 Day, P.K. 342, 343  
 de Jesus, C. 359  
 de Paula, E.R. 179  
 de Rezende, L.F.C. 179  
 De Zaeytijd, J. 58  
 Demarest, K.R. 120  
 DeMinco, N. 79  
 Dent, W.R.F. 356  
 Deshpande, P. 358  
 Devlin, M. 354  
 DeWitt, B. 66  
 Diaz, A. 45  
 Dicker, S. 354  
 Dimant, Y.S. 228, 229  
 Dobbs, M.A. 340  
 Doeleman, S. 316  
 Doherty, J.F. 192  
 Doo, S.J. 93  
 Doriese, R. 344  
 Dowgiallo, D.J. 115  
 Dowlatshahi, S. 152, 153  
 Downes, T. 338  
 Dragovan, M. 352  
 Drexler, J. 244  
 Drouet d'Aubigny, C. 355  
 Droz, P.Y. 359  
 Duband, L. 352  
 Dunare, C. 353  
 Duncan, W. 353  
 Dyrud, L. 228, 229, 246

## E

Earle, L. 352  
 Edwards, B.E. 102  
 El-Ghazaly, S. 19, 75  
 Eleftheriades, G.V. 49  
 Engargiola, G. 84  
 Engheta, N. 51, 53, 102  
 Erentok, A. 54  
 Ergun, R. 242  
 Erickson, N.R. 358  
 Erickson, P.J. 190, 191, 230  
 Erricolo, D. 95  
 Evoy, S. 102

## F

Farahat, N. 45, 63  
 Fath, V. 358  
 Fathy, A.E. 19, 75, 87, 119,  
 128, 136  
 Fear, E.C. 374  
 Fedrizzi, M. 179  
 Fehlen, R.G. 5  
 Finkbeiner, F.M. 338

Fishman, G. 294  
 Fixsen, D.J. 338, 347  
 Fomenko, A.S. 298  
 Foster, J.C. 174, 175, 204  
 Fostier, J. 58  
 Frasch, L.L. 5  
 Fraser-Smith, A.C. 297  
 Frazin, R.A. 331  
 Fukao, S. 218  
 Fuks, I.M. 113  
 Fuller-Rowell, T.J. 176,  
 208, 215  
 Fung, A.K. 109  
 Fung, S. 271  
 Furse, C. 377

## G

Gaiser, P.W. 115  
 Galindo, F. 231  
 Galkin, I.A. 203, 216, 256  
 Gallagher, D.L. 206  
 Ganguli, G.I. 237, 239, 266  
 Gao, J. 342, 343  
 Garcia, L.N. 271  
 Garner, T.W. 205, 213,  
 214, 320  
 Gasiewski, A.J. ix, 152,  
 153, 165, 166, 167, 168,  
 169  
 Gaussarian, T.L. 180, 196  
 Gaussiran II, T.L. 205, 307,  
 320  
 Gensheimer, P. 355  
 George, R.C. 193  
 Gerken, E.A. 249, 283, 284  
 Gerstoft, P. 130  
 Gibby, A.R. 276  
 Gibson, J.L. 313  
 Gigoyan, S. 87, 119  
 Giri, D.V. 94  
 Glenn, J. 352  
 Glover, T.G. 260, 261  
 Godin, O.A. 113  
 Goldberg, R.A. 264  
 Goldhirsh, J. 148  
 Goldin, A. 343  
 Goldman, M.V. 241, 243  
 Golish, D. 355  
 Gonzalez, S. 188  
 Goulding, R.H. 260  
 Gregor, R.B. 57  
 Green, J.L. 203, 271  
 Grefenstette, B.W. 286  
 Groppi, C. 355  
 Grosslein, R.M. 358  
 Grosvenor, C. 11  
 Groves, K.L. 178  
 Gupta, G. 67

## H

Habash Krause, L. 178  
 Hagness, S.C. 364, 376  
 Hailey-Dunsheath, S. 351  
 Hairston, M.R. 205  
 Hajj, G. 219  
 Halpern, M. 353  
 Hampton, J.R. 147  
 Han, Y. 19  
 Harp, G.R. 318  
 Havrilla, M.J. 5  
 Haywas, L. 178  
 Hedden, A. 355  
 Heiles, C. 301  
 Heinselmann, C.J. 187, 230,  
 232, 251  
 Henning, P.A. 307  
 Hicks, B. 333  
 Hills, R.E. 356  
 Hilton, G. 353  
 Hodgkiss, W.S. 130  
 Holdaway, M.A. 315, 326  
 Holland, W. 353  
 Holloway, C.L. 70  
 Holt, J.M. 190, 191, 218  
 Holzapfel, W.L. 84, 340  
 Holzworth, R.H. 289  
 Hood, A.Z. 124  
 Horanyi, M. 262  
 Horne, R.B. 272  
 Horsfall, D. 272  
 Hristov, V. 352  
 Hsieh, W-T. 347  
 Hu, Y. 138  
 Huang, E.X. 109  
 Huang, X. 206, 216, 278  
 Huff, G.H. 20  
 Huffines, G.R. 281  
 Hughes, B.L. 67, 77  
 Hughes, J. 251  
 Humphreys, T.E. 196  
 Hunt, C. 353  
 Hunter, T.R. 311  
 Hysell, D.L. 189, 194, 244,  
 245

## I

Ibrahim, T.S. 378  
 Iijima, B. 183, 219  
 Imura, H. 233  
 Imbriale, W.A. 357  
 Inan, U.S. 44, 253, 254,  
 276, 287, 290, 293, 294  
 Ingram, M.A. 154  
 Irisov, V.G. 165, 167, 169  
 Irwin, K. 353, 354  
 Ishikawa, S-H. 88  
 Itoh, T. 21, 52  
 Iturbide-Sanchez, F. 149



## Index

Ivarsen, K. 303  
Iyer, A.K. 49

### J

Jackson, D.R. 56, 91, 373  
Jackson, R.W. 149  
Jacobson, A.R. 215  
Jacobson, V.T. 260, 261  
Janches, D. 193, 230  
Janezic, M.D. 9, 10  
Jaugey, N.C. 281, 283, 284  
Jenkins, J. 151  
Jerab, M. 268  
Jiang, B-H. 6  
Jin, N. 69  
Jira, C.F. 276  
Johnk, R. 11  
Jones, G. 355  
Jones, S.D. 147  
Joshi, G.G. 4  
Junor, W. 307

### K

Kagan, L. 249  
Kainz, W. 373  
Kamalabadi, F. 173, 188,  
331  
Kammae, T. 282  
Kanamaluru, S. 137  
Kang, C. 234  
Kang, Y. 87, 132  
Kantor, I.J. 179  
Karacolak, T. 123  
Kassim, N.E. 307, 325, 333  
Kawakami, C.R. 68  
Kawamura, J. 341  
Kelcz, F. 376  
Kelley, M.C. 180, 249  
Kelly, J.D. 187  
Kemball, A. 331  
Kempel, L.C. 36  
Khan, Z.A. 92  
Khmyrov, G.M. 216  
Kilpatrick, S. 213  
Kim, E.M. 138  
Kim, J. 370  
Kim, S.H. 266  
Kim, Y. 64  
Kini, V. 17  
Kintner, P.M. 179, 180  
Kitrosser, D. 216  
Klein, M. 152, 153, 165,  
166, 168, 169  
Klemm, M. 365  
Knappmiller, S. 262  
Kobayashi, T. 127  
Kogut, A. 347  
Kohlberg, I. 143, 144

Kolinski, J. 17  
Koltenbah, B.E. 57  
Komjathy, A. 183  
Konanur, A.S. 67, 77  
Kooi, J. 355  
Korngut, P. 354  
Kowalski, M.E. 66  
Kozlov, A.V. 216  
Kramer, B.A. 122  
Krishnamurthy, S.H. 77  
Kucukaltun, A.N. 34  
Kudeki, E. 188, 228  
Kuester, E.F. 70  
Kuga, Y. 71  
Kuhn, M.J. 128  
Kuiper, T. 355  
Kulesa, C. 355  
Kumar, S. 342, 343  
Kuo, C.H. 110, 111  
Kuo, C-L. 343  
Kuroki, F. 37, 72, 83, 88

### L

LaBelle, J. 240  
Lam, T.A. 57  
Lane, W.M. 325  
Lang, R.H. 158, 162  
Lanting, T.M. 340  
Laskar, J. 18  
Lau, E.M. 233  
Lazio, T.J.W. 325, 333  
Lazzi, G. 67, 77, 99, 372  
Le Cocq, C. 297  
LeDuc, H.G. 342, 343  
Ledvina, B.M. 180, 196  
Lee, A.T. 84, 340  
Lee, C.-H. 18  
Lee, J. 173  
Lee, M. 122  
Lee, T.H. 64  
Lehtinen, N.G. 253  
Lertsirimit, C. 91  
Leusky, V.Y. 152, 153, 165,  
167, 169  
Li, J. 53, 284  
Li, X. 375  
Liang, J. 96  
Liao, D. 159  
Lichtenberger, A. 355  
Lim, S. 21  
Limon, M. 347  
Lin, H. 80  
Lin, S. 119, 136  
Lin, X.P. 80  
Lind, F.D. 190, 191  
Liu, N. 285, 288  
Liu, S.-Y. 311  
Liu, Y-T. 6  
Livneh, D.J. 192

Logan, D.W. 338  
Lonsdale, C. 316  
Lord, S. 341  
Losseva, T.V. 298  
Lotko, W. 237  
Loudkov, D. 341  
Lovat, G. 56  
Lueker, M. 340, 345  
Lumori, M.L.D. 138  
Lyakhov, A. 201, 208  
Lyons, W.A. 281, 283, 284  
Lysak, R.L. 238

### M

MacDougall, J. 249  
MacIntosh, M. 353  
MacMahon, D. 359  
Mahfouz, M. 128  
Mahvi, D.M. 364  
Main, D.M. 242  
Makarov, N.A. 233  
Makela, J.J. 173, 180  
Malhotra, A. 227  
Maloney, P. 352  
Mandrake, L. 219  
Mannucci, A. 183  
Marchese, J.R. 190  
Markus, T. 169  
Marriage, T. 344  
Marrone, D.P. 312, 341  
Marshall, R.A. 293  
Marshall, R.E. 150  
Masaki, K.-I. 72  
Mason, B. 354  
Masumoto, R-T. 83  
Mathews, J.D. 192, 227,  
232  
Matsuhara, H. 352  
Mattioli, V. 153  
Mazin, B.A. 342, 343  
McCarthy, M.P. 289  
McCaskill, G.E. 260  
McCready, M. 218  
McGinty, F. 137  
McHarg, M.G. 282  
McIntyre, E.M. 165, 167  
McMahon, D.H.E. 318  
McNamara, L.F. 182  
Mehdi, I. 341  
Mehl, J. 84  
Meisel, D.D. 232  
Meredith, N.P. 272  
Merheb, N.M. 147  
Merlino, R.L. 266  
Meyer, M. 197  
Meyer, S. 338  
Michielssen, E. 58  
Milikh, G.M. 229  
Minkoff, J. 319

## Index

Minter, C.F. 215  
Mitchell, C. 378  
Mitchell, C.N. 202  
Mithaiwala, M. 237, 239  
Moghaddam, M. 110, 111,  
112, 160  
Mokhtaari, M. 85  
Montgomery, M.H. 320  
Moore, R.C. 254  
Morabito, A. 197  
Morales, M. 316, 317  
Morrison, P. 144  
Moseley, S.H. 346, 347  
Moses, R. 215  
Moss, G.D. 288  
Mudaliar, S. 26  
Muella, M.T.A.H. 179  
Mukhopadhyay, R. 18  
Mumcu, G. 55  
Murata, Y-S. 83  
Mutel, R.L. 303, 332  
Myers, M.J. 84  
Myers, S.T. 324, 326  
Myoung, S.K. 93

## N

Nair, V.K. 17, 19, 75, 76  
Narayanan, G. 355, 358  
Naylor, B. 352  
Nelson, T.E. 281, 283, 284  
Nemecek, Z. 267, 268  
Nemtchinov, I.V. 298  
Newman, D.L. 241, 242,  
243  
Nguyen, H. 352  
Niemack, M. 344  
Nikitin, M. 201  
Nikola, T. 351  
Nikoukar, R. 188  
Novotny, D. 11  
Nsumei, P. 206

## O

Oberst, T. 351  
Ohta, H. 37  
Olyslager, F. 58  
Oppenheim, M.M. 224,  
226, 228, 229, 246  
O'Rourke, A.P. 364  
Oughstun, K.E. 25  
Oyoma, S. 251

## P

Padmanabhan, S. 115, 149  
Paine, S. 341  
Palo, S.E. 230, 233, 234  
Pan, H.K. 17, 19, 75, 76  
Paravastu, N. 333

Parazzoli, G.C. 57  
Parkes, W. 353  
Parshley, S.C. 351  
Parsons, A. 330, 359  
Pasko, V.P. 285, 288, 296  
Pasya, I. 127  
Pau, J. 252  
Paunil, D.E. 147  
Pautet, D. 283  
Pavlu, J. 267, 268  
Paznukhov, V. 256  
Pearson, J. 341  
Pearson, T. 327  
Perara, T. 338  
Perez-Wurfl, I. 135  
Perley, R.A. 325  
Perumana, B. 18  
Pesnell, W.D. 264  
Peter, W.B. 290  
Phillips, N. 347  
Pi, X. 219  
Pilling, S. 252  
Pinel, S. 18  
Pinto Jr., O. 289  
Pissoort, D. 58  
Platino, M. 277  
Pogorzelski, R.J. 42  
Pogrebnyak, V.A. 34  
Polisensky, E. 333  
Popa, B.-I. 50  
Prager, J. 259  
Pratap, P. 306  
Psiaki, M.L. 196  
Puetz, P. 355  
Pvillalta, J. 366, 371

## Q

Qiang, G. 129

## R

Rahmat-Samii, Y. 65, 69,  
360, 370  
Rajagopalan, A. 99  
Rajagopalan, H. 65  
Rao, R. 312  
Rao-Venkata, U. 324  
Ray, P.S. 333  
Riadle, J.D. 180  
Redman, R.O. 356  
Reinisch, B.W. 203, 206,  
216, 278  
Reising, S.C. 115, 149  
Rengarajan, S.R. 35  
Rentsiema, C. 353  
ReVelle, D.O. 223  
Rich, F.J. 204  
Richards, P.L. 84, 340  
Richer, J.S. 356  
Richterova, I. 267, 268

Rideout, W.J. 177, 190, 204  
Rivera, N.V. 363  
Roberson, B.R. 259  
Robertson, D.S. 215  
Robertson, S. 262  
Roblin, P. 93  
Rodrigues, F.S. 179, 189  
Rogers, A.E.E.R. 306  
Rogers, T. 130  
Roque, J.D. 78  
Rose, L.A. 115  
Rothwell, E. 36  
Rudakov, L.I. 237, 239  
Ruhl, J. 338

## S

Saatchi, S. 161  
Safrankova, J. 267, 268  
Sahr, J. 197  
Salah, J.E. 306  
Samay, S. 137  
Sanchez, J. 63  
Santiago, D. 45  
Sarabandi, K. 159  
Sarkar, S. 18  
Scales, J.A. 13  
Scales, W.A. 250  
Schmalbrock, P. 378  
Schneider, G. 347  
Schneider, T.L. 168  
Schreiber, A.W. 94, 95  
Scime, E. 265  
Selcher, C. 251  
Semeter, J. 246  
Sen, N. 241, 243  
Sertel, K. 55  
Shao, X. 271  
Sharp, E.H. 338  
Shiroma, G.S. 68  
Shiroma, W.A. 68, 78  
Siefiring, C.L. 181  
Siemion, A. 359  
Sill, J.M. 374  
Silveirinha, M.G. 51  
Silverberg, R.F. 338  
Simpson, J.J. 155  
Sletten, M.A. 108  
Smith, D.F. 168  
Smith, D.M. 286  
Smith, H. 356  
Song, P. 203, 278  
Song, Y. 238  
Sparks, L. 183  
Spencer, P.S.J. 215  
Spieler, H.G. 84, 340  
Spitler, L. 303  
Squire, J.P. 260, 261  
Sridharan, T.K. 341  
St-Maurice, J-P. 244

## Index

Stacey, G.J. 351  
Staggs, S. 344  
Stankov, B.B. 166, 168,  
169  
Starks, M.J. 249, 274  
Steffes, P.G. 154  
Stenbaek-Nielsen, H.C.  
282  
Stephenson, J. 377  
Stern, J. 341, 343  
Sternovsky, Z. 262  
Stevenson, T. 347  
Stewart, K. 333  
Stobie, N. 259  
Streltsov, A.V. 237  
Stutzman, W.L. 4  
Su, Y.-N. 311  
Sudiwalla, R. 353  
Sulzer, M. 188, 193, 218  
Susczynsky, D.M. 215  
Sutton, E. 328  
Swenson, C.M. 263  
Syeda, A.K. 120

## T

Tabatabaenejad, A. 112,  
160  
Taflove, A. 155, 375  
Takase, B.O. 68  
Takigawa, Y.-S. 88  
Tandradinata, H. 376  
Tanielian, H.M. 57  
Taylor, B.T. 177, 205, 214  
Taylor, G.B. 307  
Taylor, M.J. 283  
Teixeira, F.L. 101  
Tesche, F.M. 94  
Thomas, J.N. 289  
Thomson, D.J. 131  
Thorne, R.M. 272, 273  
Ting, S. 316  
Tong, E. 341  
Toporkov, J.V. 108  
Topsakal, E. 123, 124, 366,  
371  
Torrice, S.A. 158  
Torvik, J. 135  
Tran, H.T. 84  
Travers, D. 347  
Troester, G. 365  
Tucker, C. 354

## U

Ueda, T. 52  
Uslenghi, P.L.E. 28, 96  
Utku, C. 162

## V

Vale, L. 353  
Valentic, T.A. 187  
van Eyken, A.P. 218  
Van Veen, B.D. 376  
Van Zeghbroeck, B. 135  
Vayonakis, A. 342, 343  
Venkatesan, J. 86  
Venkatesh, S. 363  
Volakis, J.L. 55, 92, 93, 122  
Voronovich, A.G. 114, 168  
Voss, H.D. 264

## W

Wadefalk, N. 355  
Walker, C.K. 305, 355  
Walton, A. 353  
Wandelt, B.D. 328  
Wang, C. 219  
Wang, G. 41  
Ward, J. 341  
Watkins, B. 251  
Webb, P.A. 264  
Weber, B.L. 165, 166, 168  
Webster, J.G. 364  
Wei, E. 252  
Weiler, K. 333  
Weinreb, S. 355  
Welch, W.J. 313  
Wen, C.-H. 192  
Werner, B. 354  
Werthimer, D. 330, 359  
Westwater, E.R. 152, 153  
Whalen, J.J. 34  
Wick, G.A. 166  
Will, J.A. 364  
Williams, T.C. 374  
Wilson, B. 219  
Wilson, G.W. 338  
Wilson, J.L. 87, 132  
Wilton, D.R. 56, 91  
Winglee, R.M. 259  
Wollack, E.J. 344, 346, 347  
Wong, A.Y. 252  
Wong, K.S.Y. 68  
Wood, C. 352  
Woodcraft, A. 353  
Woodman, R.F. 231  
Wright, J.W. 195, 217  
Wright, M.C.H. 314, 318,  
329, 330, 359  
Wu, D. 373

## X

Xingzhou, Z. 129  
Xu, Y. 353

## Y

Yaghjian, A.D. 33  
Yang, D. 364  
Yang, H. 296  
Yang, S. 19, 75  
Yang, T. 121  
Yang, Y. 136  
Yardim, C. 130  
Yarga, S. 55  
Yavuz, M.E. 101  
Yin, P. 202  
Yngvesson, S. 339  
Yoneyama, T. 72, 83, 88  
Yorke, H. 341  
Young, W.F. 70  
Yumoto, K. 207

## Z

Zabotina, N.A. 195, 217  
Zabotina, L.Y. 195, 217  
Zamora, R.J. 167  
Zavorotny, V.U. 114, 167  
Zhang, C. 19, 75, 128  
Zhang, S.-R. 218  
Zhao, F. 135  
Zhao, J.-H. 311  
Zhbakov, G.A. 195  
Zheng, L. 129  
Zhou, Q.H. 227  
Ziemba, T. 259  
Ziolkowski, R.W. 54  
Zmuidzinas, J. 342, 343,  
352

